Design and Development of FPGA based Controllers for Photovoltaic Power System

Venkata Ratnam Kolluru

Department of Electronics & Communication Engineering
National Institute of Technology Rourkela, India

Design and Development of FPGA based Controllers for Photovoltaic Power System

Thesis submitted in partial fulfillment

of the requirements for the degree of

Doctor of Philosophy

in

Electronics & Communication Engineering

by

Venkata Ratnam Kolluru

(Roll: 510EC109)

under the guidance of

Prof. Kamalakanta Mahapatra

&

Prof. Bidyadhar Subudhi

Department of Electronics and Communication Engineering
National Institute of Technology Rourkela
Rourkela-769008, Odisha, India

July 2016

Department of Electronics & Communication Engineering
National Institute of Technology Rourkela
Rourkela-769008, Odisha, India.

04 July 2016

Certificate

This is to certify that the work in the thesis entitled ***Design and Development of FPGA based Controllers for Photovoltaic Power System*** by ***Venkata Ratnam Kolluru***, bearing Roll 510EC109, is a record of an original research work carried out by him under my supervision and guidance in partial fulfilment of the requirements for the award of the degree of *Doctor of Philosophy* in *Electronics & Communication Engineering*. Neither this thesis nor any part of it has been submitted for any degree or academic award elsewhere.

Prof. Bidyadhar Subudhi
Co-Supervisor

Prof. Kamalakanta Mahapatra
Supervisor

Dedicated To My Family

Acknowledgments

I would like to express my deepest gratitude towards my supervisor, Professor Kamalakanta Mahapatra and my co-supervisor Professor Bidyadhar Subudhi for their generous support, supervision, encouragement, confidence and for the valuable knowledge that they shared with me. I learned valuable lessons from their personality and visions.

I like to express my gratitude to our honourable Director, Professor Sunil Kumar Sarangi for his motivation and inspiration. I learned valuable morals from his personality, visions and dynamic activities.

I am also grateful to my Doctoral Scrutiny Committee Members, Prof. S.K. Patra, Prof. U.C. Pati, Prof. Dipti Patra, and Prof. P.K. Sahu.

I am thankful to Prof. Ayaskanta Swain, Tom, Jaganath, Rajesh, Sudeendra, Sauvagya, Jagadeesh, Srinivas, Vijay, Gokulanand, Govind, Ramakrishna, Dr. Karuppanan, Dr. Natarajamani, Satyajit, Om Prakash, Shiva, Dr. Kanhu, Dr. Preethi and Mr. P.P.K.Patro, who has given the support in carrying out the work.

My sincere gratitude to Dr. K. Veeraswamy, Prof. K. Koteswararao who encouraged me towards research.

During the course of this work, part of my work was supported by a project VLSI-SMDP sponsored by DIT, Govt. of India. I am really thankful to them.

Special thanks to my lovable friends, all ECE department faculty, staff and everybody who has helped me to complete the thesis work successfully.

Finally, and most importantly, I would like to express my deep appreciation to my beloved family members Devadattatreyulu, Bala Tripura Sundari, Jhansi Lakshmi, Nidheesh Kumar, Hanvitha, Rupa, Mr. Surendra, Sudev and Supratika for all their encouragement, understanding, support, patience, and true love throughout my ups and downs. At last but above all, I always thank and praise God for being on my side.

Venkata Ratnam Kolluru

Abstract

In the recent years owing to increased energy consumption and consequent rise in crude oil price and global climatic change have motivated researchers to focus towards harnessing power from renewable energy resources such as photovoltaic (PV), fuel cell, biomass and wind energy systems. Among the different renewable resources, PV technology is one of the fastest growing technologies, because of abundance availability of solar irradiance and it has no adverse environmental impacts. But, the cost of PV energy is higher than the other conventional sources owing to its low PV conversion efficiency. Therefore, research opportunities lie in applying power electronics and control techniques for harvesting PV power at higher efficiencies for appropriate utilization. For simulation, analysis and control design of a PV power system, an accurate model of the PV cell is essential because PV cell is the basic bulding block of a PV power system. To maximise the power generation of a PV system it is necessary that the PV array should be operated at the maximum power point. A maximum power point tracker (MPPT) is required in the PV system to enable it to operate at the MPP. The output current-voltage (I-V) and power-voltage (P-V) characteristics of a PV vell are non-linear and hence its power fluctuates in accordance with the variation in solar irradiance and temperature. During the last decade, a lot of research has been directed to develop efficient MPPT schemes. But, research opportunities are still promising for designing new MPPT algorithms and to address their digital implementation issues. Further, there lies challenge to design MPPTs that can handle partial shading conditions. The thesis first proposes development of new MPPT algorithms and different pulse width modulated-voltage source inverter control strategies for a PV system.

Firstly an integral sliding mode MPPT controller (ISMC) has been proposed for achieving an effective MPPT scheme, and then a modified P&O MPPT controller is developed which is implemented using a real-time digital simulator called Opal-RT. The performance of the modified ISMC is compared with that of the conventional proportional integral (PI) MPPT controller using both MATLAB simulation and real-time experimentation. The performance of the modified P&O MPPT controller with fixed step size is compared with that of the conventional incremental conductance (Inc Cond)

and P&O MPPT controllers, and these are validated by using Opal-RT and subsequently through FPGA implementation. A modified incremental conductance MPPT controller with variable step size is then proposed for handling partial shading conditions. The tracking performance of the proposed modified Inc Cond MPPT controller is also compared with that of the conventional Inc Cond MPPT controller, from the obtained results by using Opal-RT. Further, an experimental prototype PV set-up is developed in the laboratory to implement the proposed MPPT algorithms on the physical hardware.

After having developed efficient parameter extraction algorithms for a PV panel, the thesis subsequently proposes five new MPPT algorithms such as Integral sliding mode MPPT, modified P&O MPPT, modified Inc Cond MPPT, Model predictive MPPT, and modified Inc Cond variable step size MPPT controllers. All these developed MPPT algorithms have been implemented on a Solar array simulator (SAS) PV system, in MATLAB/SIMULINK, OPAL-RT and on a prototype hardware PV set-up. From the obtained results, it is found that these MPPTs adjust the power of a PV system effectively to its maximum power value smoothly with fast response and accuracy whilst reducing the fluctuations in its power. Tracking performance of all these proposed MPPT algorithms are found to be superior to some of the existing MPPTs such as perturb and observe (P&O), incremental conductance (INC), HCC and adaptive HCC. Further more, a PV system is observed to be stable with all these proposed MPPTs. From the results obtained it is also confirmed that the proposed modified *P&O* MPPT exhibits better MPP tracking performance in terms of quick settling time and least steady state error. Further, less voltage fluctuation and less maximum overshoot are observed in the case of the proposed modified Inc Cond MPPT among all the proposed MPPT algorithms. The proposed controllers are also well suited to all weather conditions.

A grid connected PV system involves a power conversion from DC power into AC power. Due to high switching frequencies of this conversion by inverter, there is a power loss. An efficient control scheme needs to be developed for integrating the PV system to the grid. The thesis then proposes a Model Predictive Control (MPC) for integrating a PV system to the grid. The performance of the MPC is compared with conventional hysteresis current controller (HCC) and also with that of an adaptive HCC (AHCC) through a real-time

simulatin using the Opal-RT then through FPGA implementations. FPGA implementation of the controllers such as HCC, AHCC and MPC were also performed by using LABVIEW configured with NI-cRIO-9014 platform.

For elimination of current harmonic and reactive power of the grid connected PV system, there is a need of designing a filter. The PV system based shunt active power filter (SAPF) with modified incremental conductance MPPT controller with variable step size is then designed. From the MATLAB simulation and real-time digital simulation studies it is envisaged that the proposed PV based SAPF exhibits good harmonics compensation.

Contents

List of Figures

List of Tables

List of Acronyms

(I_0) saturation current

(I_{mpp}) current at MPP

(I_{ph}) photo-generated current

(V_{mpp}) voltage at MPP

I_{d1} diffusion current

I_{d2} recombination current

I_{sc} short circuit current

R_{sh} shunt resistance

R_s series resistance

V_{oc} open circuit voltage

AC Alternating Current

AHCC Adaptive HCC

ANN Artificial Neural Network

APLC Active Power Line Conditioner

CCM Continuous Conduction Mode

CF Curve Fitting

cRIO compact Reconfigurable Input Output

CRO Cathode Ray Oscilloscope

CSI Current Source Inverter

DAQ Data Acquisition

DC Direct Current

DCM Discontinuous Conduction Mode

DSO Digital Storage Oscilloscope

DSP Digital Signal Processor

FF Fill Factor

FLC Fuzzy Logic

FPGA Field Programmable Gate Array

GCPV Grid Connected PV

GMPPT Global Maximum Power Point Tracking

GPIB General Purpose Interface Bus

HCC Hysteresis Current Controller

HIL Hardware- In the- Loop

Inc Cond Incremental Conducatnace

LAN Local Area Network

LPF Low Pass Filter

LVM Load Voltage Maximization

MPC Model Predictive Controller

MPPT Maximum Power Point Tracking

NI National Instruments

OCC One Cycle Control

P& O Perturb & Observe

PC Personal Computer

PCC Point of Common Coupling

PI Proportion-Integral

PLD Programmable Logic Devices

PLL Phase Locked Loop

PSC Partial Shading Conditions

PV Photovoltaic

PWM Pulse Width Modulation

RTDS Real Time Digital Simulator

SAPF Shunt Active Power Filter

SAPLC Shunt APLC

SAS Solar Array Simulator

SIF Shade Impact Factor

SMC Sliding Mode Controller

SMPS Switch Mode Power Supply

SRF Synchronous Reference Frame

STC Standard Test Conditions

SVPWM Space Vector PWM

THD Total Harmonic Distortion

USB Universal Serail Bus

VSI Voltage Source Inverter

VSR Voltage Source Regulator

ZCS Zero Current Switching

ZVS Zero Voltage Swithcing

Chapter 1

Introduction

1.1 Background

1.1.1 PV energy potential

The global average energy consumption is over 400 Terawatt-hour, achieved by burning of fossil fuels, hydro, nuclear power and etc. The major source of electric power comes from burning of fossil fuels. Major countries such as USA, China and India depend upon fossil fuels for electricity generation. Excessive usage of fossil fuels is likely damage the idea of sustainable development in the future [1]. Global warming is a major concern and it is for all developed and developing nations to cut down their carbon emissions. 24% of carbon emissions from China, 6% from USA and 1% from India come from burning of fossil fuels [2]. Apart from this it is known that, fossil fuels are not renewable and for exploration and processing of fossil fuels are not cost effective [3]. In recent years, there is a challenge for the researchers and engineers to develop efficient techniques for harvesting renewable energy cost effective while reducing global warming.

Developing economies e.g., China and India deliberately need pollution free, reliable, scalable, efficient, long term durability energy sources. Renewable energy sources such as solar, wind, biomass and hydro power are some of the promising solutions for sustainable development. In the list of renewable energy resources, solar energy is very promising. Photovoltaic (PV) conversion ratio currently has low efficiency, thus there is a great deal of research interest how to achieve maximum power extaction from the PV panels.

The word photovoltaic is a combination of two words, photo, which means light and voltaic that implies production of electricity [4]. Generation of electricity from

light is called PV technology. Converting solar irradiation into electricity is based on photovoltaic effect, which is a physical phenomenon of converting energy carried by optical electromagnetic radiation into electrical energy. In 1839, E. Becquerel found that, some of materials generate electric current when exposed to light. Till 1959 the photovoltaic effect remained an interesting fact in the laboratory. In 1954, Bell laboratories developed the first silicon solar cell with 6% efficiency, which was rapidly improved to 10% [5]. The PV solar cells are made with semiconductor material for absorbing a large part of the solar spectrum.

The PV energy source is free and abundant in nature, hence, it is sustainable. Usage of PV energy is pollution free, because it does not produce carbon dioxide. No noise and no mechanical moving parts in PV panles. PV converts solar irradiation into electricity directly from watts to megawatts range also. The PV modules have a very long lifetime. These are some advantages of PV.

Toxic chemicals (cadmium and arsenic) are used in the PV cell production process. These chemicals impacts in environment are negligible and can be easily controlled for disposal or recycling. PV energy is more expensive than conventional energy, because of manufacturing and cost of PV cells in the low conversion efficiencies of the equipment. The PV energy generation depends upon intensity of the sunlight on that particular day. Solar facilities will not produce power during entire periods, thus leads to shortage of energy. These are the disadvantages of PV.

1.1.2 PV energy conversion technology

Fig. 1.1 depicts the PV process. Energy from the sunlight comes in the form energy conversion which is the basic unit of light and other electromagnetic radiations. Photons include different quantity of energy corresponding to the different wavelengths of light [6].

From the energy equation $E = h\nu$, where h is Planck's constant and ν is the photon's frequency, it is observed that the energy of the photon decreases when its wavelength increases. When semiconductors are exposed to light, the photons within a certain energy band can be absorbed; rest of the photons may pass through the material or reflected without being absorbed as shown in Fig. 1.1. When a photon is absorbed, then that energy will be transferred to the electron of that material. Different semiconductors have different optical absorption coefficients.

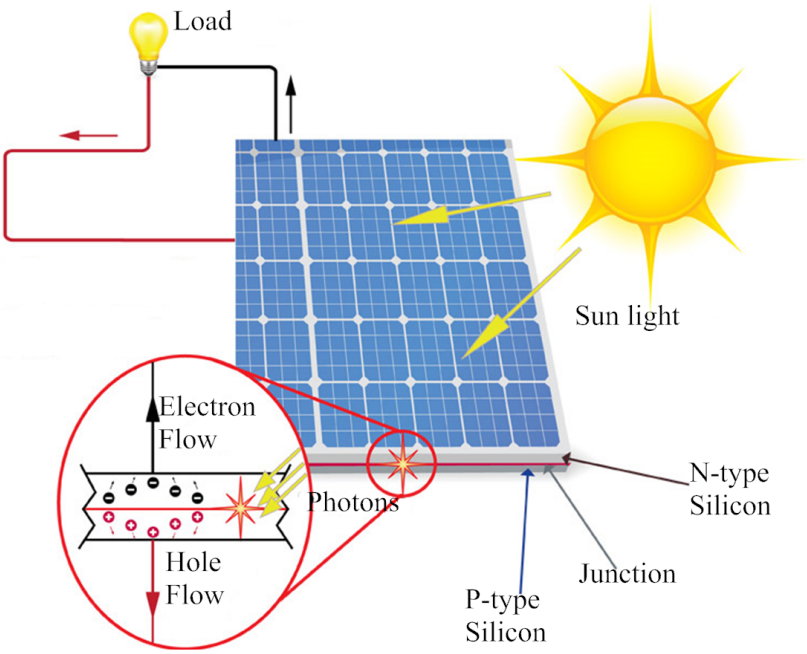

Figure 1.1: Conversion mechanism of solar radiation into electricity

Some popular technologies e.g., PV cells can be manufactured using wafer-based silicon technology and thin-film technology. The wafer based cells are made of crystalline silicon, which includes polycrystalline silicon and mono-crystalline silicon. These are the most commonly PV cells used in large scale solar electric power generation systems with grid connections. Based on a p-n junction concept these cells are developed. PV cells are made of c-Si are made from wafers between 160 to 240 micrometers thick [7].

Polycrystalline silicon cells are made from cast square ingots. These cells are the most common type used in PV fabrication because of less expensive, but less efficient than mono-crystalline silicon. Mono-crystalline silicon solar cells look like an octagon, because of the wafer material is cut from cylindrical ingots, by the ”Czochralski” process [8]. The display of mono-crystalline silicon cells are a distinctive pattern of small white diamonds. Another type PV technology called thin-film technology yield thin-film PV cells which use very thin layers of semiconducting materials, so these can be fabricated in a large quantity at low cost, but the efficiency is also low. Thin-film technology reduces the quantity of active material in a cell. Cadmium telluride (CdTe), copper indium gallium selenide (CIGS) and amorphous silicon (a-Si) are three thin-film technologies [9] often used for outdoor applications. Currently, thin film technology is mostly used to power the small consumer

electronic applications such as watches, calculators and toys.

The characteristics of these technologies are presented in Table1.1, and correponding figures are shown in Fig. 1.2. The formation of PV array from a PV cell is shown in Fig.1.3.

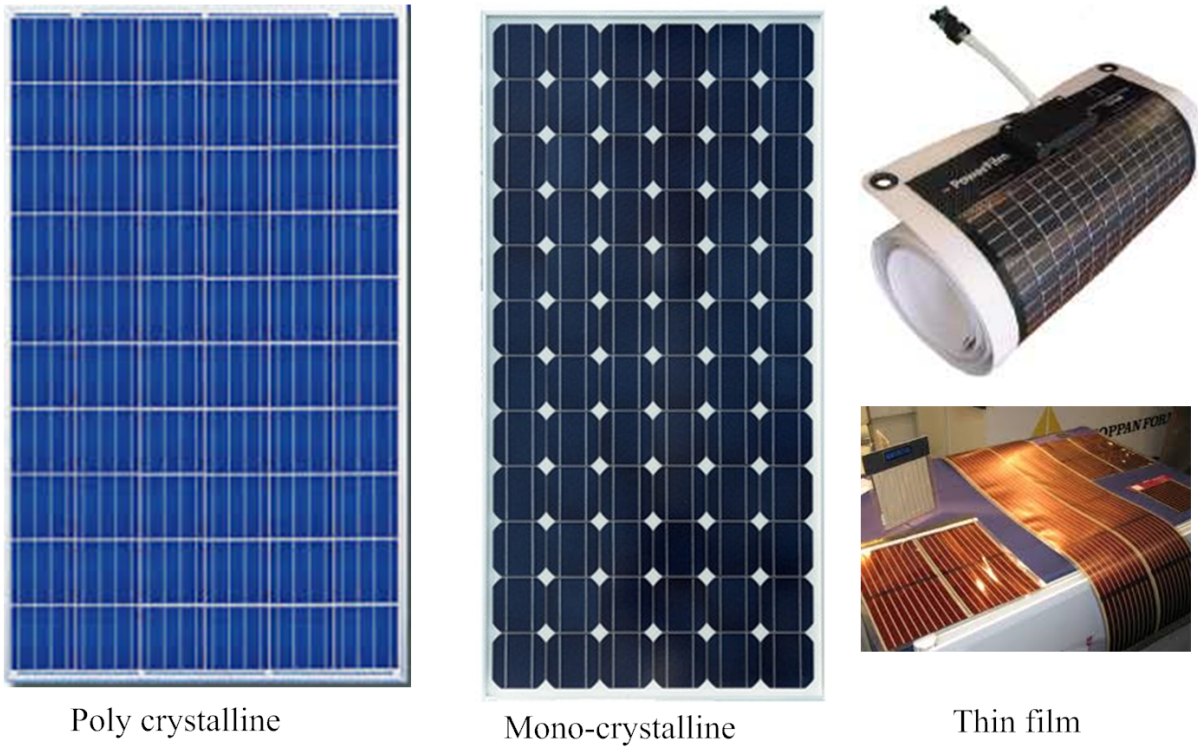

Figure 1.2: Different types PV modules

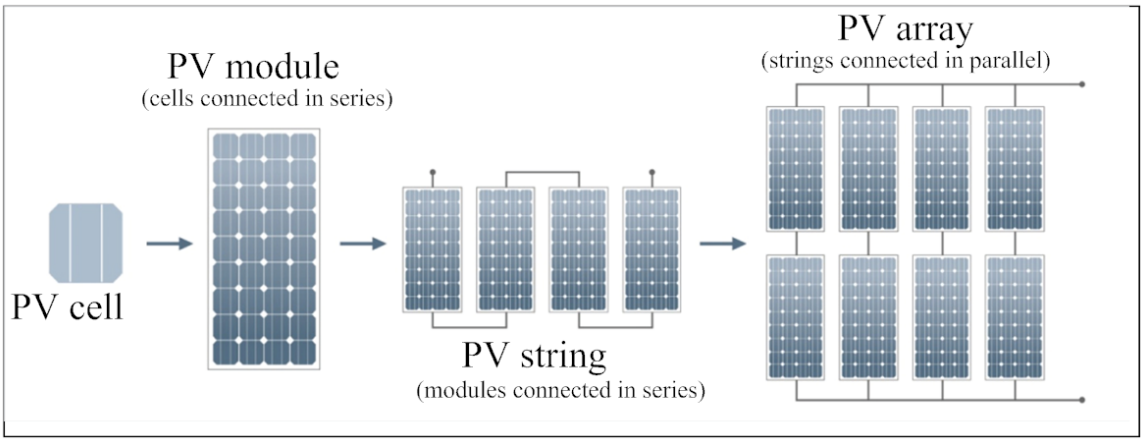

Figure 1.3: Formation of PV array from a PV cell

In addition to the above PV technologies, Hybrid PV technology which makes use of both mono-crystalline and thin-film produce PV cells benefitting for the best features of

Table 1.1: Types of PV cells

	Technology	Characteristics
1	Poly crystalline	• Made up of a poly crystalline silicon material, it is composed of small silicon crystals. • Efficient at good light conditions. • Energy conversion efficiency is 11-14%.
2	Mono crystalline	• Made up of a single silicon material. • Most efficient in good weather conditions • Energy conversion efficiency is 12-15%.
3	Thin film	• Made up of materials like CdTe, CIGS, a-Si. • Efficient at poor light conditions also. • Environmental friendly. • Energy conversion efficiency is 6-12%.

both technologies.

1.1.3 Challenges in PV system

In a PV system, the PV array converts solar energy in to electrical energy. The suitable power converter with a control strategy is required to achieve I-V and P-V charcteristics. The performance of the PV system is influenced by the nonlinear aspects of the PV array, converter topology and control strategy. To study and characterize the transient responses of a PV system one needs precise mathematical models, that includes nonlinear aspects of PV panel to facilitate for effective simulation studies. The development of PV panel needs robust mathematical models to capture I-V and P-V characteristics of PV system [10].

The energy conversion in PV systems is greatly influenced owing to shading, variation in the intensity of sunlight and generation cost per unit. Due to intermittent fluctuation and randomness, output power from PV system fluctuates substantially. The PV cell output

characteristics are nonlinear and the output power varies largely, due to difficulties in tracking the maximum power point which is affected by temperature and irradiance [11].

PV system can produce energy when there is good sunlight is available. The applications connected to solar energy systems demand more power while running few applications. The main complication to achieve the power demand is the lack of economical and efficient power converters. One more drawback is variation in solar power density because changes in temperature over day to night and summer to winter at a particular locality. Therefore, there is a need of power converter topologies to equip solar energy systems for efficient functioning of controllers, filters, inverters and storage devices economically. Another drawback of PV systems is these systems are not cost effective when compared with conventional power generation schemes. Though the customers are aware of the benefits of the PV applications, still they have a preference the buying of conventional electricity due to high cost of PV power per unit. The average power generation efficiency of an industrial PV system is around 20%. The efficiency of PV power can be improved by devising the efficient maximum power point tracker (MPPT) to extract the maximum power from the available power.

Control systems are generally implemented using microcontrollers and FPGAs. This practice started two decades ago. The availability of advanced processors in microcontrollers and FPGAs allowed faster execution of control algorithms. This has led to significant performance improvements in the system theory. The advancements in embedded systems not only helped in improving processing capabilities, but also the interfacing with the sensors, signal conditioning. Communication has became easy and robust. Microcontroller or FPGA based implementation has reduced the number of discrete components, size of the systems, better EMI and EMC compliance, measurement errors and cost of production [1]. Therefore, research on digital MPPT techniques has got a great significance in improving the efficiency of PV systems to build feasible power utilities based on solar energy for the end user.

1.1.4 Types of PV systems

PV systems are composed of interconnected components designed to achieve precise goals ranging from a small device to main distribution grid. PV systems are classified [6]

according to the diagram shown in Fig. 1.4.

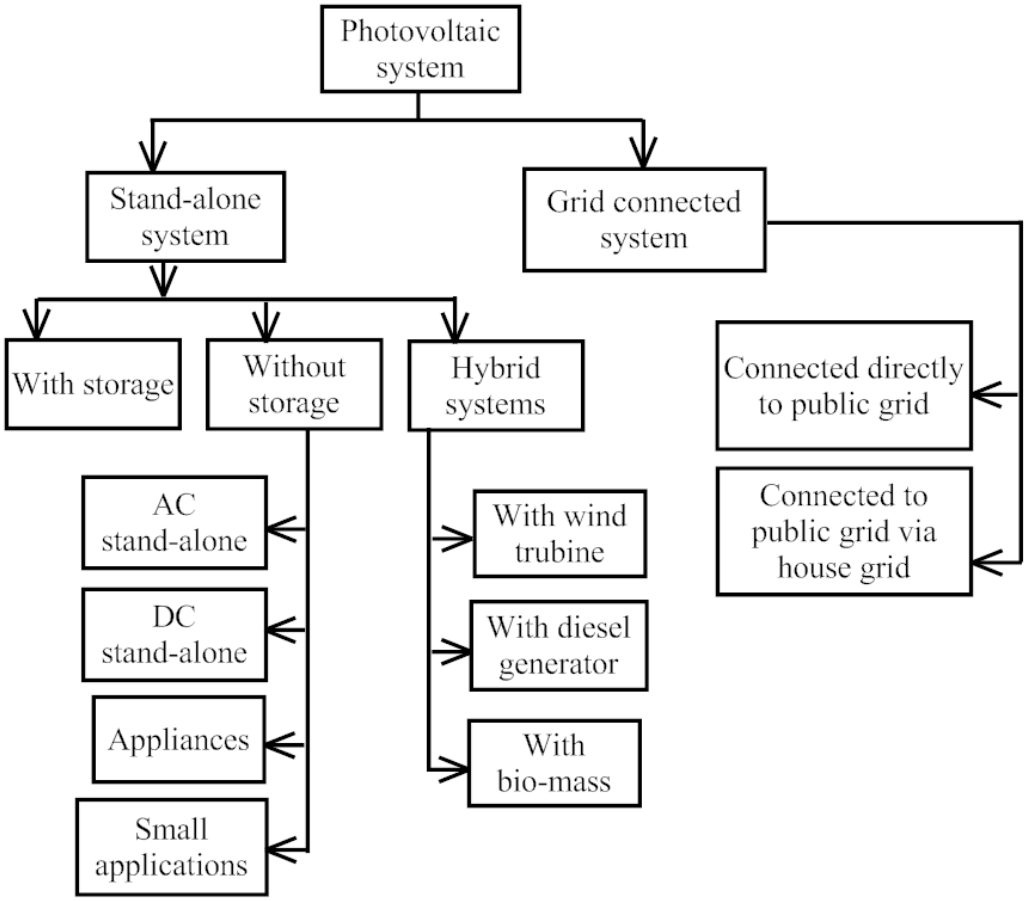

Figure 1.4: Classification of PV systems

Stand-alone PV systems: In this type, the PV array is directly connected to a battery; which stores PV generated electricity and acts as the main power supply. An inverter can be connected to a battery to convert the PV generated DC power into AC power. It enables the usage of house hold appliances without mains power.

Grid connected PV system: These types of PV systems are more popular and it can be used in residential as well as industrial areas. Here the PV system is connected to the local electrical utility network (grid) allowing the excess amount of generated PV power to be sold to the utility. During cloudy days, night power can be drawn from grid to maintain constant power supply. An inverter is connected to the PV system to convert the generated DC power in to AC power to run the all electrical equipments.

Hybrid PV system: In this type, a PV system is combined with one or more other sources of power such as diesel generator or biomass generator or wind turbine and etc. By using

this type of PV systems, user can get constant power supply. Block diagram of different PV systems are shown in Fig. 1.5.

1.1.5 Modelling of PV cell

Modelling of a PV cell is essential in order to design an efficient PV system. PV cell is the basic element of a PV system. Modelling of PV cell with different topological descriptions are reported in [11]. Choice of right topology is an important point for PV applications. Depending upon the system structure, three different classes of models [6], [12], [13] are available for PV system. They are White box, grey box and black box.

White box: It is user friendly, not require any experimental data for system identification. One can model the PV cell by using basic principles of modeling.

Grey box: For this type of models both modeling and identification are required, because some of the results obtained from modeling are not definite and must be verified by identification.

Black box: It is quite difficult to model because getting the structural information is difficult. Here also both modeling and identification are required.

Different types of PV cells along with the mathematical modelling are available in the literature [6], [14–16]. These are (i) ideal model (ii) single-diode model (iii) two-diode model. According to the law of physics, an ideal model can be represented by a photo generated current source I_{ph} and a diode is parallel to each another, shown in Fig. 1.6(a), this is the simple model and losses are very less. Here, diode D represents the p-n junction of the PV module and the current through the diode I_d represents the diffusion current. This model is not an accurate structure of a PV module.

A series resistance R_s is included in the ideal model to improve accuracy and is shown in Fig. 1.6(b), which represents the conduction loss. Another resistance R_{sh} is included for further increase of accuracy, and shown in Fig. 1.6(c), but, it adds leakage current in the p-n junction. This model is simple and non-linear, so analysis is quite easy. It responds quickly to change in system conditions. Single-diode PV cell can be represented using five parameters [17] namely, photo-generated current (I_{ph}), diode ideality factor (a), saturation current or dark saturation current (I_0), series resistance (R_s) and shunt resistance (R_{sh}). This model is widely used because easy to maintain the balance of PV module and ease of

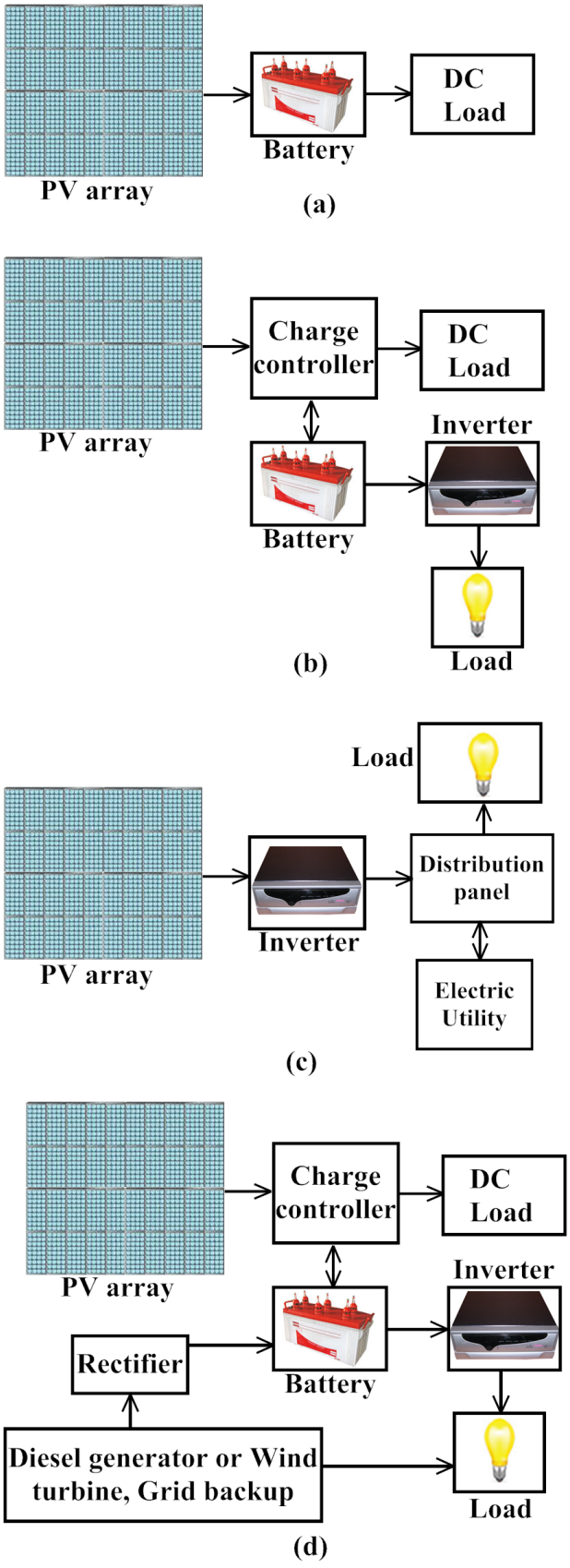

Figure 1.5: a) Direct coupled PV system b) Grid connected PV system c) Stand-alone PV system with battery storage powering DC and AC loads d) Hybrid PV system

mathematical implementation. Due to aforesaid reasons, single diode model is considered in this thesis.

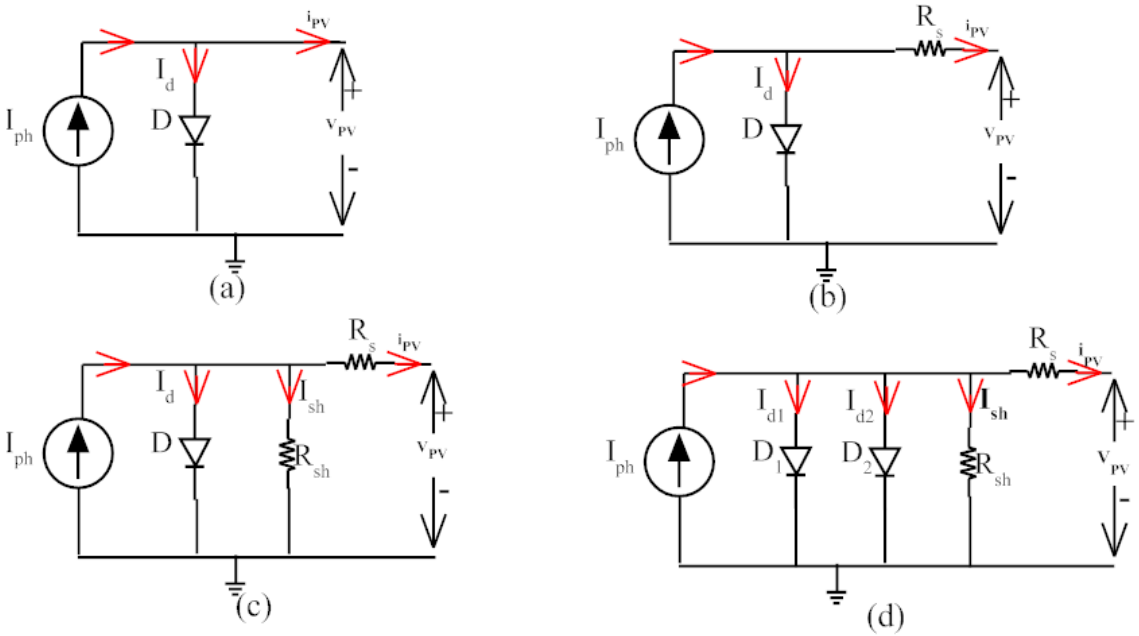

Figure 1.6: a) Ideal model b) Single diode model (four parameters) c) Single diode model (five parameters) and d) Double diode model of a PV cell

The manufacturer usually provides a data sheet of the important PV values like short circuit current (I_{sc}), current at MPP (I_{mpp}), open circuit voltage (V_{oc}) and voltage at MPP (V_{mpp}). But, the PV parameter ($I_{ph}, I_0, a, R_s, R_{sh}$) values are unknown to the user because those values will not provided in the manufacturers data sheet. These PV parameters are required for efficient design of the PV panel. Hence, first step towards the PV panel modelling is finding the values of parameters by a suitable extraction method.

In order to get more accuracy a second diode has been added to the single diode structure mentioned in Fig. 1.6(c) called two-diode model shown in Fig. 1.6(d). In this structure I_{d1} through D_1 stands for diffusion current due to major charges, I_{d2} through D_2 stands for recombination current due to minor charges. The performance of two-diode model matches with the physical PV module, but this model is complex and non-linear. Mathematical modelling of this model is also difficult.

1.1.6 Maximum Power Point Tracking (MPPT)

Even-though the PV technology is one of the best renewable energy systems converting the solar energy in to electrical energy and rapidly growing technology in many countries, but, it has some limitations such as high initial cost, low conversion energy efficiency, large area is required to capture sun light, energy can be tracked only at sunny and day time. The output is fluctuating to a large extent because of temperature and irradiance and output characteristics of PV cell are non-linear in nature. Because of weather fluctuations or varying temperature and irradiance the maximum power point of the PV cells changes a lot. Commercial PV systems have very less average power generation efficiency. With the help of better MPPT technique, with good tracking speed one can use the generated PV power practically in a short time. Therefore, research in MPPT is of great importance for maximizing the utilization of PV cells [18–22].

An adequate amount of research has been done to improve the efficiency and power quality of PV system [20]. The energy conversion efficiency of PV system is low because of the time varying characteristics (I-V, P-V) and non-linear in nature with respect to the temperature and irradiance. For this reason, the PV systems are required to operate at their MPPs because the PV panel functioning is more efficient to deliver the maximum power at MPP. To track the maximum power point in a PV system, a maximum power point tracker (MPPT) is required. The MPPT controller controls the PV system and improves the power generation efficiency. Thus the MPPT is considered as an integral component in a PV system [21].

The PV system output power will be maximum at a single point called MPP (V_{mpp}, I_{mpp}). When the load is directly coupled to PV panel shown in Fig. 1.7(a), then the operating point of the load is defined as the intersection of its I-V characteristic curve with the load line is shown in Fig. 1.7(b). There are two different operating points X and Y for two different values of RL, at these points the power is less than MPP. The operating point of a PV panel changes in accordance with the varying load. A mechanism is required to pull the operating point of the PV panel to the MPP. Techniques should be designed to operate PV panel at MPP to get maximum power out of PV system under the varying load conditions. The DC-DC converters are generally used to maintain the regulated power supply under varying

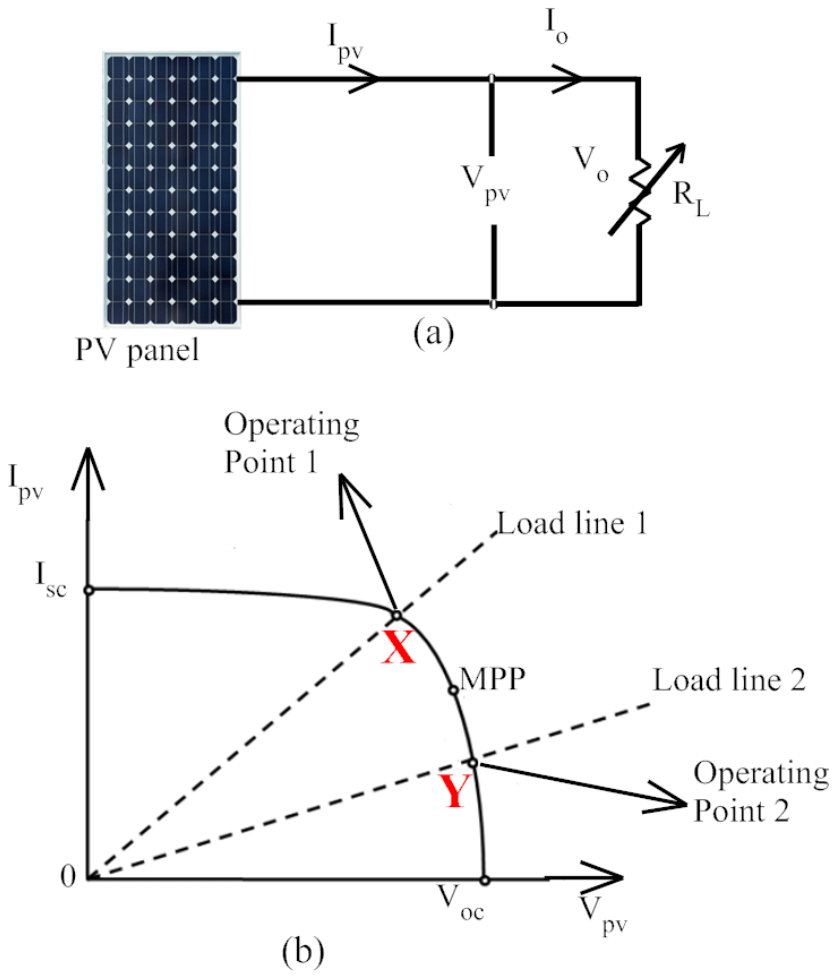

Figure 1.7: (a) PV panel connected directly to load (b) Operating point of a PV system with load

load conditions [23]. Similarly in the applications connected to a PV system also, DC-DC converters with suitable control technique for tracking MPP at varying load conditions can be used to deliver consistent power. Fig. 1.8 shows the PV system with DC-DC converter.

The MPPT algorithm calculates the reference point (V_{ref}) at which the power is maximum and through a DC-DC converter, the PV system is enabled to operate at that reference point. The PV system with MPPT is an efficient system because it changes the operating point along the MPP of the PV module and gives maximum power at all weather conditions [24] and shown in Fig. 1.9. The MPPT technique tracks the maximum power from a PV system at shading and other climatic conditions, i.e, almost extra 10% [25], [26]. The control design with MPPT technique should consider nonlinear characteristics of a PV

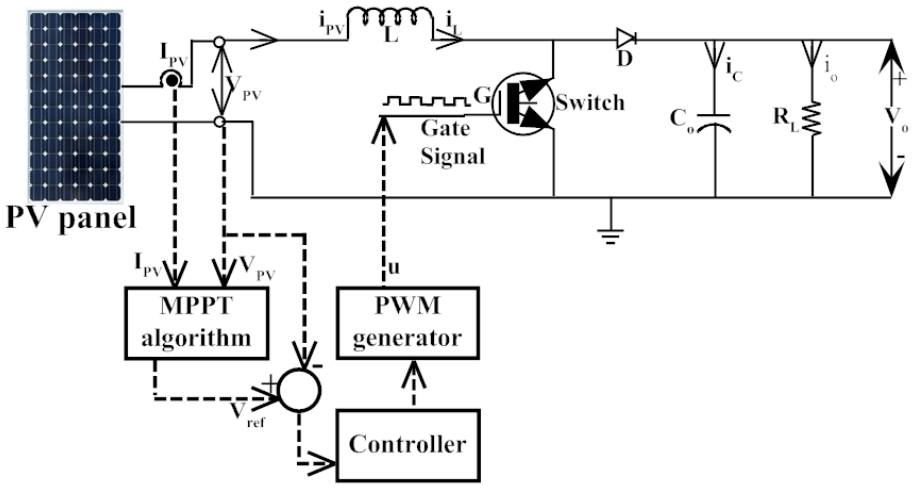

Figure 1.8: Standalone PV with MPPT

system and weather conditions [27], [28]. This MPP can be determined by mathematical calculations or search algorithms.

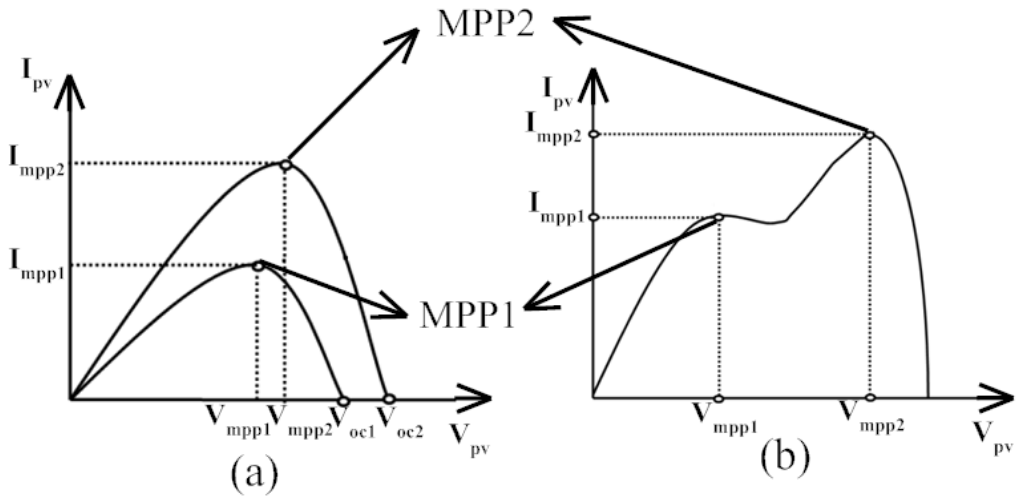

Figure 1.9: MPPs at different irradiance (a) under no shading (b) under partial shading

PV systems with MPPT techniques are already used in many applications like water pumping, satellite power supply, grid-tied, household appliances like mobile charging and etc in Germany, Japan, China and USA. The calculation of MPPT efficiency [29] is

$$Efficiency\,(\eta) = \frac{V_{PV} X\, I_{PV}}{I\, A} \tag{1.1}$$

where, I=Insolation and A=Area of the cell. Each PV cell has life expectancy. As

time progresses, the quality of the cell reduces. Therefore, checking the quality of the PV cell is compulsory and calculation of PV cell quality is called as Fill Factor (FF) and is defined [30] as follows:

$$FF = \frac{V_{mpp}\, \mathrm{I}_{mpp}}{V_{oc}\ \mathrm{I}_{sc}} \tag{1.2}$$

The ideal FF of a PV panel should be 1, generally, for a good PV panel it will be 0.7 to 0.8 and if the FF is beyond 0.4 then the panel becomes obsolete.

1.1.7 Inverters for PV applications

A PV inverter converts the direct current (DC) into an alternating current (AC) that can be fed into an electrical grid or used locally [31–41]. Solar inverters used with PV systems should have special functions like anti-islanding protection. An inverter used in a PV system is a simple circuit with low component count, which is low cost and efficient. Interfacing of an inverter to a PV application is essential in present scenario. The control circuits in a grid connected PV system should perform the following tasks:

a) To amplify and invert the generated DC power into an appropriate AC current for the grid.

b) Track the Maximum Power Point (MPP) from a PV cell for maximizing the energy generation.

High performance execution of above mentioned tasks for a wide operating range under varying weather conditions is expected from a control circuit. In addition to above tasks, the inverters should be equipped with a mechanism to address islanding problems which generally occur in solar power grids.
PV inverters can be classified into three types, they are

1. *Stand-alone inverters*: This type of inverters is used in isolated systems where the inverter draws its DC power from batteries charged by PV systems. Several stand-alone inverters integrate battery chargers to refill the battery from an AC source, when available. Usually these inverters do not interface with the utility grid, and are not required to have anti-islanding protection.

2. *Grid-tie inverter*: This type of inverters can match the phase with a utility-supplied sine wave. These are designed to shutdown automatically upon the loss of utility supply for safety causes. They do not provide backup power during utility outages.

3. *Battery backup inverters*: These types of inverters are designed to draw energy from batteries; which are capable of supplying AC energy to selected loads during a utility outage, and are required to have anti-islanding protection.

The centralized inverter technology is shown in Fig. 1.10(a) was based on centralized inverters, which interfaced a large number of PV modules to the grid [36]. The series connected PV modules (strings) generates sufficient high voltage, which needs no amplification circuits. The series connected PV modules are connected in parallel through string diodes to reach high power levels. This technology has some limitations, they are: 1) It requires high voltage DC cables among PV modules and inverter. 2) Due to centralized MPPT, power losses are more. 3) Mismatch losses occurs between PV modules. 4) Risk of hotspots in the PV modules during partial shading conditions, and 5) Individual design for each installation. Due to disadvantages, this technology cannot be used for large scale power generation.

The string inverter technology is shown in Fig. 1.10(b), which is the modified version of centralized inverter. Here the required numbers of single string of PV modules are connected to the inverter [31], [37]. Here the losses with string diodes are completely omitted and separate MPPT can be applied to each of the string, and the overall efficiency is increased when compared to the centralized technology.

The multi string inverter technology is shown in Fig. 1.10(c), which is a modified version of string inverter. Here several series connected PV strings are interfaced to individual DC-DC converter. The outputs of the DC-DC converters are connected to a common DC-AC inverter [31]. In this technology, each series of PV panel will have DC-DC converter so that, better control action on output of each series of PV panel is possible when compared to the aforementioned technologies. This design is flexible to achieve high efficiency, and further enlargement is easy.

The AC module inverter technology is shown in Fig. 1.10(d), which is a customized version of the string inverter. Here each PV module has its own DC-AC inverter connection

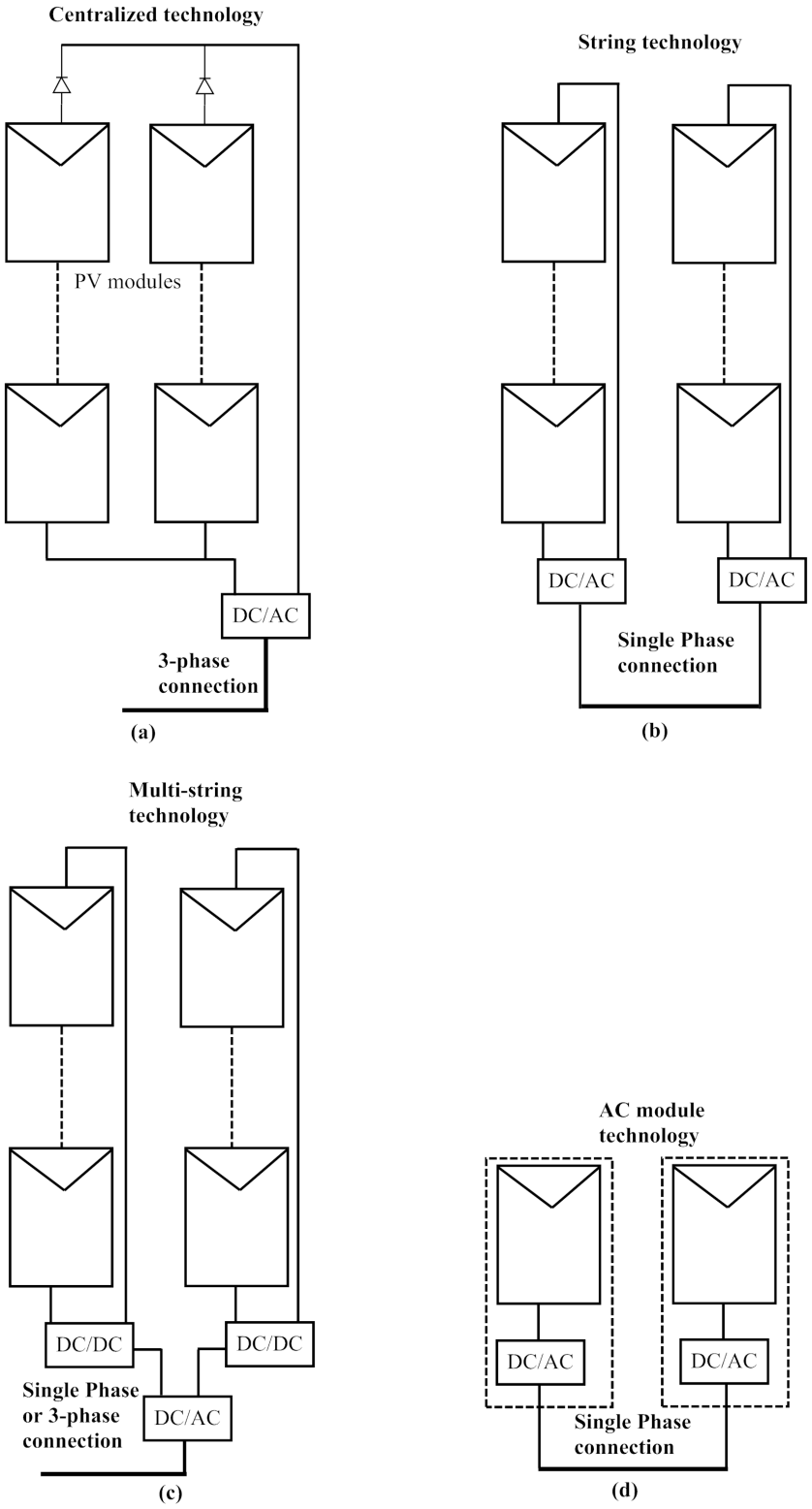

Figure 1.10: PV system technologies for inverter (a) centralized technology, (b) string technology, (c) multi string technology and (d) AC module technology

[33]. The constant losses in the inverter are same as like string technology, but power losses of the system is less. The AC module technology supports the best operation, which results to a high performance, and it can be used as a plug-in device by individuals without specialized knowledge [34].

1.2 Literature Review on control of PV system

The global energy demand is increasing. The developing countries like India are supposed to add 5000MW of generation capacity every year to meet their energy demand. The fluctuations in pricing of fossil fuels, pressure to address the global warming and climate change from international community have forced the governments to focus on clean and sustainable energy sources like Solar power. The PV power generation has seen a rapid growth in the last few years leads to the wide usage of PV energy; a PV system has the advantages of low maintenance, and free from environmental pollution. These PV systems can serve as an alternating source for generating electric power to stand-alone as well as grid connected applications. This section reviews relevant literature of PV cell modelling, MPPT, power conditioning circuits and inverters.

1.2.1 Review on modelling of a PV cell

To develop a PV power system, the mathematical modelling of a PV cell is a key aspect. Recently, significant amount of research is being conducted to develop an accurate mathematical model of PV cell. This section reviews about the modelling approaches of different PV cells. The illuminated solar cell parameter evaluation by considering series and shunt resistances with a single diode model in [10]. Five different parameter (I_s, R_s, a, R_{sh} and I_{ph}) values were extracted from experimental I-V characteristics of solar modules. Mono-crystalline PV module using four and five parameter modelling and experimental verification of operating current is reported in [11]. Analytically described the I-V characteristic of PV module for the operative temperature and irradiance with single diode and five parameter with rapid convergence in [14] provides accurate results. A commercial silicon solar module and a plastic solar module are used with an auxiliary function in [15] to evaluate the four parameter (R_s, a, I_s, R_{sh}) values extracted

for illuminated solar cells. The performance of this model is compared with simulation and experimental results. A theoretical approach is presented in [16] to evaluate the series and shunt resistances estimated by seven parameters with two diode model and measured environmental parameters and semi empirical equations. A newton-raphson based extraction method is discussed in [42]. The authors presented the analysis for PV panel modelling with experimental verification. In this paper the panel dynamics would approach very quickly and estimated with both I-V and P-V characteristic curves. The modelling of the different PV array characteristics such as I-V and P-V curves at partial shading conditions demonstrated in [43]. The authors compared the simulated and experimental results at partial shading conditions.

To develop a PV power system, an accurate mathematical model of PV cell along with power conditioning circuits are required. Model of a PV cell is non-linear in nature as depicted in characteristic curves (I-V and P-V curves). It is observed that almost all the PV models along with power conditioning units only consider ohmic losses. However, it is also quite important to consider activation loss and concentration losses. While one develops models for a PV cell along DC-DC and DC-AC converters of the activation loss and concentration losses also need to be considered. When these effects are measured, an accurate and a better model of the PV cell evolves; hence the PV system along with power conditioning systems would provide superior result as compared to the real-time simulation or experimental results. In 1839, the photovoltaic effect was discovered by Edmund Becquerel in Paris. He experimented with two silver coated platinum electrodes immersed in a dilute acid to form a sort of battery. He kept one electrode in sunlight and the second one in shaded and observed that these two electrodes altered their electric powers. A system of this type is called an electrochemical cell [5]. In 1876, the photovoltaic effect was reported for the first time in a solid selenium by William G. Adams and Richard E. Day in London. They observed that selenium changes its conductivity under illumination, which means the electric power is produced under illumination. Subsequently in 1954, the first silicon solar cell was developed in the Bell laboratory ofcourse with a very low efficiency (i.e., 6%). In 1955, Hoffman Electronics- Semiconductor Division created a first commercial solar cell with 2% efficient for 25/cell or 1, 785/Watt [6].

A DC-DC converter is required for a PV system to connect a load, which is step up or step down the PV output voltage. This section describes mathematical modelling and control strategy of DC-DC converters. Modern electronic systems require DC power supplies to regulate the output at a specified value, reduce AC voltage ripple on the DC output voltage and achieve multiple outputs that may differ in voltage and currents [44]. The principle operation of power regulators is based on current/voltage divider, whereas the semiconductor switching devices are operated in the active region. At higher power levels, the power electronic switches control the regulators by switch ON and switch OFF states. The power loss is also less in both the states and there is no external power supply is required to operate in the active region, and results higher efficiency. Due to the ability of the switches to operate at high frequency, the transformers and filters can be made smaller and lighter.

With the help of DC-DC converter applications, it is possible to get more efficient conversion of power from PV system to load [45]. A DC-DC converter has the objective of converting the power from the PV system to a desired level, usable form, and these converters are largely used for switch mode power supplies (SMPS). The input to the DC-DC converters is generally an unregulated DC voltage [46] which fluctuates due to the changes in the operating conditions. Switch mode DC-DC converters are used to convert the unregulated DC input into a regulated DC output at a desired voltage level. That means, the converter can produce the DC output voltage at a desired level still it has any variations at input voltage and at load also. This is possible with the control ON and OFF timings of the switches present in the converters [47].

Pulse width modulation (PWM) is one of the techniques to control the output voltage. It employs switching at constant frequency and adjusts the switch ON time to control the output voltage, called as duty cycle. This is defined as the ratio of ON time to the one switching time period (i.e., both ON and OFF timings), is generated by comparing a signal level control voltage with a saw tooth or triangular wave forms [48]. This control voltage signal can be obtained by amplifying the error in between the reference signal and the actual signal. The frequency of the repetitive waveform depends on the switching frequency, which is generally in few kilohertz. The advantages of PWM switched converters are

a) Less component count, b) Operating at constant frequency, c) Easy to implement d) Economical.

1.2.2 Review on Maximum Power Point Tracking(MPPT) techniques

Several MPPT techniques applied on different applications of PV systems at standard test conditions (STC) and partial shading conditions (PSC) is found in [17], [18], [20], [22], [26], [29] and [38].

It is very difficult to analyze all of these MPPT techniques by studying their structures, because each MPPT technique has its own advantages as well as disadvantages. The control strategy classification is one of the options to analyze the MPPTs. There are three types of control strategies available; they are direct control, indirect control and evolutionary computational methods.

Direct control strategies can seek MPP directly by taking the variations of the PV panel operating points without any prior knowledge of the PV panel parameters. Direct Control techniques can be classified into two types; a) sampling methods, b) modulation methods. In sampling methods, a sample is made from PV panel voltage (V_{PV}) and current (I_{PV}) and gather the present and past information of the sample to track the MPP location. In modulation methods, MPP can be tracked by generating oscillations automatically by the feedback control. Indirect control strategies are based on the use of a database that includes parameters and data. This means that characteristic curves of the PV at different temperatures and irradiances are stored in look up table or using some mathematical formulae to approximate the MPP. Evolutionary computational methods like, FLC (Fuzzy Logic) and ANN (Artificial Neural Network) etc are also used to get the optimal value of MPP. Evolutionary methods do not require exact mathematical models; they can work with indefinite inputs and can handle nonlinearities. These are rule based techniques which are adaptive in nature and very difficult to generate. The classification of MPPT control techniques is shown in Fig. 1.11, and Table 1.2 gives a comparison of different MPPT techniques according to the classification.

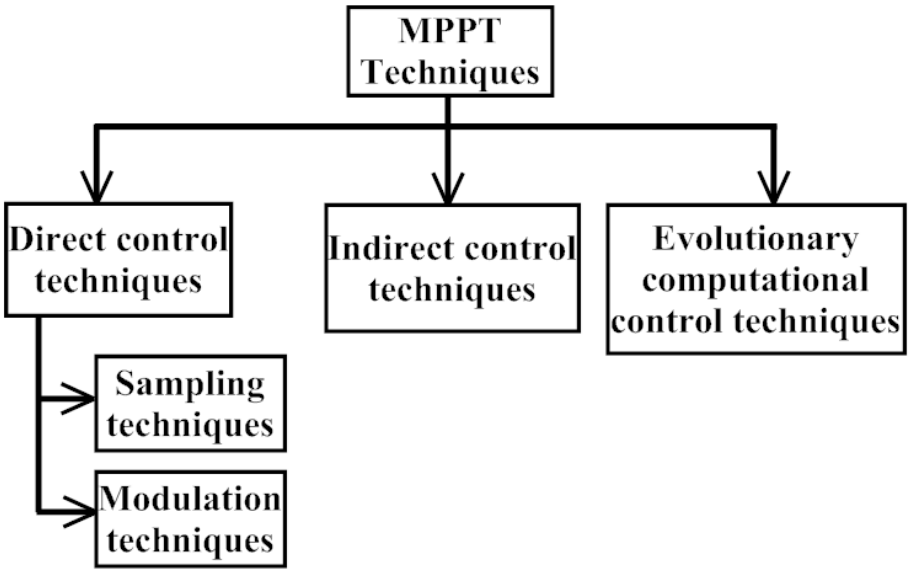

Figure 1.11: Classification of MPPTs according to control techniques

List of MPPT techniques

1. Curve Fitting (CF) MPPT technique [40]
2. One Cycle Control MPPT [49]
3. Feedback voltage (FV) or current MPPT technique [50]
4. Perturb & Observe (P& O) and Hill climbing MPPT technique [51]
5. Incremental Conductance (Inc Cond) MPPT technique [52]
6. Steepest Decent MPPT technique [53]
7. Intelligent MPPT techniques
    a) Fuzzy logic based MPPT technique [54]
    b) Artificial Neural Network (ANN) based MPPT technique [55]
8. Sliding mode control (SMC) based MPPT technique [56]
9. Load current/voltage maximization (LVM) MPPT technique [57]

Table 1.2: Comparison of different MPPT techniques

Name of MPPT	Type of control technique	Control variable	Analog/ Digital circuitry	Parameter tuning	Complexity (calculation and hardware implementation)
CF	Indirect control	V_{PV}	Digital	Yes	Simple
OCC	Direct control (sampling techniques)	V_{PV} and I_{PV}	Both	Yes	Simple
FV	Direct control (sampling techniques)	V_{PV} and I_{PV}	Digital	No	Simple
P&O	Direct control (sampling techniques)	V_{PV} and I_{PV}	Both	No	Complex
Inc Cond	Direct control (sampling techniques)	V_{PV} and I_{PV}	Digital	No	Complex
SD	Direct control (sampling techniques)	V_{PV} and I_{PV}	Digital	No	Medium
FLC	Evolutionary control	V_{PV} and I_{PV}	Digital	Yes	Medium
ANN	Evolutionary control	V_{PV} and I_{PV}	Digital	Yes	Medium
SMC	Evolutionary control	V_{PV} and I_{PV}	Digital	No	Complex
LVM	Direct control (Modulation techniques)	V_{PV}	Analog	No	Medium

1.2.3 Review on DC-DC converters

This section presents different DC-DC converters with control techniques by using analog and digital domains. A DC-DC boost converter is a power conditioning device, which boosts the output voltage. The converters are controlled according to the pulses generated by the feedback or feed forward control circuits [23], the converter circuits are simulated in MATLAB/SIMULINK for fast switching actions. The DC-DC boost converter steps up the output voltage, which stores the energy through an inductor and that energy delivers to the capacitor at switch actions regulated by PWM. Then the charged capacitor will supply a higher voltage to the load [36]. A DC-DC multilevel boost converter (MBC) based on PWM is analysed in [58] which combines the boost converter and the switched capacitor

Table 1.3: Advantages and Disadvantages of MPPT techniques

S.No	Name of MPPT	Advantages	Disadvantages
1	CF	• Simple and low cost (does not require voltage or current sensors to measure voltage and current during MPP tracking).	• It requires accurate information of the PV system. • Complex Mathematical calculations.
2	OCC	• The system (PV with a single -stage inverter) inexpensive and reliable. • Operating in constant switching frequency mode and it does not require DSP for hardware implementation	• MPPT tracking performance is not so good at variable weather conditions
3	FV	• Simple and inexpensive.	• Cannot be used these systems with battery as load. • Not suitable for environmental changing conditions.
4	P&O	• Easy to implement and produce accurate results.	• Accuracy is dependent on the size of perturbation. • Suitable for steady state environmental conditions.
5	Inc Cond	• Efficiency is almost same as P&O. • It can track MPPT at fast changing weather conditions.	• Circuitry is complex and cost is high. • Sensors are required to accomplish MPPT action.
6	SD	• Less complex and fast MPPT performance.	• The stability, speed and accuracy are depending on initial conditions and step-size. • Range of operation is less for fixed step, and algorithm is lengthy for variable step operation. • The convergence error is slow on derivative terms (if Euler method is used for calculation).

S.No	Name of MPPT	Advantages	Disadvantages
7	FLC	• Response performance is good, no overshoot and prior knowledge of PV is not required. • Suitable for fast temperature and irradiance variations.	• This technique is based on rules and construction of rules is difficult.
8	ANN	• No detailed PV knowledge is required to operate whole system. • On-line tracking is possible and is independent of weather conditions. • Accurate and fast once it is tuned.	• Tuning and MPP calculation takes large time. • Obtained rules for MPP tracking are applicable to same type of PV panels.
9	SMC	• Simple control laws and fast MPP tracking. • Considers nonlinear behaviour of PV panel and converter. • Hardware implementation is easy because it is compatible with DSP, microcontroller, FPGA, etc.	• Chattering occurs at steady state. • Extra circuitry is necessary to change variable operating frequency to fixed frequency.
10	LVM	• Algorithm is simple and implementation is possible with simple circuitry. • Prior knowledge of panel characteristics is not required.	• Applicable to limited range, tuning takes large time (power loss at tuning). • Not suitable to fast changing conditions.

function to provide different output voltages by using only one switch and one inductor. The converter operates with wide output voltage variations without penalizing the efficiency. As a result, the converter can be used in several self balancing and unidirectional current flow application like PV, fuel cell. The converter topologies are useful at higher power levels as well as lower power levels. A novel solar harvester implementation based on a boost converter topology can be found in [59], and the circuit is able to harvest solar energy up to a power level of 1.6W. The core of a solar harvester is a DCDC switching converter, which is controlled and operate the PV module at its maximum power and low power levels too. The main advantages of this method are reduction of switch ON and OFF losses, high efficiency and design modularity. A Sheppard-Taylor topology is developed in [60] for low power applications. The switch of the converter is tuned on to zero-current-switching and the rectifier diodes are tuned off with zero-voltage-switching (ZVS). This topology can regulate the output voltage under input voltage variations or load variations. A new pulsed power supply topology is based on positive buck boost converters presented in [61]. The main use of this proposal is utilization of low and medium voltage semiconductor switch for high voltage generation, and switch diode capacitor units are designed at output to change the current source energy into voltage and generate a pulsed power with sufficient voltage magnitude. This converter is flexible and efficient. Experimental result confirms the operation of this converter which matches with proved theoretical analysis. In [46] the diode-capacitor multipliers are combined with boost converter to operate at high switching frequency. This approach reduces the capacitor values, and it can also be used for a three phase network through a rectifier. The final output voltage is dependent on the internal resistance of the circuit, if it is high then output voltage is low and vice versa.

A zero current soft switching pulse width modulation (ZCS-PWM) DC-DC boost converter with an active edge resonant cell (AERC) is developed in [45]. The converter operates with AERC and suppresses the voltage surges and current ringings. As a result, the voltage ratings of the switches can be reduced as compared to the classical converters, and conversion efficiency is more. Experimental validation is performed on a 1.6kW-40kHz prototype. A ZCS DC-DC full bridge boost converter is compared with a ZVS active clamp converter in [62]. The main advantages of ZCS converter is, the switches can operate with

ZCS due to an active auxiliary circuit that diverts the current away from the switch before it is turned off, and also helps to remove unwanted voltage spikes across the full bridge converter. The ZCS approach is better than ZVS for a low input, high output voltage converters operating under heavy load conditions. A ZVT-ZCT-PWM boost converter with an active snubber cell is proposed in [47]. The active snubber cells provides turn ON with ZVT and turn OFF with ZCT to the main switch in converter, and operates with soft switching at high frequencies also. No additional voltage stress across the main and auxiliary components is the added advantage of this approach. The presented analysis is verified with 100kHz and 1kW converter.

A transformer less high gain boost converter is proposed in [63] in which modularity, low ripple for input current and output voltage, lower voltage and current ratings is compared with basic boost converter. Finally, the design structure and analysis are verified with 1 kW and 60 kHz lab prototype experimental setup. In [64], [65] at a selectable duty cycle is used in the high gain transformer less boost converter with input current ripple cancellation. This converter features a high voltage gain without utilizing extreme values of duty cycle or boosting transformers, and the converter is validated through laboratory hardware prototype. Grid interaction operation for multi input buck boost converter is utilized as an interface between microsources and the dc bus in [66]. For grid interconnection, an LC filter, double tuned filters, and a C-type high-pass filter are used to eliminate high-frequency switching oscillations, high order and selected harmonics. This approach is a better choice for microsources. Single stage multi input DC-DC/AC boost converter is proposed in [67], consists of two sets of parallel boost converters, which are actively controlled to produce two independent output voltage components. The validity and effectiveness of this converter and its control performance are verified by simulation and experimentally. The low cost electronic converters are utilized in photovoltaic applications such as PV generator [62] and water pumping system [64]. The experiment performed with DC-DC converters and three phase and single-phase DC-AC converters found the peak efficiency as 91% at 210W power.

DC-DC converter topologies

Different topologies of DC-DC converters have been proposed in literature. Depending on the application, DC-DC converters are either step up or steps down the input voltage. Single stage converters do not provide any isolation between the input and output. Single stage DC-DC converters are categorized as follows:

- Boost Converter
- Synchronous Boost Converter
- Buck-Boost Converter

Apart from single stage DC-DC converters we can find multistage converters in the literature. Multistage converters first convert the DC power to AC power and again back to DC. A high frequency transformer is integrated in the DC-DC converter design; it will boost the AC signal easily to the required level [65], [66]. These systems offers electrical isolation between the input and output, as the transformer uses different grounds, and also assists continuous noise filtering. The converter topologies under this scheme include

- Unidirectional full-bridge DC-DC power converter
- Push-pull DC-DC boost converter

In this thesis, we concentrate brief on single stage converters. Mathematical modelling and descriptions of these converters are provied next.

1.2.4 Review on PWM-current control techniques

This section reviews various control techniques of DC-AC inverter and its implementation schemes. The DC-AC power converters are called as inverters, that means the inverter is to change a DC input voltage to AC output voltage at a desired frequency level. The output waveforms of ideal inverters must be sinusoidal. However, the waveforms of practical inverters are non-sinusoidal and contain some harmonics.

Xue *et al*, presented [68] a general overview of single phase inverters for small distributed power generators at low cost, high efficiency and tolerance for an extremely

wide range of input voltage variations. Single-stage inverters offer simple structure with low cost, but suffer from input voltage variations and characterized by the system performance. The multiple-stage inverters accept a wide range of input voltage variations, but efficiency is low, expensive with complicated structure. Single phase grid connected PV central inverters with discrete control structure and energy balance modelling is proposed in [69]. The overall aim is to implement a two control loop design with nonlinear time varying characteristics of single phase grid connected PV full bridge inverter for stability of the system at all operating conditions of PV. The analysis and simulation results compared with a set of experimental results. A fast response low harmonic distortion control structure is proposed in [70] to combine the features of SMC and repetitive control. The control methodologies are combined into a single control by using the Laplace domain equivalent control principle. This system performs excellent transient and steady-state in voltage source inverters (VSI) with a specific low pass filter (LPF). The advantages are fast dynamic response with low harmonic distortions. Single phase inverters between grid-tied and stand-alone modes can be used with a novel seamless transfer is proposed in [71] to operate in grid-tied and off grid connected modes at a same time. However, the grid-tied current controller and the voltage controller at the output are switched between the two modes, so the outputs of both controllers may not be equal during the transfer, which will cause the current or voltage spikes during the switching process. In grid-tied mode, the voltage controller and current controllers are used to compensate the filter capacitor current and control the grid current respectively. In stand-alone mode also both controllers are used, voltage controller is to regulate the output voltage and the output of the current controller is zero. The simulation and experimental results verified with theoretical analysis. Energy balancing is required for grid-tied inverters. This balancing has done with predictive DC voltage control in three phase grid connected PV inverters in [72], and also reduces the DC capacitance and improves system reliability as well as MPPT performance. A micro-inverter is connected to a PV system [73] and operating in grid connected and island modes by reconfigurable control strategy. The advantage is that in grid connected mode, the microinverter works as a current source in phase with the grid voltage, injecting power to the grid, in island mode, the microinverter control is reconfigured to work as a voltage

source using droop schemes. These techniques consist in implementing P/Q strategies in the inverters, in order to properly share the power delivered to the loads. Finally, simulation and experimental results on an 180-W PV microinverter are provided. Recently transformerless grid connected PV inverters [74] are designed with optimization and reliability, and lower order harmonics mitigated in single phase grid tied PV inverter [75].

In recent years, the control algorithms are developed in high level language and implemented in FPGA / DSP processor for efficient performance and fast processing [76], [77]. Here, the PWM-switching pulses applied to PWM-inverter should meet the requirements of harmonics of the load and maintains the dc-voltage constant. An FPGA based step up PV array emulator for grid connected inverters is presented in [76] to meet the performance metrics. An FPGA based hardware-in the-loop (HIL) simulation of VSI used for PV system power conversion, which is capable to operate at switching frequencies up to 3 kHz. Thus it is capable to support the high switching frequency requirements of modern single-phase DC/AC power converters.

1.2.5 Review on shunt active power filter for PV system

The power quality issues are increasing and sensitive consumer electronic products demand prcised power supplies. Some additional power electronic circuits have to be installed to solve the power quality issues. To maintain the power quality in a grid connected PV system, the active power filter usage is compulsory [78] - [79]. A PV active power filter can supply active and reactive power to the grid when solar radiation is available. This section describes the literature review on power conditioning circuits with PV system.

Patel *et al*, investigated the performance of PV based active power filters for string inverter configurations (SIC), multi string inverter configurations (MSIC) and centralized inverter configurations (CIC) and tested for all weather conditions in [78]. Based on reference current generation of PV active power filter with control schemes, the authors concluded that the power taping is similar in case of uniform radiation conditions but not in the case of partial shading conditions. For better performance of grid connected PV, a novel digital EMI filter [80] is used to suppress the common mode electromagnetic interference. The analog EMI controller is replaced with the digital controller to eliminate limitations. The digital controller consists of Digital Active EMI Filter (DAEF) to remove the unwanted

interference signal and tested with a 200w microinverter. To compensate the harmonics and reactive power, a shunt active power filter is connected to PV system in [81]. A synchronous d-q-o reference frame algorithm (SRF) is used for reference current computation and carrier based PWM is used to generate switching pulses of voltage source inverter. With this model the current THD is reduced from 32.31% to 2.87%.

From the above discussion it can be concluded that there is a scope to research in design of active power filters for improvement of power quality in a grid connected PV system. In this work; we design and develop an active power filter for a PV system. Inclusion of power quality circuits is costly. Some applications demand for quality power and inclusion of power quality circuits is mandatory.

The power generation from renewable energy sources is one of the finest areas of research where researchers are working to develop distributed generation system for low cost power. PV is one of the best alternative sources which can generate electricity from solar irradiation. The major issue of PV is depending on sun light. To develop a PV based power system; proper modelling, accurate design of power conditioning circuits and controller are necessary. Therefore, in this thesis we develop a prototype with novel power conditioning and control circuits which fit into the practical scenario. FPGA based solution has been proposed to implement the control circuit to achieve the maximum possible performance. FPGA based solutions are also flexible, such that system can be tuned according to the requirement in the future.

1.3 Research motivation

PV cell is the basic element in a PV power system. In order to analyze the characteristics of PV system dynamics it is necessary to accurately model the dynamic behaviour of PV array. A DC-DC converter is required to adjust the operating point of PV system such that PV panel can be operated at MPP to transfer the maximum power to the load. The control strategy of DC-DC converters and DC-AC inverters will have major impact on performance and conversion efficiency of the PV system. There is a need to develop fast, reliable and low cost digital control technique for converter as well as inverter topologies which will eventually lead to a better PV based energy management system, which supplies energy to

household and industries at a reasonable cost per unit.

1.4 Aim of the thesis

The aim of the thesis is to design and develop FPGA based controllers for a PV system for load and grid connected applications.

1.5 Objectives of the thesis

The objectives of the thesis are as follows.

- To develop a maximum power extraction algorithm for a PV system at uniform weather conditions and to design a DC-DC boost converter considering the implementation of algorithms.
- To implement MPPT algorithms using FPGA.
- To develop a MPPT scheme for extraction of maximum power from a PV system with rapidly changing conditions and partial shading conditions.
- To develop control schemes for achieving efficient grid synchronization of a PV system.
- To develop an active power filtering scheme for grid connected PV system for achieving THD satisfying IEEE-1547 grid code.
- To develop an experimental set up for verification of PV system algorithms as mentioned above.

1.6 Scopes of the Thesis

The scopes of this work can be outlined as follows

- DC-DC boost converter is analyzed and developed to boost the PV output voltage to a required level.
- The effects of PV at partial shading is observed and validated with a PV simulator.

- Different control techniques are analyzed and simulated through MATLAB/SIMULINK and opal-RT system.
- Different PWM-VSI current control techniques like HCC and MPC are developed to generate the PWM pulses for inverter.
- Single phase PV power system using HCC technique is validated experimentally with NI-cRIO-9075, which includes FPGA.
- Design and development of an active power filter to improve the power quality with a PV system employing adaptive HCC technique.

1.7 Thesis Organization

The thesis is structured into six chapters.
Chapter 1 introduces the need of PV systems which can be used as an alternating source of power supply. Subsequently, the chapter also reviews on different approaches to parameter extraction techniques of PV with MPPT at uniform conditions and partial shading conditions. Later, the review continues on DC-AC inverter and active power filter for PV system. The objective of the thesis and outline of thesis are also presented.

Chapter 2 focuses different MPPT control techniques of a PV system at STC. This chapter includes mathematical modelling of single diode PV cell with Newton-Raphson method, state space analysis of DC-DC converter with results, advantages and disadvantages.The conventional and modified MPPT control algorithms are implemented for a DC-DC converter in a feedback and feed forward approach. The simulation results of different control schemes (PI, modified SMC, Inc Cond, P&O and modified P&O) are verified with Real Time Digital Simulator (Opal-RT) system results. Finally, the models are validated with experimental results.

Chapter 3 demonstrates the PV system under partial shading conditions (PSC). For global maximum power point tracking (GMPPT), the conventional and proposed control techniques are implemented for a DC-DC boost converter. The simulation of PV under

PSC with different MPPT control algorithms (modified P&O, Inc Cond and modified Inc Cond) in MATLAB/SIMULINK, and the results are verified with Real Time Digital Simulator (Opal-RT) system results. Finally, the models are validated with experimental results.

Chapter 4 presents various PWM-VSI current control schemes for a load or grid connected PV system. The Hysteresis Current Controller(HCC), Adaptive Hysteresis Current Controller(AHCC) and Model Predictive Controller (MPC) techniques are discussed and those are used to generate the required switching signals of the PWM-inverter. The Three phase PV power system using HCC, AHCC and MPC control schemes are simulated and the results are validated through Opal-RT and experimental setup. The control algorithms are developed and executed with NI-cRIO-9014.

Chapter 5 describes an application of PV based system for shunt active power filtering with a modified variable step incremental conductnace MPPT controller . It describes the shunt active power line conditioner topology, system configuration, characteristics of harmonics as well as compensation principle. The active power line conditioner topology is developed with voltage source inverter. The simulated results validated with the opal-RT system results.

Chapter 6 concludes the thesis and briefly discusses about the future scope for extension of the work described in the thesis.

1.8 Chapter Summary

This chapter gives the literature review on various topics such as single diode and double diode models of PV cells, MPPT controllers, DC-DC converters, DC-AC inverters and shunt active power filters.

Chapter 2

Development of new integral sliding mode and P&O MPPT controllers for handling standard test conditions

2.1 Introduction

We have already discussed regarding MPPT controllers for PV systems in Chapter 1. The importance of these controllers along with advantages and disadvantages are brought out during the discussion on related work. Therefore, in this chapter we are proposing new control schemes for MPPT. From the literature review pursued on parameter extraction methods described in Chapter 1, it is found that Newton-Raphson based methods are fast and accurate initial conditions for PV cells [29]. Mathematical modelling of PV cell and state space analysis of DC-DC boost converter are developed in this chapter. Analysis and simulation of different feedback and feedforward control techniques have been developed for handling of standard test conditions in chapter 2.

Modern electronic applications require DC-DC converters to regulate the output to a precise value in addition to reduction of ac ripples if any [63]. The PV system generated power is expected to be of good quality, be reliable and efficient. However, semiconductior switches are using in swithcing modes for obtaining regulation. The switching devices control ON and OFF states of the switches at higher power levels. High efficiency can be achieved due to power losses at ON and OFF states only,and with no requirement of any other power devices to operate in the linear region. The transformers and filters can be made small because of the capability of the switch to operate at high frequency. A DC-DC

converter is required for more efficient conversion of power from PV system to the load, and it converts the solar power to usable form. DC-DC converters usually find applications in switch mode power supplies. Converters are used for obtaining regulated DC output from an unregulated DC input. The converter input is generally an unregulated DC voltage, which fluctuates because of the changes in operating conditions. The average DC output voltage must be controlled and hence the converter delivers a desired voltage level in spite of any variations in the input side or at the output load. This is accomplished through the switch ON and OFF timings in the converter.

Pulse Width Modulation technique is a method to control the output voltage of the DC-DC converter. PWM technique employs switching at a constant frequency and adjusts ON time of the switch to control the output voltage. The ratio of the ON time to the total switching time period is known as duty cycle, and is generated by comparing a signal level control voltage with a repetitive waveform. The frequency of the repetitive waveform establishes the switching frequency, which is in few kHz to hundreds of kHz range. These PWM controlled DC-DC converters have advantages like low component count, constant switching frequency. Further more, these are readily available in the market off the rack.

2.2 Chapter objectives

- To develop an efficient MPPT controllers for handling standard test conditions.
- To verify the simulated results with real time results (Opal-RT).
- To validate the simulated results with experimental results.

2.3 Mathematical modelling of a PV cell

PV cell converts solar energy into electrical energy. First, for any given temperature and irradiance the parameters of the PV model must be determined. After these parameters are determined, then solution of final PV equation can be obtained by using Newton-Raphson method. The modelling process for a PV model as described in [6], [82], is shown in Fig. 2.1.

Generally, the PV cell or module is represented either by single exponential model or by double exponential model. The single diode (exponential) circuit model [1], [82] and double diode (exponential) model [42] are shown in Fig. 2.2(a) and Fig. 2.2(b) respectively, suitable to generate electrical power at all weather conditions. When the solar irradiation falls on photovoltaic material, it will convert irradiation into direct current. Models proposed with constant parameters in [83], [84] are inaccurate and not suitable for weather varying conditions. Some of researchers have been developed single diode models without shunt resistance in [85].

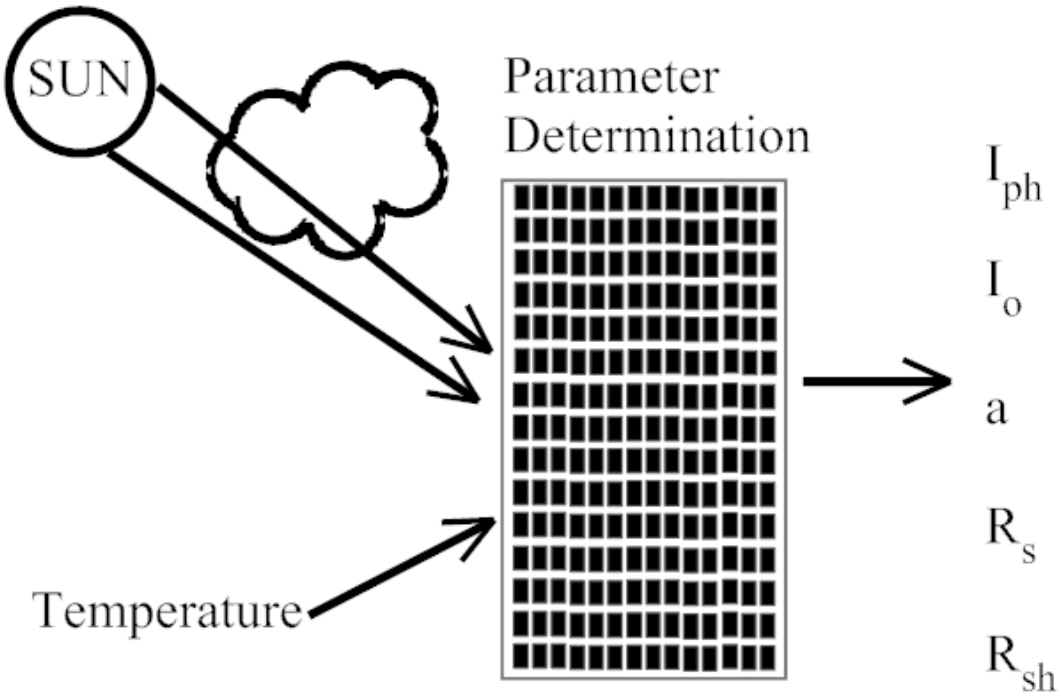

Figure 2.1: Modelling process for PV

The diode current equation is expressed in [17] as

$$I_d = I_0[e^{qV_d/akT} - 1] \tag{2.1}$$

Applying Kirchhoffs current law (KCL) in PV cell shown in Fig.2.2(a), the equation can be expressed as

$$I_{ph} - I_d - \frac{V_d}{R_{sh}} = I_{pv} \tag{2.2}$$

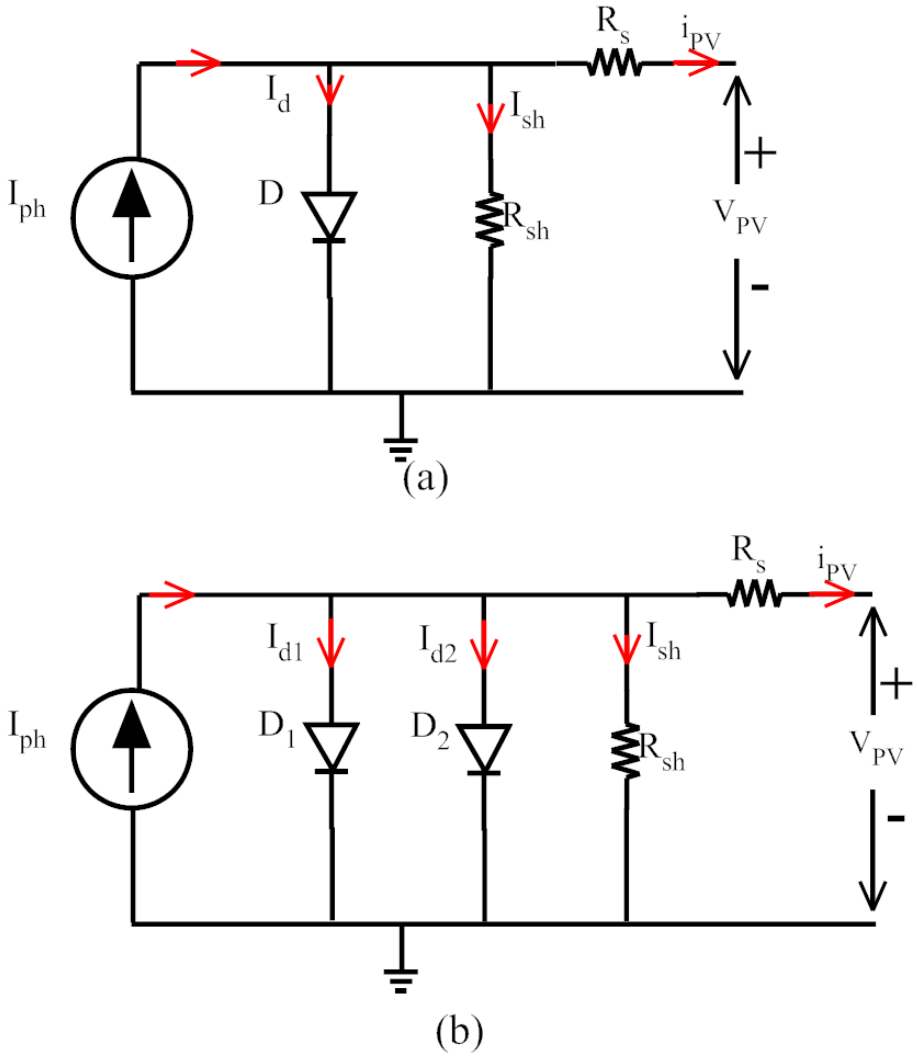

Figure 2.2: Schematic of PV cell (a) Single diode, (b) Double diode

Substituting equation(2.1) into equation(2.2) yields

$$I_{ph} - I_0[e^{qV_d/nkT} - 1] - \frac{V_d}{R_{sh}} = I_{pv} \tag{2.3}$$

PV current for single diode model is expressed in terms of voltage is as follows

$$I_{pv} = I_{ph} - I_o\left\{\exp\left[\frac{q(V_{pv} + I_{pv}R_s)}{nkT}\right] - 1\right\} - \frac{V_{pv} + I_{pv}R_s}{R_{sh}} \tag{2.4}$$

where I_{ph}= The photo generated current,

I_o= Dark saturation current,

V_d = Voltage across diode,

q = Charge of the electron (1.6X10^{-19} C),

I_{pv}= Final PV cell current (at load),

V_{pv}= Final PV cell voltage (at load),

a= Diode ideality factor,

k = Boltzmanns constant (1.3X10^{-23} J/K),

T=Absolute temperature,

R_s= Series resistance,

R_{sh}= Shunt resistance.

Equation(2.4) is non-linear in nature. The PV parameters (I_{ph}, I_o, a, R_s, R_{sh}) vary with temperature and irradiance. Curve fitting and Newton- Raphson methods are using to derive PV system modeling for single and double diode models (shown in Fig. 2.2.)

Single diode model

The single diode model assumes that the dark saturation current of a PV cell which can be described by a single exponential term, and it can be modified by using the diode ideality factor. Five parameters in equation (2.4) must be determined to reproduce the I-V characteristic curve, and five equations are required containing five unknown parameters that will be solved concurrently to obtain the unknown parameters [14], [43, 86, 87].

There are three key points on the I-V characteristic curve of a PV cell, they are 1) short circuit current (I_{sc}), 2) maximum power point (MPP) and 3) open circuit voltage (V_{oc}). At the open circuit voltage point on the I-V curve, $V_{pv} = V_{oc}$ and $I_{pv} = 0$. Substituting these values in equation (2.4), the first needed equation can be obtained as

$$0 = I_{ph} - I_o \left\{ \exp\left[\frac{q(V_{oc})}{akT} \right] - 1 \right\} - \frac{V_{oc}}{R_{sh}} \tag{2.5}$$

At the short circuit current point on the I-V curve, $I_{pv} = I_{sc}$ and $V_{pv} = 0$. Substituting these values in equation (2.4), the second required equation is obtained as

$$I_{sc} = I_{ph} - I_o \left\{ \exp\left[\frac{q(I_{sc}R_s)}{akT} \right] - 1 \right\} - \frac{I_{sc}R_s}{R_{sh}} \tag{2.6}$$

At the maximum power point on the I-V curve, $I_{pv} = I_{mpp}$ and $V_{pv} = V_{mpp}$, after substituting

these values in equation (2.4), the third equation can be obtained that follows

$$I_{mpp} = I_{ph} - I_o \left\{ \exp\left[\frac{q(V_{mpp} + I_{mpp}R_s)}{akT} \right] - 1 \right\} - \frac{V_{mpp} + I_{mpp}R_s}{R_{sh}} \tag{2.7}$$

The other equations are obtained by taking derivative of equation (2.4) with respect to V_{pv}, then the equation becomes

$$\frac{dI_{pv}}{dV_{pv}} = -I_o \left\{ \left[\frac{q}{akT} \left(1 + \frac{dI_{pv}}{dV_{pv}} R_s \right) \right] \exp\left[\frac{q(V_{mpp} + I_{mpp}R_s)}{akT} \right] \right\} - \frac{1}{R_{sh}} \left(1 + \frac{dI_{pv}}{dV_{pv}} R_s \right) \tag{2.8}$$

At the open circuit voltage point on the I-V curve, voltage and current values are V_{pv}=V_{oc} and I_{pv}=0, that means $\frac{dI_{pv}}{dV_{pv}} = \frac{dI_{pv}}{dV_{pv}} \big|_{I_{pv}=0}$ Substitute the above condition in equation (2.8), then

$$\frac{dI_{pv}}{dV_{pv}} \big|_{V_{pv}=0} = -I_o \left\{ \left[\frac{q}{akT} \left(1 + \frac{dI_{pv}}{dV_{pv}} \big|_{V_{pv}=0} R_s \right) \right] \exp\left[\frac{qI_{sc}R_s}{akT} \right] \right\} - \frac{1}{R_{sh}} \left(1 + \frac{dI_{pv}}{dV_{pv}} \big|_{V_{pv}=0} R_s \right) \tag{2.9}$$

Again, at the short circuit current point on the I-V curve, voltage and current values are V_{pv}=0 and I_{pv}= I_{oc}, that means $\frac{dI_{pv}}{dV_{pv}} = \frac{dI_{pv}}{dV_{pv}} \big|_{V_{pv}=0}$.

$$\frac{dI_{pv}}{dV_{pv}} \big|_{V_{pv}=0} = -I_o \left\{ \left[\frac{q}{akT} \left(1 + \frac{dI_{pv}}{dV_{pv}} \big|_{V_{pv}=0} R_s \right) \right] \exp\left[\frac{qI_{sc}R_s}{akT} \right] \right\} - \frac{1}{R_{sh}} \left(1 + \frac{dI_{pv}}{dV_{pv}} \big|_{V_{pv}=0} R_s \right) \tag{2.10}$$

The power can be calculated using P =VxI. the power equation can be differentiated with respect to voltage V_{pv}, then the above power equation becomes:

$$\frac{dP_{pv}}{dV_{pv}} = \left(\frac{dI_{pv}}{dV_{pv}} \right) V_{pv} + I_{pv} \tag{2.11}$$

To find the voltage at MPP, the derivative is equated to zero, then

$$\frac{dP_{pv}}{dV_{pv}} = 0 \tag{2.12}$$

Substituting equation (2.12) in equation(2.11), gives

$$\frac{dI_{pv}}{dV_{pv}} = -\left(\frac{I_{MPP}}{V_{MPP}} \right) \tag{2.13}$$

Substituting equation(2.13) in equation(2.8), which gives

$$-\frac{I_{MPP}}{V_{MPP}} = -I_o \left\{ \left(\frac{q}{nkT} \right) \left[1 - \frac{I_{MPP}}{V_{MPP}} R_s \right] \exp \left[\frac{q(V_{MPP} + I_{MPP} R_s)}{akT} \right] \right\} - \frac{1}{R_{sh}} \left[1 - \frac{I_{MPP}}{V_{MPP}} R_s \right] \quad (2.14)$$

Equation (2.14) can be used to obtain the five PV parameters (I_{ph}, I_o, a, R_s, R_{sh}). Therefore, substitute the values of V_{oc}, I_{sc}, V_{MPP}, I_{MPP}, and into the independent equations. The non-linear equations can be solved by using Newton-Raphson method. For notational convenience the above values can be written as

$$R_s^1 = \frac{dV_{pv}}{dI_{pv}} \Big|_{V_{pv}=V_{oc}} \quad (2.15)$$

$$0 = \left(R_s^1 - R_s \right) \left(\frac{1}{R_{sh}} + \frac{I_o}{aV_T} \exp \frac{V_{oc}}{aV_T} \right) - 1 \quad (2.16)$$

$$V_T = \frac{kT}{q} \quad (2.17)$$

Substituting equation(2.15), equation(2.16) and equation(2.17) in the above independent equations, then new set of equations are as follows

$$0 = I_o \left(\exp \frac{V_{oc}}{aV_T} - \exp \frac{I_{sc} R_s}{aV_T} \right) - I_{sc} \left(1 + \frac{R_s}{R_{sh}} \right) + \frac{V_{oc}}{R_{sh}} \quad (2.18)$$

$$0 = \left(R_s^1 - R_s \right) \left(\frac{1}{R_{sh}} + \frac{I_o}{aV_T} \exp \frac{V_{oc}}{aV_T} \right) - 1 \quad (2.19)$$

$$0 = \frac{1}{R_{sh}} - \frac{1}{R_{sh}^1 - R_s} + \frac{I_o}{aV_T} \exp \frac{I_{sc} R_s}{aV_T} \quad (2.20)$$

$$0 = I_o \exp \frac{V_{oc}}{aV_T} + \frac{V_{oc} - V_{mpp}}{R_{sh}} - \left(1 + \frac{R_s}{R_{sh}} \right) \mathrm{I}_{mpp} - I_o \exp \frac{V_{mpp} + \mathrm{I}_{mpp} R_s}{aV_T} \quad (2.21)$$

To obtain the initial values of PV parameters, the algorithm uses analytical expressions, based on that the initial values can be calculated. The diode ideality factor can be obtained

by the following equation

$$n = \frac{V_{mpp} + \mathrm{I}_{mpp} R^1_{sh} - V_{oc}}{V_T \left[\ln\left(I_{sc} - \frac{V_{mpp}}{R^1_{sh}} - I_{mpp}\right) - \ln\left(I_{sc} - \frac{V_{oc}}{R_{sh}}\right) + \frac{I_{mpp}}{I_{sc} - \left(\frac{V_{oc}}{R^1_{sh}}\right)} \right]} \tag{2.22}$$

Rest of the initial values of the PV parameters can be found from the following equations

$$R_{sh} = R^1_{sh} \tag{2.23}$$

$$I_o = \left(I_{sc} - \frac{V_{oc}}{R_{sh}}\right) \exp\left(-\frac{V_{oc}}{aV_T}\right) \tag{2.24}$$

$$R_s = R^1_s - \frac{nV_T}{I_o} \exp\left(-\frac{V_{oc}}{aV_T}\right) \tag{2.25}$$

$$I_{ph} = I_{sc}\left(1 + \frac{R_s}{R_{sh}}\right) + I_o\left(\exp\frac{I_{sc}R_s}{aV_T} - 1\right) \tag{2.26}$$

Newton-Raphson method: This method is using to solve the non-linear equations of the system. It finds the roots of a non-linear equation by computing the Jacobian linearization of the function assuming the initial value, and tending closer to zero. A set of non-linear equations in matrix form is given as

$$f(i) = \begin{bmatrix} f_1(i) \\ f_2(i) \\ \vdots \\ f_N(i) \end{bmatrix} = j \tag{2.27}$$

where i, j and N are vectors, and f(i) is a function having N vectors. The aim is to find the i value for a given j and f(i), therefore the equation (2.27) can be rewritten as

$$0 = j - f(i) \tag{2.28}$$

By adding a NxN square matrix K_i on both sides of equation (2.28), which gives

$$Kx = Kx + j - f(i) \tag{2.29}$$

Multiplying equation (2.29) with K^{-1} then the equation becomes

$$x = x + K^{-1}[j - f(i)] \tag{2.30}$$

The Newton-Raphson method states that the matrix K is based on Taylor series expansion of i about a point i_0.

$$j = f(i_0) + \frac{df}{di}\Big|_{i=i_0} \ (i - i_0)..... \tag{2.31}$$

Neglecting higher order terms in equation (2.31) and solve for i, then equation(2.31) becomes

$$i = i_0 + \left[\frac{df}{di}\Big|_{i=i_0}\right]^{-1} \ [j - f(i_0)] \tag{2.32}$$

Replace i_0 by a old value i(n) and i by a new value i(n+1): then equation(2.32) as

$$i(n+1) = i(n) + J_b^{-1}(n)\left[j - f\{i(n)\}\right] \tag{2.33}$$

Where J_b is a Jacobian matrix, it can be defined as

$$J_b(n) = \frac{df}{di}\Big|_{i=i(n)} = \begin{bmatrix} \frac{\partial f_1}{\partial i_1} & \frac{\partial f_1}{\partial i_2} & \cdots & \frac{\partial f_1}{\partial i_N} \\ \frac{\partial f_2}{\partial i_1} & \frac{\partial f_2}{\partial i_2} & \cdots & \frac{\partial f_2}{\partial i_N} \\ \vdots & \vdots & \ddots & \vdots \\ \frac{\partial f_N}{\partial i_1} & \frac{\partial f_N}{\partial i_2} & \cdots & \frac{\partial f_N}{\partial i_N} \end{bmatrix} \tag{2.34}$$

From above equations one can use five unknown PV parameters of Jacobian matrix by

considering equation(2.5), then f_1(i) obtains

$$J_b(1,1) = 1$$

$$J_b(1,2) = -\exp\left(\frac{qV_{oc}}{akT}\right) + 1$$

$$J_b(1,3) = -\frac{qI_oV_{oc}\exp\left(\frac{qV_{oc}}{akT}\right)}{a^2kT} \tag{2.35}$$

$$J_b(1,4) = 0$$

$$J_b(1,5) = -\frac{V_{oc}}{R_{sh}^2}$$

By considering equation (2.6) for Jacobian matrix and the function f_2(i) one can write the following terms of the Jacobian matrix,

$$J_b(2,1) = 1$$

$$J_b(2,2) = -\exp\left(\frac{qI_{sc}R_s}{akT}\right) + 1$$

$$J_b(2,3) = -\frac{qI_oI_{sc}\exp\left(\frac{qI_{sc}R_s}{akT}\right)}{a^2kT} \tag{2.36}$$

$$J_b(2,4) = -\frac{qI_oI_{sc}\exp\left(\frac{qI_{sc}R_s}{akT}\right)}{akT} - \frac{I_{sc}}{R_{sh}}$$

$$J_b(2,5) = -\frac{I_{sc}}{R_{sh}^2}$$

Considering equation (2.9) for Jacobian matrix, and the function f_3(i) obtains

$$
\begin{aligned}
J_b(3,1) &= 0 \\
J_b(3,2) &= -\frac{q\left(1-\frac{R_s}{R_s^1}\right)\exp\left(\frac{qV_{oc}}{akT}\right)}{akT} \\
J_b(3,3) &= -\frac{qI_o\left(R_s^1-R_s\right)\exp\left(\frac{qV_{oc}}{akT}\right)(akT+qV_{oc})}{a^3k^2T^2R_s^1} \\
J_b(3,4) &= -\frac{qI_o\left(R_s-R_s^1\right)\exp\left(\frac{qV_{oc}}{akT}\right)}{akTR_s^1} + \frac{1}{R_{sh}R_s^1} \\
J_b(3,5) &= \frac{1-\frac{R_s}{R_s^1}}{R_{sh}^2}
\end{aligned}
\tag{2.37}
$$

Considering equation(2.10) for Jacobian matrix, and the function f_4(i) obtains

$$
\begin{aligned}
J_b(4,1) &= 0 \\
J_b(4,2) &= -\frac{q\left(1-\frac{R_s}{R_s^1}\right)\exp\left(\frac{qI_{SC}R_s}{akT}\right)}{akT} \\
J_b(4,3) &= -\frac{qI_o\left(R_{sh}^1-R_s\right)\exp\left(\frac{qI_{SC}R_s}{akT}\right)(akT+qI_{SC}R_s)}{a^3k^2T^2R_{sh}^1} \\
J_b(4,4) &= \frac{qI_o\left(R_{sh}^1-R_s\right)\exp\left(\frac{qI_{SC}R_s}{akT}\right)}{akTR_{sh}^1} - \frac{q^2I_o\left(1-\frac{R_s}{R_{sh}^1}\right)I_{sc}\exp\left(\frac{qI_{SC}R_s}{akT}\right)}{a^2k^2T^2} + \frac{1}{R_{sh}R_{sh}^1} \\
J_b(4,5) &= \frac{R_{sh}^1-R_s}{R_{sh}^2R_{sh}^1}
\end{aligned}
\tag{2.38}
$$

Considering the equation(2.14) for Jacobian matrix, and the function f_5(i) obtains

$$J_b(5,1) = 0$$

$$J_b(5,2) = -\frac{q\left(1-\frac{I_{mpp}R_s}{V_{mpp}}\right)\exp\left(\frac{q(V_{mpp}+I_{mpp}R_s)}{akT}\right)}{akT}$$

$$J_b(5,3) = \frac{\left(V_{mpp}+I_{mpp}R_s\right)\left[akT+q\left(V_{mpp}+I_{mpp}R_s\right)\right]qI_o\exp\left(\frac{q(V_{mpp}+I_{mpp}R_s)}{akT}\right)}{V_{mpp}n^3k^2T^2} \tag{2.39}$$

$$J_b(5,4) = \frac{qI_oI_{mpp}\exp\left(\frac{q(V_{mpp}+I_{mpp}R_s)}{akT}\right)}{V_{mpp}akT} - \frac{q^2I_o\left(1-\frac{I_{mpp}R_s}{V_{mpp}}\right)I_{mpp}\exp\left(\frac{q(V_{mpp}+I_{mpp}R_s)}{akT}\right)}{a^2k^2T^2} + \frac{I_{mpp}}{R_{sh}V_{mpp}}$$

$$J_b(5,5) = \frac{1-\frac{I_{mpp}R_s}{V_{mpp}}}{R_{sh}^2}$$

The equations describing the Jacobians for the unknown PV parameters are computed using MATLAB symbolic toolbox, a numerical solution can be obtained by using the optimization toolbox. After mathematical modeling of a PV cell is done, simulated in MATLAB/SIMULINK, PV characteristic curves are obtained. The obtained characteristic curves for Standard Test Conditions (STC) are shown in Fig.2.3. The standard test conditions for a PV cell are temperature is 25^o C, and irradiation is 1000 W/m^2. The simulated PV model extracted 23 V voltage and 3.4 A current. The electrical parameters of PV panel are given in Table 2.1. Due to change of weather, the temperature and irradiation levels will be changed. Therefore, changes occurs in PV characteristic curves. Multiple PV characteristic curves at different temperatures and irradiations are shown in Fig. 2.4.

Table 2.1: Electrical parameters of PV array

Maximum power (P_{max})	62 W
Voltage at MPP (V_{MPP})	20 V
Current at MPP (I_{MPP})	3.1 A
Open circuit voltage (V_{oc})	23 V
Short circuit current (I_{SC})	3.36 A

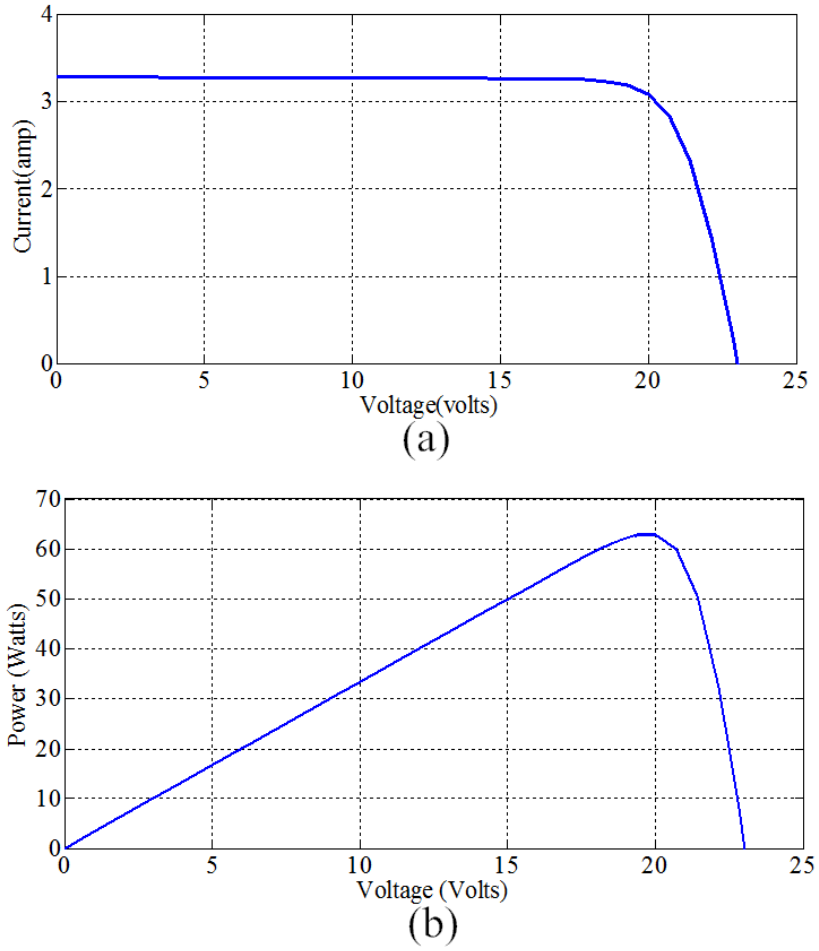

Figure 2.3: PV characteristic curves at STC

2.4 Design of DC-DC boost converter

A DC-DC boost converter is a power converter with an output voltage greater than its input voltage. It belongs to the class of SMPS containing a minimum of two semiconductor switches (a diode and a transistor) and at least one energy storage element, either capacitor, or inductor, or both [88]. Filters are used to reduce the output voltage ripple. The advantage of boost converter includes higher efficiency with fewer components. To reduce ripples at output the values of capacitor and inductor are chosen precisely. However, the large inductance tends to increase the start-up time slightly while small inductance allows the coil current to ramp up to higher levels before switch turns OFF [61]. The duty cycle is varied at high switching frequency to convert the unregulated voltage into a regulated supply.

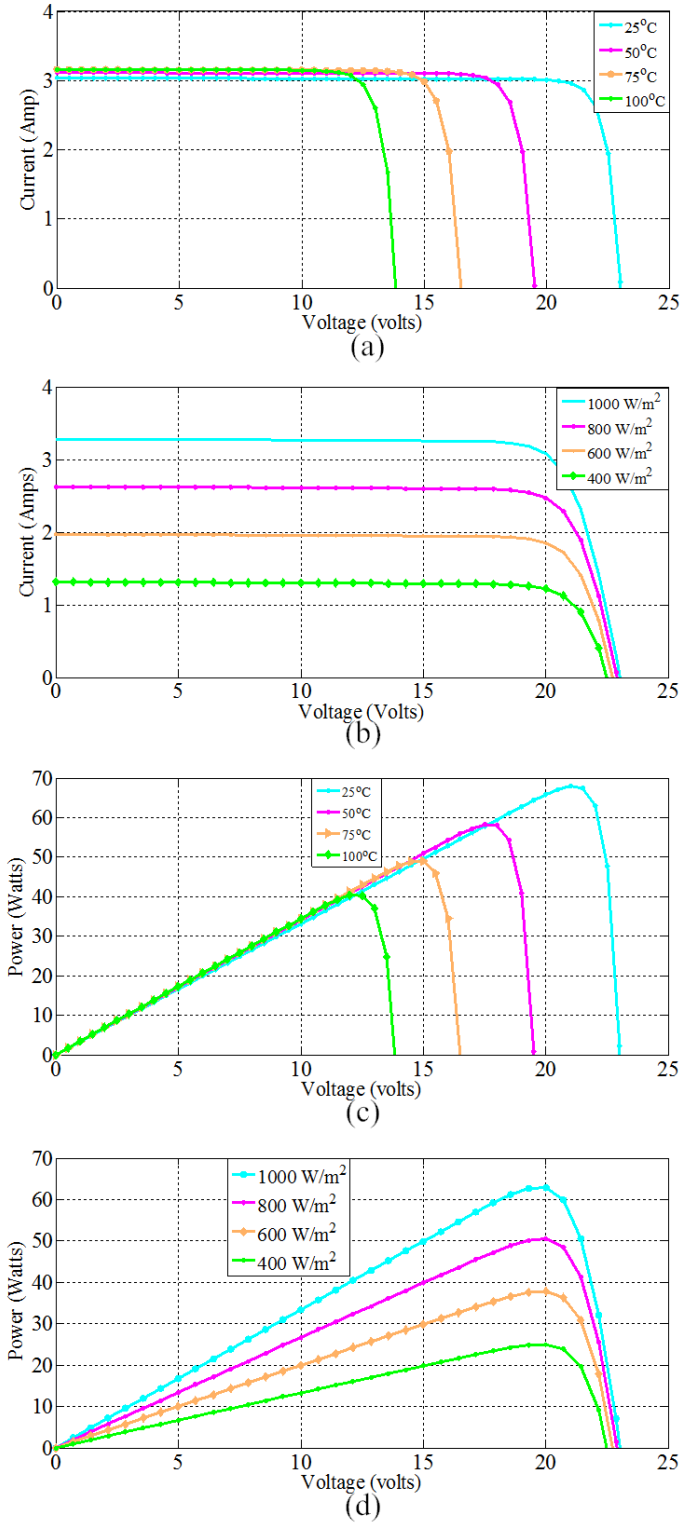

Figure 2.4: PV characteristic curves at different weather conditions (a) and (c) varying temperature with constant $1000W/m^2$ irradiance, (b) and (d) varying irradiance with constant 25^oC temperature

Modeling of DC-DC boost converter:

The state-space averaging technique is widely used to derive the expressions and analysis for the small signal characteristics of pulse width modulated controlled DC-DC converters. The dynamics of this converter can be determined by applying Kirchhoffs voltage law on the loop containing the inductor and Kirchhoffs current law at the node with the capacitor branch connected to it. The circuit diagram of the DC-DC boost converter is shown in Fig. 2.5, and the functioning will depend on the switch ON and OFF.

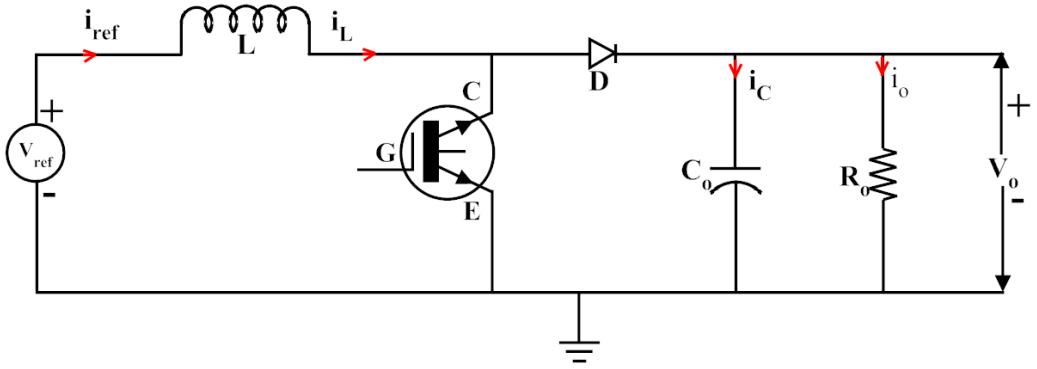

Figure 2.5: DC-DC boost converter circuit diagram

When the switch is ON, the equivalent circuit diagram is shown in Fig. 2.6, the current flows from the supply to the inductor L. At this condition the diode D is reverse biased and it does not conduct. Hence the inductor stores energy and the inductor current rises, and the capacitor C maintains the voltage V_o and supplies current i_o. The state space equations are:

$$\begin{bmatrix} \frac{dI_L}{dt} \\ \frac{dV_o}{dt} \end{bmatrix} = \begin{bmatrix} 0 & 0 \\ 0 & -\frac{1}{C_o R_L} \end{bmatrix} \begin{bmatrix} I_L \\ V_o \end{bmatrix} + \begin{bmatrix} \frac{1}{L} \\ 0 \end{bmatrix} V_{ref} \tag{2.40}$$

$$V_o = \begin{bmatrix} 0 & -\frac{1}{C_o R_L} \end{bmatrix} \begin{bmatrix} I_L \\ V_o \end{bmatrix} \tag{2.41}$$

When the switch is OFF, the inductor generates a high voltage to maintain the current i_L in the same direction and now the diode D is forward biased and it starts conducting. Hence the output voltage can be expressed as

$$V_o = V_{ref} + L\frac{di_L}{dt} \tag{2.42}$$

The circuit diagram of the boost converter when the switch is OFF is shown in Fig. 2.7.

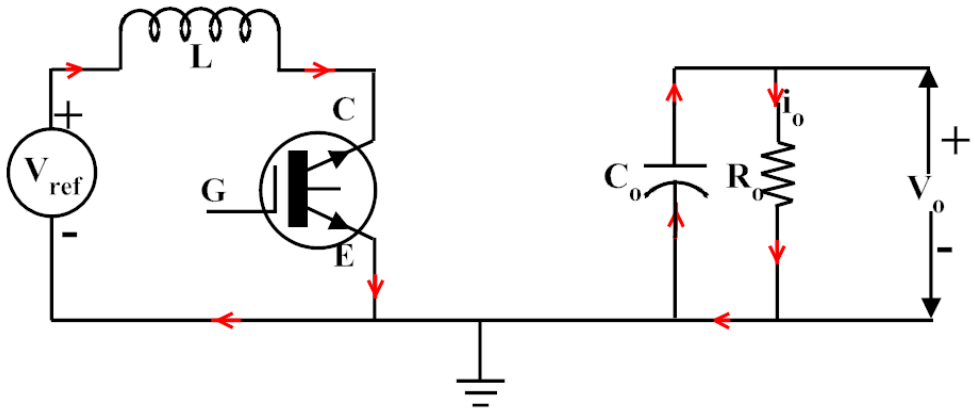

Figure 2.6: Boost converter current flow at switch ON condition

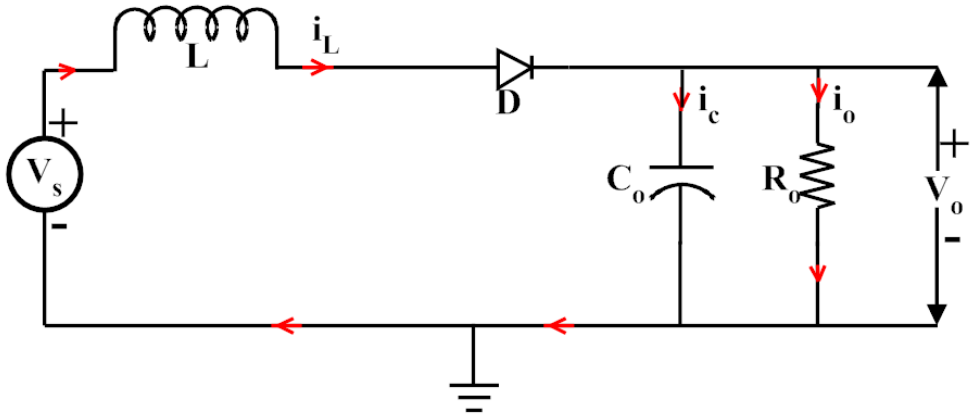

Figure 2.7: Boost converter current flow at switch OFF condition

The voltage induced in the inductor adds to the supply voltage and this total voltage appears as output voltage, at that situation the capacitor C also charges to the boosted voltage. The inductor and supply provides the energy to the load when the transistor is turned OFF. The current through the inductor decreases because its stored energy goes on reducing. After some time the transistor is again turned ON and the cycle repeats. The mathematical model of a boost converter when the transistor is OFF can be expressed in state space as follows

$$\begin{bmatrix} \frac{dI_L}{dt} \\ \frac{dV_o}{dt} \end{bmatrix} = \begin{bmatrix} 0 & -\frac{1}{L} \\ \frac{1}{C_o} & -\frac{1}{C_o R_L} \end{bmatrix} \begin{bmatrix} I_L \\ V_o \end{bmatrix} + \begin{bmatrix} I_L \\ 0 \end{bmatrix} \begin{bmatrix} V_{ref} \end{bmatrix} \tag{2.43}$$

$$V_o = \begin{bmatrix} \frac{1}{C_o} & -\frac{1}{C_o R_L} \end{bmatrix} \begin{bmatrix} I_L \\ V_o \end{bmatrix} \tag{2.44}$$

2.5 Control techniques

DC-DC converter is one of the primary power-conditioning systems in a PV system. To get the required output voltage from DC-DC converter, closed loop control is essential. There are different linear and non-linear control strategies for DC-DC converter. The main objective of the controller is to maintain the desired output voltage and compensate for any disturbances. The most widely used linear control strategy for DC-DC converter is voltage mode control using PI controller and one of the promising non-linear control strategy is Sliding Mode Control strategy. One of the main advantages of sliding mode control is its robustness to unknown disturbances [23].

2.5.1 PI MPPT Controller

A proportional-integral (PI) controller is a feedback control strategy widely used in industrial applications. This control structure is simple. The block diagram of control strategy of PI controller with PV arrays and boost converter is shown in Fig. 2.8. The PI controller calculates error value as the difference between desired set point or reference value with measured value [23]. The PI control structure involves two constant parameters such as proportional and integral values denoted as K_P and K_I. P depends on the present error; I depends on the accumulation of past errors based on current rate of change. The weighted sum of these two actions is used to adjust the process via a control element.

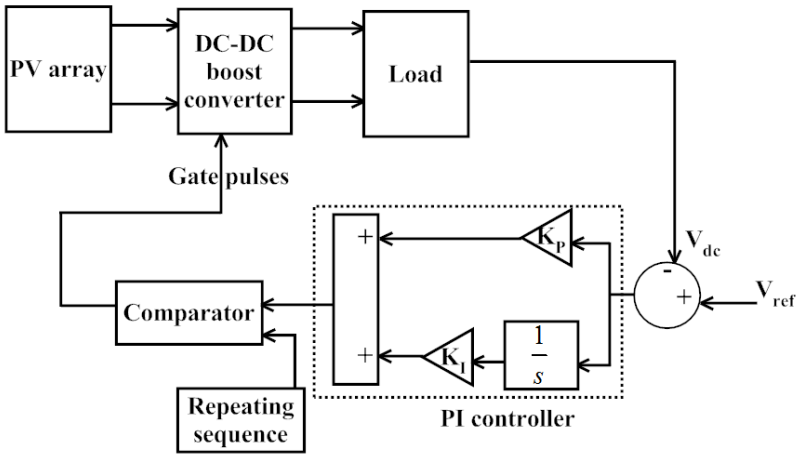

Figure 2.8: Control Strategy of PI for PV array with DC-DC boost converter

DC-DC boost converter is an integral part of the PV system for boosting the output

voltage to a certain desired level. Therefore, PI MPPT controller has been used for a PV system along with a DC-DC boost converter to maintain desired output voltage. The PI controller output is given to a comparator to compare with a standard repetitive signal. This PWM controller operates at a constant frequency constant and the variations in duty cycle regulates output voltage. For the given PI MPPT controller, the duty cycle varies between 0.5 to 1. Hence, the mean duty-cycle is in between 0.5 and 1. The comparator output which is the PWM signal is fed to gate terminal of transistor of the converter. The K_P and K_I are 0.9 and 103 respectively these values are obtained heuristically so that it provides undistorted output. The reference voltage V_{ref} is 250 V, and the design parameters of PI MPPT controller are given in Table 2.2.

Table 2.2: Simulation parameters of PV with DC-DC boost converter

Parameters	Values
Voltage Ripple	0.1 %
Inductance (L)	1 mH
Capacitance (C)	500 μF
K_P	0.9
K_I	103
Switching Frequency (f_s)	10 kHz
Desired DC output voltage	250 V

2.5.2 Modified integral sliding mode controller for MPPT

Sliding mode controllers are used for MPPT tracking [56]. However, with this control approach there is a delay in reaching steady state condition. Sliding mode controller enhances robustness regulation of the system [89]. Considering above, we have added an integral component in the proposed modified sliding mode control (named as integral sliding mode control(ISMC)) represented in equation(2.47). This control method is simple and would provide better control performance. SMC is a combination of system states, which has the same order as that of the converter [59]. The block diagram ISMC with PV and boost converter is shown in Fig. 2.9.

The fundamental principle of an SMC is to design a particular sliding manifold in its control law that will preside over the trajectory of the state variables towards the required operating point. In case of a boost converter as it has a single switch, it is apt to adopt a

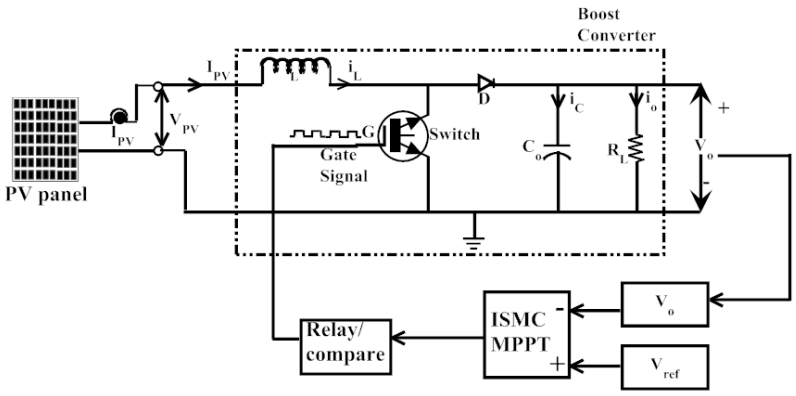

Figure 2.9: Block diagram of ISMC with PV system and DC-DC boost converter

control law for switching function [90] as

$$u = \frac{1}{2}(1 + sgn(S)) \tag{2.45}$$

where, u= switching logic of converter, 'S' is an instantaneous state trajectory. In this case, 'S' is illustrated as

$$S = \alpha_1 x_1 + \alpha_2 x_2 + \alpha_3 x_3 = K^T x \tag{2.46}$$

with $K^T = [\alpha_1 \ \alpha_2 \ \alpha_3]$ and $\alpha_1, \alpha_2, \alpha_3$ representing the control parameters also considered as sliding coefficients, x_1, x_2, x_3 are the desired state feedback variables which are to be controlled. By equating S=0, a sliding plane can be acquired. The aim of the designer is to determine the state of switching function u and also to choose appropriate values of α_1, α_2 and α_3 such that the controller satisfies (i) hitting, (ii)SM existence and (iii)stability conditions [56].

(i) Hitting condition

The design of SMC to meet the hitting condition is straight forward in the case of power converters. Now the state variables can be expressed in the form of

$$\begin{bmatrix} x_1 \\ x_2 \\ x_3 \end{bmatrix} = \begin{bmatrix} V_{ref} - \beta V_o \\ \frac{d(V_{ref} - \beta V_o)}{dt} \\ \int (V_{ref} - \beta V_o) dt \end{bmatrix} \tag{2.47}$$

In order to design the hitting condition, it is sufficient to depend only on the immediate

state variable x_1, which is predominant during the reaching phase of 'S'. The resulting control function in this configuration is

$$u = \begin{cases} 1 = ON, \ When\, S > 0 \\ 0 = OFF, When\, S < 0 \end{cases} \tag{2.48}$$

Thus, the method ensures fulfillment of hitting condition of the SMC, which is nearly related to the way in which the hysteresis controller switching states are designed.

(ii) SM Existence condition

With the switching states of the converter are determined, the next step is to select the sliding coefficients $\alpha_1, \alpha_2, \alpha_3$ that fulfill the condition for SM existence. Now, by inspecting a local reachability condition of the state trajectory, i.e.,

$$\lim_{s\to 0} S.\ \dot{S} < 0 \tag{2.49}$$

$$\dot{S} = K^T \dot{x} \tag{2.50}$$

$$\dot{x} = Ax + Bu + D \tag{2.51}$$

Now it can be written as

$$\begin{cases} \dot{S}_{s\to 0^+} = K^T A_x + K^T B v_{s\to 0^+} + J^T D < 0 \\ \dot{S}_{s\to 0^-} = K^T A_x + K^T B v_{s\to 0^-} + J^T D < 0 \end{cases} \tag{2.52}$$

Case 1: $S \to 0^+, \dot{S} < 0$ Substitution of $v_{s\to 0^+} = \bar{u} = 0$ gives

$$-\alpha_1 \frac{\beta i_c}{C} + \alpha_2 \frac{\beta i_c}{r_L C^2} + \alpha_3 (V_{ref} - \beta V_o) < 0 \tag{2.53}$$

Case 2: $S \to 0^-, \dot{S} > 0$ Substitution of $v_{s\to 0^-} = \bar{u} = 1$ gives

$$-\alpha_1 \frac{\beta i_c}{C} + \alpha_2 \frac{\beta i_c}{r_L C^2} + \alpha_3 (V_{ref} - \beta V_o) - \alpha_2 \frac{\beta V_i}{LC} + \alpha_2 \frac{\beta V_o}{LC} > 0 \tag{2.54}$$

Finally, the combination of equation (2.53) and equation (2.54) gives the simplified

existence condition as follows

$$0 < \beta L\left(\frac{\alpha_1}{\alpha_2} - \frac{1}{r_L C}\right) i_C - LC\frac{\alpha_3}{\alpha_2}(V_{ref} - \beta V_o) < \beta(V_o - V_i) \tag{2.55}$$

The array of sliding coefficients (α_1 , α_2 and α_3) for the controller of the boost converter must obey to its stated inequalities. It is important to make sure that the circuit tolerances and operating range of conditions are taken into consideration when evaluating the stated inequalities. This confirms the fulfillment of the SM existence condition for the full operating range of the converters.

(iii) Stability Condition

The selected sliding coefficients (α_1 , α_2 and α_3) should satisfy the stability condition simultaneously, apart from the fulfillment of SM existence condition. The relation between the sliding coefficients to the dynamic response of the converter during SM operation is

$$\alpha_1 x_1 + \alpha_2 \frac{dx_1}{dt} + \alpha_3 \int x_1 \, dt = 0 \tag{2.56}$$

Equation(2.56) can be rearranged into standard second order system form in which the design of the sliding coefficients (α_1 , α_2 and α_3) will give one of the three possible types of responses like under damped, critical damped and over damped. Therefore, selection of sliding coefficients can be easily done by converter response time and voltage peak over shoot specifications.

For an SM voltage controller the switching logical function 'u' is obtained by the combination of control parameters x_1, x_2 and x_3 by utilizing the computation of state trajectories.

$$S = \alpha_1 x_1 + \alpha_2 x_2 + \alpha_3 x_3 = K^T x \tag{2.57}$$

where α_1 , α_2 and α_3 are considered as control parameters.

By imposing S=0, a sliding line is obtained. The main aim of using sliding line is to serve as a periphery to split the phase trajectory, which reaches and tracks the sliding line declaring that the system is stable. From Fig. 2.10, it can be observed that the phase trajectory is at any arbitrary position below the sliding line (S=0) e.g., point 'P', u=1 is employed such that the trajectory is directed towards the sliding line. Similarly, when the

trajectories above the sliding line e.g., point 'Q', u=0 is employed for the trajectory to be directed towards the sliding line is shown in Fig. 2.11.

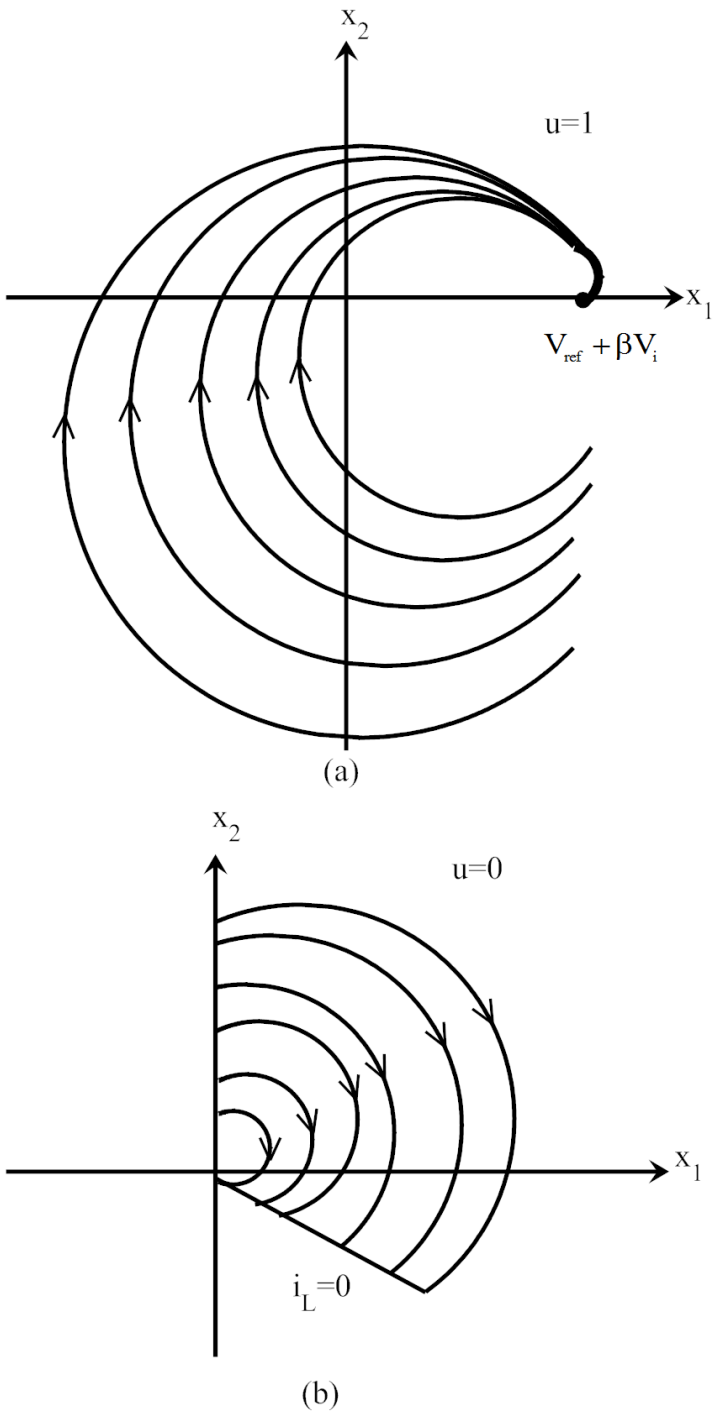

Figure 2.10: Phase trajectories of the substructures at (a) u=1, (b) u=0 for different starting positions of x_1 and x_2.

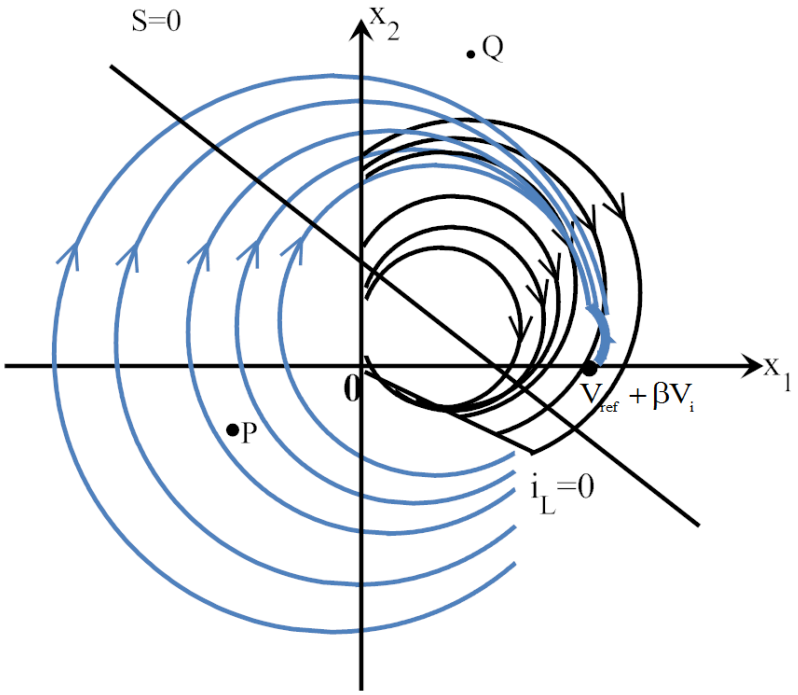

Figure 2.11: Combined plot of phase trajectories of the substructures corresponding u=1 and u=0 for different starting positions of x_1 and x_2.

$$\lambda_1 = (LC\frac{\alpha_3}{\alpha_2} + 1)x_1 + LC(\frac{\alpha_1}{\alpha_2} - \frac{1}{LC})x_2 < 0 \tag{2.58}$$

$$\lambda_2 = (LC\frac{\alpha_3}{\alpha_2} + 1)x_1 + LC(\frac{\alpha_1}{\alpha_2} - \frac{1}{R_LC})x_2 - (V_{ref} + \beta V_{in}) > 0 \tag{2.59}$$

The aforementioned conditions are shown in Fig.2.11, for the two situations a) $\frac{\alpha_1}{\alpha_2} > \frac{1}{R_LC}$, $\frac{\alpha_3}{\alpha_2} < \frac{-1}{LC}$ and b) $\frac{\alpha_1}{\alpha_2} < \frac{1}{R_LC}$, $\frac{\alpha_3}{\alpha_2} < \frac{-1}{LC}$. In both figures, region 1 depicts $\lambda_1 < 0$ and region 2 represents $\lambda_2 > 0$. The SM operation is only valid on the portion of the sliding line S=0, that covers both regions 1 and 2. In this case the portion is within A and B, where A is intersection of S=0 and $\lambda_1 < 0$, and B is the intersection of S=0 and $\lambda_2 > 0$. Trajectory touches the sliding line S=0 within AB, and slides through it. When trajectory goes beyond sliding line outside AB, it results an overshoot, when $\frac{\alpha_1}{\alpha_2} > \frac{1}{R_LC}$, $\frac{\alpha_3}{\alpha_2} < \frac{-1}{LC}$. Both these regions are shown in Fig.2.12.

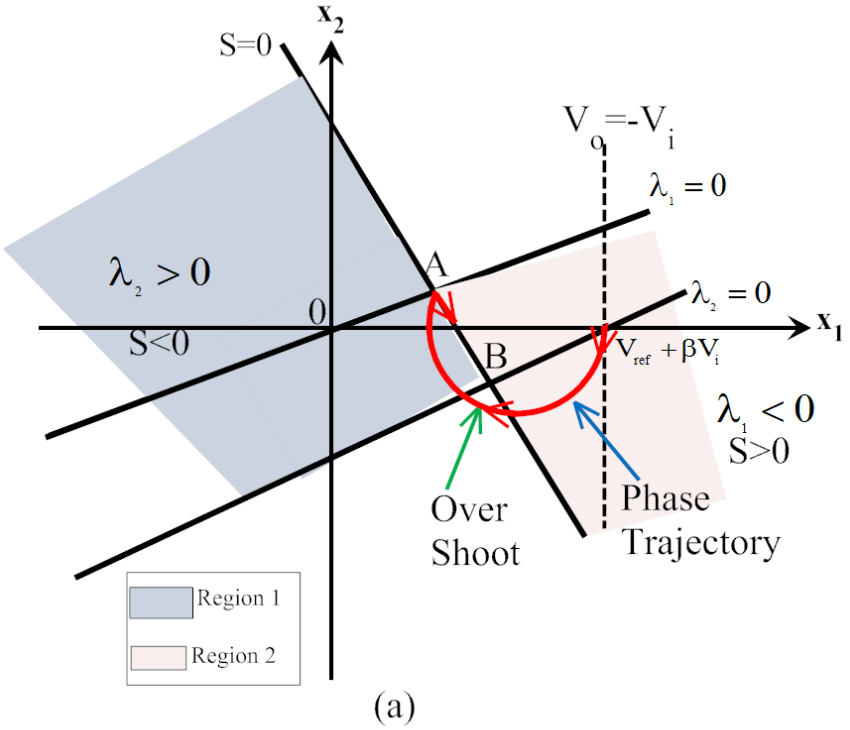

(a)

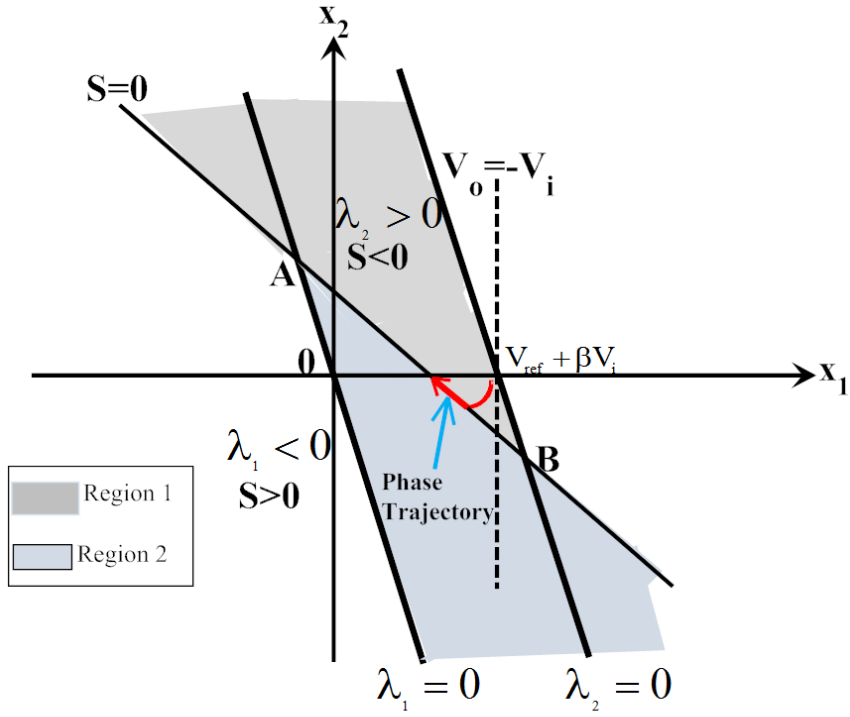

(b)

Figure 2.12: Regions of SM existence in phase plane a) $\frac{\alpha_1}{\alpha_2} > \frac{1}{R_L C}$, $\frac{\alpha_3}{\alpha_2} < \frac{-1}{LC}$ and b) $\frac{\alpha_1}{\alpha_2} < \frac{1}{R_L C}$, $\frac{\alpha_3}{\alpha_2} < \frac{-1}{LC}$

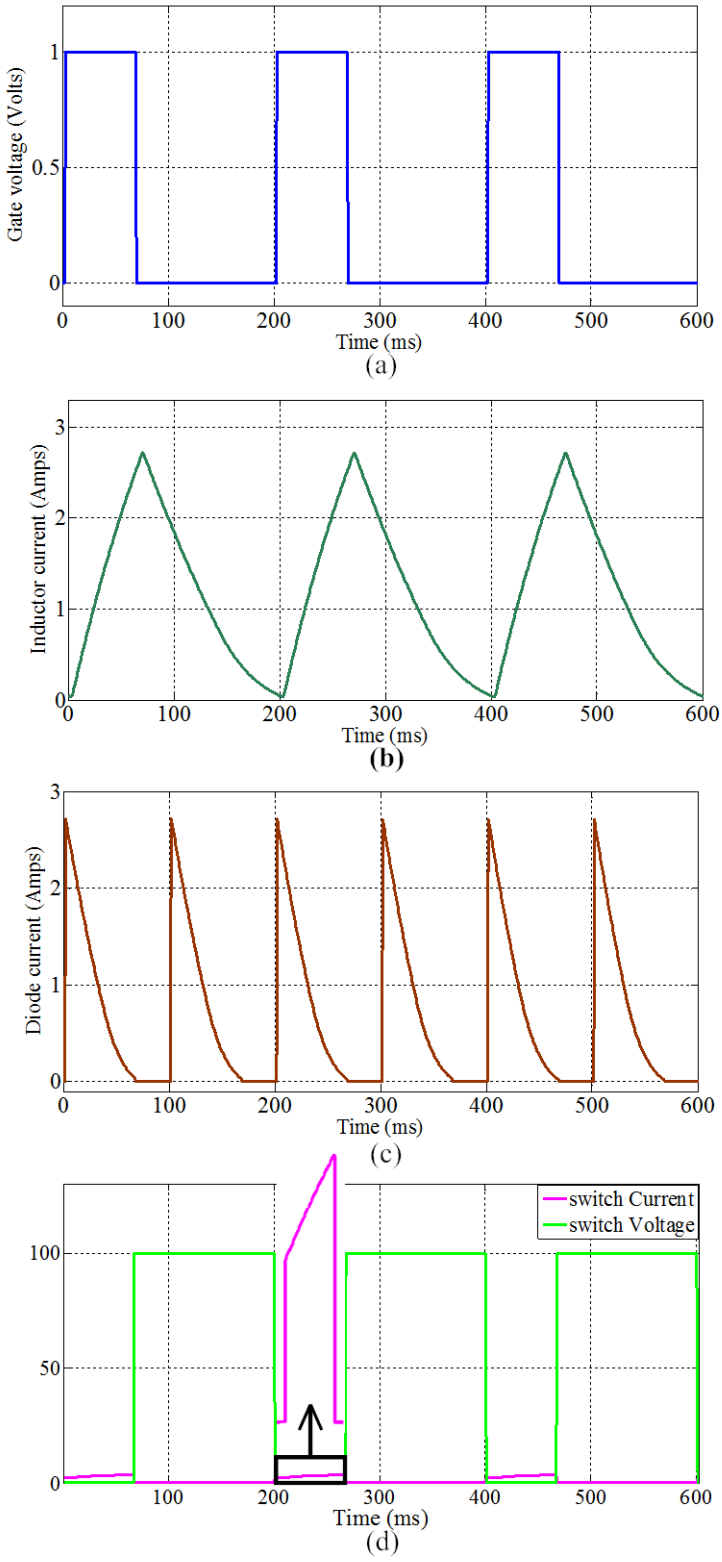

Figure 2.13: Outputs obtained from boost converter

2.5.3 Simulation Results

Fig. 2.13 shows the results of the boost converter. Fig. 2.13(a) shows the gate voltage of the converter. The inductor gets charged when switch is ON and thereby current increases linearly, when switch is OFF inductor gets discharged through the main diode of the boost converter is shown in Fig. 2.13(b). The diode current is shown in Fig. 2.13(c). The switch voltage and current waveforms of the boost converter are shown in Fig. 2.13(d). The results of both PI and ISMC MPPT controllers are shown in Fig. 2.14. Both PI and ISMC MPPT controller results are compared in Fig. 2.15.

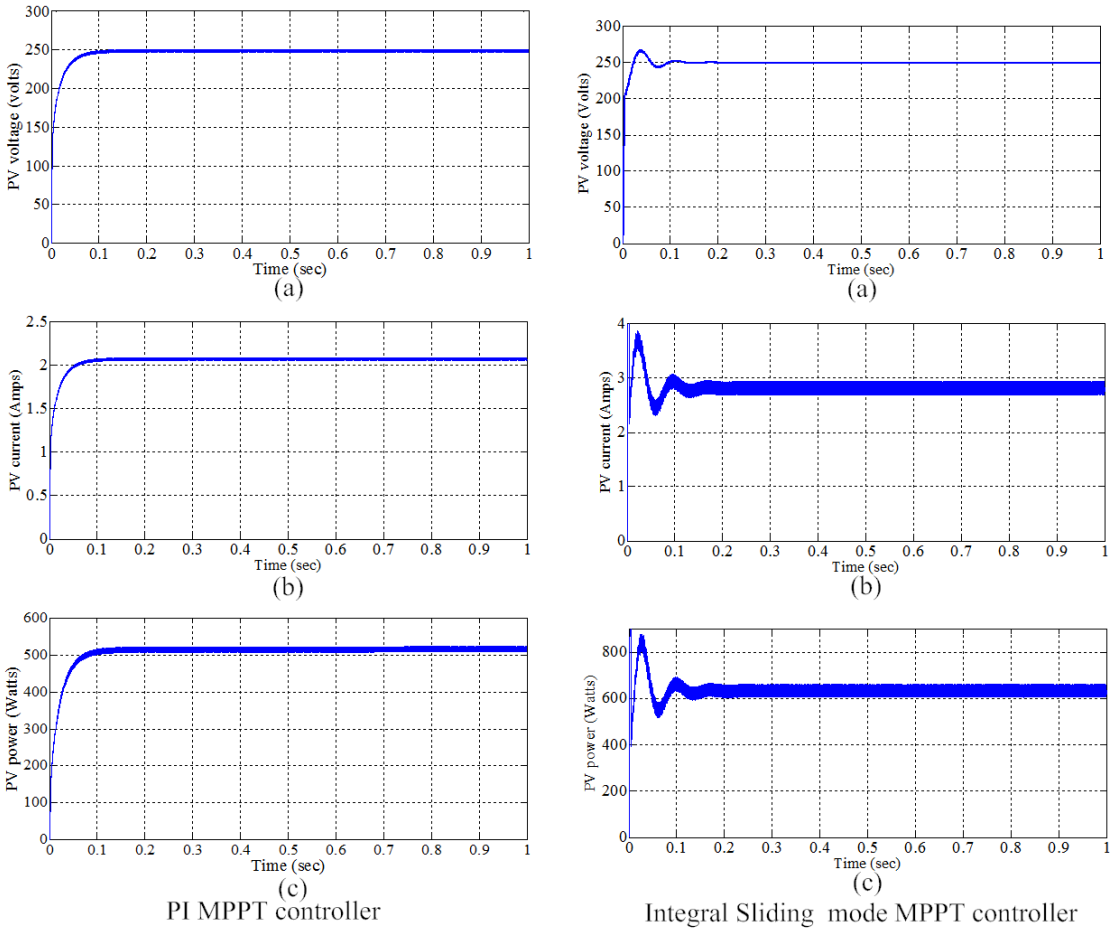

Figure 2.14: Simulation results of PI and modified ISMC MPPT controllers

Voltage is compared in Fig. 2.15(a), observed that the ISMC and PI MPPT controllers are tracking the voltage, but the steady state occured in ISMC is faster than the PI controller. Current is compared in Fig. 2.15(b), and observed that the ISMC is tracking around 0.5 A

more current than PI MPPT controller, but the steady state occured in PI controller faster than the ISMC controller. Power is compared in Fig. 2.15(c), and observed that the ISMC is tracking around 75 W more power than PI MPPT controller, but the steady state occured in PI controller little faster than the ISMC controller. Finally, one can observe that the ISMC is tracking more power than the existing PI controller.

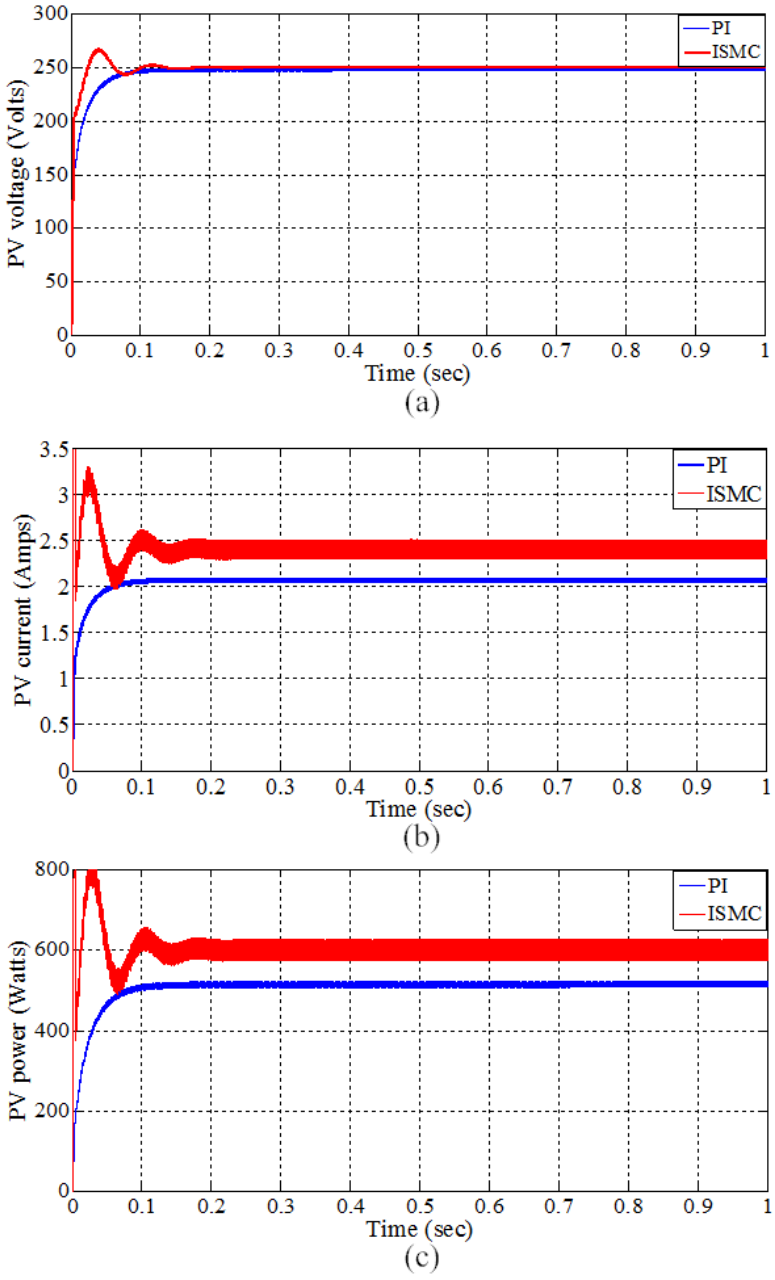

Figure 2.15: Simulation results comparison of PI and modified SMC MPPT controllers

2.6 MPPT control techniques

We have already discussed MPPT controllers with feedback. There are two approaches to implement MPPT controllers, such as feedback and feedforward. Among these two approaches feedforward approach is more popular [25], because the implemenatation is quite easier than feedback approach. In this section we proceed feedforward approach. The block diagrams of feedforward controllers are shown in Fig. 2.16(a). The switch ON/OFF conditions are shown in Fig. 2.16(b) and Fig. 2.16(c).

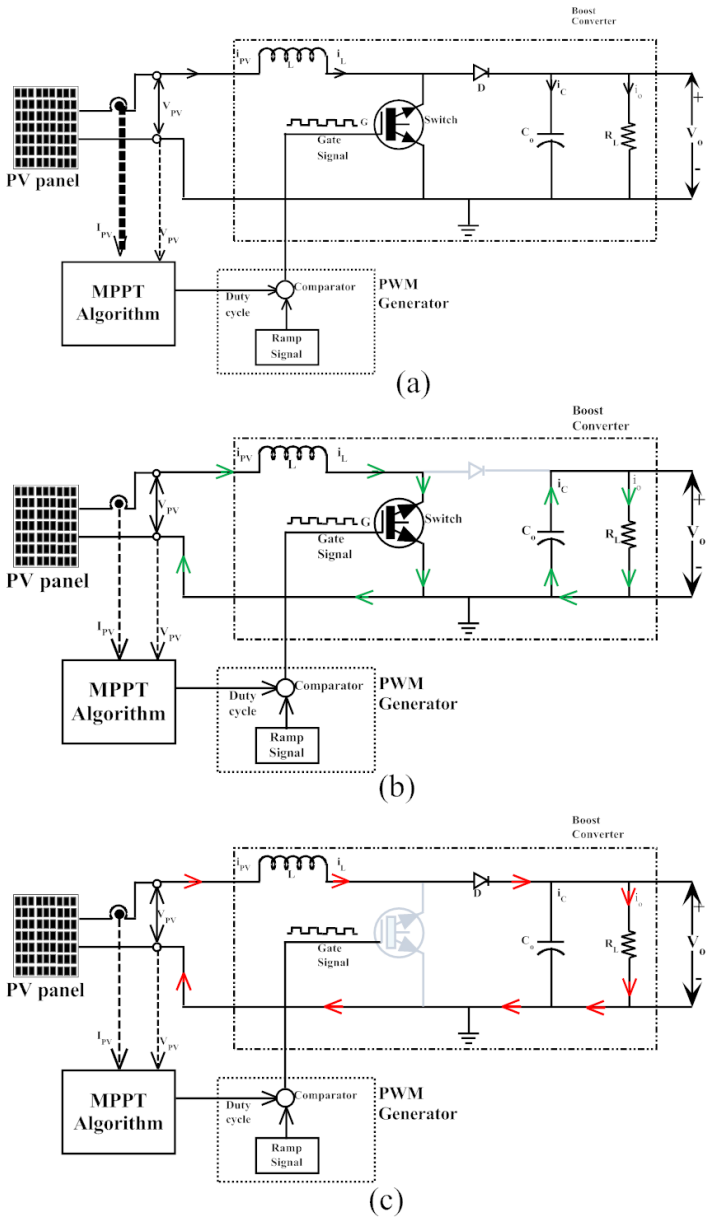

Figure 2.16: Block diagram of MPPT controller with PV panel and DC-DC boost converter

2.6.1 Incremental Conductance MPPT Controller

Incremental conductance (Inc Cond) MPPT controller algorithm with a fixed step size tracks MPP accurately and tracking speed is high, when compared to the other MPPT techniques. The controller is connected in an open loop [20]. A DC-DC boost converter is connected in between the PV panels and load to regulate the PV output voltage. The controller measures the incremental changes in PV array current and voltage to predict the effect of voltage change. This method utilizes incremental conductance (dI/dV) of a PV array to compute the sign of change in power with respect to voltage (dP/dV). Inc Cond MPPT control algorithm is shown in Fig. 2.17.

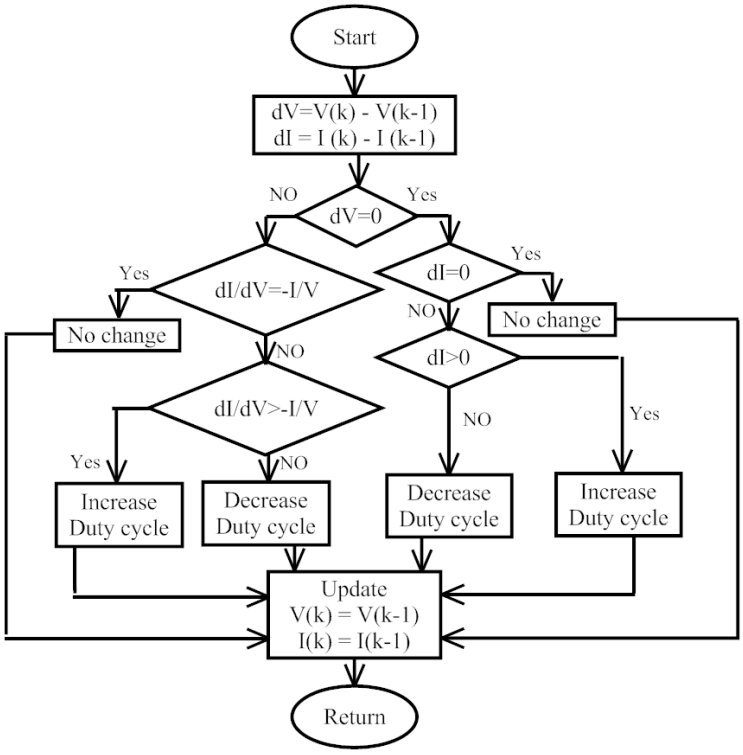

Figure 2.17: Flowchart model of Inc Cond MPPT algorithm

The Inc Cond controller compares incremental conductance (dI/dV) to array conductance (I/V), and when the difference of these two is zero then that voltage is MPP voltage, and the corresponding current is MPP current. Inc Cond controller maintains the MPP voltage until the irradiation changes and the process is repeated. MPP is located at the knee of the I-V curve, where the resistance is equal to the negative of differential

resistance [18].

$$\frac{dV}{dI} = -\frac{V}{I} \tag{2.60}$$

The slope of the PV curve at MPP is equal to zero.

$$\frac{dP}{dV} = 0 \tag{2.61}$$

After mathematical calculations on equation(2.61), the final equation is as follows

$$I + V\frac{dI}{dV} = 0 \tag{2.62}$$

Based on equation (2.60) and equation (2.61) if any small error occurs then, equation (2.62) becomes

$$I + V\frac{dI}{dV} = e \tag{2.63}$$

2.6.2 Perturb & Observe (P&O) MPPT controller

The Perturb and Observe algorithm operates periodically perturbing the control variable and comparing the PV output power immediately. In an initial P&O MPPT controller using P&O method the adjustment of the operating point is achieved by changing the reference voltage of the controller [51]. The adjustment can be made through the duty cycle D. The block diagram of P&O MPPT with a PV system is shown in Fig. 2.18, and algorithm is shown in Fig. 2.19.

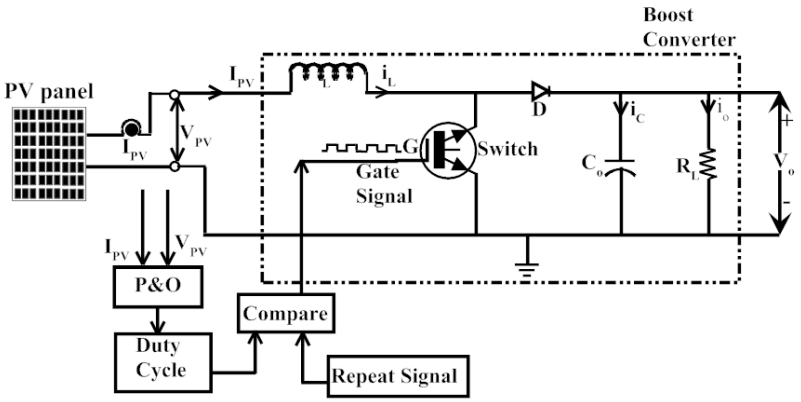

Figure 2.18: Block diagram of a PV system with P&O MPPT

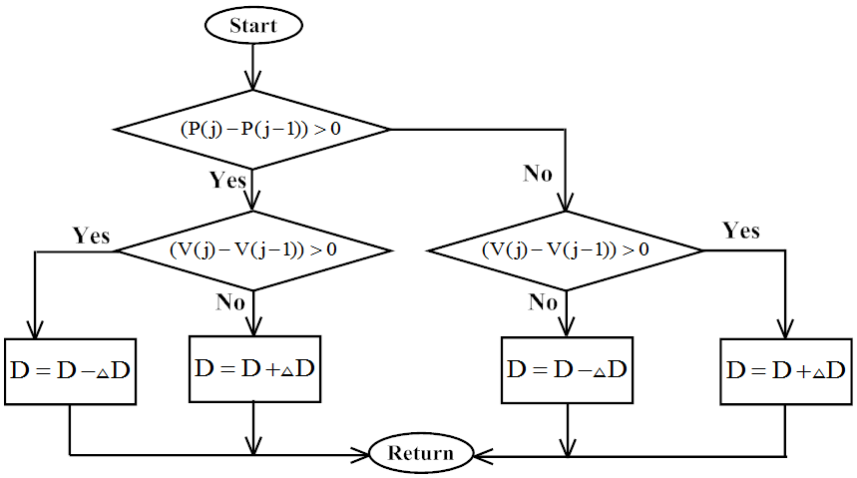

Figure 2.19: Flowchart model of perturb & observe MPPT algorithm

Note that P(j) and V(j) are the output power and voltage of PV. The power can be calculated from V(j) x I(j) at jth time. D and ΔD are the duty ratio and change in duty ratio. In-order to attain faster and precise MPPT response under standard test conditions, variable step size perturbation (ΔD) can be required. This will be selected as a function of PV power, denoted as follows:

$$\Delta D(j) = \alpha.\beta\left[P(j) - P(j-1)\right] \tag{2.64}$$

where α and β are the constant values to control the movement towards MPPT, it depends on perturbation direction.

2.6.3 Modified P&O MPPT controller

Fig. 2.20 shows the flowchart of the modified Perturb & Observe (P&O) MPPT algorithm. Implementation of the algorithm is very simple, and all variables are initialized at the beginning. The algorithm changes the duty cycle accoring to the maximum power point tracking. In this algorithm, the MPPT occurs based on calcultations of variation in power and variation in voltage. The duty cycle values will be changed at the end of the algorithm. The P&O algorithm perturbs the voltage in one direction and evaluates the corresponding difference of the power [18]. If the power is increasing, then the algorithm will move the voltage in the same direction till the peak power. After the peak power occurred, the perturbation will reverses the direction, which means, the P&O MPPT algorithm can track

the maximum power point (MPP) in the wrong direction also [51]. The P&O algorithm is optimized with respect to the change in step size, ΔD in order to follow certain irradiance. Here, value of step size is chosen directly by different initializations at the starting of the algorithm, therefore, no more calculations are required to set duty cycle always within the range. In this algorithm the duty cycle varies with respect to the change in temperature. That means, this is best suited for standard test conditions.

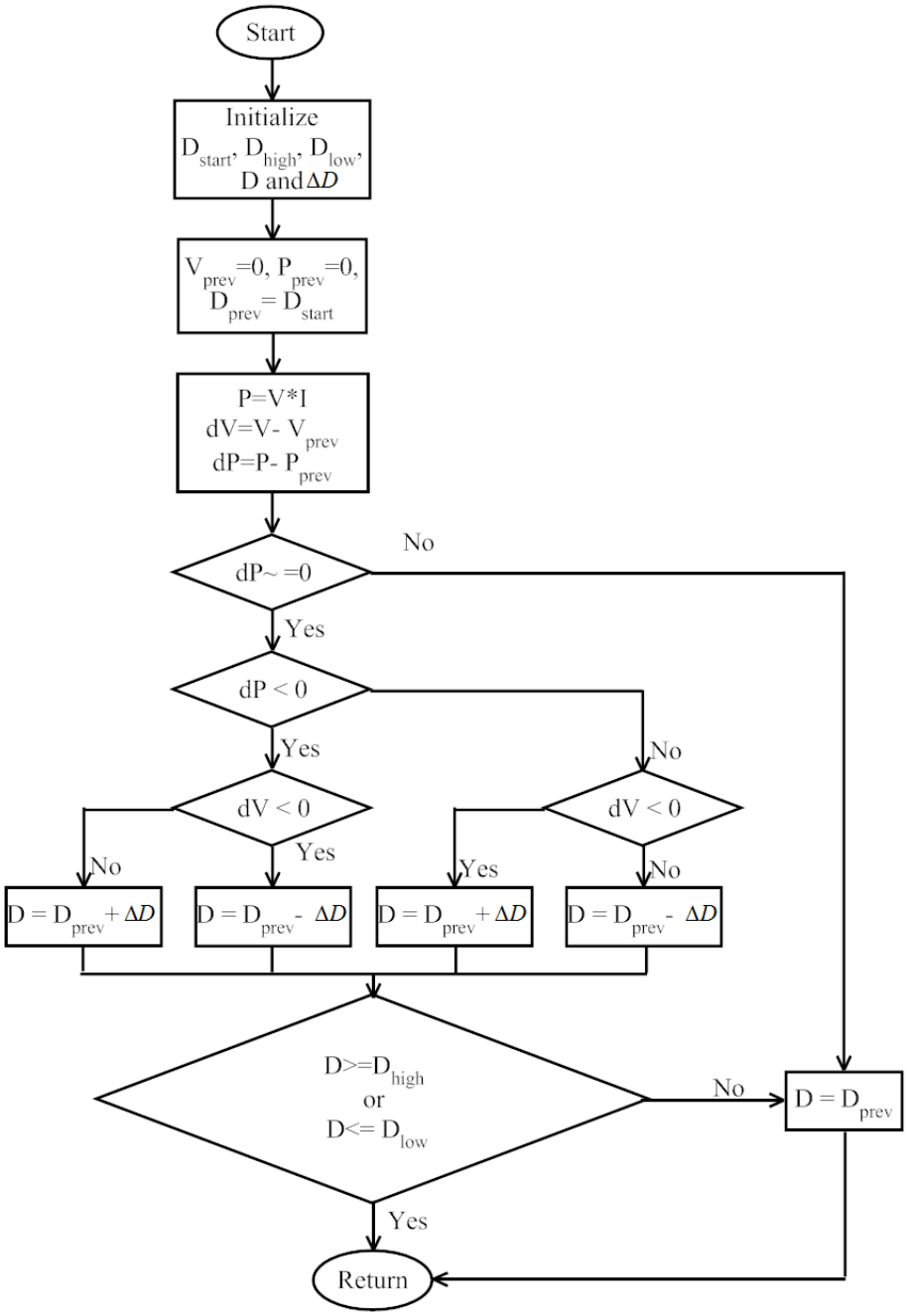

Figure 2.20: Flowchart model of modified perturb & observe MPPT algorithm

The algorithm execution steps are follows:

- Initialization of different duty cycle conditions such as D_{start}, D_{high}, D_{low} and calculate the change in duty cycle (ΔD) with the initial values. Fix the V_{prev} and P_{prev} as zero and D_{prev} as D_{start}. Calculate power, change in power (dP) and change in voltage (dV) when the algorithm start its execution.

- Check the conditon of change in power, if it is equal to zero, then no change in the duty cycle, otherwise, check the change in power is positive or negative.

- If the change in power is positive, then check the change in voltage is positive or negative and then fix the duty cycle. Likewise, check the condition for change in power is negative and then check the change in voltage is positive or negative and then fix the duty cycle (this duty cycle should be in the specified range).

- If the duty cycle is not in the given range, then change the duty cycle with initial condition and repeat the above process.

2.6.4 Simulation Results

Inc Cond and P&O MPPT controller simulation results are shown in Fig. 2.21. From Fig. 2.21, one can observe that the Inc Cond MPPT controller is tracking little more power than the existing P&O MPPT controller. The modified P&O MPPT controller and comparision all feedforward MPPT controller results are shown in Fig.2.28. The voltage comparison of all (Inc Cond, P&O and modified P&O) feed forward MPPT controllers are shown in Fig. 2.22(a), observed that the modified P&O MPPT controller is tracking more voltage than the conventional MPPT controllers. Current is compared in Fig. 2.22(b), and observed that the proposed P&O MPPT controller is tracking less current than the conventional MPPT controllers. Power is compared in Fig. 2.22(c), and observed that the modified P&O MPPT controller is tracking around 90 W more power than conventional MPPT controllers. In all the cases, steady state occured is faster in modified P&O MPPT controller than Inc Cond and P&O MPPT controllers.

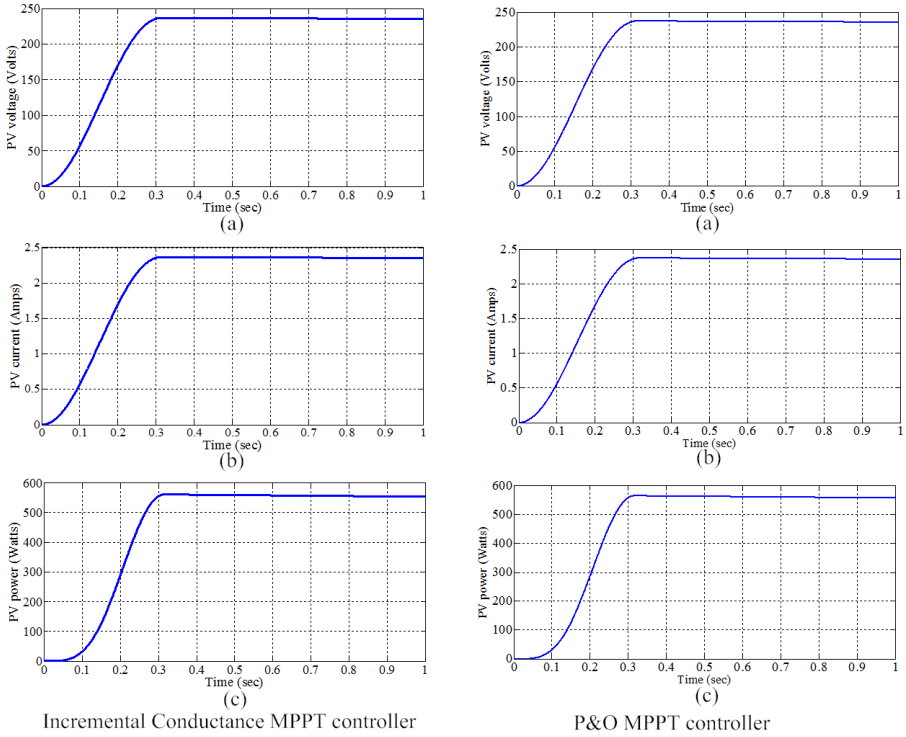

Figure 2.21: Simulation results of Inc Cond and P&O MPPT controllers

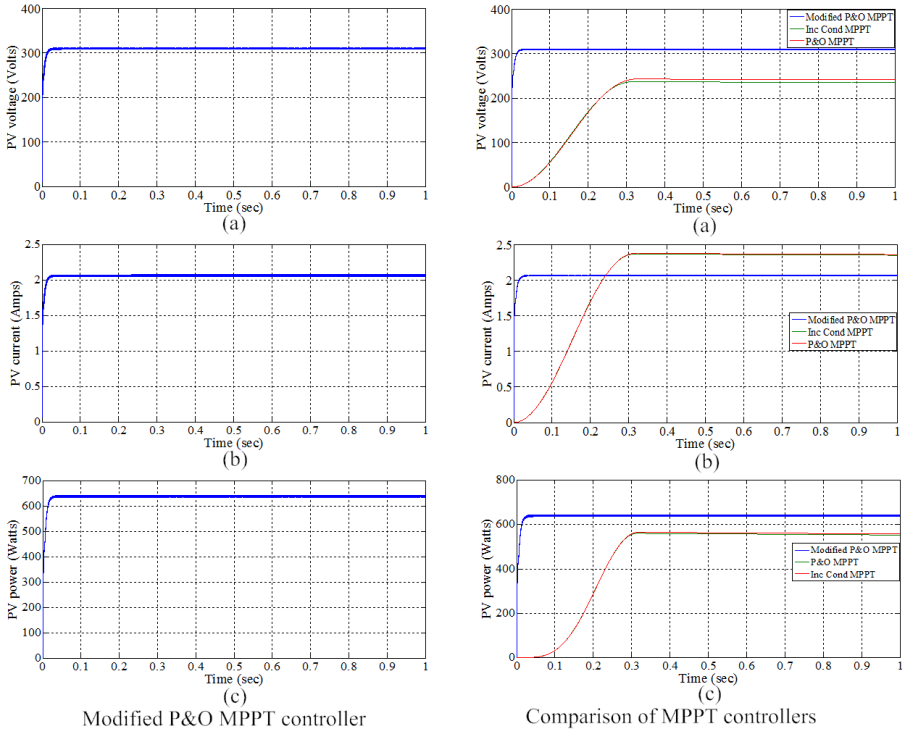

Figure 2.22: Simulation results of modified P&O and all feedforward MPPT controllers

Finally, the feedback and feedforward MPPT controller results are compared, and is shown in Fig. 2.23. From the results, the modified P&O and ISMC MPPT controllers are tracking more voltage and power than the existing MPPT controllers. Reaching the steady state condition in proposed controller is faster than the conventional controllers. From the aforesaid points, the proposed controllers are well suited for standard test conditions.

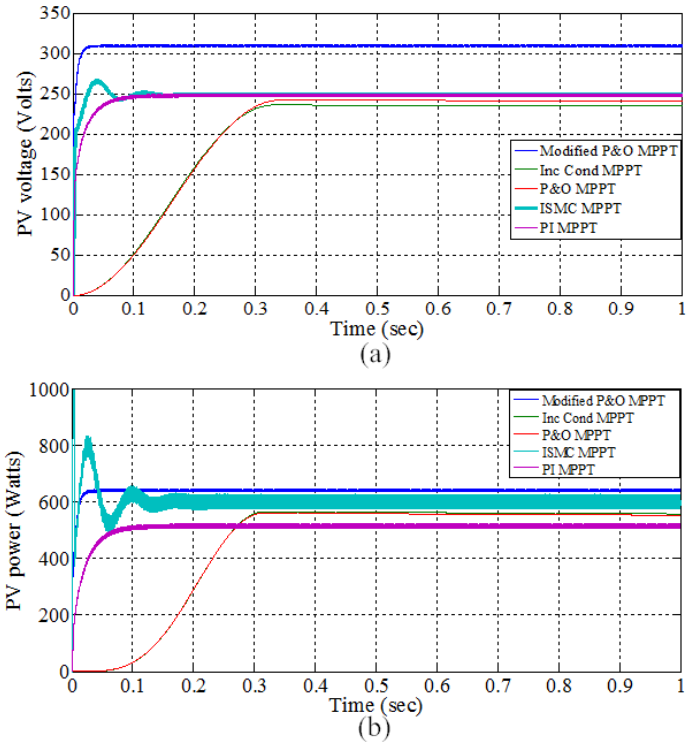

Figure 2.23: Simulation results comparison of all MPPT controllers

2.7 Real Time Digital Simulator (Opal-RT) platform

In order to justify the results obtained by simulation, the model has been tested using opal-RT. RTDS permits the users to simulate the electrical power system models with precision and this method is quiet efficient [91]. The RTDS simulator not only runs in real time but also tests the physical protection and control structure of the model. This gives the users to test and prove their prototype and final products in a pragmatic and practical environment [92]. Being a digital power system simulator, the RTDS is able to perform simulation with a typical time step of 50 μs [93] and operates in a continuous real time

approach. The RTDS simulator meets the dead line within the specified time for every simulation. In order to relate with the simulated power system, it is perfect for testing, designing, and advancement of power system shielding and control methods with a huge competence for digital and analog signal exchange together.

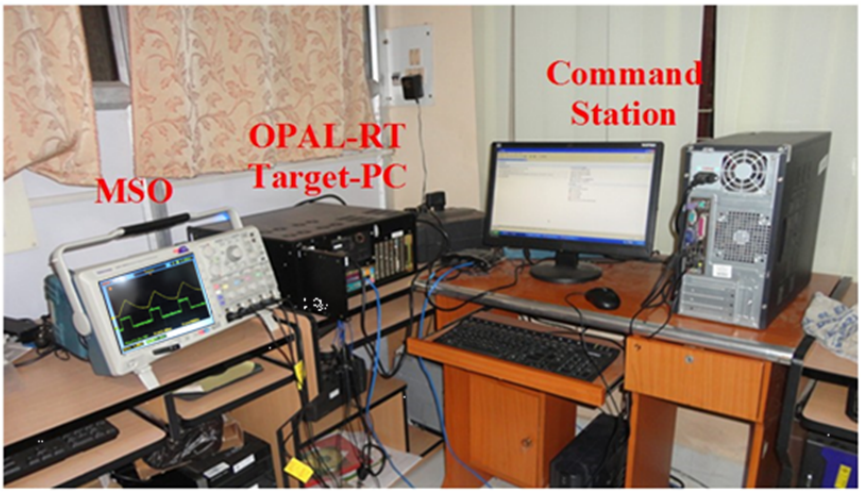

Figure 2.24: Picture of RTDS hardware implementation

The RTDS consists of two main tools, these are 1) for a PC-cluster to execute simulink block diagrams, real time distributed simulation package (RT-LAB), and 2) algorithmic toolboxes intended for the fixed-timestep simulation of electric circuits along with its controllers [94]. Being acknowledged as a vital tool for engineering design, Real-time simulation and Hardware-In-the- Loop (HIL) applications are particularly intended for power electronics and electrical systems [95]. On behalf of power system components and network equations, the mathematical calculations are executed based on Opal-RT simulation system by means of either a Wanda 3U module or Wanda 4U module. The intended PC is communicated through a PCI-Express ultra-low-latency real-time bus interface [89]. The picture of RTDS hardware implementation is shown in Fig. 2.24. The simulated results are validated through Opal-RT results. The real time hardware results of DC-DC boost converter generated by using RTDS hardware are shown in Fig. 2.25. The Opal-RT results of PI MPPT and modified SMC MPPT controllers are shown in Fig. 2.26 and Fig. 2.27. The Opal-RT results of Inc Cond MPPT, P&O MPPT, modified P&O MPPT controllers are shown in Fig. 2.28, Fig. 2.29, and Fig. 2.30 respectively.

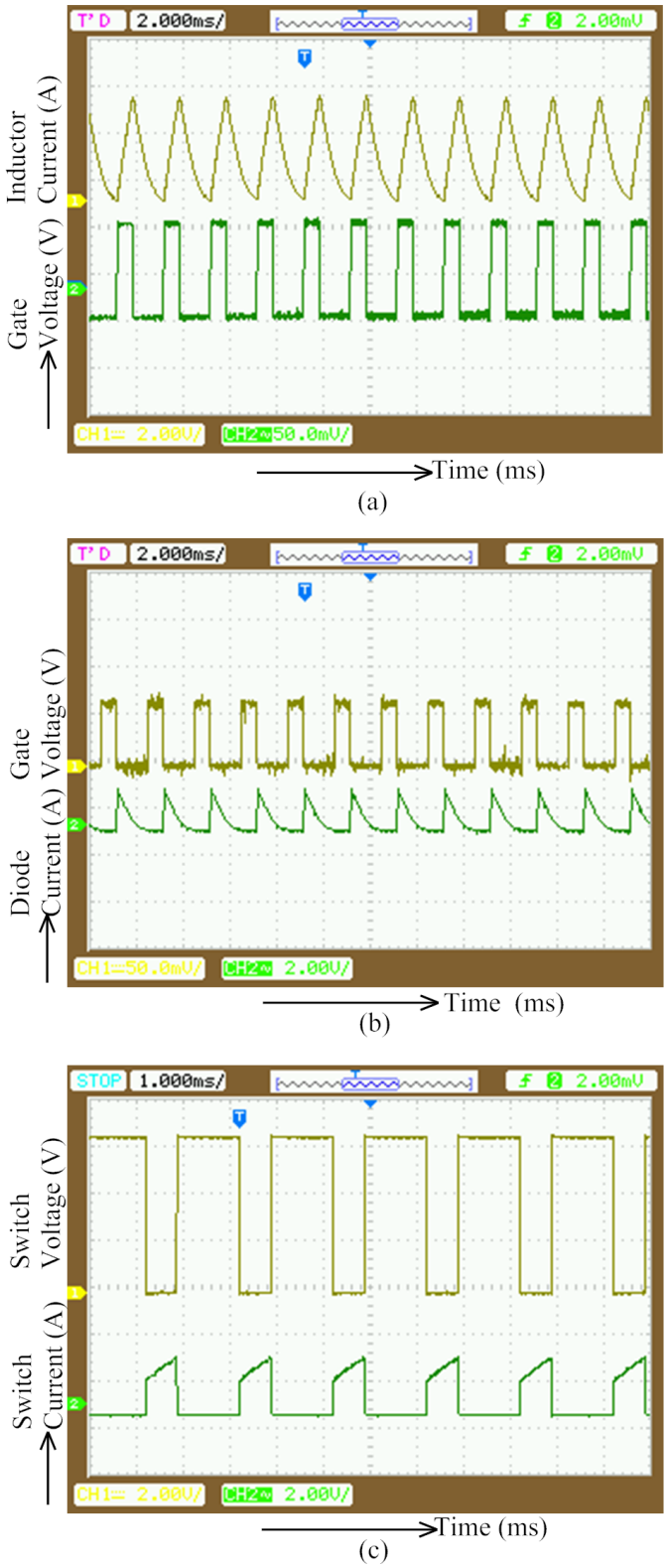

Figure 2.25: Opal-RT results of Boost converter

The Opal-RT results of PI MPPT controller is shown in Fig. 2.26. PV output voltage is shown in Fig. 2.26(a), observed that the PI MPPT controller is tracking 250 V. PV output current is shown in Fig. 2.26(b), observed that the PI MPPT controller is tracking 2.1 A. PV output power is shown in Fig. 2.26(c), and observed that the PI MPPT controller is tracking 525 W. Simulation results and Opal-RT results are matched.

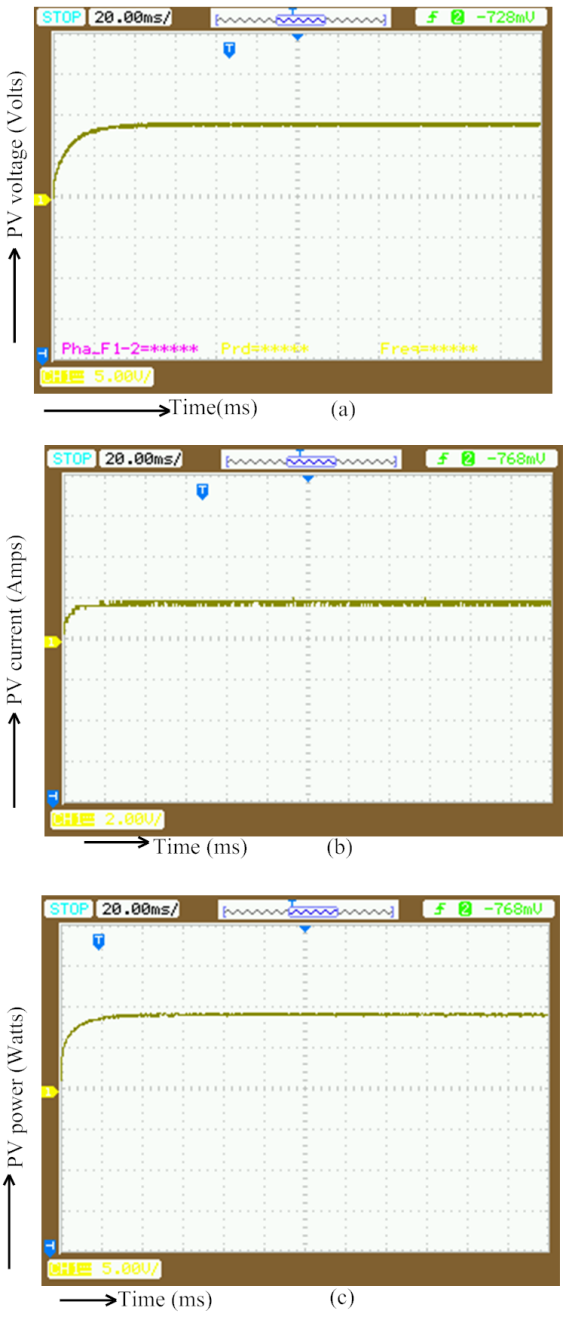

Figure 2.26: Opal-RT results with PI MPPT controller

The Opal-RT results of ISMC MPPT controller is shown in Fig. 2.27. PV output voltage is shown in Fig. 2.27(a), observed that the ISMC MPPT controller is tracking 250 V. PV output current is shown in Fig. 2.27(b), observed that the ISMC MPPT controller is tracking 2.5 A. PV output power is shown in Fig. 2.27(c), and observed that the ISMC MPPT controller is tracking around 600 W. Simulation results and Opal-RT results are matched.

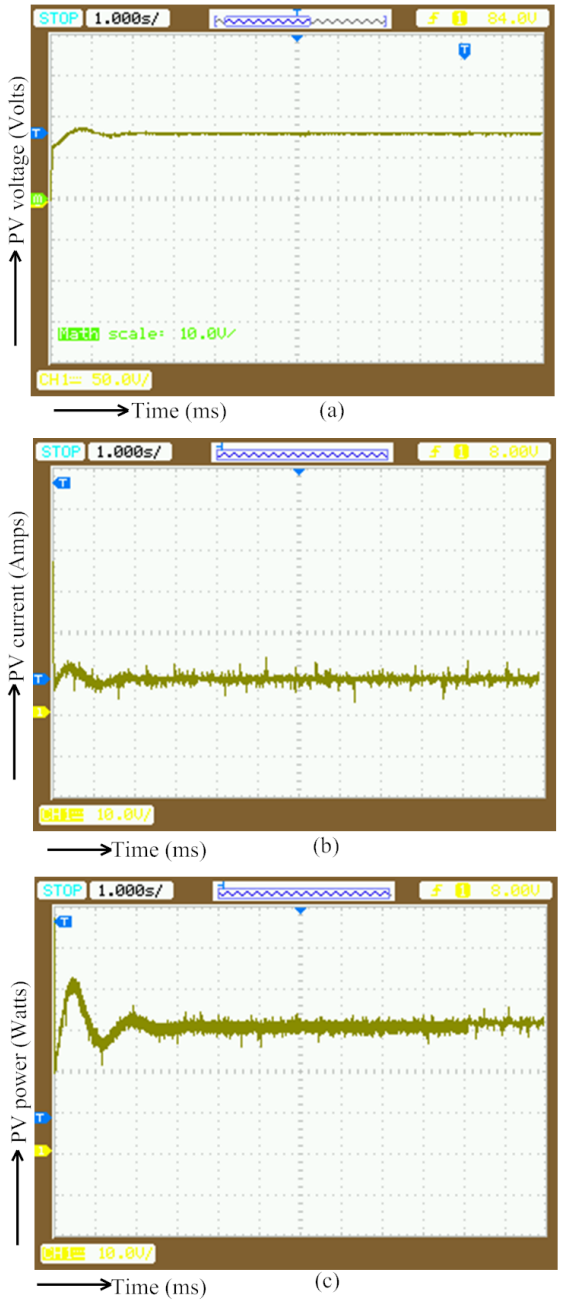

Figure 2.27: Opal-RT results of modified Sliding mode MPPT controller

The Opal-RT results of Inc Cond MPPT controller is shown in Fig. 2.28. PV output voltage is shown in Fig. 2.28(a), observed that the Inc Cond MPPT controller is tracking 235 V. PV output current is shown in Fig. 2.28(b), observed that the Inc Cond MPPT controller is tracking 2.4 A. PV output power is shown in Fig. 2.28(c), and observed that the Inc Cond MPPT controller is tracking around 560 W. Simulation results and Opal-RT results are matched.

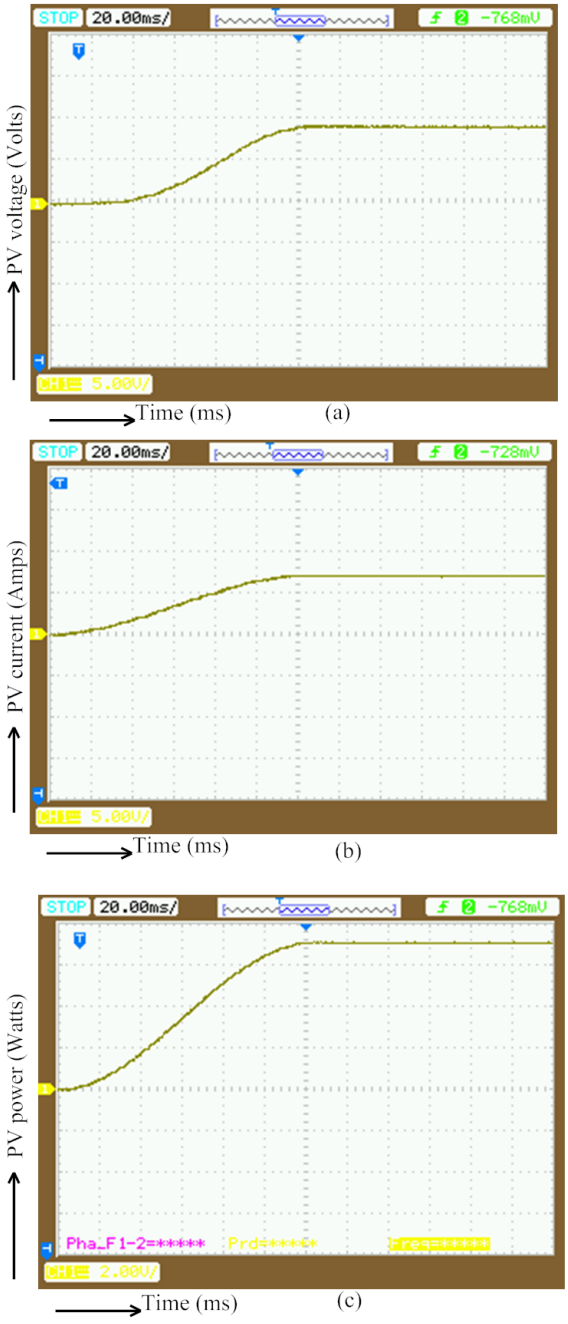

Figure 2.28: Opal-RT results of incremental conductance MPPT controller

The Opal-RT results of PI MPPT controller is shown in Fig. 2.29. PV output voltage is shown in Fig. 2.29(a), observed that the P&O MPPT controller is tracking 230 V. PV output current is shown in Fig. 2.29(b), observed that the P&O MPPT controller is tracking 2.35 A. PV output power is shown in Fig. 2.29(c), and observed that the P&O MPPT controller is tracking around 540 W. Simulation results and Opal-RT results are matched.

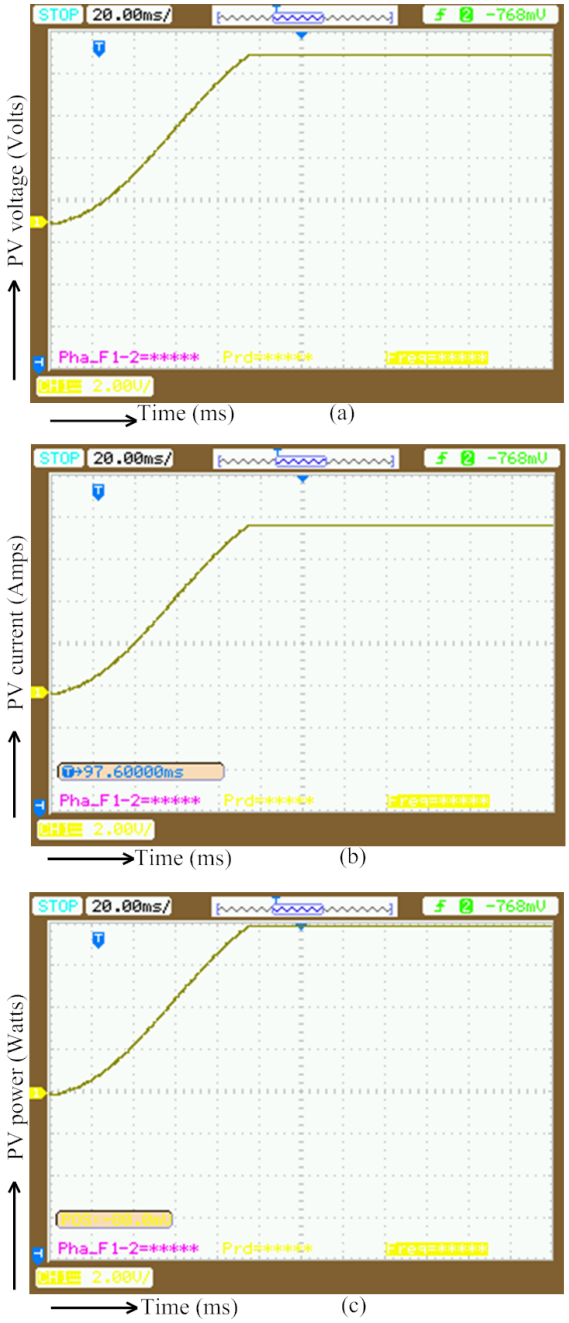

Figure 2.29: Opal-RT results of P&O MPPT controller

The Opal-RT results of PI MPPT controller is shown in Fig. 2.30. PV output voltage is shown in Fig. 2.30(a), observed that the P&O MPPT controller is tracking 310 V. PV output current is shown in Fig. 2.30(b), observed that the P&O MPPT controller is tracking 2.1 A. PV output power is shown in Fig. 2.30(c), and observed that the P&O MPPT controller is tracking around 650 W. Simulation results and Opal-RT results are matched.

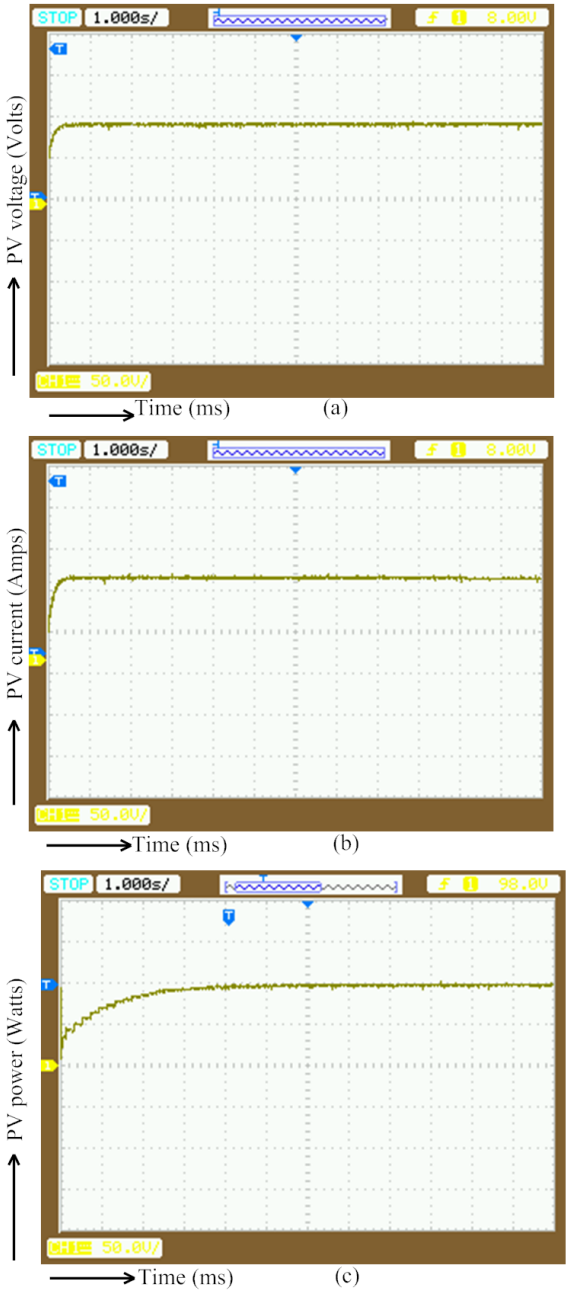

Figure 2.30: Opal-RT results of modified P&O MPPT controller

2.8 Experimental results and analysis

Fig. 2.31 shows the picture of hardware setup for a PV system at standard test conditions. The brief introduction about the setup is described in this section (complete description is presented in chapter 3).

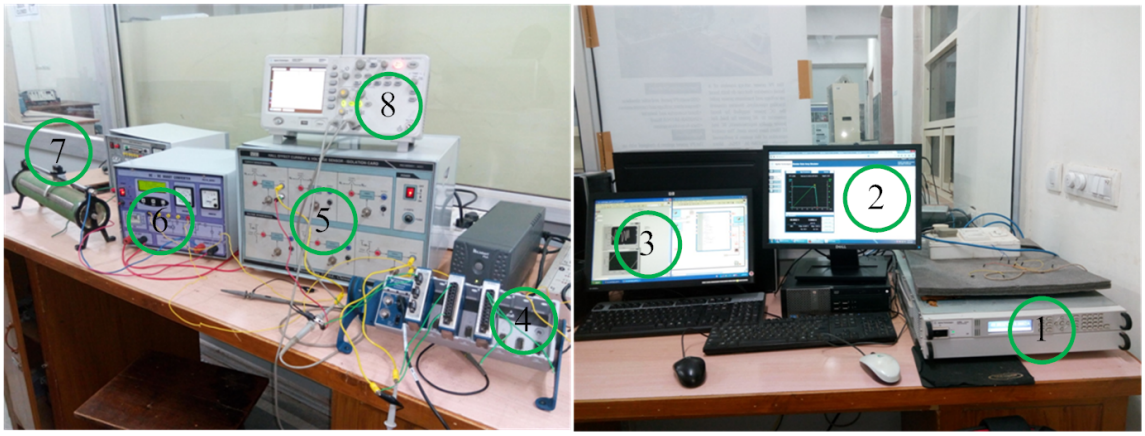

1) Agilent Solar Array Simulator (E4360A)
2) PC connected to SAS
3) PC for Control Algorithm (LabView)
4) cRIO-9014
5) Hall Effect Sensor device
6) DC-DC boost converter
7) Load
8) D S O

Figure 2.31: Experimental setup

2.8.1 SAS simulator

The E4360A standard Solar Array Simulator (SAS) is a dual output programmable dc power source, which emulates the I-V and P-V characteristic curves of different arrays under various weather conditions like partial shading, full shading, rotation and temperature. It is a current source with low output capacitance, and provides 1200 W output in a small 2U-high mainframe with two channels (each channel can provide 600W output). The size of SAS simulator is small and can save high power. The SAS simulator is a full turn-key SAS system configured to exact specifications. The simulator operates in three different modes namely fixed mode, SAS mode and Table mode. The experiment requires single peak characteristic curves after which the SAS mode can be used. Table mode is used when the user requires multiple peaks evaluating partial shading condition (PSC). Two possibilities to connect a PC with simulator are LAN and GPIB USB 2.0 interface. One can access the simulator remotely through built in web server as well.

2.8.2 Compact Reconfigurable Input/ Output (cRIO)

National Instruments (NI) compact Reconfigurable Input/Output (cRIO) is a small industrial control and acquisition system, and is a reconfigurable input/output FPGA technology for customization and high performance. It integrates a real-time processor and reconfigurable FPGA for stand-alone or distributed embedded applications. The I/O modules can swap the positions easily with built-in signal conditioning of sensors and actuators. With this NI- cRIO, one can rapidly build embedded control or acquisition systems that rival the performance and optimization of custom-designed hardware circuitry. cRIO embedded systems are developed using LabVIEW, LabVIEW Real-Time (RT) Module and LabVIEW FPGA Module. The Hall Effect sensor device contains current and voltage sensors, and senses high voltage as input and gives the low voltage as output. By using these sensors one can take the readings in DSO or CRO or MSO. The SAS simulator is connected to a PC by using Local Area Network (LAN) for remote operation with the help of web browser to check the output characteristics. The control algorithm is implemented with LabView in another PC. The output of the simulator is connected to a sensor device as well as boost converter. The sensors outputs are connected to cRIO input modules which are mentioned in the control strategy. PWM generation is required for the boost converter operation, so, these signals are given from the output module of cRIO. Finally, load is connected to the boost converter and results are taken from DSO or CRO.

Solar simulator outputs with different controllers are shown in Fig. 2.32. When the control algorithm is not running, the MPPT tracking is showing 0% as shown in Fig. 2.32(a) and after running the Inc Cond MPPT control algorithm; it tracks the MPPT and is shown in Fig. 2.32(b). The P&O MPPT and modified P&O control algorithms outputs along with its MPP tracking are shown in Fig. 2.33(a) and Fig. 2.33(b).

Different FPGA based control techniques such as Incremental Conductance, P&O and modified P&O has been implemented by using NI-cRIO 9014 platform. The NI-cRIO 9014 based FPGA controller implementation simplifies the control circuit and adds flexibility to the system. The experimental results of different MPPT controllers such as Inc Cond, *P&O* and modified *P&O* are shown in Fig. 2.34. PV voltage, current and power are collected from each controller. These results are taken from PV (i.e., before boost converter).

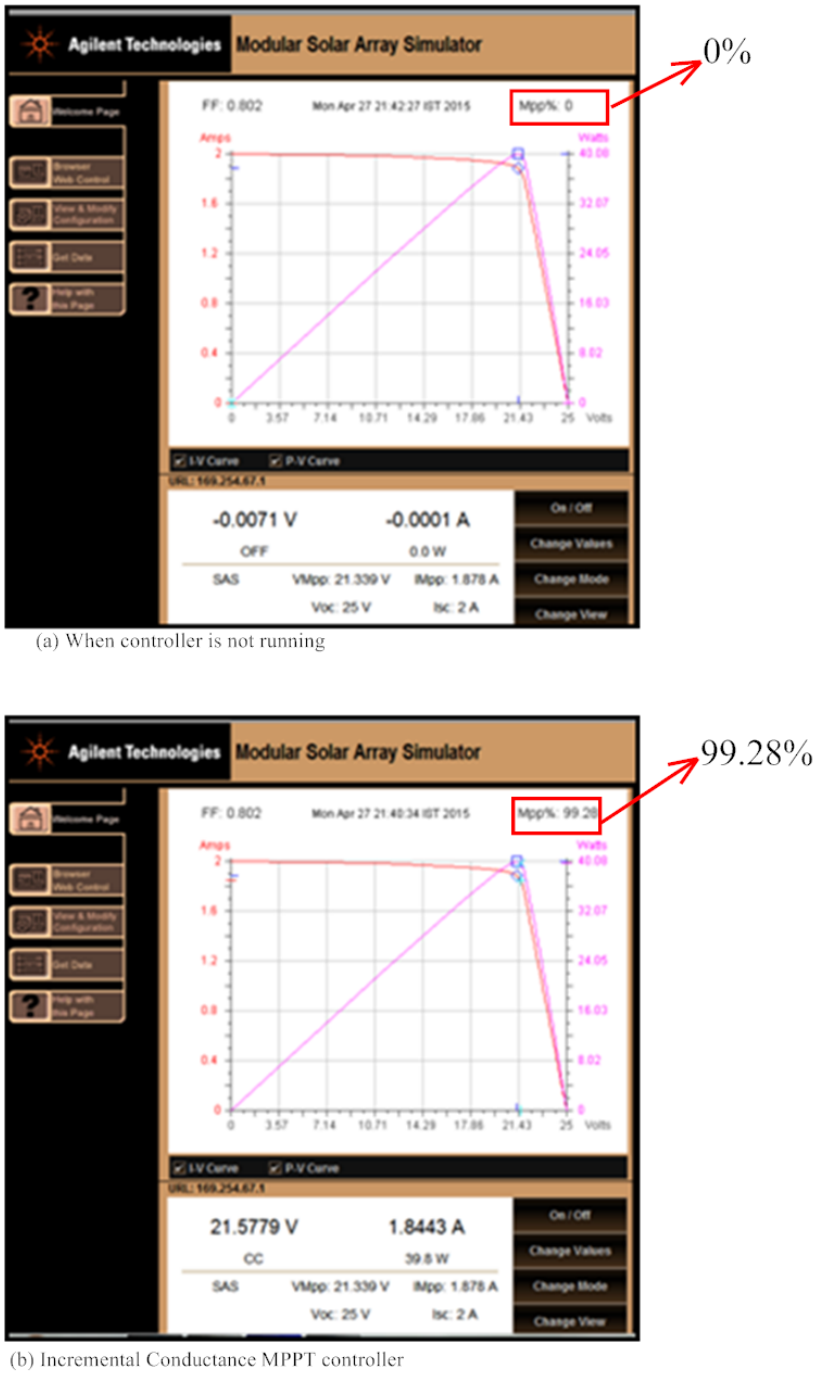

(a) When controller is not running

(b) Incremental Conductance MPPT controller

Figure 2.32: SAS simulator outputs

The experimental results of different MPPT controllers such as Inc Cond, *P&O* and modified *P&O* are shown in Fig. 2.35. PV voltage, current and power are collected from each controller. These results are taken from PV (i.e., after boost converter). The tracking values of simulation, Opal-RT and experimental results are same.

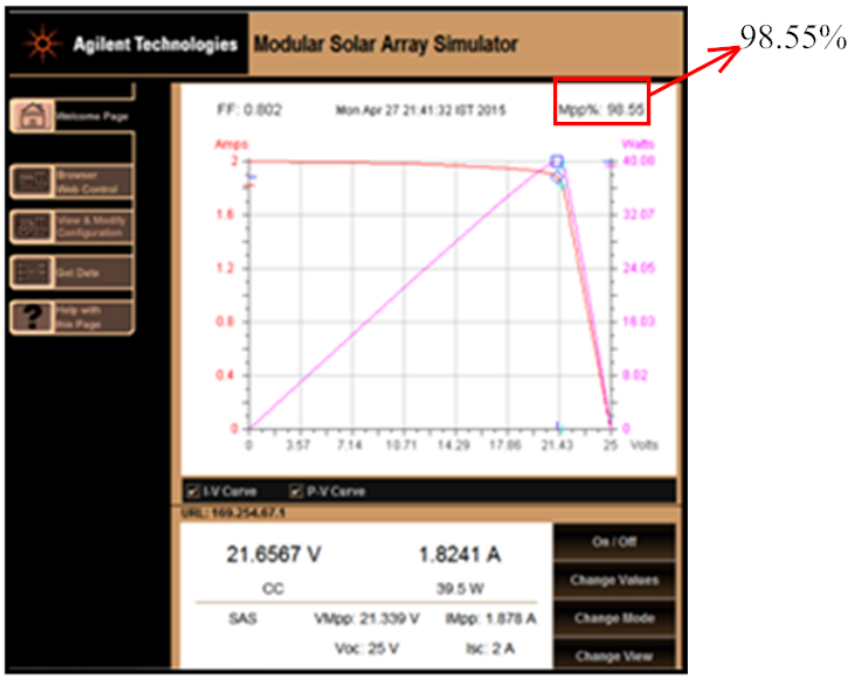

(a) P&O MPPT controller

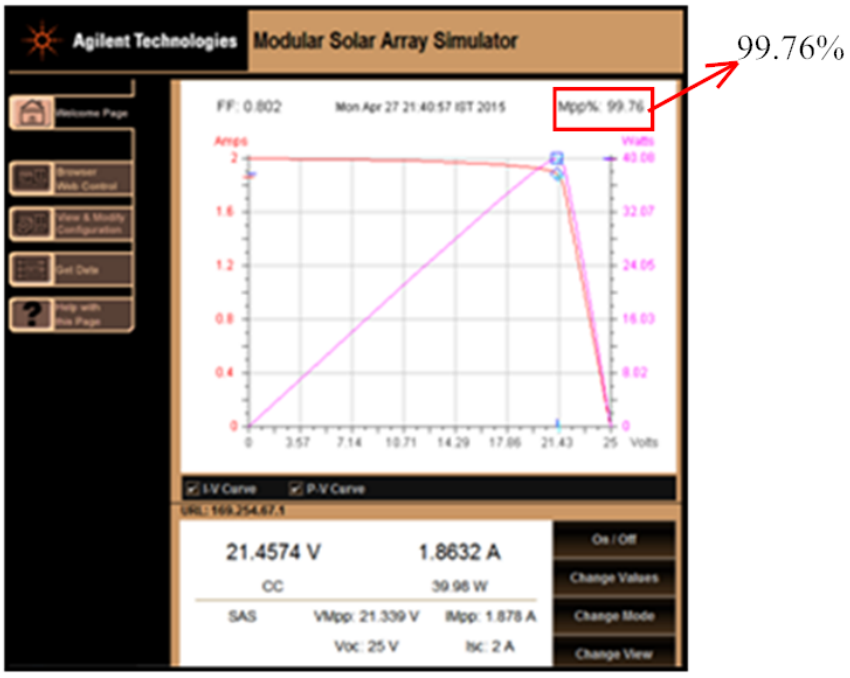

(b) Modified P&O MPPT controller

Figure 2.33: SAS simulator outputs

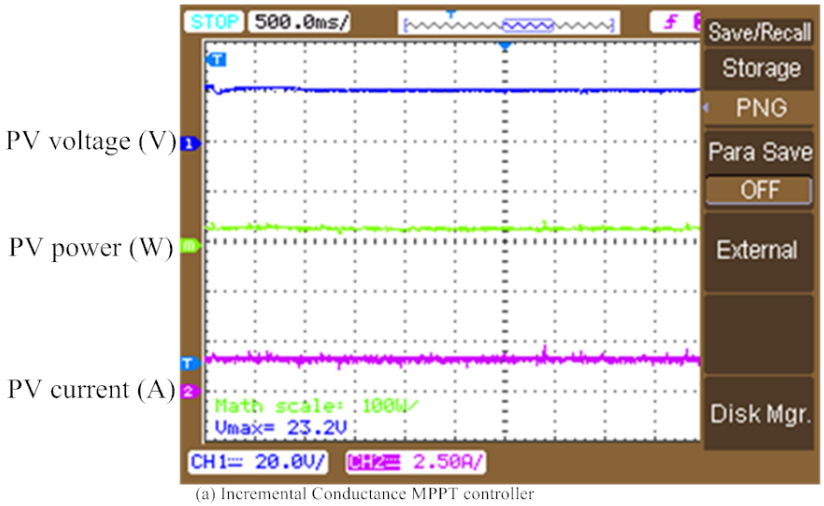

(a) Incremental Conductance MPPT controller

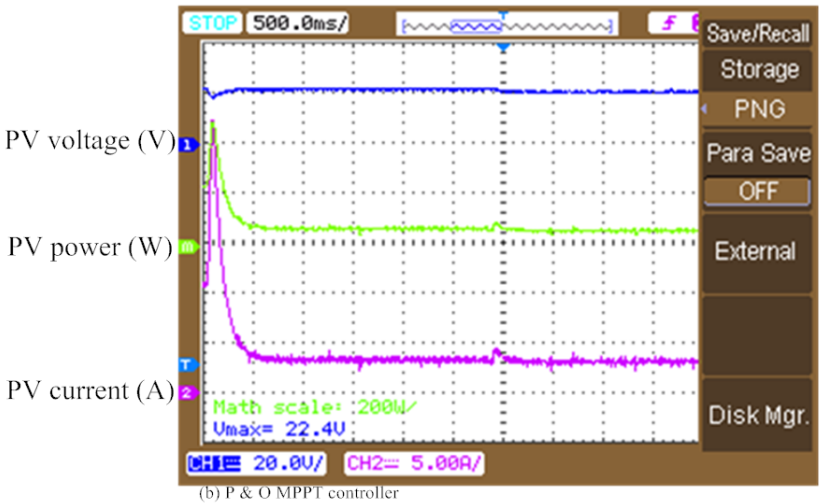

(b) P & O MPPT controller

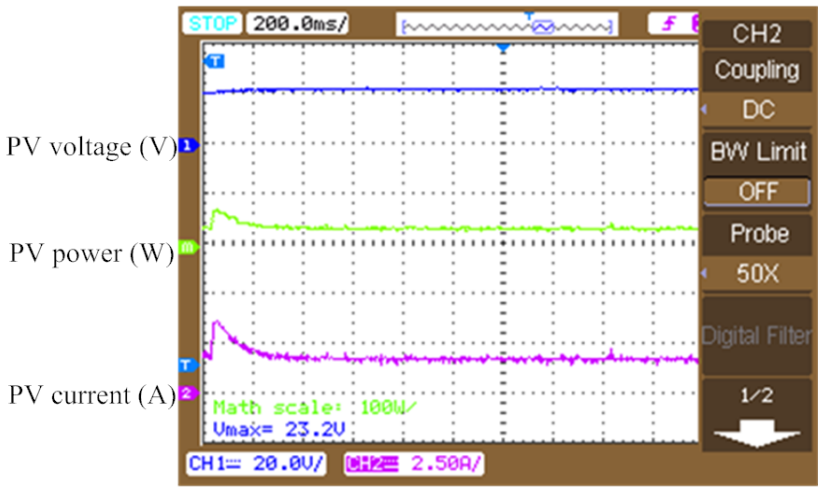

(c) Modified P & O MPPT controller

Figure 2.34: Experimental results before boost converter

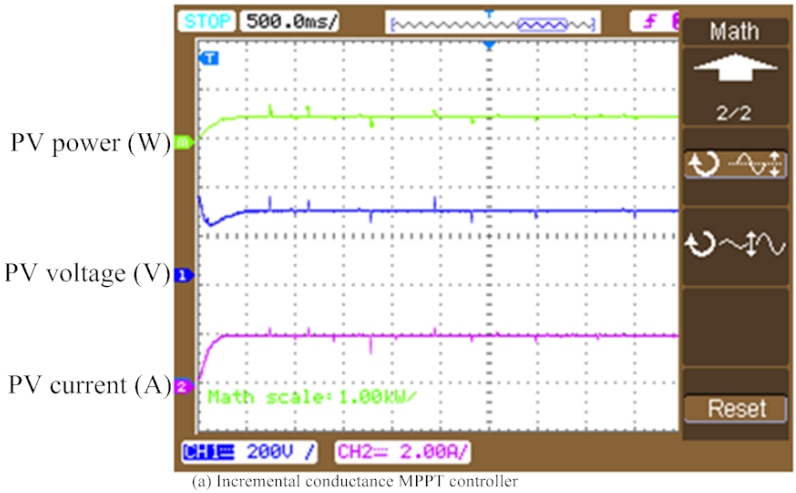

(a) Incremental conductance MPPT controller

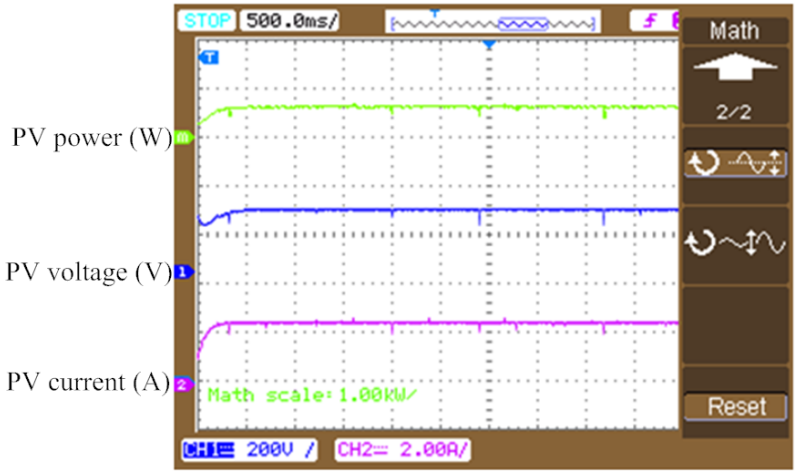

(b) P&O MPPT controller

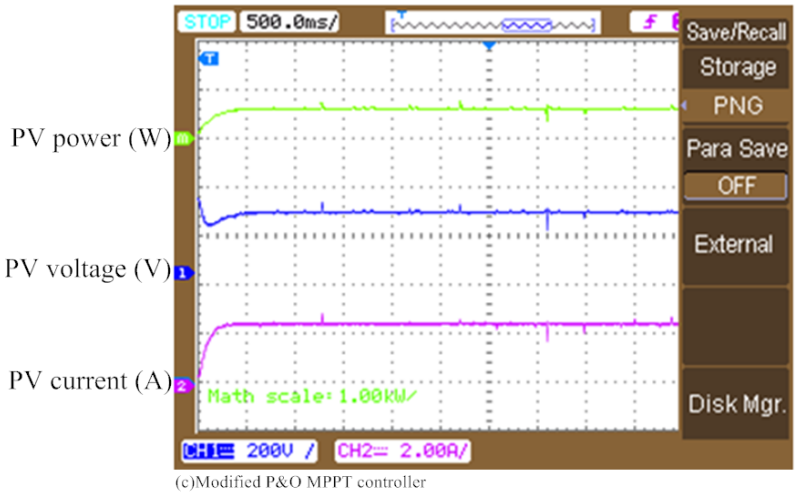

(c)Modified P&O MPPT controller

Figure 2.35: Experimental results after boost converter

2.9 Chapter Summary

A new integral sliding mode MPPT controller is proposed in this chapter for PV systems at standard test conditions. The proposed controller is compared with existing PI MPPT controller. A modified P&O MPPT controller is proposed for handling standard test conditions. The proposed controller is compared with the conventional incremental conductance, Perturb & Observe (P&O) controllers. The simulation results are verified with RTDS and experimental results using prototype set-up are presented to validate the efficiency of the proposed approaches. The FPGA implementation simplified the control circuit and added flexibility to the system. Experimental setup contains E4360A solar array simulator, LabView-2012, NI-cRIO 9014, Hall Effect sensor and DC-DC boost converter. The simulation and experimental results demonstrated that the proposed controllers provides effective tracking of MPP so that maximum power can be extracted from the PV panel at standard test conditons.

Chapter 3

Development of a new Incremental Conductance MPPT Algorithm for handling Partial Shading Conditions

3.1 Introduction

In Chapter 2, control techniques for a PV system to track MPPT have been described at standard test conditions. But with varied weather conditions, temperature and solar irradiations also vary. If the temperature and irradiation are not uniform, then energy yield from the the PV varies. Partial shading occurs due to clouds or building shadows. Owing to partial shading, the shaded panels receive non-uniform solar irradiances thus there would be multiple peaks in the I-V and P-V characteristic curves of the PV array [27]. This in turn affects not only the energy yield but also non-uniform current, and the shaded panels may be damaged. Hence, there is a need to develop suitable maximum power extraction algorithms such that the PV system power can be maximized at all weather conditions and under partial shading conditions (PSC).

Among all the peaks, the voltage and power are maximum at one particular peak, that is called as the global peak. This chapter describes development of a new Incremental Conductance MPPT algorithm for a PV system to track global maximum power point (GMPP) under partial shading conditions. Fig. 3.1 shows a simple description of a PV system with a MPPT algorithm. The conventional incremental conductance MPPT fails to handle PSCs with fixed step size of duty cycle. In this chapter, a modified Inc Cond MPPT controller is proposed with variable step size of duty cycle to handle PSCs with simplified

control algorithm.

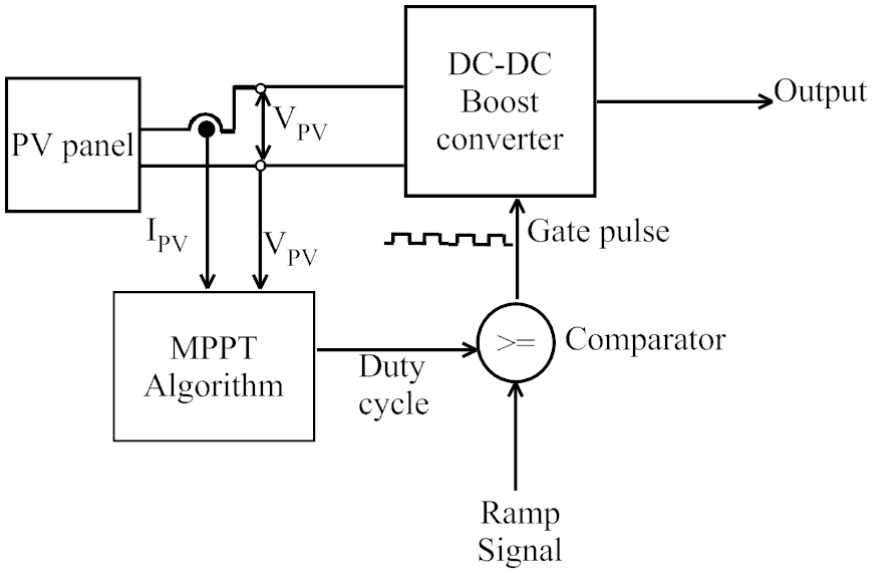

Figure 3.1: Block diagram of PV with MPPT

In view of implementing the aforesaid MPPT algorithm, a DC-DC boost converter is connected in between the PV system and load. This converter regulates the DC output voltage from the unregulated DC input for a desired voltage level. The controlled average DC output voltage delivers a desired voltage level in spite of variations either at input or at output load. This is accomplished through duty ratio control of the converter. PWM technique is a popular method to control the output voltage of the converter. This technique employs switching at a constant frequency and adjusts ON time of the switch to control the output voltage. The PWM signal is generated by comparing a signal level control voltage with a triangular repetitive waveform. This control voltage signal is obtained by amplifying the error signal, which is the difference between reference signal and actual signal.

Sometimes the installed PV modules are affected by shadows of the other modules. Sub-optimal deployments may be selected for compromise and shade impact factor (SIF) should be considered. This SIF parameter is used to quantify power loss due to shading [96]. The SIF compares the fractional power loss to the fraction of the module area and is defined as follows

$$SIF = \left(\frac{P_{normal} - P_{shaded}}{P_{normal}}\right)\frac{A_{normal}}{A_{shaded}} \tag{3.1}$$

where, P_{normal} is the PV system power without shade, P_{shaded} is the PV system power when shaded, A_{normal} is the area of the PV panels and A_{shaded} is the area of shaded cells.

If SIF is greater than one, more power is assumed to be lost. This SIF depends on bypass diodes, sub-strings. Though the little shadow on a string PV cells also, the output power can be reduced drastically. The PV modules are connected either in series or in parallel. If the series connected PV module is shaded, then it acts like a resistor or open circuit and slows down the flow of current from rest of the PV cells in a network. In Fig. 3.2 the characteristic curves (I-V and P-V) of a PV system shows simulation results when it is shaded.

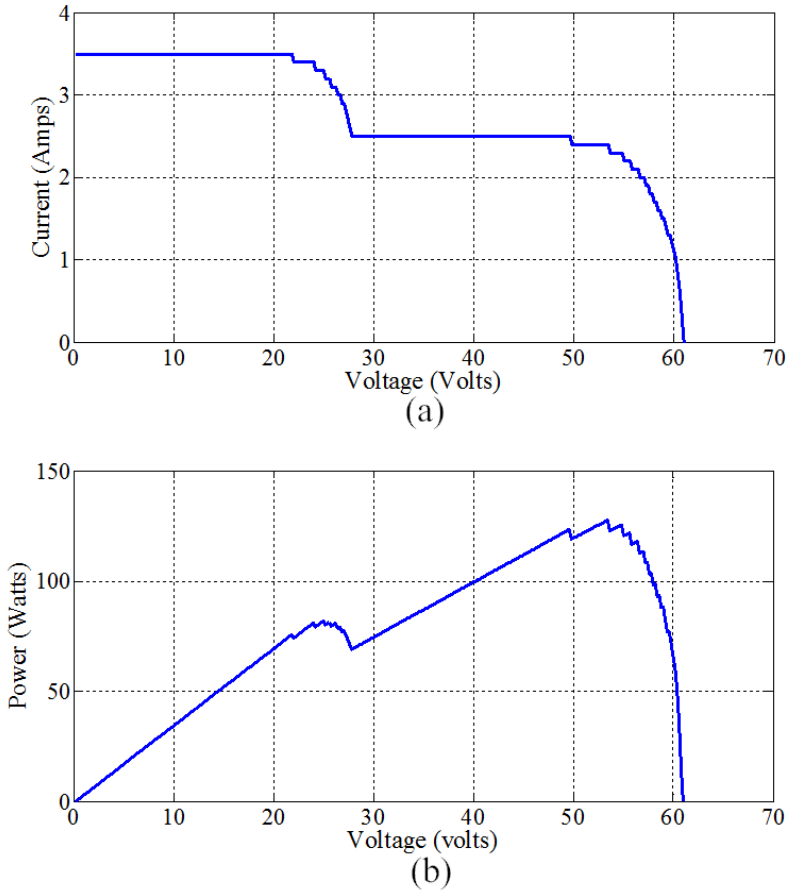

Figure 3.2: PV characteristic curves at partial shading conditions (a) I-V curve and (b) P-V curve

3.2 Chapter objectives

- To develop a modified Incremental Conductance MPPT controller for handling partial shading conditions of a PV system.
- To simulate the proposed modified Incremental Conductance MPPT algorithm using a Real-time simulator.
- To validate the simulated results with experimental results.

3.3 Global MPPT techniques

As described in the introduction, under partial shading conditions, I-V and P-V curves of a PV array exhibit multiple MPPs. Out of these there is only one global peak and remaining are the local peaks. For efficiency concern, the control algorithm should track GMPP always. That means,one can get higher voltage and power at GMPP. Thus in order extract maximum power from PV arrays under partial shading conditions the MPPT scheme shoud be able to identify the global peak. There is a single MPP in PV characteristic curve under uniform insolation. Generally, some of PV modules in a PV array are partially shaded, then the PV characteristic curves (I-V and P-V) consist more than one peaks. Among all, one peak has high voltage and power. That peak is called as global MPP (GMPP) and other peaks in the characteristic curve is called as local MPP(LMPP).

3.3.1 Incremental conductance MPPT algorithm

The conventional incremental conductance MPPT control technique detects the slope of the P-V curve to track maximum power point (MPP). This inc cond algorithm uses the instantaneous conductance (I/V) and incremental conductance (dI/dV) for MPPT. By using these two values, the algorithm determines the operating point of the PV module in the P-V (power-voltage) curve. Calculations for tracking the maximum power point can be accomplished by using the following equations.

$$\frac{dI}{dV} = -\frac{I}{V} \qquad at \;\; MPP \tag{3.2}$$

$$\frac{dI}{dV} > -\frac{I}{V} \qquad left\ of\ MPP \tag{3.3}$$

$$\frac{dI}{dV} < -\frac{I}{V} \qquad right\ of\ MPP \tag{3.4}$$

Equation (3.2) shows that the PV module operates at the MPP, equation (3.3) shows PV module operates at left side of MPP and equation (3.4) shows MPP to be on its right side. These equations are obtained from the slope of the P-V curve at MPP is equal to zero, as shown in the following equation.

$$\frac{dP}{dV} = 0 \tag{3.5}$$

On rewriting equation (3.5), one obtains

$$\frac{dP}{dV} = I\frac{dV}{dV} + V\frac{dI}{dV} \tag{3.6}$$

$$\frac{dP}{dV} = I + V\frac{dI}{dV} \tag{3.7}$$

Equating (3.5) and (3.7), yields

$$I + V\frac{dI}{dV} = 0 \tag{3.8}$$

For tracking of the MPP, the conventional Inc Cond algorithm is used as given equation (3.8). If equation (3.3) satisfies then the converter duty cycle needs to be decreased, on the other hand the duty cycle should be increased if equation(3.4) is satisfied. In case equation (3.8) holds good then there is no need to change the duty cycle. The fixed step algorithm takes less tracking speed than the variable step [97]. The variable step algorithm is computed as

$$Step = N * abs\,(dP/dV) \tag{3.9}$$

where N denotes the scaling factor.

Fig. 3.3 shows the conventional inc cond MPPT algorithm. This algorithm also depends

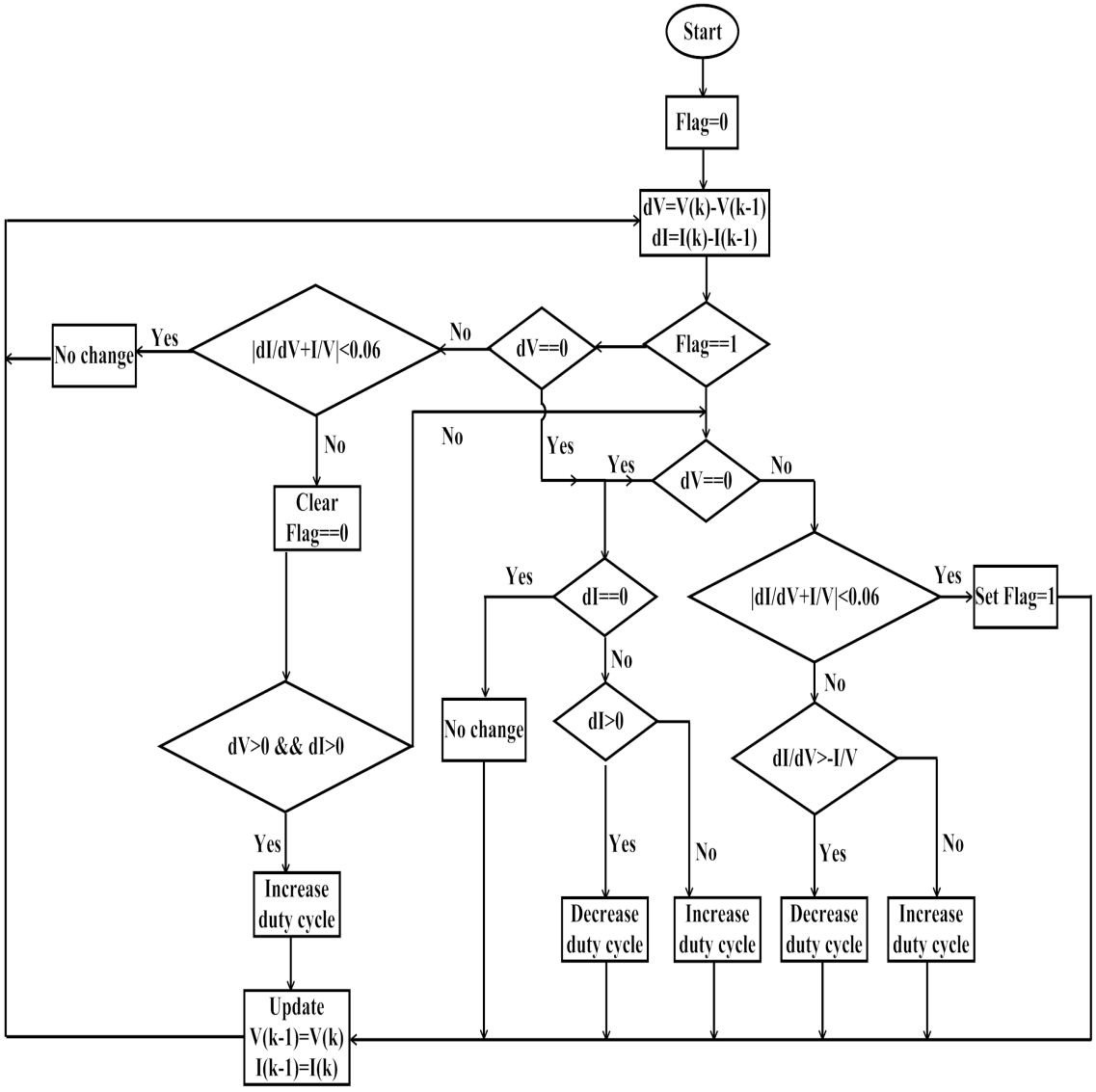

Figure 3.3: Flow chart of conventional incremental conductance MPPT algorithm

on the slope of the P-V characteristic curve, which is affected by the load impedance and solar irradiation. This algorithm uses PV current and voltage in the calculation. When the load impedance decreases, then the PV voltage also decreases and current increases resulting a steady state oscialltion. In order to a small value of error is chosen as a measure of this reduced oscillation. Thus, equation (3.8) can be re-written as [52]

$$\left| I + V\frac{dI}{dV} \right| < 0.06 \tag{3.10}$$

With the permitted error and step size of 0.005 the steady state oscillation error can be greatly reduced.

In this algorithm, first the flag value is set be zero. This flag value indicates the MPP position. If the flag value is zero, then the algorithm executes for standard test conditions using equation (3.10). When the MPP condition reached, the flag value will be one, and then checks the remaining algorithm for other MPPs. If there is no variation on the duty cycle, then irradiation and load resistance are constant. When changes occur in irradiation or load, then the algorithm sets the flag value to be zero and decides changes in current and voltage of PV module. If the algorithm finds the current and voltage to be increased then the duty cycle also increases.

Issues in the conventional inc cond algorithm is discussed in this section. The algorithm is well established and checks all conditions. But, (i) the implementation of FPGA controller is difficult, (ii) instead of a fixed step size, the variable step size duty cycle tracks more power for partial shading conditions [18], and (iii) the permissible error (0.06) value should be less. In order to resolve the aforesaid problems a modified algorithm with variable step size and the permissible error is reduced to 0.03 with a step size of 0.005. The modified inc cond MPPT algorithm is discussed in next section.

3.3.2 Modified Incremental Conductance MPPT algorithm

Fig. 3.4 shows the modified incremental conductance MPPT algorithm with variable step size. This algorithm is intended to improve the performance of the conventional Inc Cond MPPT. The conventional incremental conductance MPPT control algorithm takes more. After the checking of the states of the flag, the same condition is checked twice in the conventional control algorithm. Based on the aforementioned reasons the control algorithm is time taking to track power from PV panels. Therefore, flags are eliminated in modified incremental conductance MPPT algorithm with variable step size. Instead of fixed step, variable step plays key role at partial shading conditons [87]. Hence,variable step is introduced in modified MPPT control algorithm. The permissible error value is decreased to 0.03 in modified algorithm for proper checking of PV curve. Inc Cond algorithm searches for the slope and try to stay at that position to track the MPP. At this position, the difference between the present value and previous value is zero [54]. In modified algorithm, equation

(3.10) can be rewritten as follows.

$$\left| I + V\frac{dI}{dV} \right| < 0.03 \tag{3.11}$$

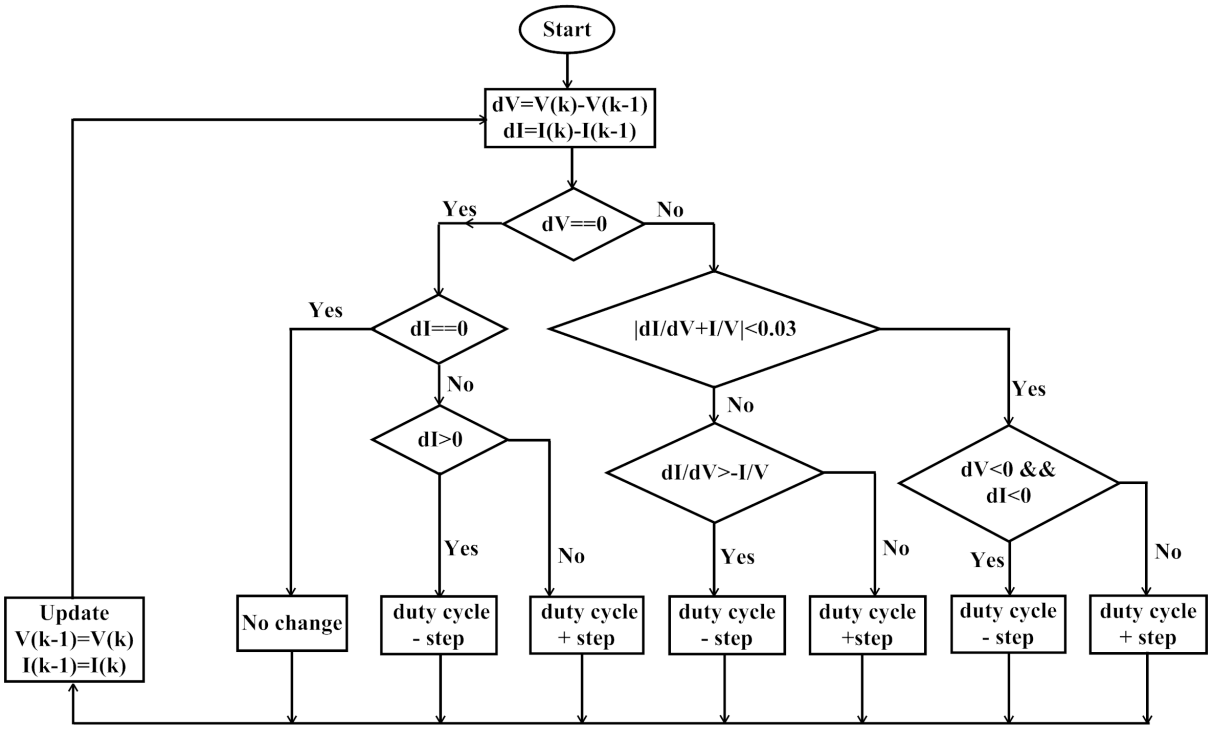

Figure 3.4: Modified incremental conductance algorithm with variable step

In this algorithm, voltage and current variation conditions is checked and assigned appropriate duty cycle immediately. When the MPP condition reached, the remaining algorithm can check for other MPPs. If any greater MPP is found by the algorithm, then the controller leaves the earlier MPP and keeps the GMPP value as MPP. Here the duty cycle is constant and adding a step size to vary the duty cycle. When changes occur in irradiation levels or load, then the algorithm founds changes in current and voltage of PV module and tracks GMPP position. If the algorithm finds the current and voltage to be increased then the duty cycle also increase with the step size. It is easy to check different conditions in the modified incremental conductance MPPT control algorithm and practical implementation also easy. The algorithm responds and allocates different duty cycles immediately when changes occur at the PV panel output. Therefore, the tracking speed is also increased by comparing with the conventional Inc Cond algorithm. When the controller tracks the MPP

faster, then the output also gets increased. The steady state time is drastically reduced with modified MPPT control algorithm. The simulation results of conventional and modified Inc Cond MPPT algorithms are shown in Fig. 3.5 and Fig. 3.6 respectively.

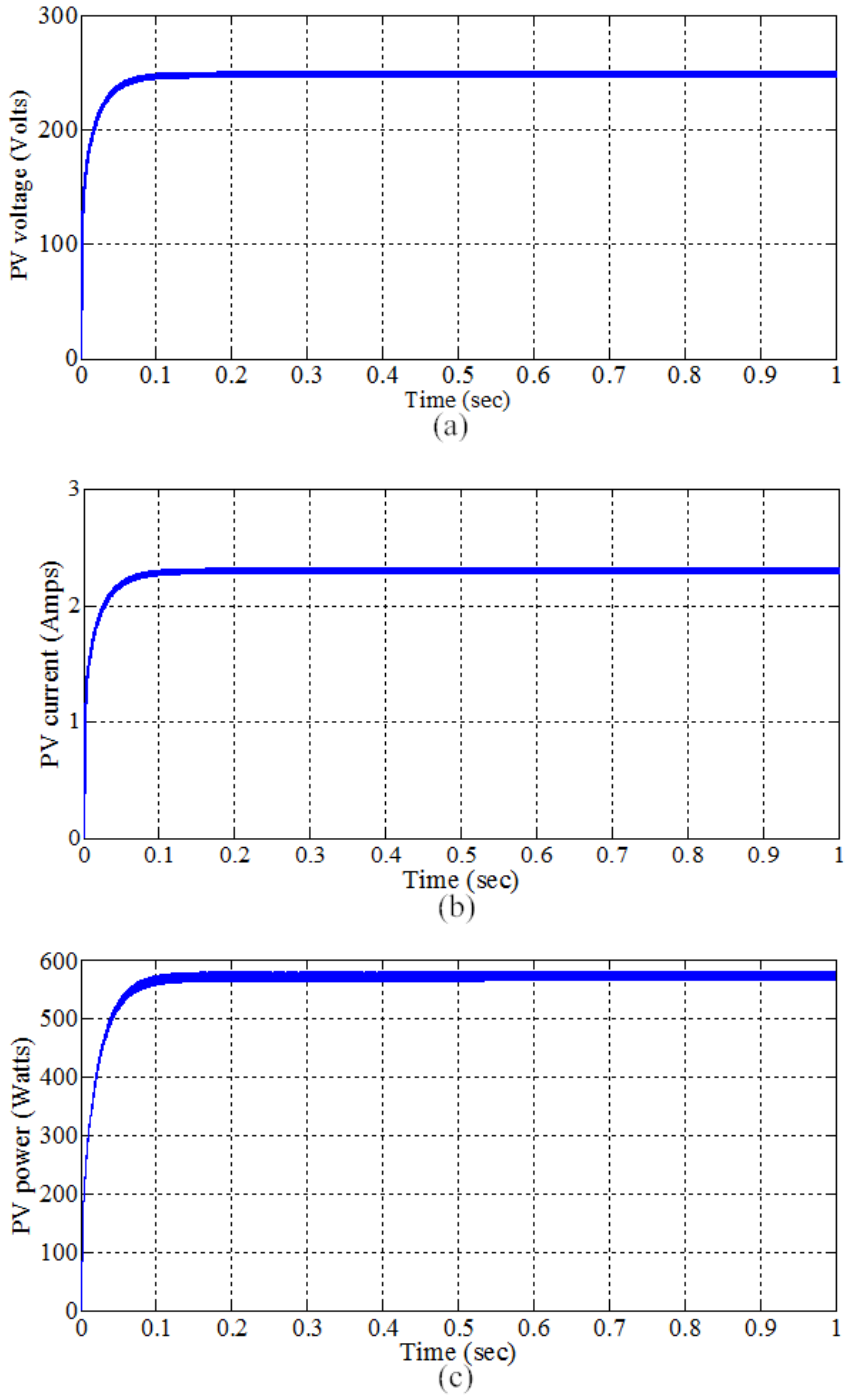

Figure 3.5: Simulation results of conventional incremental conductance MPPT controller

The modified Inc Cond MPPT control algorithm is tracking around 1% more power than the conventional. Reaching the steady state condition in voltage tracking and power tracking is faster than the conventional Inc Cond algorithm.

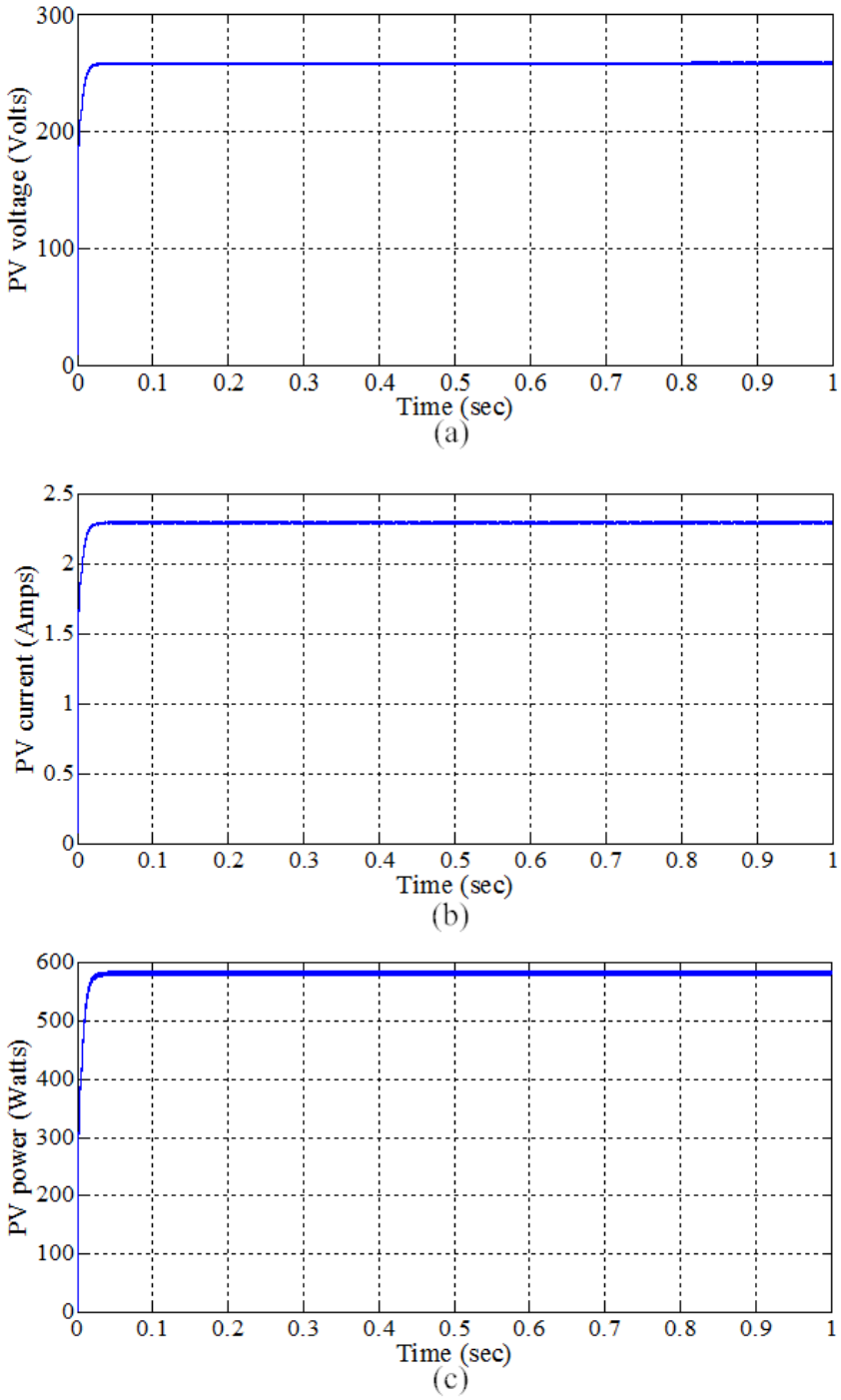

Figure 3.6: Simulation results of modified incremental conductance MPPT controller

3.4 Experimental results and analysis

Fig. 3.7 shows the picture of an experimental setup of PV system for varying the efficiencies of the propoed MPPT algorithm under partial shading conditions. The description of the hardware setup is as follows.

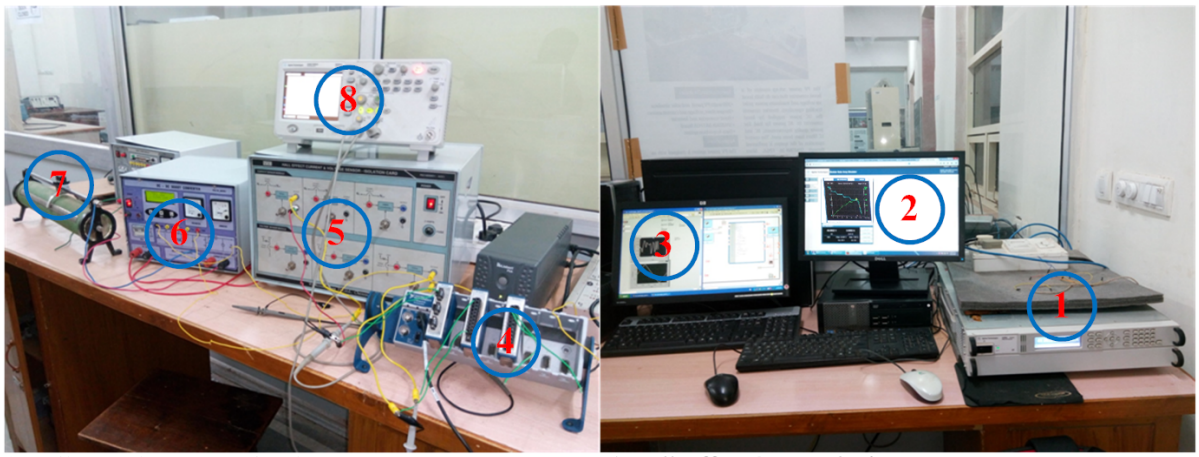

1) Agilent Solar Array Simulator (E4360A)
2) PC connected to SAS
3) PC for Control Algorithm (LabView)
4) cRIO-9014
5) Hall Effect Sensor device
6) DC-DC boost converter
7) Load
8) D S O

Figure 3.7: Picture of the experimental setup for a PV system

3.4.1 Solar array simulator (E4360A)

The description of E4360A standard Solar Array Simulator is as follows.

Operating in SAS mode

This mode uses an exponential model to approximate the characteristic (I-V, P-V) curves. It is programmed in terms of the key parameters like open circuit voltage (V_{oc}), Short circuit current (I_{sc}), voltage maximum power point (V_{mpp}) and current maximum power point (I_{mpp}) at the approximate peak power point. The SAS mode of operation is achieved by sampling output voltage, and applying a low pass filter by adjusting the constant current loop continuously by using the filtered voltage as an index in to the exponential model. When V_{oc}, I_{sc}, V_{mpp}, and I_{mpp} at the maximum power point are provided

the simulator internal algorithm uses the following equations.

$$V = \frac{\frac{V_{oc} * \ln\left[2-\left(\frac{I}{I_{sc}}\right)^{N}\right]}{\ln(2)} - R_s * (I - I_{sc})}{1 + \frac{R_s * I_{sc}}{V_{oc}}} \tag{3.12}$$

$$R_s = \frac{V_{oc} - V_{mpp}}{I_{\,mpp}} \qquad N = \frac{\ln(2 - 2^{\alpha})}{\ln\left(\frac{\mathrm{I}_{mpp}}{I_{sc}}\right)} \tag{3.13}$$

$$\alpha = \frac{V_{mpp} * \left(1 + \frac{R_s * I_{sc}}{V_{oc}}\right) + R_s * \left(\mathrm{I}_{\,mpp} - I_{sc}\right)}{V_{oc}} \tag{3.14}$$

where V= Final PV voltage, R_s Series resistance, N= Number of PV units, α=Difference of voltage between V_{oc} and V_{mpp}

Operating in Table mode

In this mode, the output characteristics of a PV system are obtained by a user defined table of I-V points. The operation is achieved by sampling the PV simulator output voltage applying to an LPF with continuous constant current loop adjustments by using the filtered voltage as an index into the stored table of points. Here, linear interpolation is used to set the current when the filtered voltage does not match with the table entry. This means that the I-V curve of the PV panel is generated by connecting the points in the table as straight lines. The minimum table size is 256 points and which can go up to a maximum size of 4096 points. Accurate characteristic curves can be obtained even when the table size is large. Each point in the table is defined by an I-V coordinate pair that defines a location in the I-V characteristic curve. Here in table mode, the first value is the voltage and next value is the current. If the voltage value V=0 is not provided, then the current associated with the lowest voltage value is treated as I_{sc} and the curve will be extended horizontally to the current axis. If the current value I=0 is not provided, then the slope of the current values will be extended to the voltage axis. The SAS simulator accepts the entries for maximum power point current (I_{mpp}) equal to I_{sc}, and entries for V_{mpp} must be less than V_{oc}. The slope ($\frac{\Delta V}{\Delta I}$) of the output curve must meet the minimum requirements. The simulator checks the slope of the curve thoroughly and terminates at V_{oc}.

3.4.2 Compact Reconfigurable IO (cRIO) - 9014

National Instruments (NI) cRIO is an ideal device which can perform distributed control applications. NI-cRIO is small in size and is a rugged Data Acquisition (DAQ) control system powered by a real time processor and reconfigurable FPGA for embedded and distributed applications. The controller can be developed by using LabVIEW in real-time operating system and FPGA that interfaces with the computer to control a variety of modules that are installed in chassis [98]. The chassis and a host computer communicate through TCP/IP protocol. The cRIO contains modules like (i) Power supply, (ii) 4 or 8 slots of reconfigurable chassis, (iii) Real time embedded processor, and (iv) Interchangeable I/O modules. Fig. 3.8 shows the block diagram of a programmable controller. The power supply module of NI-cRIO-9014 provides DC output of 24V, 5A to the embedded processor and I/O modules. The reconfigurable chassis is a metal structure and the main part of NI-cRIO system can characterize the entire cRIO platform. The cRIO embedded processor gives high performance through an FPGA chip whose power consumption is low. A peripheral control interface (PCI) bus connection provides high performance to the processor. The cRIO has built in data transfer mechanism to pass data to the embedded processor for real time analysis, post processing and data communication to the host computer. NI-cRIO features as follows.

The cRIO processor capacity is 200MHz, which can execute real time applications. It is having real time clock and watchdog timer, and the ethernet provides 10 to 100 Mbps data transfer rate. The range of input supply 9V to 35V (DC) and 20W power.

The FPGA chip is connected to I/O modules in a star topology to access each module directly. The I/O modules contain built in signal conditioning and screw terminal with D-sub connectors. The connector junction box integrates the I/O modules, significantly reducing the space necessities and wiring. Fig. 3.9 shows the picture of NI-cRIO.

NI-9201 is 8 channel analog input module; each channel has an analog input (AI) terminal for input and COM for common terminal. This COM terminal is internally connected to the ground of the module [99]. The salient features of the input module has 8 inputs, sampling rate is 500kS/s. The operating voltage is $\pm 10V$. The over voltage protection circuit is presented inside the module, and it swap the higher/lower voltages. The

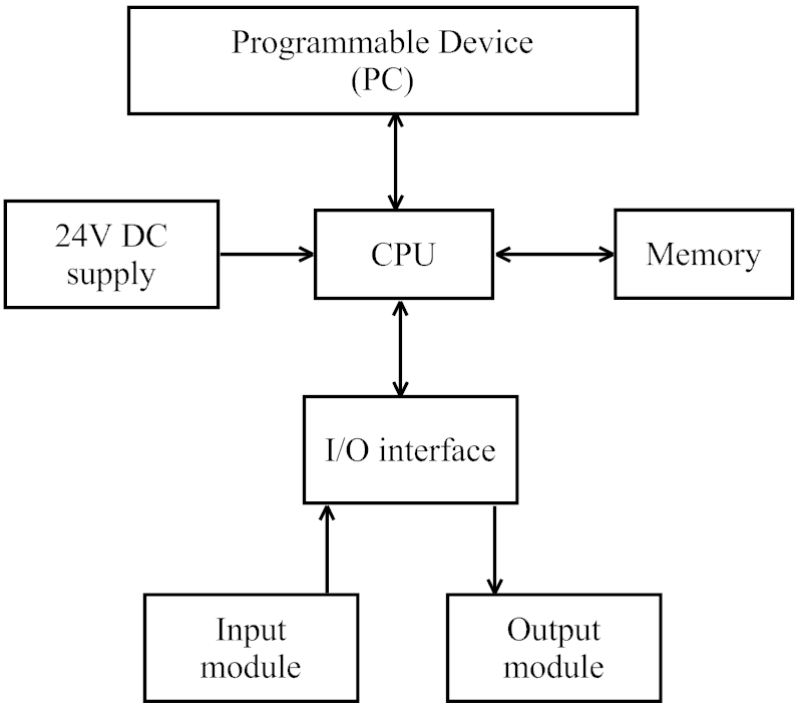

Figure 3.8: Block diagram of NI-cRIO programmable controller

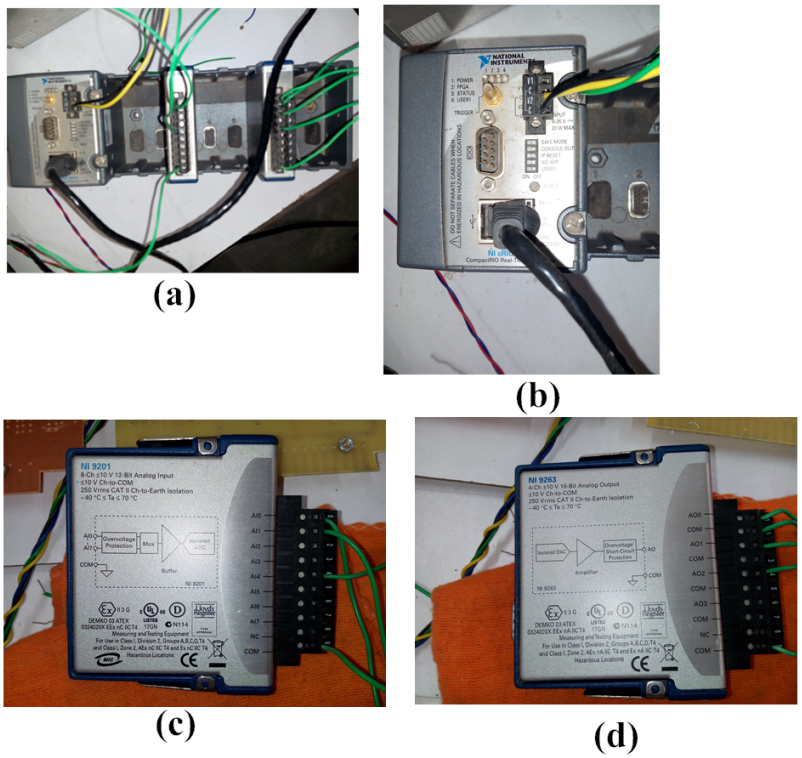

Figure 3.9: Pictures of NI-cRIO (a) reconfigurable chassis, (b) Embedded Processor, (c) Input module and (d) Output module.

operating temperature range of the input module is in between -40 to 70^0C.

NI-9263 is a 4 channel analog voltage output module; each channel has AO (analog output) and COM (common) terminals [100]. The salient features of the 9263 module are given below.

The module has 4 outputs and each output has a transfer capacity of 100kS/s. The resolution is 16-bit size. The operating voltage is $\pm 10V$. An over voltage protection circuit is presented inside the module, and it swap the higher/lower voltages. The operating temperature range of the input module is in between -40 to 70^0C.

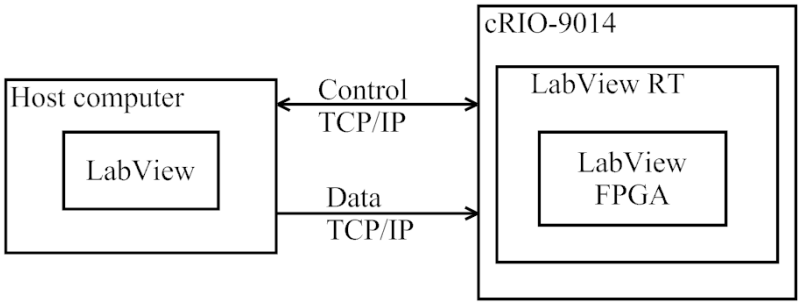

Figure 3.10: Block diagram of control architecture of cRIO-9014

The LabView executable real time module contains LabView FPGA module code; it waits for the incoming TCP/IP connection from the host computer to pass control messages. Later, the cRIO initiates a second TCP/IP connection to transfer back the data to host when the host establishes an acquisition. Fig. 3.10 shows the block diagram of the control architecture and Table 3.1 describes cRIO modules used in experimental setup.

Table 3.1: Simulation parameters of PV system with DC-DC boost converter

Slot	Module type	Description
	NI-cRIO-9014	Real time controller with 2 GB storage,128MB DRAM
3	NI-9201	8 channel analog input module, 500kS/s
6	NI-9263	4 channel analog output module, 100kS/s, 16-bit

3.4.3 Hall Effect sensor

A Hall Effect sensor is necessary to provide isolation between the power and signal conditioning circuits. The power or voltage or current quantities are sensed and altered in to low voltage signals by using Hall Effect voltage and current sensors. or transducers.

For sensing the voltage and current in the experimental set up LEM LV 25-P voltage sensor and LEM LA 55-P current sensor are used in the Hall Effect sensor circuits to convert the higher level voltages and currents to a low level analog signal in the range of ±5V peak to peak.

Design of voltage sensor circuit

In this experimental set up, the voltage is scaled down from 250V to 5V. Fig. 3.11 shows the circuit of the Hall Effect voltage sensor.

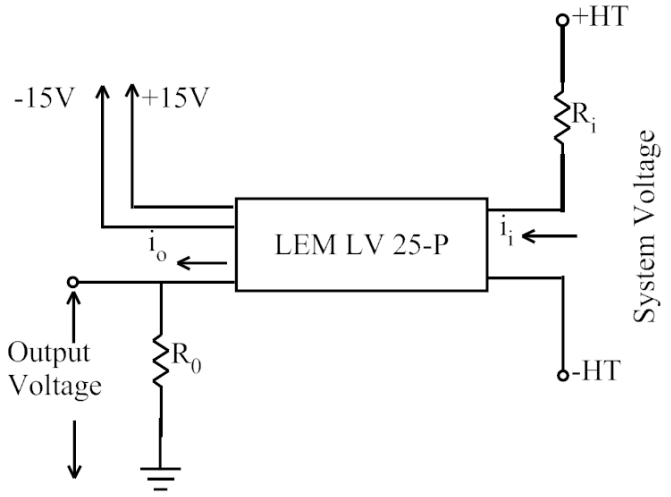

Figure 3.11: Circuit diagram of voltage sensor

From the transducer data presented in the data sheet [101], we choose the value of input resistance Ri such that the output resistance must be in the range of 100Ω to 350Ω. For input current i_i calculation, V_i=250V is selected and choose R_i=40kΩ. Then

$$i_i = \frac{V_i}{R_i} = \frac{250V}{40k\Omega} = 6.25mA \tag{3.15}$$

The conversion ratio for Hall Effect transducer is 2500:1000. Therefore, the output current i_o will be $i_o = i_i$* conversion ratio=6.25*2.5=15.625 mA

The output measuring resistance is obtained by the ratio of output voltage and output current. The output voltage of the sensor is 5V and output current is 15.625mA. Therefore,R_{vo} is calculated as follows

$$R_{vo} = \frac{V_o}{I_o} = \frac{5}{15.625 * 10^{-3}} = 320\Omega \tag{3.16}$$

Design of current sensor circuit

In this experimental set up, there is a need of converting current of 5A is into 2V signal for measuring the values in voltage. The circuit diagram of the current sensor is shown in Fig. 3.12. The picture of Hall Effect sensor is shown in Fig. 3.13.

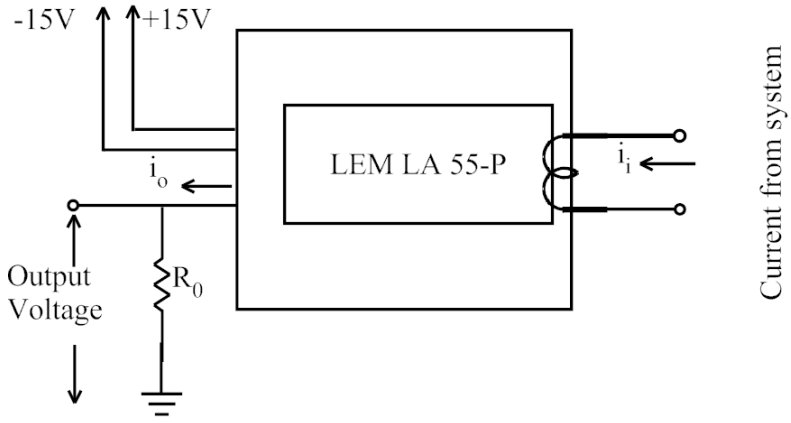

Figure 3.12: Circuit diagram of current sensor

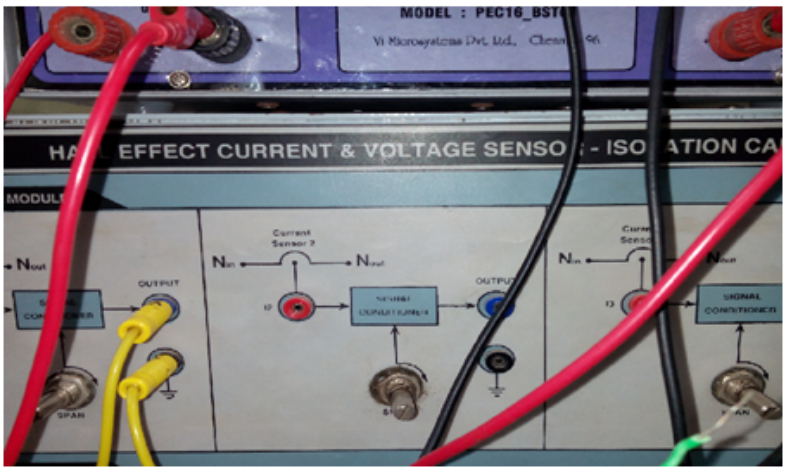

Figure 3.13: Picture of Hall Effect sensor

The number of turns on the current sensor (shown in Fig.3.12) is chosen such that the output resistance should lie in between 15-160 Ω, specified in the current transducer data sheet [102]. The conversion ratio is 1:1000. The number of turns are 9 and the primary

current is 5 A, therefore, the output current is calculated as follows

$$i_o = \frac{Number\,of\,turns * i_i}{conversion\,ratio} = \frac{9 * 5}{1000} = 0.045A \tag{3.17}$$

where i_o= Sensor output current, i_i= Senosr input current

The output resistance is adjusted to get the output from current sensor is 2 V with input current of 5 A. So, the output resistance is

$$R_{vo} = \frac{V_o}{i_o} = \frac{2}{0.045} = 44.4\Omega \tag{3.18}$$

where R_{vo}= Output resistance of sensor

Characteristic curves of a PV simulator for different controllers are shown in Fig. 3.14 and Fig. 3.15. When no control algorithm is applied, the MPP tracking is 0% as shown in Fig. 3.14(a), and after running the conventional Inc Cond MPPT control algorithm it tracks the MPPT and is shown in Fig. 3.14(b). When the modified Inc Cond MPPT control algorithm is running, and when it tracks MPPT is shown Fig. 3.15. From the results it is observed that, the proposed Inc Cond MPPT controller is tracking 0.32% more power than the conventional Inc Cond MPPT controller.

(a) When control algorithm is not running

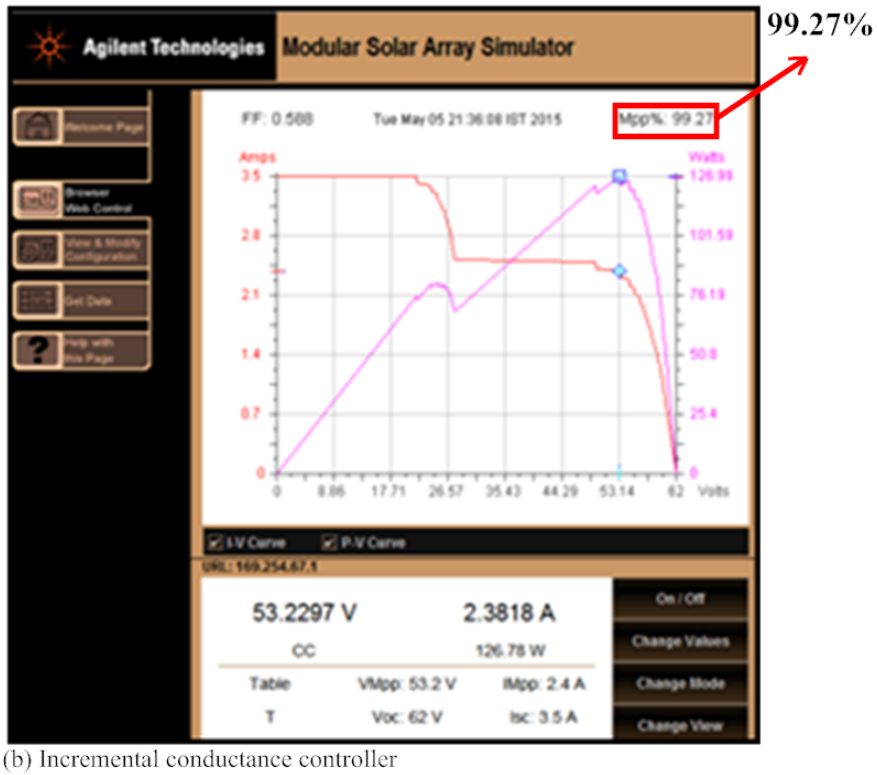

(b) Incremental conductance controller

Figure 3.14: SAS simulator outputs of conventional Inc Cond MPPT controller

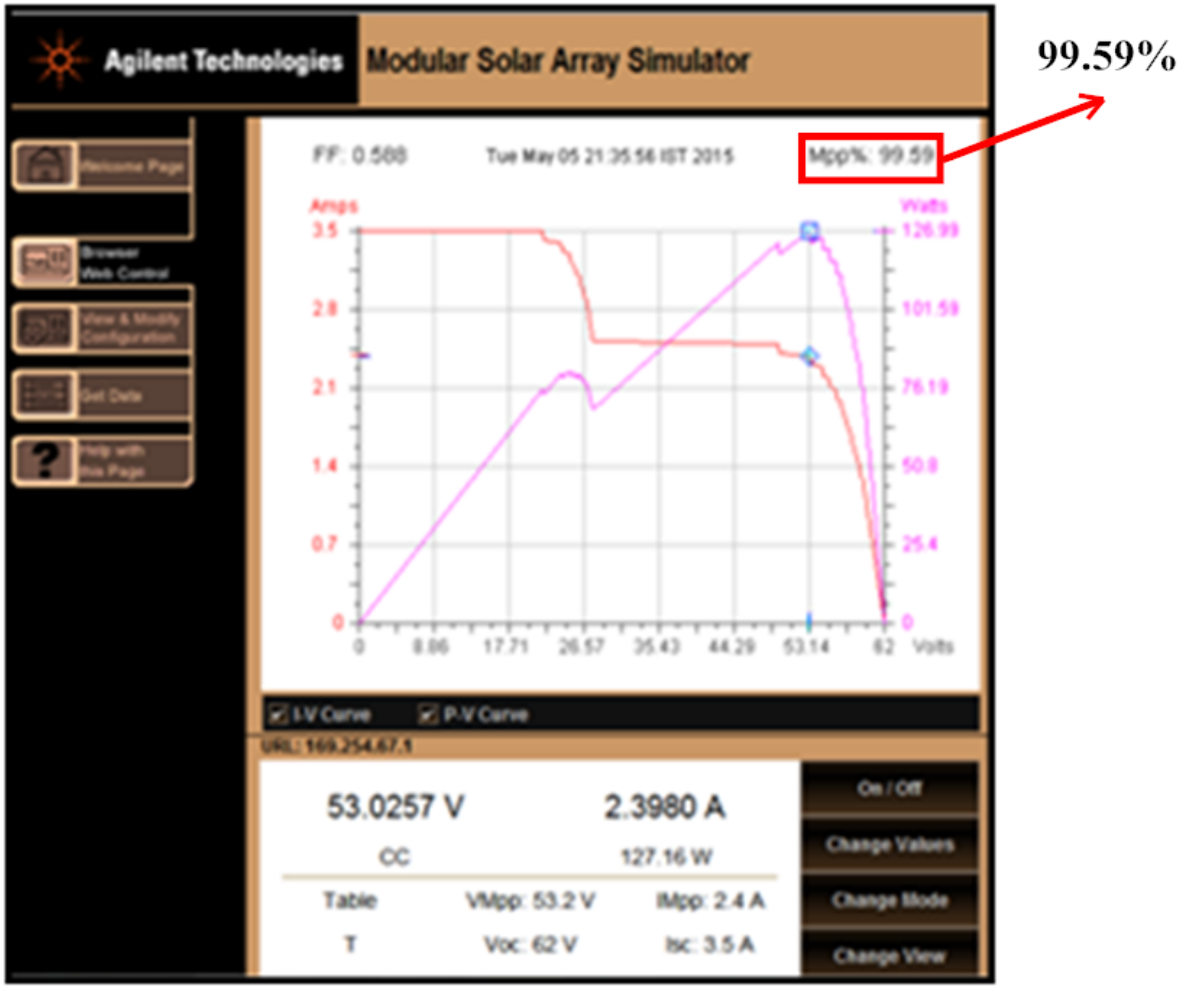

(c) Modified Incremental conductance Controller

Figure 3.15: SAS simulator outputs of modified Inc Cond MPPT controller

The simulation results are validated with Real-time digital simulation results. These Opal-RT results of conventional and modified Inc Cond MPPT controllers are shown in Fig. 3.16, Fig. 3.17 respectively.

The Opal-RT results of Inc Cond MPPT controller for PSC is shown in Fig. 3.16. PV output voltage is shown in Fig. 3.16(a), observed that the Inc Cond MPPT controller is tracking 250 V. PV output current is shown in Fig. 3.16(b), observed that the Inc Cond MPPT controller is tracking 2.5 A. PV output power is shown in Fig. 3.16(c), and observed that the Inc Cond MPPT controller is tracking around 575 W. Opal-RT results are matched with simulation results.

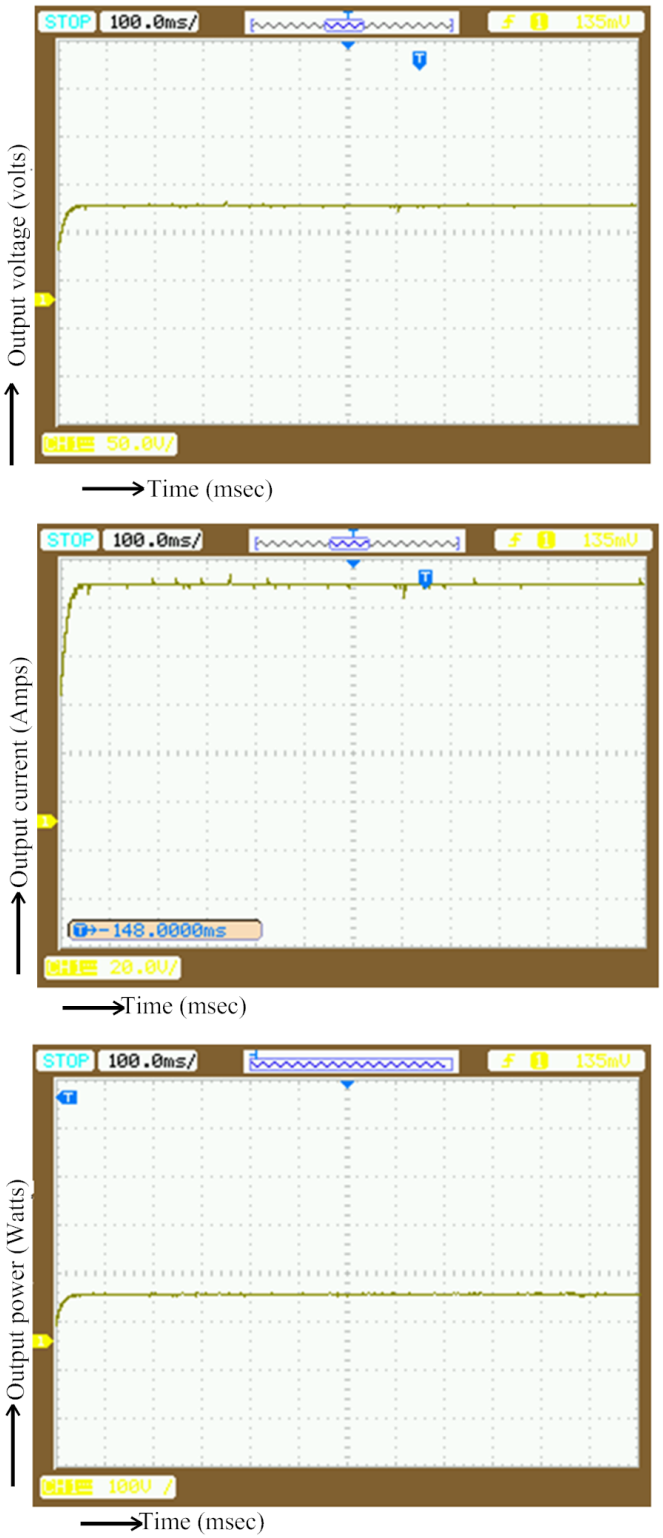

Figure 3.16: Opal-RT results of Incremental conductance MPPT controller

The proposed Inc Cond MPPT control algorithm is tracking around 1% more power than the conventional. Reaching the steady state condition in voltage tracking and power

tracking is faster than the conventional Inc Cond algorithm. Opal-RT results are matched with simulation results.

Figure 3.17: Opal-RT results of modified Incremental conductance MPPT controller

The simulation results are verified with experimental prototype setup results. The experimental results are taken from DSO are shown in Fig. 3.18 (before DC-DC boost converter) and Fig. 3.19 (after DC-DC boost converter) respectively.

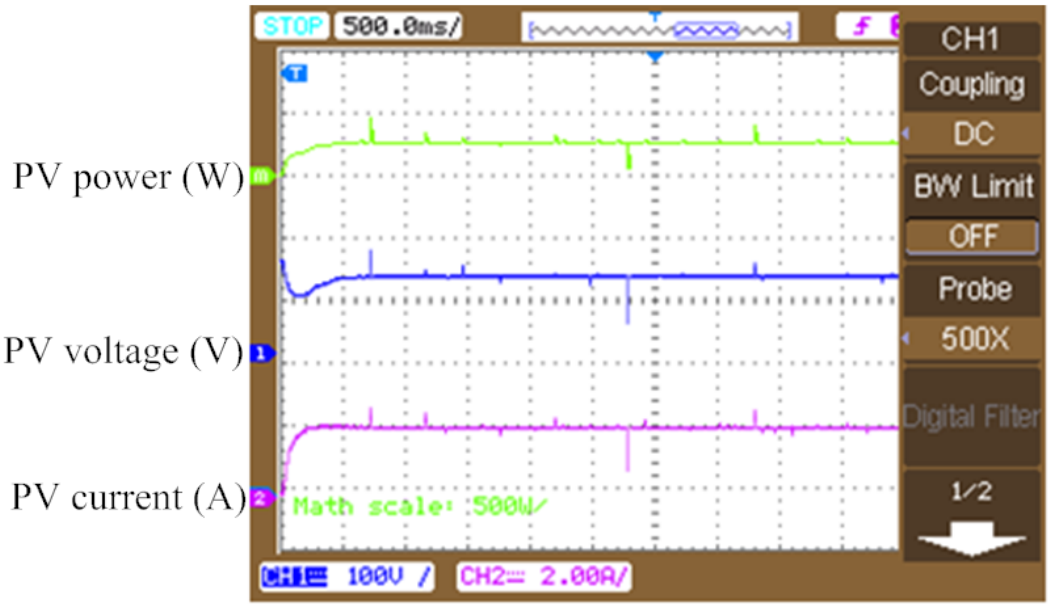

(a) Incremental Conductance MPPT controller

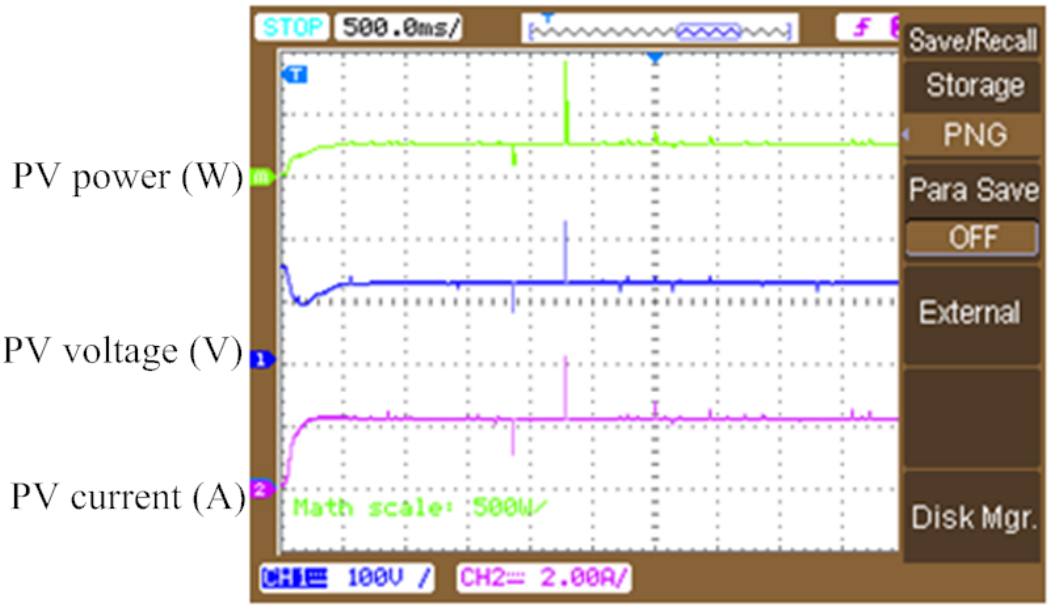

(b) Modified Inc Cond MPPT controller

Figure 3.18: Experimental results (Output of PV array)

The simulation results are verified with experimental prototype setup results. The experimental results are taken from DSO are shown in Fig. 3.19 (after DC-DC boost

converter). From these results one can observe that the experimental results, Opal-RT results and simulation results are matched. The modified Inc Cond MPPT controller is tracking more power than the conventional

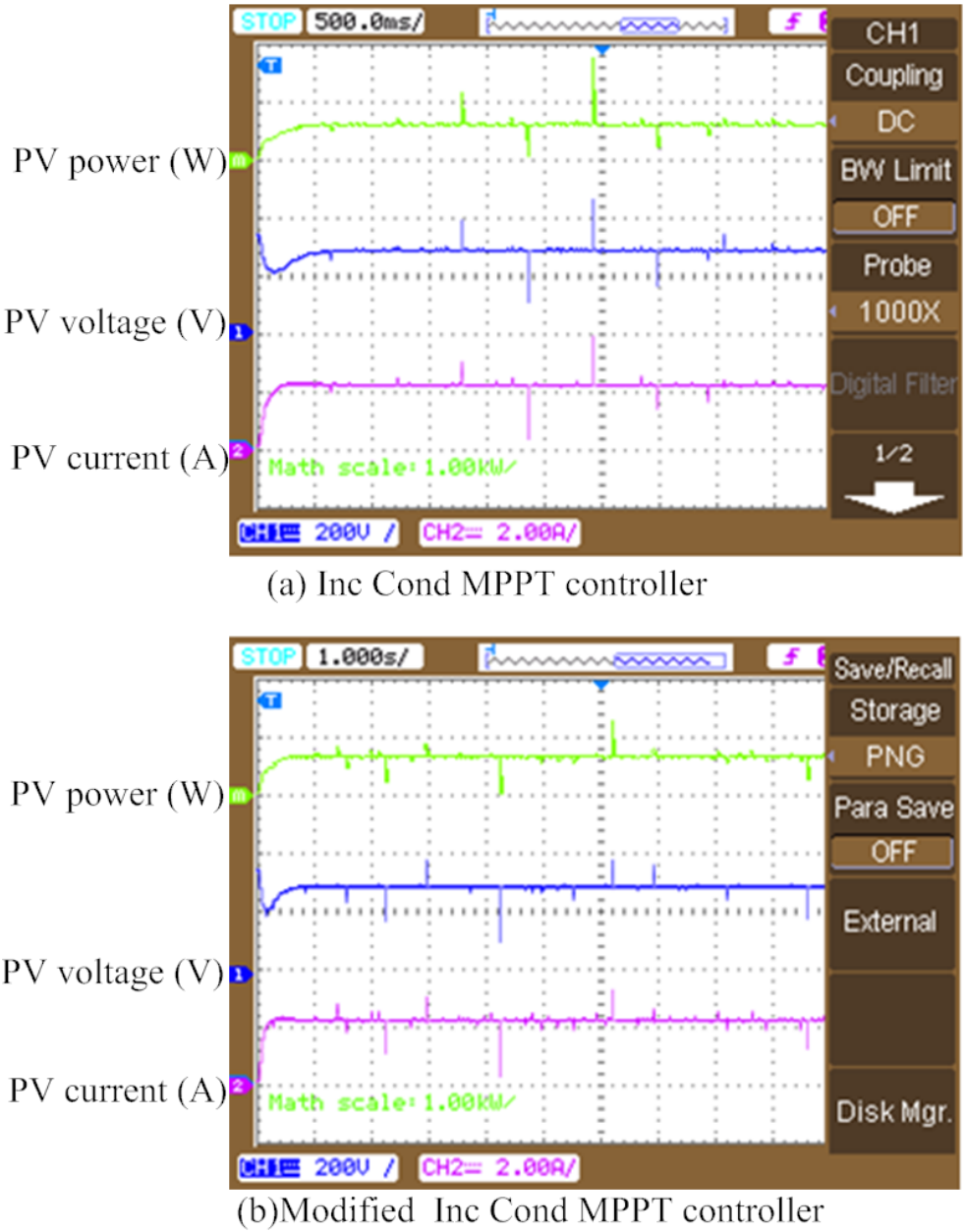

Figure 3.19: Experimental results (Output of boost converter)

3.5 Chapter Summary

A modified incremental conductance MPPT controller with variable step size is proposed in this chapter for PV systems and its effectiveness are verified. The step size is varied according to the weather conditions. The performance of the proposed controller is compared with the existing incremental conductance controller. Simulation in MATLAB/SIMULINK, real-time simulation in Opal-RT and experimental results using prototype set-up are used to validate the efficacy of the proposed approach. The simulation and experimental results demonstrate that the new incremental conductance controller provieds effective tracking of MPP so that maximum power can be extracted from the PV panel and regulates the load voltage at partial shading conditions and all weather conditions.

Chapter 4

Development of a new Model Predictive Controller MPPT Algorithm for Grid Connected PV

4.1 Introduction

In Chapter 2 and Chapter 3, control techniques for a PV stand-alone system to track MPPT at standard test conditions and partial shading conditions are described respectively. However, a grid connected PV system is mostly desirable for integrating to the utility grid. This chapter describes PWM-VSI current control strategies for a grid connected PV system with global maximum power point tracking. In a voltage source inverter (VSI), the DC source has very less impedance (almost negligible) and constant terminal voltage with different loads [103]. An LC filter can be used at the output side of the inverter to obtain sinusoidal waveform [104]. Most of the grid connected PV systems use current control techniques with PWM-VSI control strategy. This thesis has been described a VSI current control strategy to develop control techniques for Grid Connected PV (GCPV) .

PV cell provides DC output voltage, whose magnitude is raised by a boost converter. For utility and grid connected applications the boost converter output is connected to the inverter. A DC-link capacitor is connected in between the boost converter and inverter. The DC-AC inverter is controlled by PWM-VSI technique. In this chapter, a model predictive controller (MPC) has been developed to overcome the switching losses due to high frequency.

4.2 Chapter objectives

- To develop a model predictive MPPT controller for grid connected PV system.
- To compare the simulated results with real-time results (Opal-RT), and experimental results.

4.3 Mathematical modelling of PWM-VSI

The PWM-VSI technique is used in both single phase and three phase modes. A generic topology of a grid connected PV system is shown in Fig. 4.1. For grid/utility supply the output DC voltage of PV panel has to be fed to an inverter. A DC-link capacitor is connected in parallel to the DC bus. The aim of DC-link capacitor is (i)to supress the ripple produced by switching current and voltage in DC-DC converter, (ii) to decouple the DC power source from the AC source by charging and discharging. To operate an inverter, PWM signals are necessary. For providing accurate switching pulses to the inverter, the basic components such as controller, unit sine vector, reference current generator are essential. The reference current extraction process can be obtained by unit current vector and magnitude analyser. The magnitude analyser is used to estimate the required amplitude of load current. The maximum value of load current is multiplied with the unit current templates to generate the required reference current. The reference current is compared with actual current to generate PWM signals, and these signals are fed to the inverter gate. The inverter is connected with an LC filter, which supresses the ripple of inverter output voltage. The inverter is connected to the grid by an interfacing inductance. Subsequently, the grid is connected to the load.

4.3.1 Modelling of Single Phase PWM-VSI

The PWM-VSI includes a single phase AC voltage applied through a DC-link capacitor. Normally, an inverter is powered from a DC source or from a battery. In this thesis, a DC-link capacitor is added after the DC-DC boost converter that follows PV to maintain the DC voltage. Fig. 4.2 shows a schematic diagram of single phase DC-AC VSI. It contains a capacitor rather than a DC source or battery, single phase voltage v_a (expressed in terms

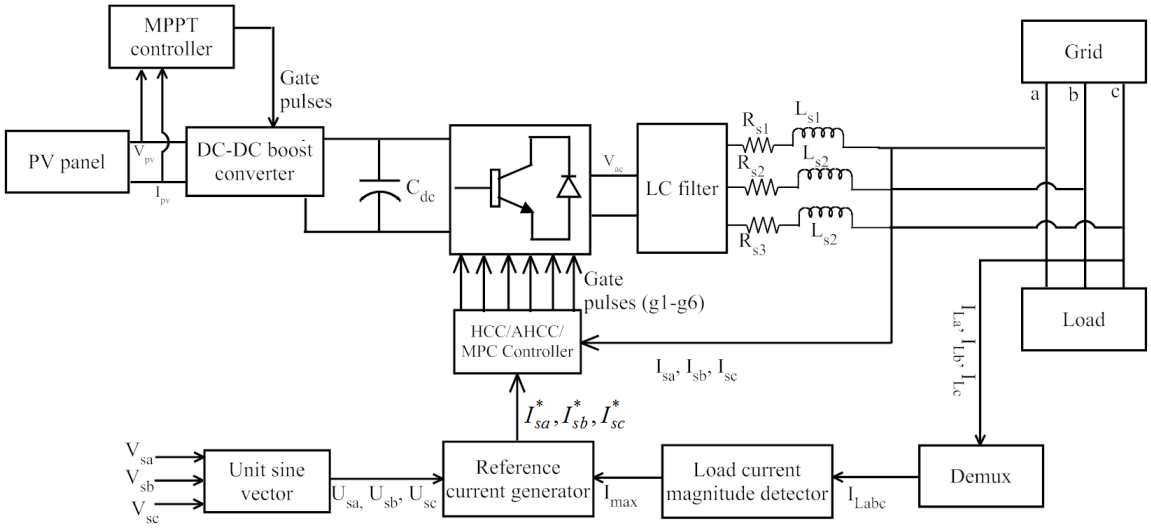

Figure 4.1: Topology of grid connected PV

of DC-link capacitor voltage V_{dc}) and current i_a at the input side, two switching devices S_a and S_b for ON/OFF states [105]. A series connected resistor R_c and an inductor L_c are connected in series with the source/grid.

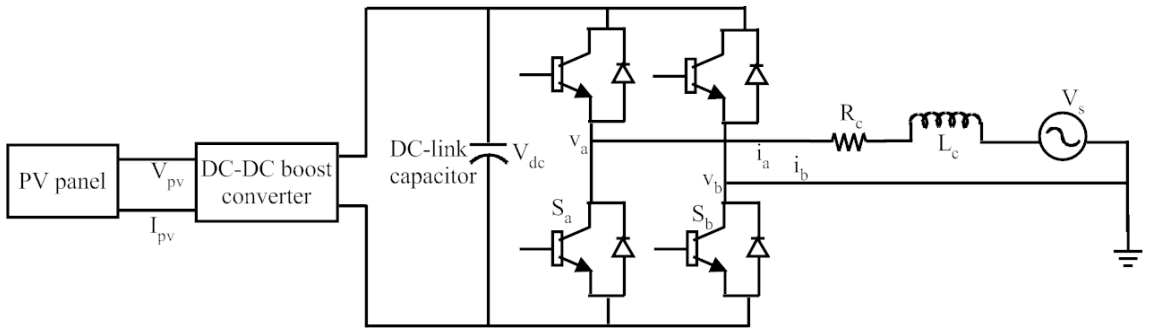

Figure 4.2: Single phase DC-AC VSI

The single phase voltage V_a (shown in Fig. 4.2) and single phase current i_a can be calculated as follows

$$v_a = (S_a)\, V_{dc} \tag{4.1}$$

$$\frac{di_a}{dt} = \frac{1}{L_c}(V_s - v_a - R_c L_c) \tag{4.2}$$

The DC-link capacitor current I_{dc} can be obtained in terms of phase current i_a and

switching status of the switching devices S_a, S_b as follows

$$I_{dc} = i_a S_a - i_a S_b \tag{4.3}$$

From equation(4.3), the DC-link capacitor voltage (V_{dc}) can be written as

$$\frac{dV_{dc}}{dt} = \frac{1}{C_{dc}} (i_a S_a - i_a S_b) \tag{4.4}$$

The DC-link capacitor can be used as an energy storage element, and the stored energy should supply as real power. In the steady state condition, the real power supplied by the source is equal to the demand at the load, other than this; a small amount of power is required to compensate the losses in PV system.

4.3.2 Modelling of a three phase PWM-VSI

The PWM-VSI includes an AC voltage of three phase which is applied through a DC-link capacitor. Fig. 4.3 shows the schematic diagram of a three phase DC-AC VSI. In this circuit, v_{ca}, v_{cb} and v_{cc} are the three phase voltages at the input side and these can be expressed in terms of DC-link capacitor voltage (V_{dc}) and switching function states of the devices S_a, S_b and S_c [106].

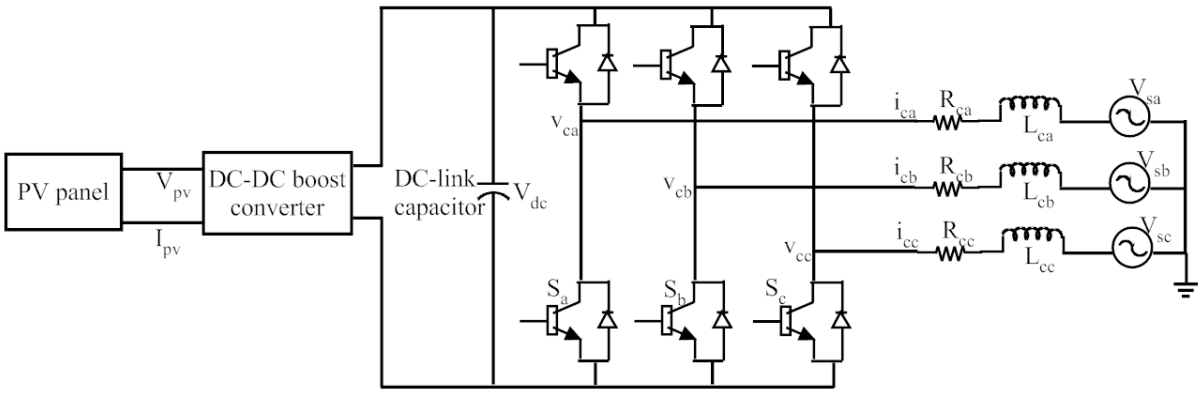

Figure 4.3: Three phase DC-AC VSI

Calculation of three phase voltages v_{ca}, v_{cb} and v_{ca} are as follows:

$$\begin{aligned} v_{ca} &= \tfrac{V_{dc}}{3}(2S_a - S_b - S_c) \\ v_{cb} &= \tfrac{V_{dc}}{3}(-S_a + 2S_b - S_c) \\ v_{cc} &= \tfrac{V_{dc}}{3}(-S_a - S_b + 2S_c) \end{aligned} \tag{4.5}$$

Three phase currents i_{ca}, i_{cb} and i_{cc} flow through RL filter, which can be obtained as follows

$$\begin{aligned} \tfrac{di_{ca}}{dt} &= \dot{i}_{ca} = -\left(\tfrac{R_{ca}}{L_{ca}}\right) i_{ca} + \tfrac{(V_{sa}-V_{ca})}{L_{ca}} \\ \tfrac{di_{cb}}{dt} &= \dot{i}_{cb} = -\left(\tfrac{R_{cb}}{L_{cb}}\right) i_{cb} + \tfrac{(V_{sb}-V_{cb})}{L_{cb}} \\ \tfrac{di_{cc}}{dt} &= \dot{i}_{cc} = -\left(\tfrac{R_{cc}}{L_{cc}}\right) i_{cc} + \tfrac{(V_{sc}-V_{cc})}{L_{cc}} \end{aligned} \tag{4.6}$$

The calculation of DC-link capacitor current in terms of phase currents (i_{ca}, i_{cb} and i_{cc}) and switching devices (S_a, S_b, S_c) status is as follows

$$I_{dc} = i_{ca} S_a + i_{cb} S_b + i_{cc} S_c \tag{4.7}$$

From equation(4.7), the DC-link capacitor voltage can be written as

$$\frac{dV_{dc}}{dt} = \dot{V}_{dc} = \frac{i_{ca} S_a + i_{cb} S_b + i_{cc} S_c}{C_{dc}} \tag{4.8}$$

The DC-link capacitor serves as an energy storage element that supplies real power to the inverter. This real power can be supplied by the source when the control output reaches to the steady state condition, and it should be equal to the power demand of the load along with small power losses in the PV system.

4.4 Hysteresis current controller (HCC)

The existing fixed hysteresis current controller is used for a PV system to generate switching pulses to the inverter. This controller is widely used either for single level inverter or for multilevel inverters. Some of the researchers have developed HCC for multilevel inverter by using the programmable logic devices (PLD) [107]. The HCC can be categorized into two types; they are two-level HCC and three-level HCC. Fig.4.4 shows the block diagram of three phase HCC for a GCPV system. In this thesis, hysteresis current controller for three phase PV system is simulated, verified with Opal-RT and validated through experimental setup.

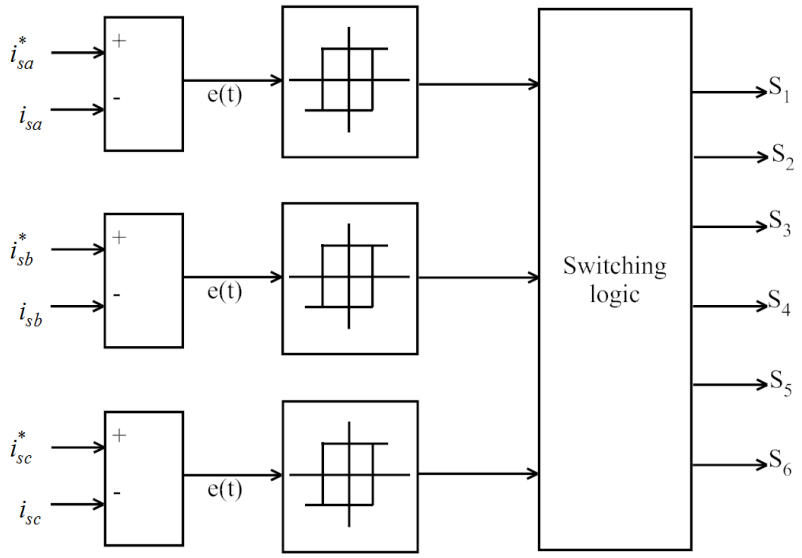

Figure 4.4: Block diagram of three phase HCC

In Fig. 4.4, e(t) is the error current; which is the difference between the reference currents (i^*_{sa}, i^*_{sb}, i^*_{sc}) and the actual currents (i_{sa}, i_{sb}, i_{sc}). When the error current exceeds the upper limit of the hysteresis band then the inverter upper switch should be OFF and lower switch should be ON. When the error current exceeds the lower limit of the hysteresis band then the inverter lower switch should be OFF and upper switch should be ON.

4.4.1 Two level hysteresis current controller

The two level hysteresis current controller is shown in Fig. 4.5, it operates the VSI by comparing the error current e(t) against the hysteresis bands. The error current is the

difference between reference and actual currents. When the error current exceeds the upper limit of the hysteresis band, then the lower switch should be ON, after which the current starts decaying [105], [108]. If the error current crosses the lower limit of the hysteresis band, then the upper switch is ON, then the current get backs into the hysteresis band. Therefore, the actual current is forced to track the reference current within the band limits. The switching pattern of the two level HCC is shown in Fig. 4.6.

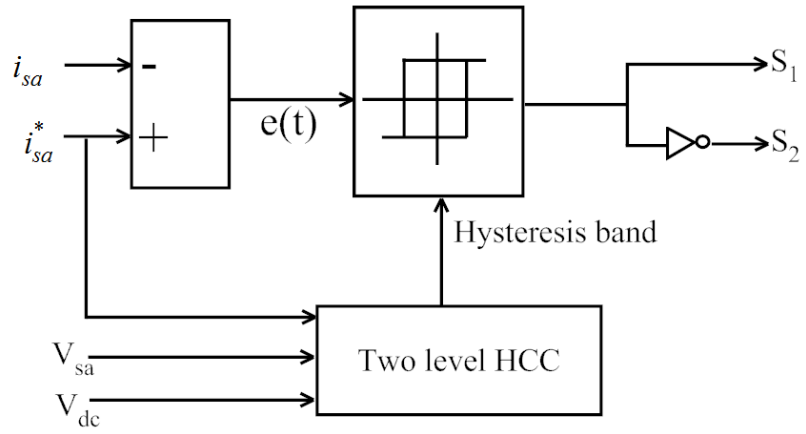

Figure 4.5: Block diagram of two level hysteresis current controller

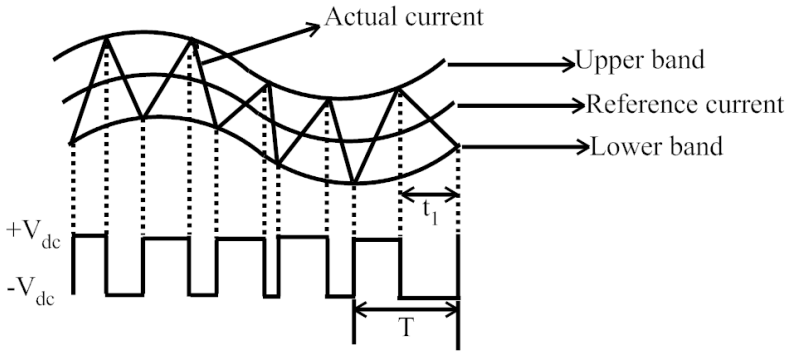

Figure 4.6: Switching pattern for two level hysteresis band

The switching performance of phase A is defined as

$$S = \begin{cases} ON\ if\ i_{sa}(t) < i^*_{sa}(t) - hb \\ OFF\ if\ i_{sa}(t) > i^*_{sa}(t) + hb \end{cases} \tag{4.9}$$

Similarly, the switching performance of phases B and C can be derived by using hysteresis bandwidth (hb). Two level HCC are used because of circuit simplicity in PV

power system applications [109]. However, it does not use zero voltage from the inverter DC side, only negative and positive DC supply voltages are used to generate the required switching pulses. The two level generates significant side band harmonics around the switching frequency because two level modulation is lower than the three level modulation [104]. To overcome the above problems, three level hysteresis modulation is implemented with three level switching process.

4.4.2 Three level hysteresis current controller

The three level hysteresis controller block diagram is shown in Fig. 4.7. The implementation of the controller is set as upper band and lower band overlap boundaries and displacement of small offset current. When the error current e(t) (difference among the reference and actual currents) crosses an outer boundary, then the inverter output is set to positive or negative output to force a reversal of the current error. Similarly, when the error current reached to an inner boundary then the inverter output is set to zero and the error current will be forced to reverse direction without reaching the next boundary. If the zero selection output does not reverse the current trajectory, then it will go on through the inner boundary to the subsequent outer boundary where an opposite polarity inverter output will be controlled and then the current will be reversed in any direction [110].

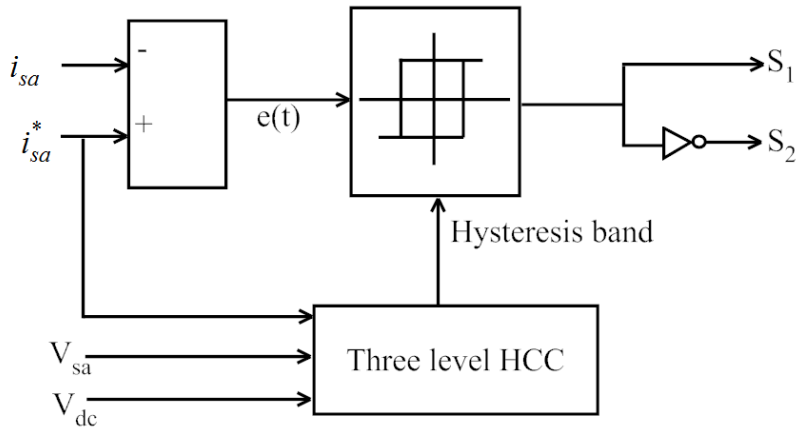

Figure 4.7: Block diagram of three level hysteresis current controller

The switching process of three level hysteresis current controller is shown in Fig. 4.8. Here, the error current is surrounded in the middle of the upper-inner and lower-outer boundaries for a positive inverter output. Likewise, for a negative inverter output, the error

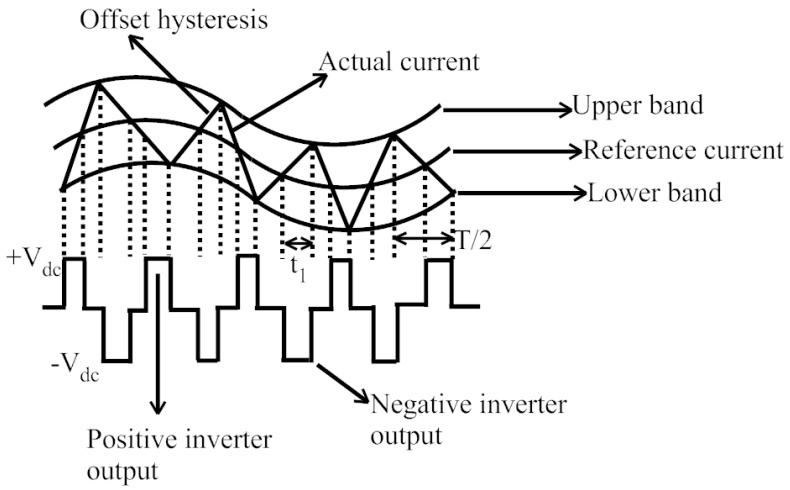

Figure 4.8: Switching pattern for three level hysteresis band

current is surrounded in between the lower-inner and upper-outer boundaries.

The complete switching cycle for two level and three level HCC is $0 \rightarrow t_1 \rightarrow T$ and $0 \rightarrow t_1 \rightarrow T/2$ respectively. Depending on the polarity of output voltage, the switching process introduces either positive or negative DC offset error at the average output current. However, this error can be corrected by adding a compensation factor of the half hysteresis band offset magnitude to the phase current reference. The switching process introduces a positive or negative DC-offset error in the average output current, depending on the polarity of the active output voltage. The switching operation of an inverter for phase-A switching logic is presented in [111], and flow chart of three level HCC for phase-A is shown in Fig. 4.9.

The advantages of fixed-HCC are simple design, accuracy and unconditioned stability. The disadvantages of fixed-HCC are slope of current waveform may vary widely and the peak amplitude of current waveform may exceed the hysteresis-band. Consequently, inverter switches will be operated at high switching frequency in order to track reference current.

4.5 Adaptive HCC

The hysteresis current control strategy has some disadvantages such as uneven switching frequency at a particular band limit. Adaptive HCC overcomes those limitations. The

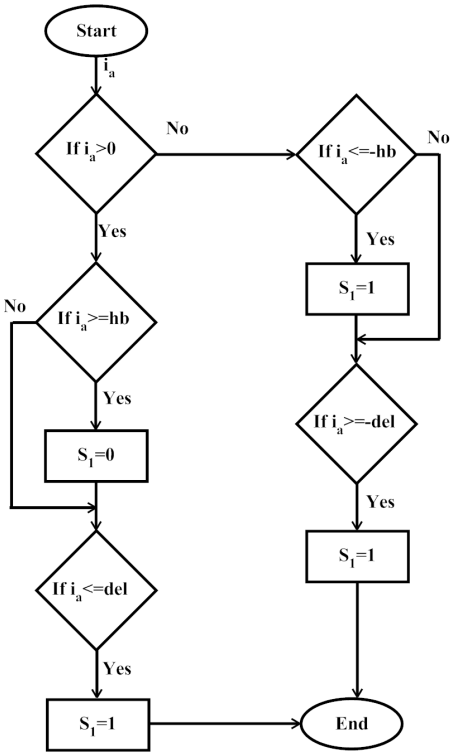

Figure 4.9: Flow chart of three level HCC for Phase A

adaptive hysteresis current controller based switching pulse generator for PWM-VSI is shown in Fig. 4.10. This proposal by Bose [112] for the machine drive system is adopted here for PV power system based on theory of indirect current control. When e(t) (error current) crosses the lower limit of the band, then the upper switch should be ON and when it exceeds the upper limit, then the lower switch is ON. Therefore, the actual current is forced to track the reference current within the hysteresis band. The single line switching representation is shown in Fig. 4.11, and the switching interval equations [106], [113] are as follows

$$\frac{di_{sa}^{+}}{dt} = \frac{1}{L}(V_{dc} - v_s) \tag{4.10}$$

$$\frac{di_{sa}^{-}}{dt} = -\frac{1}{L}(V_{dc} + v_s) \tag{4.11}$$

where L = Phase inductance, i_{sa}^{+} =rising current segment, i_{sa}^{-} =falling current segment. From Fig. 4.11, the equations for switching intervals of hysteresis band curvature can be written

as

$$\frac{di_{sa}^{+}}{dt}t_1 - \frac{di_{sa}^{*}}{dt}t_1 = 2HB \tag{4.12}$$

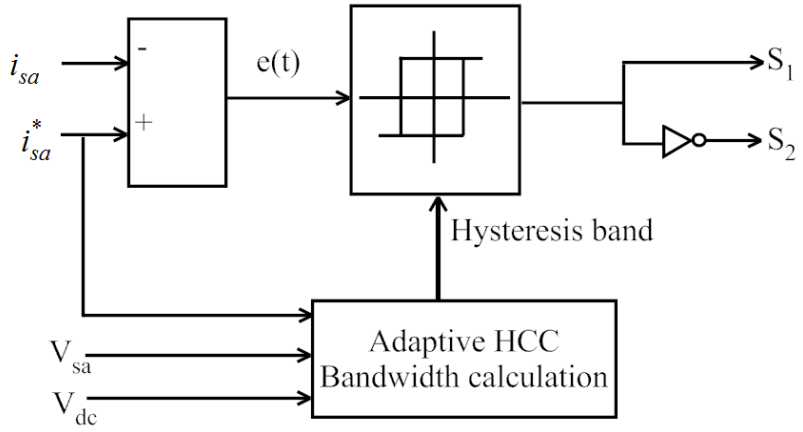

Figure 4.10: Block diagram of an adaptive hysteresis current controller

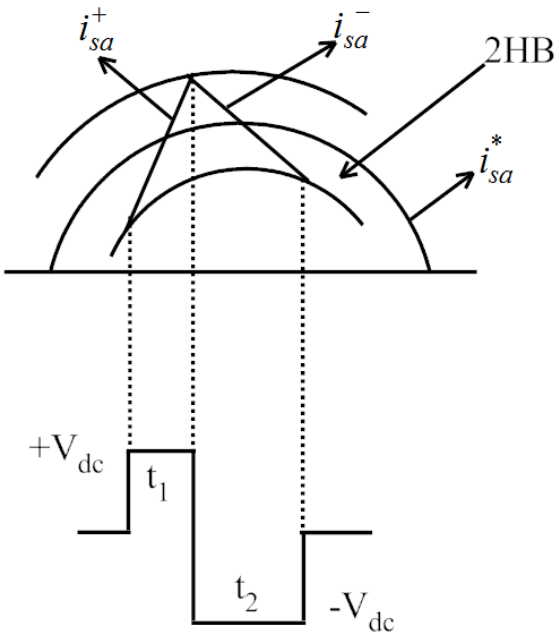

Figure 4.11: Single line switching pattern for 2 level hysteresis band

$$\frac{di_{sa}^{-}}{dt}t_2 - \frac{di_{sa}^{*}}{dt}t_2 = -2HB \tag{4.13}$$

$$t_1 + t_2 = T_c = 1/f_c \tag{4.14}$$

where, t_1 and t_2 are switching intervals and f_c is modulation frequency. Adding equation(4.12) and equation(4.13), yields

$$\frac{di_{sa}^{+}}{dt}t_1 + \frac{di_{sa}^{-}}{dt}t_2 - \frac{di_{sa}^{*}}{dt}(t_1 + t_2) = 0 \tag{4.15}$$

Substituting equation(4.10), equation(4.11) and equation(4.14) in equation(4.15), then

$$\frac{(V_{dc} - v_s)}{L}t_1 - \frac{(V_{dc} + v_s)}{L}t_2 - \frac{1}{f_c}\frac{di_{sa}^{*}}{dt} = 0 \tag{4.16}$$

After simplification, equation(4.16) as

$$(t_1 - t_2) = \frac{L}{V_{dc} - f_c}\left[\frac{v_s}{L} + \frac{di_{sa}^{*}}{dt}\right] \tag{4.17}$$

Subtracting equation(4.13) from equation(4.12), yields

$$\frac{di_{sa}^{+}}{dt}t_1 - \frac{di_{sa}^{-}}{dt}t_2 - \frac{di_{sa}^{*}}{dt}(t_1 - t_2) = 4HB \tag{4.18}$$

Substitute equation(4.10), equation(4.11), equation(4.14) and equation(4.17) in equation(4.18), the final equation is as follows

$$4HB = \frac{V_{dc}}{Lf_c} - \frac{L}{V_{dc}f_c}\left[\frac{v_s}{L} + \frac{di_{sa}^{*}}{dt}\right]^2 \tag{4.19}$$

On simplifying the equation(4.19), gives

$$HB = \frac{0.25V_{dc}}{Lf_c}\left[1 - \frac{L^2}{V_{dc}^2}\left[\frac{v_s}{L} + \frac{di_{sa}^{*}}{dt}\right]^2\right] \tag{4.20}$$

The equation(4.20) can be re-written as

$$HB = \frac{0.25V_{dc}}{Lf_c}\left[1 - \frac{L^2}{V_{dc}^2}\left[\frac{v_s}{L} + m\right]^2\right] \tag{4.21}$$

where

v_s = supply voltage,

V_{dc}=DC-link capacitor voltage,

L= Coupling inductor,

m= slope of the reference current signal.

The adaptive hysteresis band current controller (AHBCC) changes the bandwidth according to instantaneous current variation and V_{dc} to minimize the current distortion [114]. To control the inverter switching pulses, the hysteresis band (HB) can be modulated at different point of fundamental frequency. Calculated HB is applied for the switching operation of HCC. The switching operation is created by an S-function in MATLAB/SIMULINK model to generate switching pulses to drive the inverter. The block diagram of adaptive HB calculation is shown in Fig. 4.12. By using the ABHCC, the PWM performance will be increased and effects of dc-link voltage variations on current quality should be decreased. Due to high frequency, the ABHCC ensures more switching power losses.

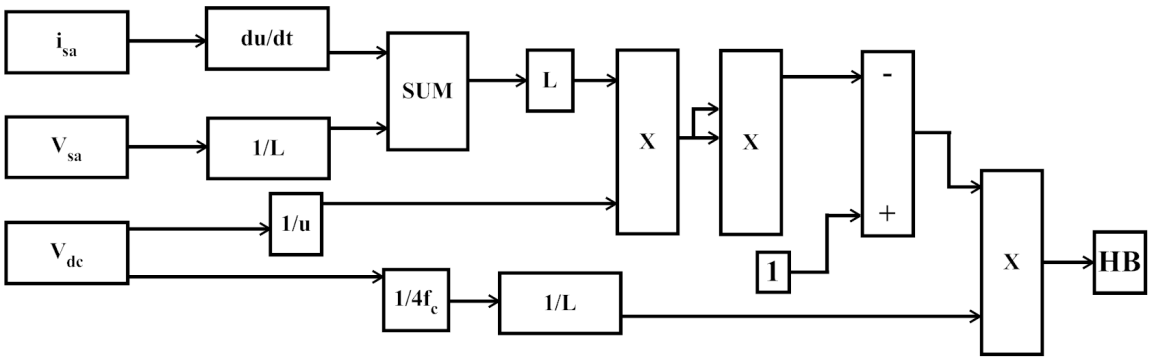

Figure 4.12: Block diagram of an adaptive hysteresis bandwidth calculation

4.6 Model Predictive Controller

The adaptive HCC yields more power loss due to high frequency switching, this limitation can be overcome by using a model predictive controller. The model predictive control has been proposed for reconfiguration due to its ability to handle constraints and changing the model dynamics systematically. MPC is also called as model based predictive control (MBPC), receding horizon control (RHC), generalized predictive control (GPC), dynamic matrix control (DMC) and sequential open-loop optimizing control (SOLO) [115]. The control strategy of MPC has become an advanced control technology in chemical industry, and its usage is spreading to other application areas [116]. It uses a model to compute the trajectory of a future variable u to optimize the behaviour of the control variable 'x'. MPC uses the current measurements to calculate the future actions of the manipulated variables

and make sure that the controlled and manipulated variables to satisfy the constraints. The topology of MPC is shown in Fig. 4.13, and block diagram of MPC control strategy is shown in Fig. 4.14.

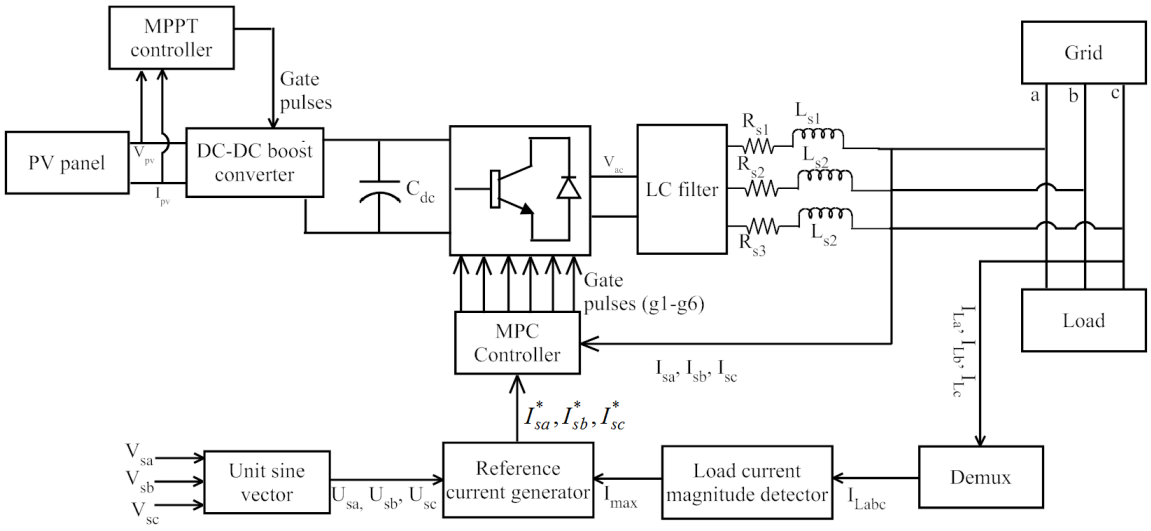

Figure 4.13: Topology of model predictive MPPT controller

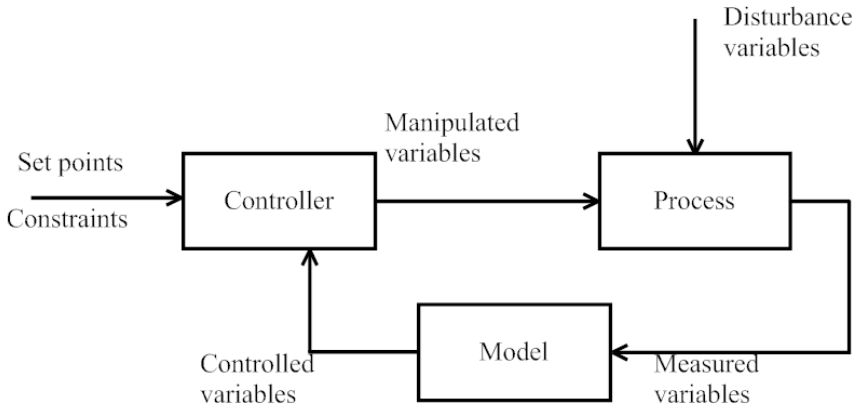

Figure 4.14: Block diagram of model predictive controller

At the time instant k, the initial controlled variable x_k is computed with the n sampling instants of manipulated variables u(k), u(k+1), ...,u(k+n-1). Here, n is the prediction horizon. The manipulated variables are calculated to minimize the cost function C. for the quadratic programming, the first element in the manipulated variables u(k) will be applied to the system at the time interval of (k) to (k+1), next sampling instant is (k+1) to (k+2), and so on. The quadratic programming equation for manipulated variables for all sampling

time instants is as follows

$$\min C = \frac{1}{2}\sum_{k=0}^{n-1} [x_r(k+1) - x(k+1)]^T Q [x_r(k+1) - x(k+1)] + [u_r(k) - u(k)]^T R [u_r(k) - u(k)] \tag{4.22}$$

where, Q and R are weighting matrices for prediction error and control actions. If Q and R are positive then the quadratic problem would be convex. One advantage of this MPC is to block the violations of input and output constraints, for example, limitation on rate of change in input, product quantity and quality. The cost function C with inequality constraints is

$$C = \begin{cases} \underline{u} \le u_k \le \bar{u}, \ 0 \le k \le n-1 \\ \underline{x} \le x_k \le x, \ 1 \le \bar{k} \le n \end{cases} \tag{4.23}$$

where, $\underline{u}\, and\, \underline{x}$ and $\bar{u}\, and\, \bar{x}$ are the lower bounds and upper bounds of u and x respectively. It is important to justify the nonlinear MPC before it should be applied, because nonlinear optimization consumes more time than the linear MPC [117]. The implementation of MPC for power converters is a difficult task due to high amount of computations to solve the optimization problem. This problem can be solved with the development of high speed DSP or FPGA.

4.6.1 MPC in power converters

Four different models are used in MPC; they are (i) impulse response models, (ii) state space models, (iii) transfer function models and (iv) step response models. Two important methods are there for using MPC to control the power converters, they are (a) finite control set MPC [116] and (b) predictive direct power control (PDPC) [118]. Finite control set (FCS) signifies finite number or limited number of switching states in power converter. There are eight switching states in three phase half bridge rectifier and the switching state minimizes the selected cost function. In [119], a two level VSI was tested with FCS-MPC and it was observed that no need of modulation stages for the switching states was necessary. PDPC implemented by using space vector PWM (SVPWM), it computes voltage vectors and their durations of action to minimize the power errors in prediction time

interval. Several model predictive algorithms has been applied to inverter [120]; but those are limited to control the three phase rectifiers. In this thesis, a discrete time state space model for an inverter is used for development of MPC.

4.6.2 Modelling of Voltage Source Regulator (VSR)

To predict the future behaviour, discrete time state space model is used. In order to minimize the cost function of the PWM rectifier, its input voltage is calculated. Furthermore to solve the variable frequency and drawback of finite control set, a desired voltage by the converter is generated via the Space Vector PWM (SVPWM). There are many design parameters in MPC like n (prediction horizon), Q, R (weighting matrices) and sampling period. Fig. 4.15 shows the topology of three phase voltage source PWM rectifier.

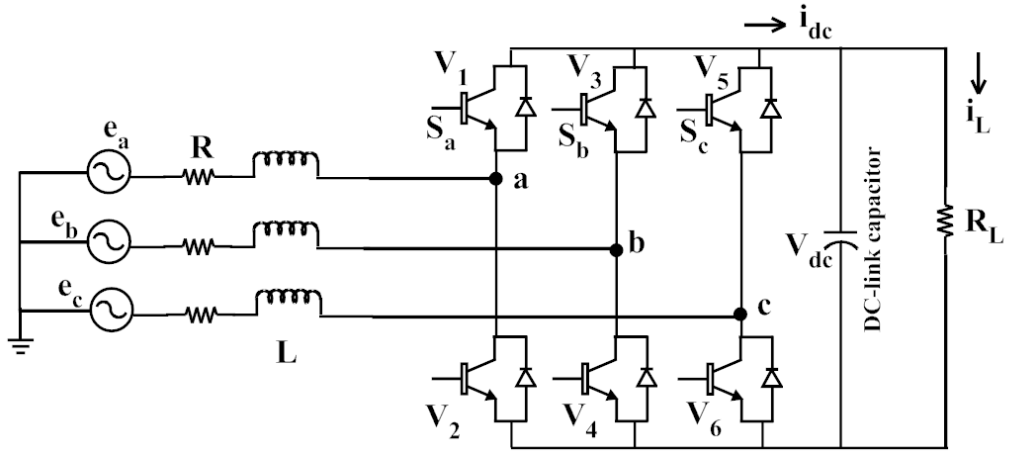

Figure 4.15: Three phase PWM topology

The dynamic model for the three phase model is given by

$$\begin{cases} L\frac{di_a}{dt} = e_a - Ri_a - \left(S_a - \frac{S_a+S_b+S_c}{3}\right)V_{dc} \\ L\frac{di_b}{dt} = e_b - Ri_b - \left(S_b - \frac{S_a+S_b+S_c}{3}\right)V_{dc} \\ L\frac{di_c}{dt} = e_c - Ri_c - \left(S_c - \frac{S_a+S_b+S_c}{3}\right)V_{dc} \\ C\frac{dV_{dc}}{dt} = i_a s_a + i_b s_b + i_c s_c - \frac{V_{dc}}{R_L} \end{cases} \tag{4.24}$$

where, S_a, S_b, S_c are manipulated variables, i_a, i_b, i_c, v_{dc} are controlled variables, which suppresses the AC current harmonics and regulate the DC output voltage. We can apply the park transformation to get the dq coordinate model from abc coordinate model. The

equations are as follows:

$$\begin{cases} L\frac{di_d}{dt} = e_d + \omega L i_q - R i_d - V_{dc} s_d \\ L\frac{di_q}{dt} = e_q - \omega L i_d - R i_q - V_{dc} s_q \\ C\frac{dV_{dc}}{dt} = \left(i_q s_q + i_d s_d\right) - i_L \end{cases} \tag{4.25}$$

where, s_d, s_q are manipulated variables and i_d, i_q, V_{dc} are controlled variables. From the equation(4.25), one can observe that the system is non-linear. The losses on AC side resistors and switches are ignored using the energy conservation law, which states that the grid input power and the load power along with the capacitor charging power should be equal, in order to achieve the regulated DC voltage, assuming a steady state system with $v_{dc} = v_{dco}$, where v_{dco} is the reference value of the DC output voltage.

$$p = e_d i_d + e_q i_q = V_{dco}(i_q s_q + i_d s_d) \tag{4.26}$$

From equation(4.25), we know that $\left(i_q s_q + i_d s_d\right) = C\frac{dV_{dc}}{dt} + i_L$, $i_L = \frac{V_{dc}}{R_L}$

Substitute the above values in equation(4.26), then the equation becomes

$$p = e_d i_d + e_q i_q = v_{dco}\left(C\frac{dV_{dc}}{dt} + \frac{V_{dc}}{R_L}\right) \tag{4.27}$$

Therefore,

$$C\frac{dV_{dc}}{dt} = \frac{e_d i_d}{V_{dco}} - \frac{V_{dc}}{R_L} \tag{4.28}$$

From the above equations, the dynamic model of the power rectifier is expressed as

$$\begin{cases} L\frac{di_d}{dt} = e_d + \omega L i_q - R i_d - V_{dc} s_d \\ L\frac{di_q}{dt} = e_q - \omega L i_d - R i_q - V_{dc} s_q \\ C\frac{dV_{dc}}{dt} = \frac{e_d i_d}{V_{dco}} - \frac{V_{dc}}{R_L} \end{cases} \tag{4.29}$$

Equation(4.29) can be expressed in state space is as follows

$$\begin{bmatrix} \dot{i}_d \\ \dot{i}_q \\ \dot{V}_{dc} \end{bmatrix} = \begin{bmatrix} -\frac{R}{L} & \omega & 0 \\ -\omega & -\frac{R}{L} & 0 \\ \frac{e_d}{CV_{dco}} & 0 & -\frac{1}{CR_L} \end{bmatrix} \begin{bmatrix} i_d \\ i_q \\ V_{dc} \end{bmatrix} + \begin{bmatrix} \frac{1}{L} & 0 \\ 0 & \frac{1}{L} \\ 0 & 0 \end{bmatrix} \begin{bmatrix} e_d - V_{dc} s_d \\ e_q - V_{dc} s_q \end{bmatrix} \tag{4.30}$$

Future value of the controlled variables can be predicted by a discrete time model with T sampling time. This can be achieved by the Euler's approximation $\frac{di}{dt} = \left(\frac{i(k+1)-i(k)}{T}\right)$ thus converting equation(4.30) as shown below:

$$\begin{bmatrix} i_d(k+1) \\ i_q(k+1) \\ V_{dc}(k+1) \end{bmatrix} = \begin{bmatrix} 1-\frac{R}{L} & \omega T & 0 \\ -\omega T & 1-\frac{RT}{L} & 0 \\ \frac{e_d T}{CV_{dco}} & 0 & 1-\frac{T}{CR_L} \end{bmatrix} \begin{bmatrix} i_d(k) \\ i_q(k) \\ V_{dc}(k) \end{bmatrix} + \begin{bmatrix} \frac{T}{L} & 0 \\ 0 & \frac{T}{L} \\ 0 & 0 \end{bmatrix} \begin{bmatrix} e_d - V_{dc}s_d \\ \\ e_q - V_{dc}s_q \end{bmatrix} \tag{4.31}$$

Thus quickly regulating the DC output voltage and with unity power factor suppressing the input current harmonics, the aim of MPC is attributed again in this section, which states that $i_q = 0$, $V_{dc} = V_{dco}$ and required power to the load is supplied by id thus making these traceable by the MPC controller. Furthermore, by solving equation(4.22) and equation(4.30), then the final equation is as follows

$$x(k) = \begin{bmatrix} i_d(k) \\ i_q(k) \\ V_{dc}(k) \end{bmatrix}, u(k) = \begin{bmatrix} e_d - V_{dc}s_d \\ e_q - V_{dc}s_q \end{bmatrix}, Q = \begin{bmatrix} 2 & 0 & 0 \\ 0 & 2 & 0 \\ 0 & 0 & 2 \end{bmatrix}, R = \begin{bmatrix} 2 & 0 \\ 0 & 2 \end{bmatrix} \tag{4.32}$$

The desired input voltage to PWM rectifier u(k), and $V_{dcsd}(k)$and $V_{dcsq}(k)$ derived control action minimizes the cost function of MPC, which is obtained in d_q format. To frame the desired space vector the input voltage is transformed from d_q frame to $\alpha\beta$ frame.

$$V^* = \sqrt{(V_{dc}s_d)^2 + (V_{dc}s_q)^2} \angle \left(\omega t + \arctan \frac{V_{dc}s_d}{V_{dc}s_q}\right) \tag{4.33}$$

Space vector control strategy was introduced by Japanese in 1980s for AC motors. It is a new control strategy to control converters. The SVPWM technique increases the voltage utilization rate by 15% when compared with the conventional sinusoidal PWM method [115]. The main advantage of SVPWM is having lower switching frequency.

4.6.3 Synthesis of voltage space vector

The objective of SVPWM is to synthesize the desired AC input voltage space vector. For any given voltage space vector $V*$, it can be synthesized by the eight basic space vectors is

shown in Fig. 4.16.

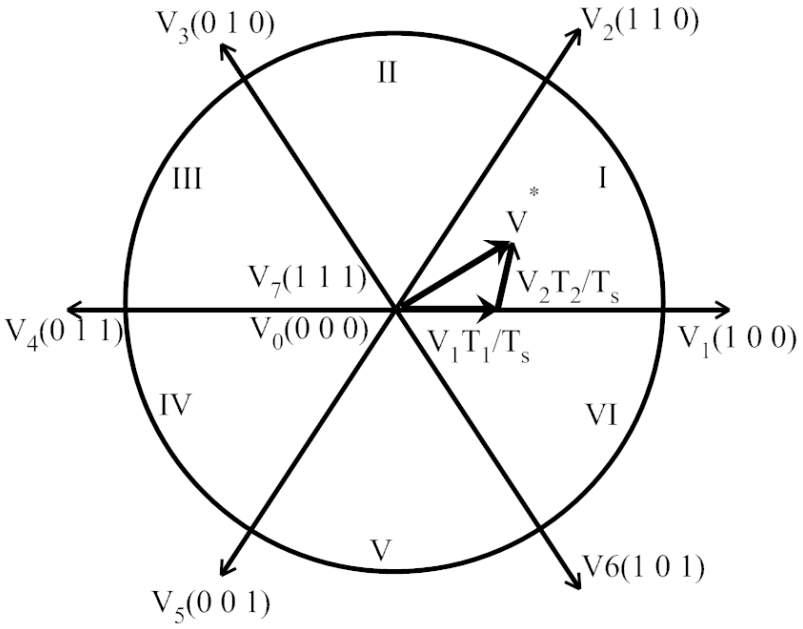

Figure 4.16: Basic vectors and sectors

The voltage vector can be expressed from Fig. 4.16 as

$$T_1 V_1 + T_2 V_2 = V^* T_s \tag{4.34}$$

The angle between $V^* and\, V_1\ is\ \alpha$, using the sinusoidal law, one can write

$$\frac{|V^*|}{\sin\frac{2\pi}{3}} = \frac{\left|\frac{T_2}{T_s}V_2\right|}{\sin\alpha} = \frac{\left|\frac{T_1}{T_s}V_1\right|}{\sin(\frac{\pi}{3}-\alpha)} \tag{4.35}$$

From the above equations the time interval can be calculated as

$$\begin{cases} T_1 = \frac{\sqrt{2}|V^*|}{v_{dc}} T_s \sin\left(\frac{\pi}{3}-\alpha\right) \\ T_2 = \frac{\sqrt{2}|V^*|}{v_{dc}} T_s \sin(\alpha) \\ T_{0,7} = T_s - T_1 - T_2 \end{cases} \tag{4.36}$$

Constraint of linear SVPWM modulation is

$$T_1 + T_2 \leq T_s \tag{4.37}$$

Combine equation(4.35) and equation(4.36), then

$$\frac{\sqrt{2}\,|V^*|}{v_{dc}} T_s \sin\left(\frac{\pi}{3} - \alpha\right) + \frac{\sqrt{2}\,|V^*|}{v_{dc}} T_s \sin(\alpha) \leq T_s \tag{4.38}$$

A modulation in the three phase sinusoidal voltages takes place when V^* is rotated in the complex plane at a fixed speed, which due to switching frequency and limited switch combinations rotates in a constant speed. As shown in Fig. 4.17 to prevent any changes at AC currents, there is a limitation to amplitude of VS vector V^*. The saturation of SVPWM condition where by the V+ can be bigger than $\frac{V_{dc}}{\sqrt{2}}$ is depicted as a flowchart of MPC-SVPWM in Fig. 4.17.

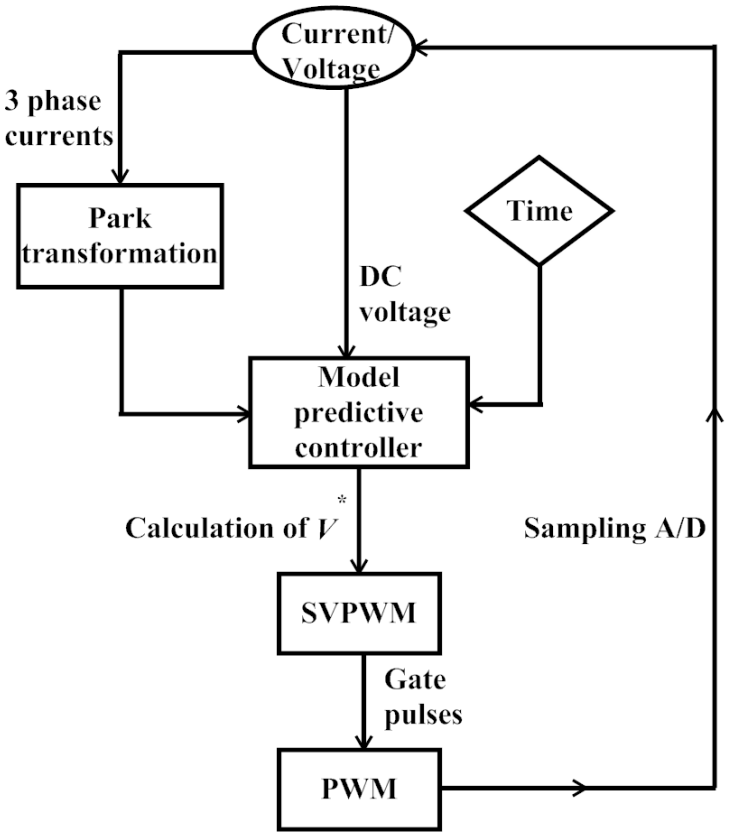

Figure 4.17: Flow chart of MPC-SVPWM

4.7 Results and Discussion

The GCPV system with different controllers is simulated in MATLAB/SIMULINK, and simulation results are validated with Opal-RT and experimental setup.

The supply voltages are sensed to get the unit sine vector templates, which are given as

$$V_{sa} = V_m \sin(\omega t)$$

$$V_{sb} = V_m \sin(\omega t - 120^0) \tag{4.39}$$

$$V_{sc} = V_m \sin(\omega t + 120^0)$$

where V_m = peak value of source voltage, $\omega = 2\pi f$ =angular frequency.

Three phase current is considered to generate unit sine vector templates, derived as follows

$$u_{sa} = \frac{V_{sa}}{V_m} = \sin(\omega t)$$

$$u_{sb} = \frac{V_{sb}}{V_m} = \sin(\omega t - 120^0) \tag{4.40}$$

$$u_{sc} = \frac{V_{sc}}{V_m} = \sin(\omega t + 120^0)$$

The magnitude analyser estimates the peak current I_{max}, and it multiplies with output of unit sine vector to generate the required reference current.

$$i^*_{sa} = \mathrm{I}_{max} u_{sa} = \mathrm{I}_{max} \sin(\omega t)$$

$$i^*_{sb} = \mathrm{I}_{max} u_{sb} = \mathrm{I}_{max} \sin(\omega t - 120^0) \tag{4.41}$$

$$i^*_{sc} = \mathrm{I}_{max} u_{sc} = \mathrm{I}_{max} \sin(\omega t + 120^0)$$

The VSI generates switching pulses by using PWM controller after comparing reference current with actual current. The inverter parameters are given in Table 4.1.

The unit sine vector and load current magnitude detector with HCC, AHCC and MPC PWM current controller is simulated under balanced load conditions. The simulated results are shown in Fig. 4.18, Fig. 4.19, and Fig. 4.20 respectively. Here, 6 PV panels are

Table 4.1: Inverter parameters

Parameter	**Value**
Supply voltage/frequency	280V/50Hz
Interface inductor (RCLC)	1 ohm, 1.5 mH
Capacitance (C)	500 μF
DC-link capacitance (C_{dc})	2.2 nF
Reference voltage (V_{dcref})	400V
VSI	6 IGBTs

considered and connected in series. PV generates 280V output after losses like ohmic losses, activation losses.

The PV output voltage is shown in Fig. 4.18(a). A DC-DC boost converter is used to step up the PV voltage to 400V (specifications given in Chapter 1), output waveform is shown in Fig. 4.18(b). The output of boost converter is connected to an inverter through a DC-link capacitor. The inverter output is given to an LC filter for ripple suppression. Fig. 4.18(c) shows grid voltage and Fig. 4.18(d) inverter output voltage. The current from grid, reference current, inverter output current and unit sine vector are shown in Fig. 4.18(e), Fig. 4.18(f), Fig. 4.18(g) and Fig. 4.18(h) respectively.

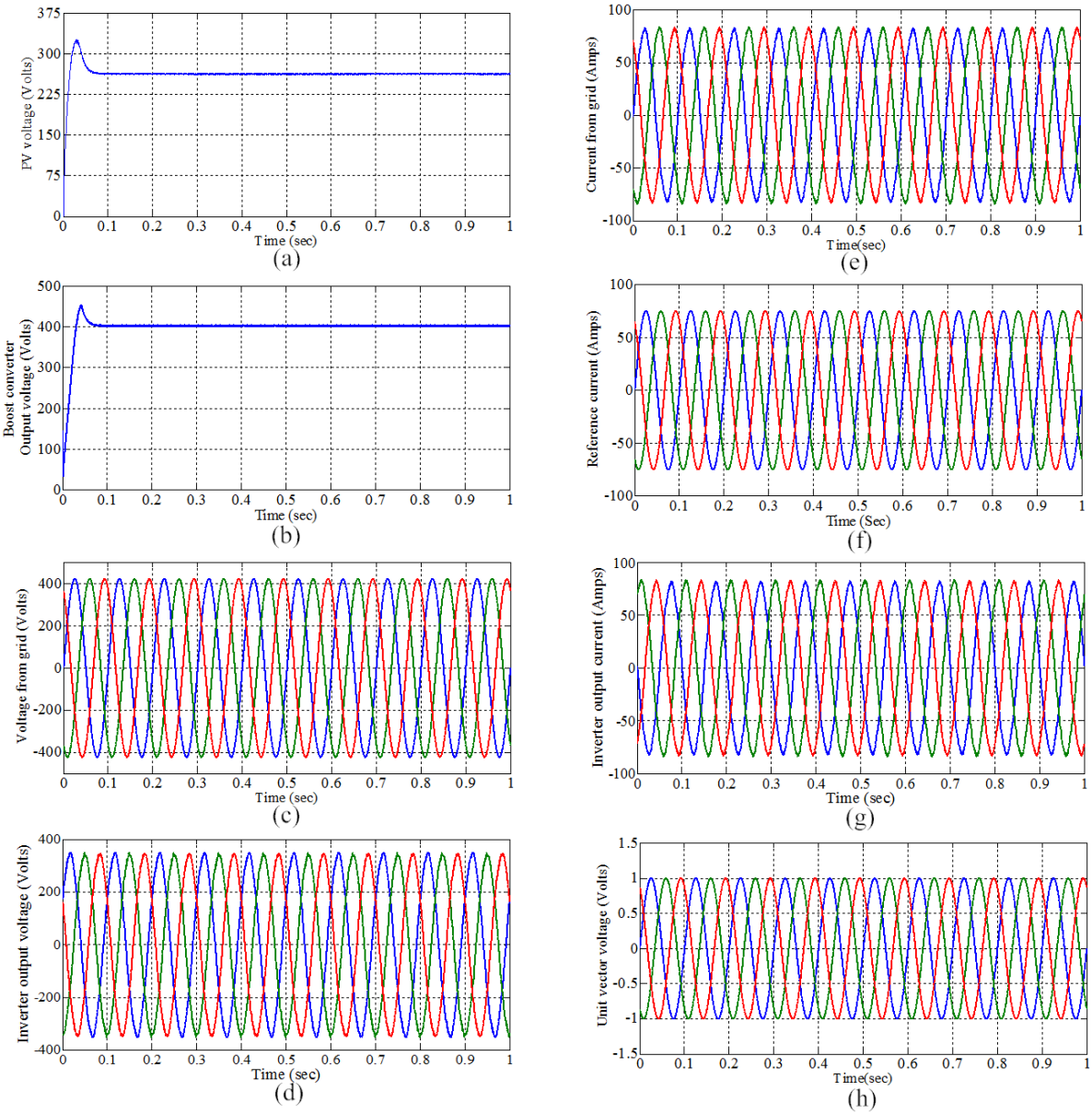

Figure 4.18: Simulation results of Hysteresis current controller

The PV output voltage is shown in Fig. 4.19(a). A DC-DC boost converter is used to step up the PV voltage to 400V (specifications given in Chapter 1), output waveform is shown in Fig. 4.19(b). The output of boost converter is connected to an inverter through a DC-link capacitor. The inverter output is given to an LC filter for ripple suppression. Fig. 4.19(c) shows grid voltage and Fig. 4.19(d) inverter output voltage. The current from grid, reference current, inverter output current and unit sine vector are shown in Fig. 4.19(e), Fig. 4.19(f), Fig. 4.19(g) and Fig. 4.19(h) respectively.

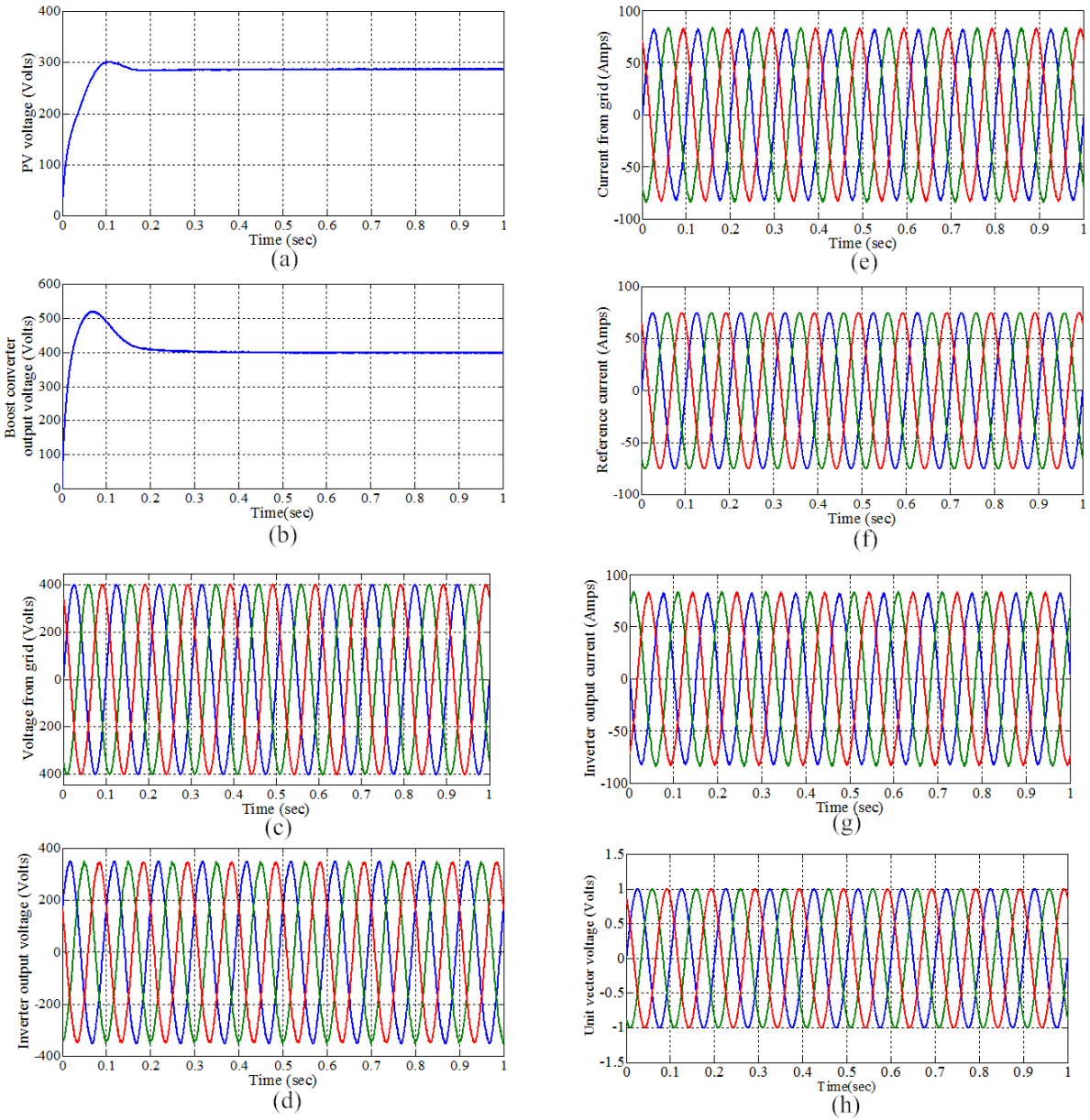

Figure 4.19: Simulation results of Adaptive hysteresis current controller

The PV output voltage is shown in Fig. 4.20(a). A DC-DC boost converter is used to step up the PV voltage to 400V, output waveform is shown in Fig. 4.20(b). The output of boost converter is connected to an inverter through a DC-link capacitor. The inverter output is given to an LC filter for ripple suppression. Fig. 4.20(c) shows grid voltage and Fig. 4.20(d) inverter output voltage. The current from grid, reference current, inverter output current and unit sine vector are shown in Fig. 4.20(e), Fig. 4.20(f), Fig. 4.20(g) and Fig. 4.20(h) respectively.

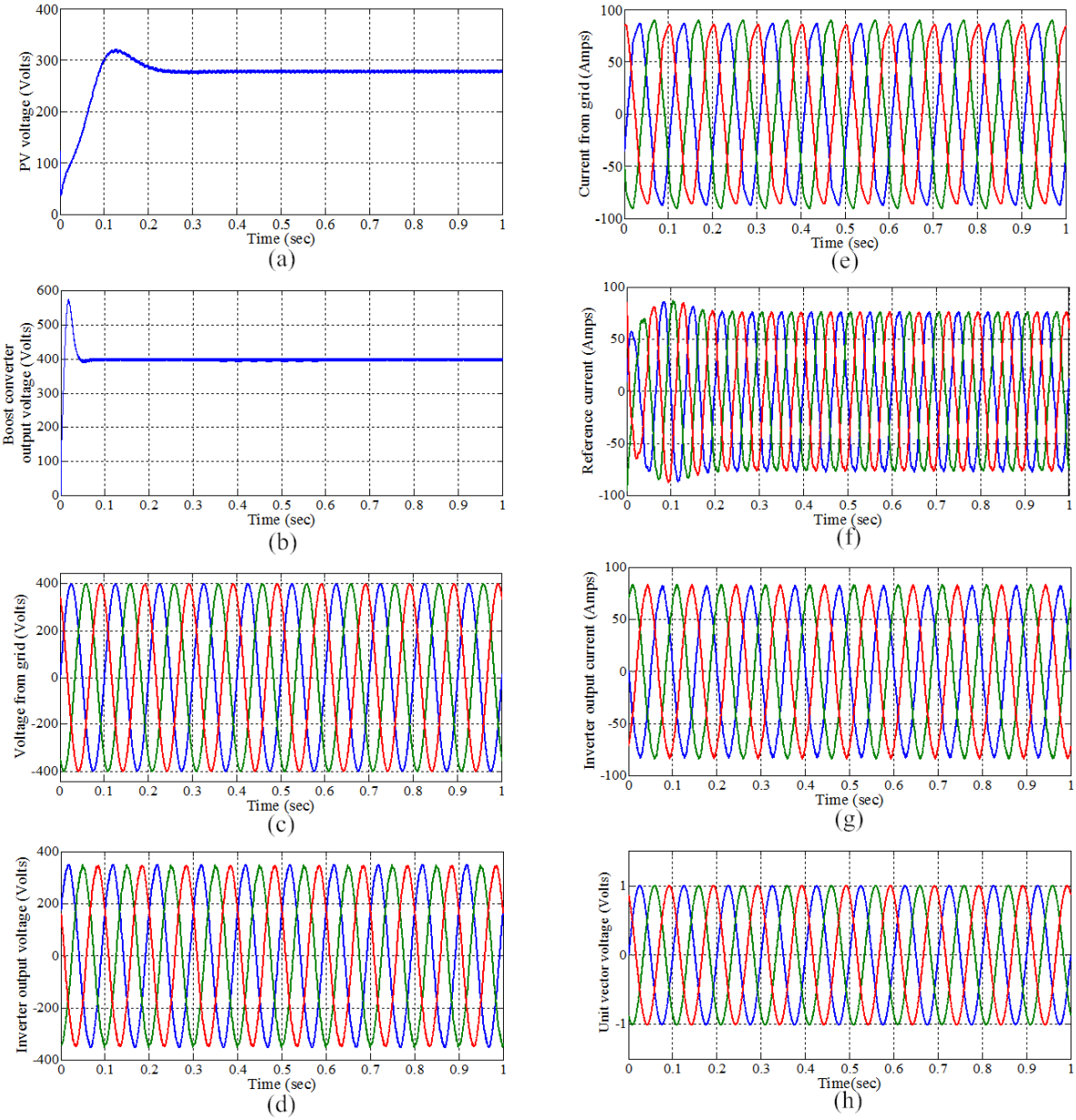

Figure 4.20: Simulation results of Model predictive controller

Fig. 4.21 shows the picture of complete hardware setup. The hardware setup has been described in chapter 3 except voltage source inverters. The PV system prototype model consists of six IGBT (SKM75Gb063d), an inductor (5mH) and a DC-link capacitor (6800). The three pahse supply voltages, load currents and DC voltage signals are the input to the controller, which are sensed and computed.

The HCC/AHCC/MPC techniques are used to generate the switching sequences; these

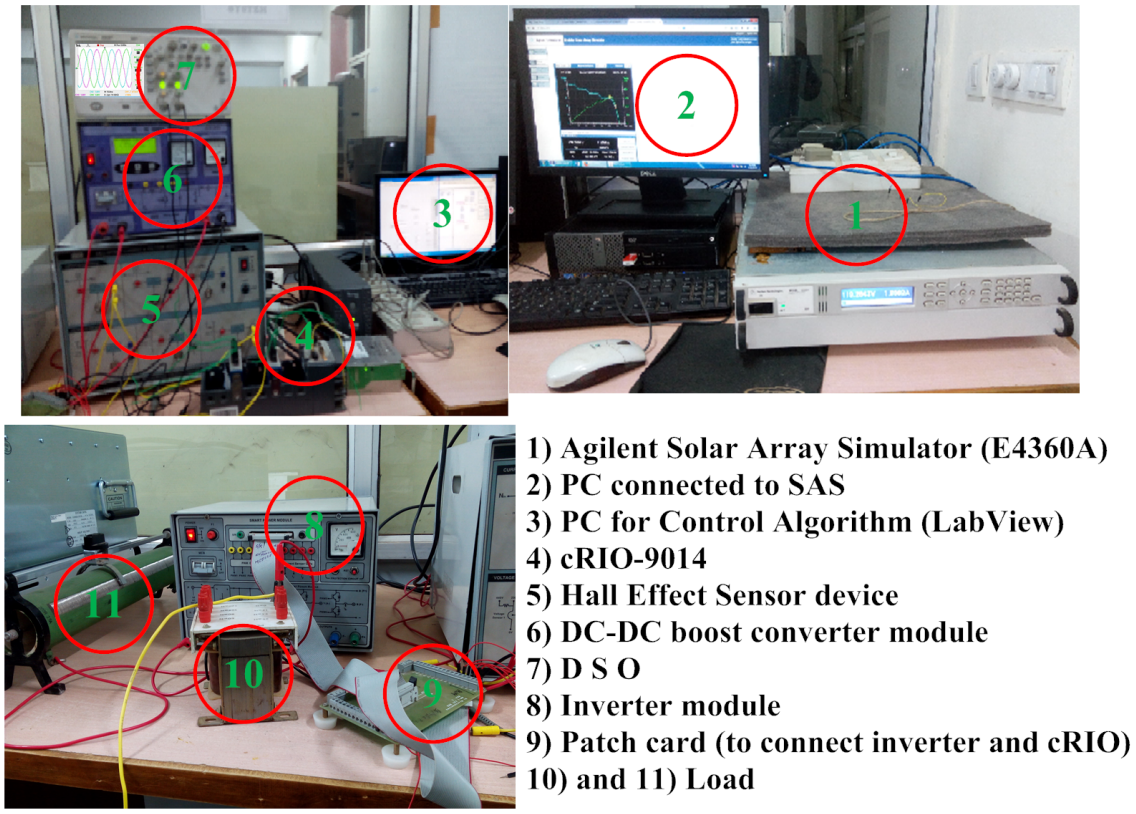

Figure 4.21: Picture of complete hardware setup

are provided to IGBT via cRIO through gate driver circuit. The VSI generates necessary voltage and current with the help of control circuit. A VSI consists of IGBT/MOSFET along with anti parallel diodes and DC voltage source. In VSI design interface inductance and DC-link capacitor are important. HCC/AHCC/MPC strategies are used to generate the control signal. The task of the controller (HCC/AHCC) is to compute the current error and generates switching pulses to the inverter and regulates the error within the band region. The MPC controller predicts the future and reduces the harmonics, generates PWM signal to the inverter. The blanking circuit uses the generated signal for all the switches and ensures that the outgoing switches are turned OFF and incoming switches are turned ON. Fig. 4.22 shows the schematic of the blanking circuit.

Blanking circuit The controllers generate the PWM pulses for the inverter. These pulses are not directly given to switches (IGBT) to prevent the short circuit of DC-link capacitor during ON and OFF of both switches in the same leg. Therefore, a dead time is necessary in between the ON and OFF conditions of the switches which are presented in the same leg.

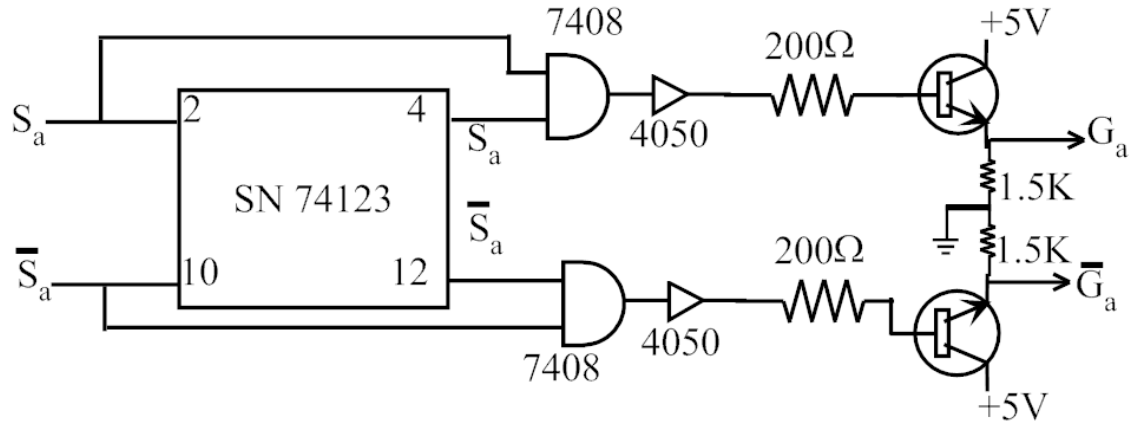

Figure 4.22: Schematic diagram of blanking circuit

The inputs of this circuit are controller switching pulses generated by the controller. The IC74SN123 has two similar units of monostable multivibrator.

The analog controller design has some limitation like structure and control law is fixed and complex circuit connections. Because of improvement of digital technology, now a days digital controllers are used for power electronic applications. It provides design flexibility with less time. FPGA implementation of MPC is one of the challenging tasks for digital controllers. FPGA is a matrix of configurable logic blocks (CLB) which are interconnected and reprogrammable [76]. FPGA approach can design exact hardware according to the control structure and reduces the execution time [77]. In this experimental setup, three pahse load connected PV system is developed. NI-cRIO-9014 is used to implement HCC/AHCC/MPC, which provides accurate PWM pulses to drive the inverter. The block diagram of PV power system is shown in Fig. 4.23.

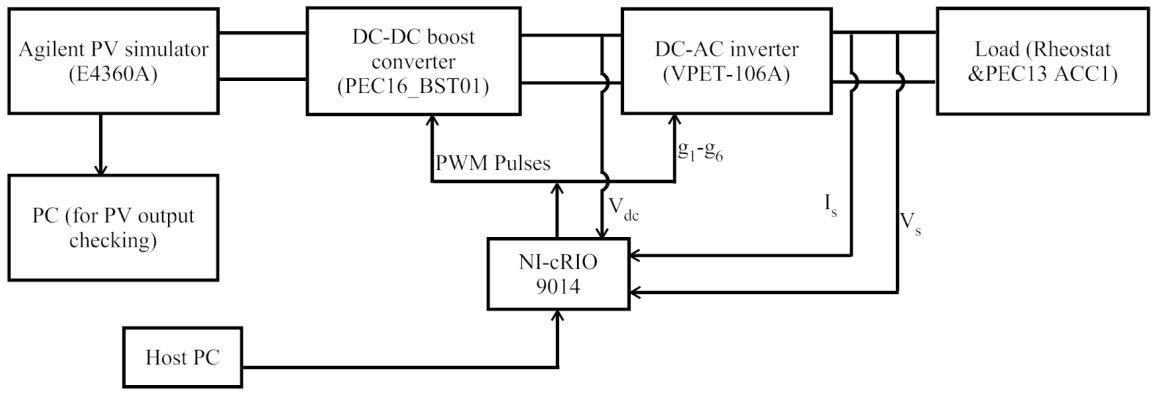

Figure 4.23: Block diagram of experimental setup

The blancking circuit will provide delay is about 6 µsec, it is sufficient to turn OFF or ON the IGBT. Hall Effect current sensors are used to measure the actual current. This signal is compared with the reference signal. Simulation results are validated with real-time digital simulation results. The opal-RT results of HCC, AHCC and MPC are shown in Fig. 4.24, Fig. 4.25 and Fig. 4.26 respectively ((a) PV output voltage, (b) DC-DC boost converter output voltage, (c) inverter output voltage and (d) inverter output current).

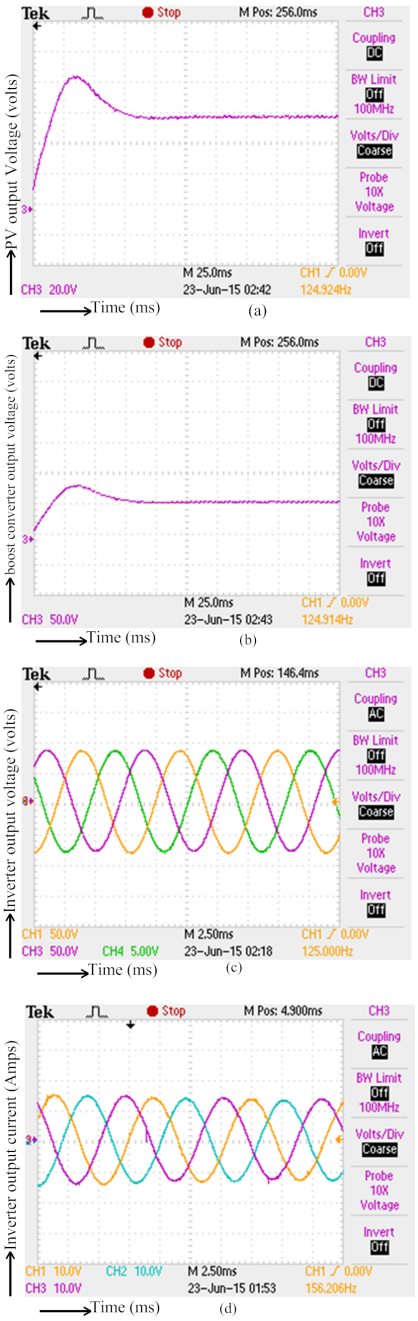

Figure 4.24: Hysteresis current controller Opal-RT results

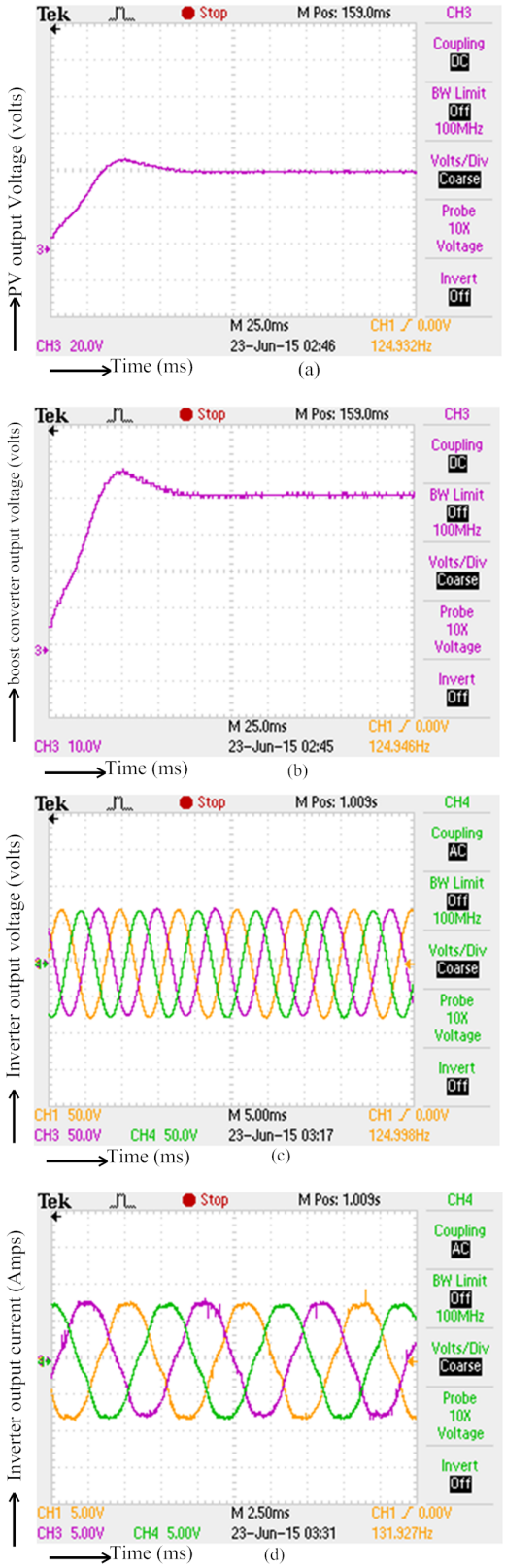

Figure 4.25: Adaptive hysteresis current controller opal-RT results

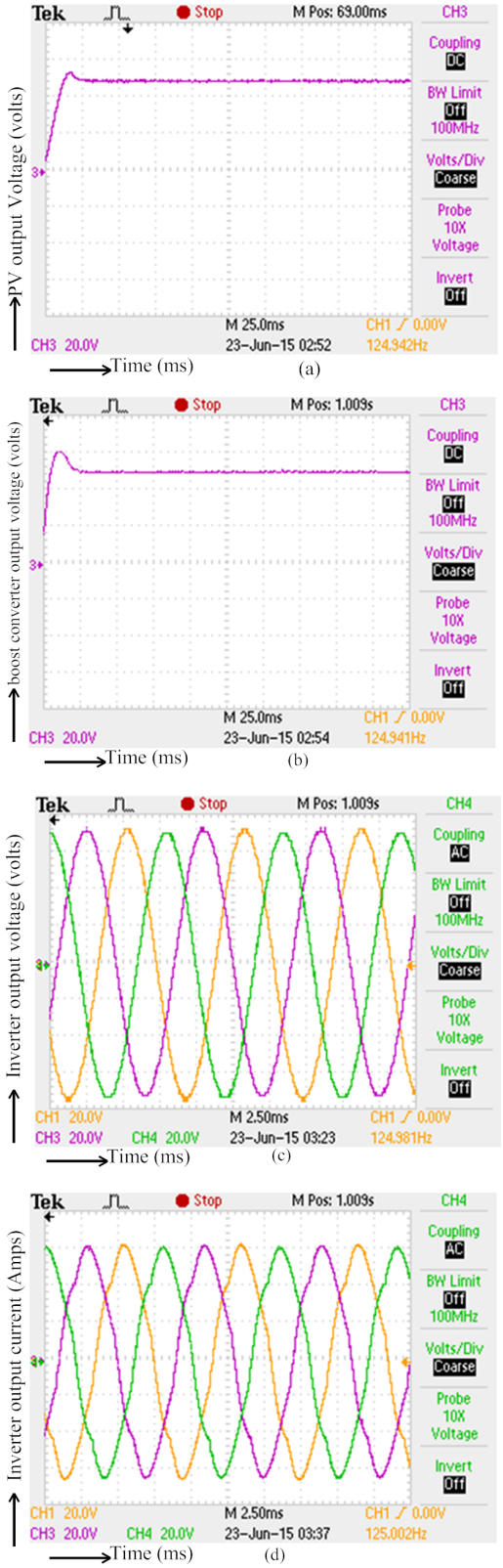

Figure 4.26: Model predictive controller opal-RT results

Simulation results are verified with experimental results. The experimental results of HCC, AHCC and MPC are shown in Fig. 4.27, Fig. 4.28 and Fig. 4.29 respectively ((a) PV output voltage, (b) DC-DC boost converter output voltage, (c) inverter output voltage and (d) inverter output current).

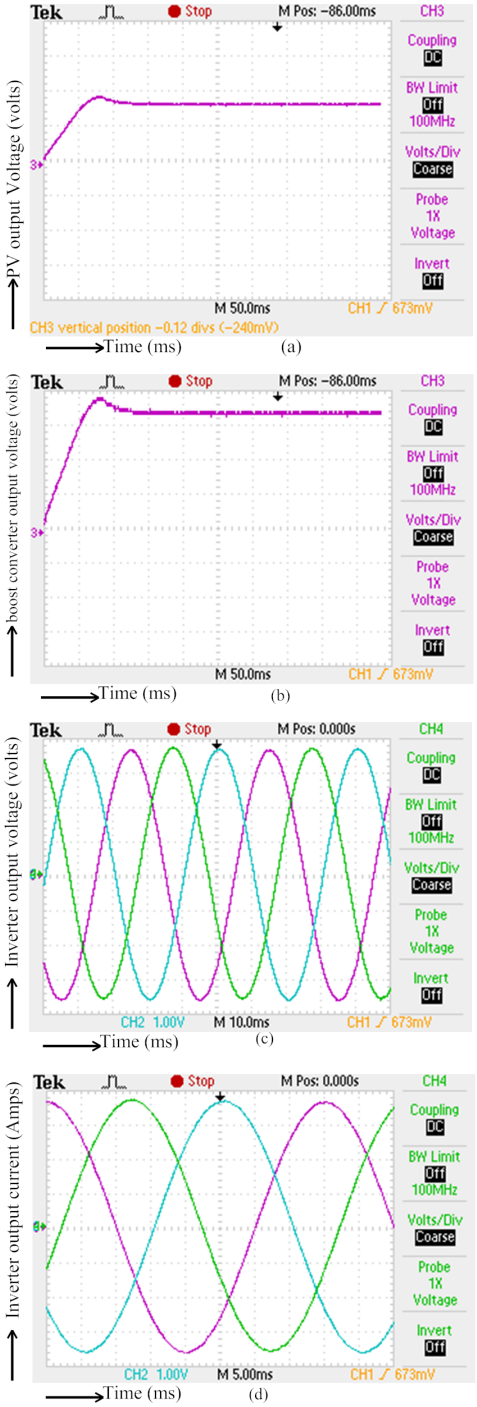

Figure 4.27: Hysteresis current controller Experimental results

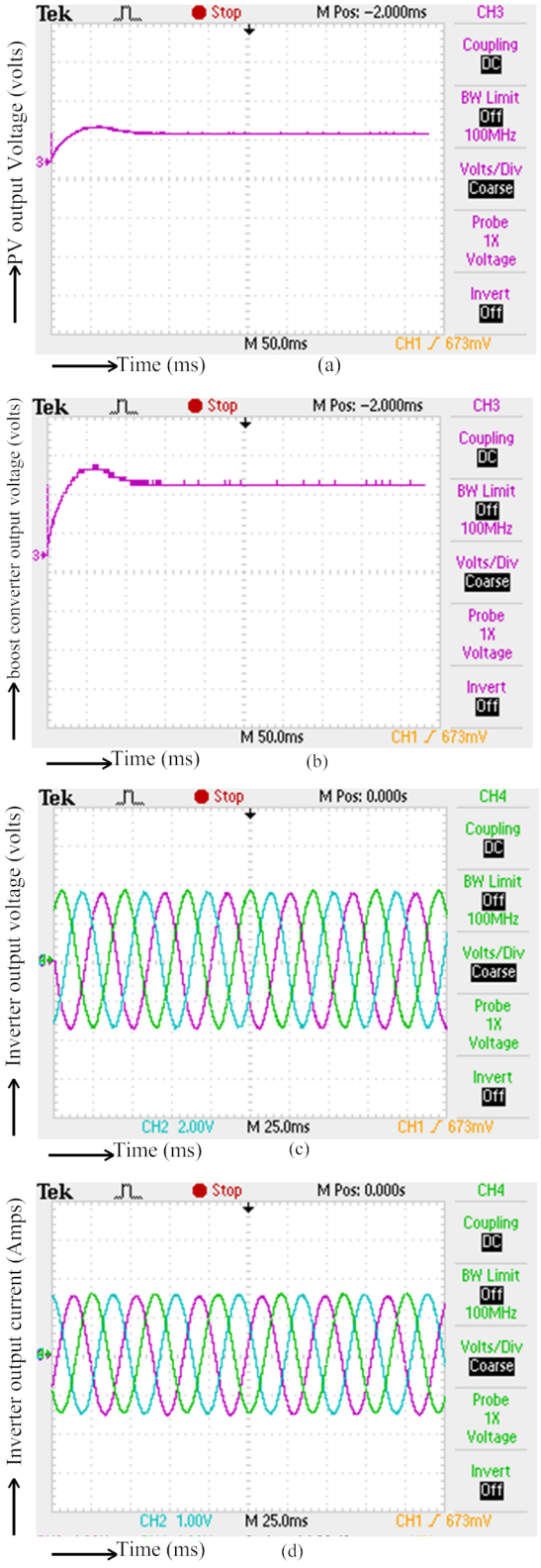

Figure 4.28: Adaptive hysteresis current controller Experimental results

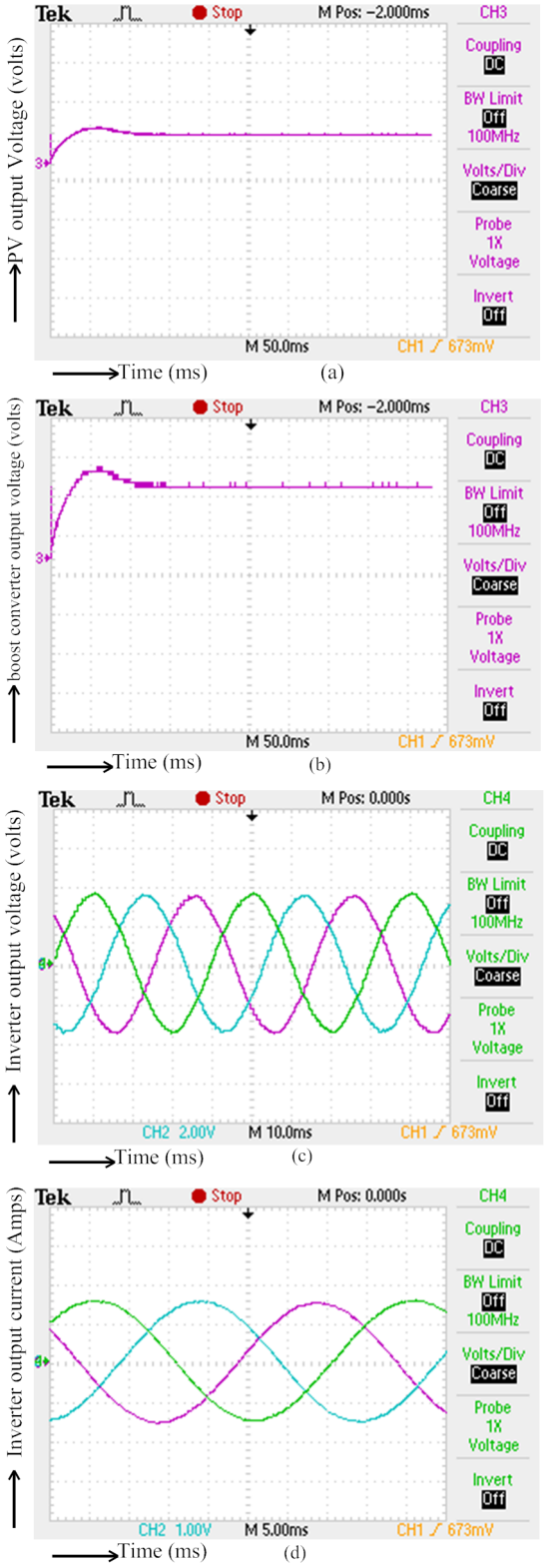

Figure 4.29: Model predictive controller Experimental results

4.8 Chapter Summary

A new model predictive MPPT controller is proposed in this chapter for PV systems and its effectiveness are verified. The proposed controller is compared with existing hysteresis current controller and adaptive hysteresis current controller. The HCC control strategy having advantages like simple design, unconditioned stability and easy to implement. This control strategy has some disadvantages like uneven switching frequency at a particular band limit. AHCC overcomes those limitations. The bandwidth of AHCC changes according to the current variation, but, it yields more power loss due to high frequency switching. The power loss problem is solved with MPC. The model predictive controller reaches the trajectory within the specified time with the help of future prediction. The implementation time is too high in case of MPC. Simulation in MATLAB/SIMULINK, real-time simulation in Opal-RT and experimental results using prototype set-up are presented to validate the efficacy of the proposed approach. The simulation and experimental results demonstrate that the new incremental conductance controller provieds effective tracking of MPP so that maximum power can be extracted from the PV panel and regulates the load voltage.

Chapter 5

Modified Variable Step Incremental Conductance MPPT with Active Power Filter for a Grid Connected PV system

5.1 Introduction

In Chapter 4, different control techniques for a grid connected PV system have been described. However, current harmonics and reactive power are present at GCPV output. To eliminate current harmonics and reactive power a filter is necessary. This chapter describes design, analysis and control structure of a three phase grid connected PV (GCPV) system with active power filter topology. The PV based shunt active power filter (SAPF) is designed for current harmonic compensation and reactive power compensation in AC power distribution system. It is used in all types of power (low, medium and high) levels and it consists of power circuit and control unit. This chapter proposes a variable step modified Incremental Conductance MPPT controller for DC-DC boost converter in the PV system. The thesis considers a two stage grid connected PV system in which the first stage involves a DC-DC boost converter and the second stage is through a VSI [111].

Shunt active power filter comprises a capacitor, VSI and interfacing inductor. This SAPF is connected in parallel with the load. We are discussing PV systems in our thesis and we are aiming at a specific application, i.e., active filtering. PV system is usually used for back-up power supply. The same PV can be utilized for active filtering purpose if required. This is being demonstrated in this chapter.

The PV based shunt active power filter design consists of power transistors, DC link

capacitor, interface inductor and control unit [121]. The control unit employs the reference current extraction and PWM current control techniques [122]. The research is going on implementation of digital controller for active power line conditioners (APLC) by using microcontrollers/FPGA/DSP for real time implementations [123]. Shunt active power filter is controlled using different controllers like PI [124] and FLC [125] for PV system that can be used for active power filter if required.

5.2 Chapter Objectives

- To develop a variable incremental conductance MPPT controller with active power filter.
- To implement the above MPPT control algorithms in MATLAB and in Opal-RT.

5.3 Active power filter (APF) techniques for a PV system

The PV array based shunt active power stage is a bidirectional current converter which consists of switching circuit and filter component. Every switch in the network is an IGBT along with anti parallel diode to allow current flow in both the directions. The inverter output is connected to the grid through an interfacing inductor. The PV based SAPF can inject power into distribution line for reactive power compensation. APF is connected in parallel with the non-linear load to compensate harmonic currents. The APF injects compensating current in opposite phase identical to the harmonic current for compensation. This ensures that the current drawn from the distribution network at the point of common coupling (PCC) is a sinusoidal current at fundamental frequency.

5.3.1 Shunt active power filter configurations

This system can be classified as

- Single phase system
- Three phase system
  - Three phase three wire system

– Three phase four wire system

Single phase system

The harmonics present in single phase system can be mitigated by using a APF. The extensive use of industrial electronic components such as computers and printers can produce harmonic related problems in distributed power systems. These problems can be solved by using a single phase active power line conditioner [78]. The single phase PV based Shunt APLC (SAPLC) can be implemented using a VSI. The circuit schematic of a shunt active power line conditioner with PV source is shown in Fig. 5.1. It consists of two-legs, four switching power transistors and a DC link capacitor. The inverter is connected in parallel with the load through an interfacing inductor. The single phase PV system based shunt APLC compensates current harmonics by introducing an equal and opposite harmonic compensation current. Hence, compensated current becomes sinusoidal and it is in-phase with the voltage. In our system we have PV system in addition to normal APF. We have additional components like PV array, MPPT controller and DC-DC boost converter. These components are apparently redundant for an APF, however, as we pointed out we are only using our back-up system for achieve filtering. If active-filtering is not demanded, then our system would only supply normal power.

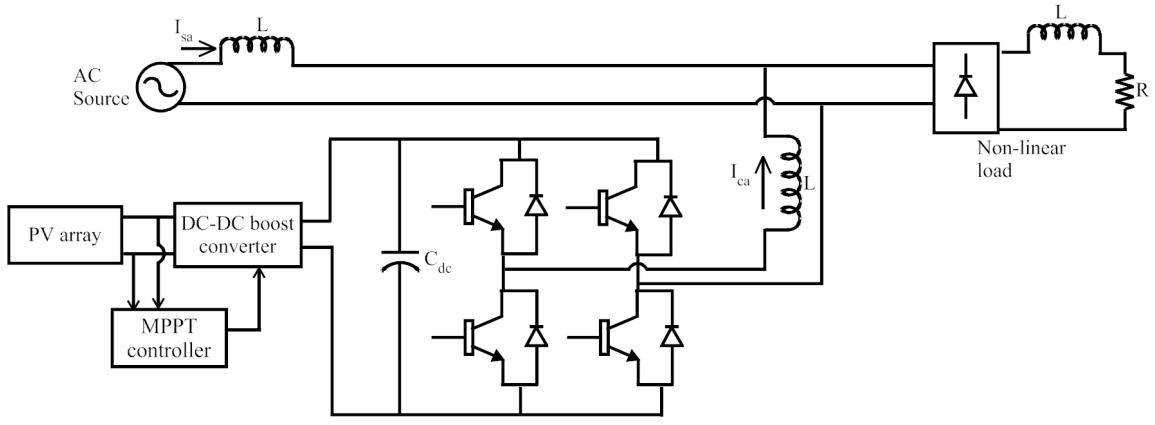

Figure 5.1: Single phase shunt active power line conditioner system

Three phase three wire PV based system

Three phase three wire PV system based shunt APLC includes two level PWM voltage source inverter as shown in Fig. 5.2. The PWM-VSI consists of six IGBTs, a DC link capacitor, and it is connected with PCC through an interface inductor. This interfacing inductor suppresses the higher order harmonic components caused by switching action of power transistors. Reduction of current harmonics present in the distribution line is achieved by injecting equal and opposite amount of compensating current at the PCC [80], [81].

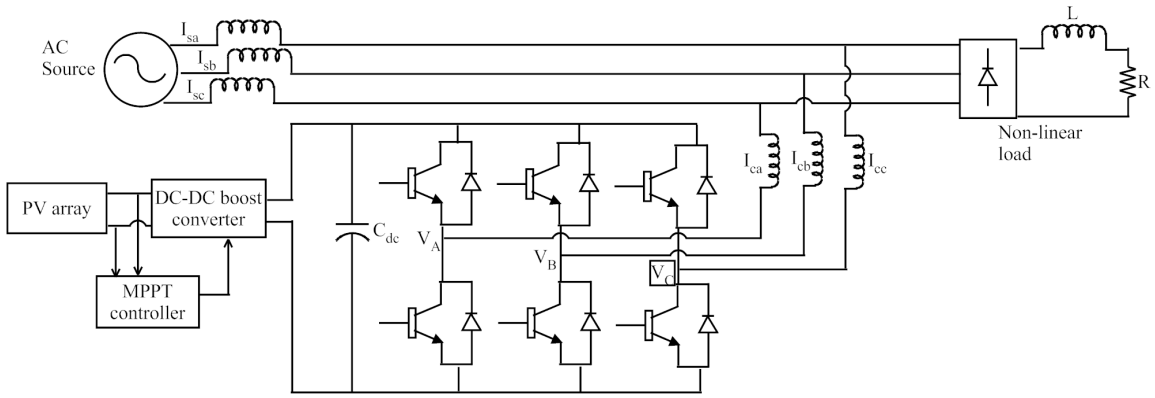

Figure 5.2: Three phase three wire shunt active power line conditioner system

Modified Variable Step Incremental Conductance MPPT algorithm

Due to the controller, swithcing losses are more in GCPV system. To eliminate these losses the Inc Cond MPPT controller is again modified and simplified. With the modified Inc Cond MPPT controller the swithcing losses have been reduced. The simiplified and modified Inc Cond MPPT control algorithm is shown in Fig. 5.3.

The incremental conductance control technique measures the incremental changes in PV current and voltage to predict the effect of voltage change [18]. This method always finds the knee point (I-V curve) and tries to maintain to stay at that position. Because of more computation in the controller, it can track more power at rapidly changing conditions. Instead of a fixed step size duty cycle, variable step size duty cycle tracks more power at all conditions. Fig.5.3 shows the modified variable step incremental conductance controller algorithm to stabilize the DC-link capacitor voltage. The incremental conductance control

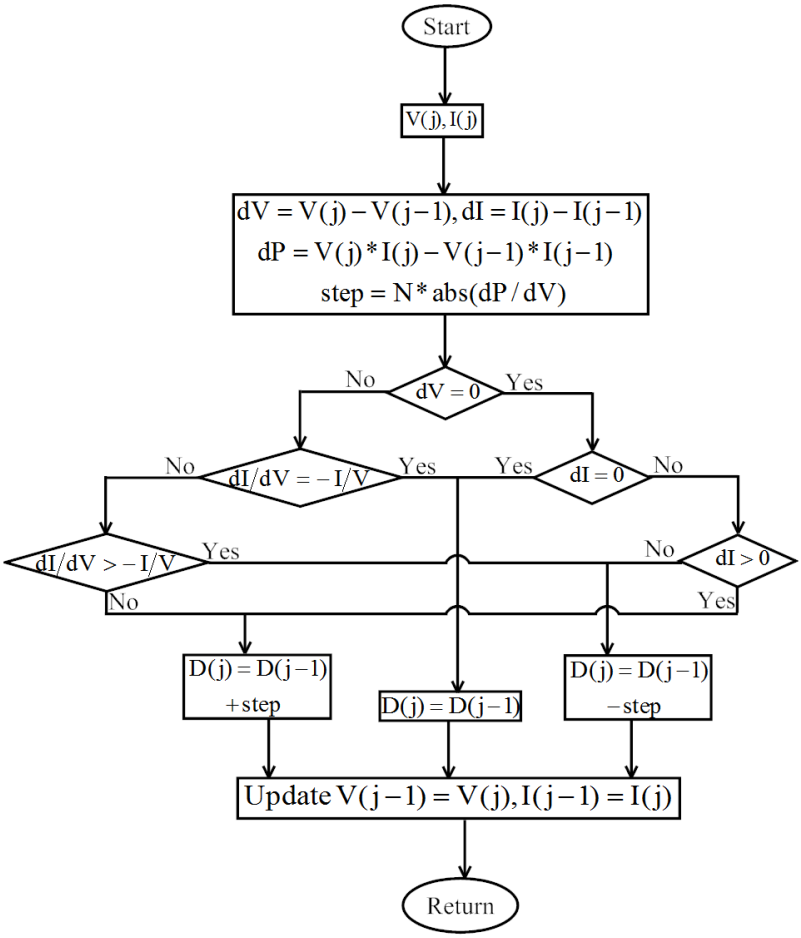

Figure 5.3: Modified incremental conductance MPPT controller with variable step size

technique computes the MPP by comparing the incremental conductance dI/dV with array conductance (I/V). The MPP position occurs when these two conductances(dI/dV and I/V) are equal. The controller maintains the voltage until the irradiation gets changed and the process is repeated. In this algorithm (Fig. 5.3), the first step is initialization and calculation of voltage variation, current variation and step size. The second step is checking voltage variation, if it is zero, and then checks the current variation. If voltage and current variations are zero, then that position is the MPP position, and the algorithm update duty cycle. If dV value is not zero, then checks with incremental conductance and array conductance. According to the position of MPP the duty cycle gets changed along with the step size. The algorithm runs continuously and updates the voltage and current values till MPP reaches. The procedure continues till the change occurs in irradiation. The mathematical calculations for incremental conductance algorithm are presented in chapter 2 as well as in

chapter 3.

$$\frac{dP}{dV} = 0 \tag{5.1}$$

$$I + V\frac{dI}{dV} = 0 \tag{5.2}$$

5.3.2 Principle of PV based Shunt Active Power Filter System

The basic principle of APF was proposed during 1970s. However, in 1976 the actual design of APF was proposed by Gyugyi and Strycula [121]. Fig. 5.4 shows a schematic diagram of PV based shunt active power line conditioner, which compensates current harmonics and reactive power. The basic principle of shunt APF system is to compensate current harmonics by injecting equal and opposite harmonic components. This principle is applicable to all non-linear loads which produce harmonics. A non-linear load is connected in parallel with the shunt APF to detect the harmonic current and reactive power. This system consists of an inductor and resistor per phase on the AC-side of three phase IGBT bridge current controlled VSI with a DC-link capacitor C_{dc} [78], [89].

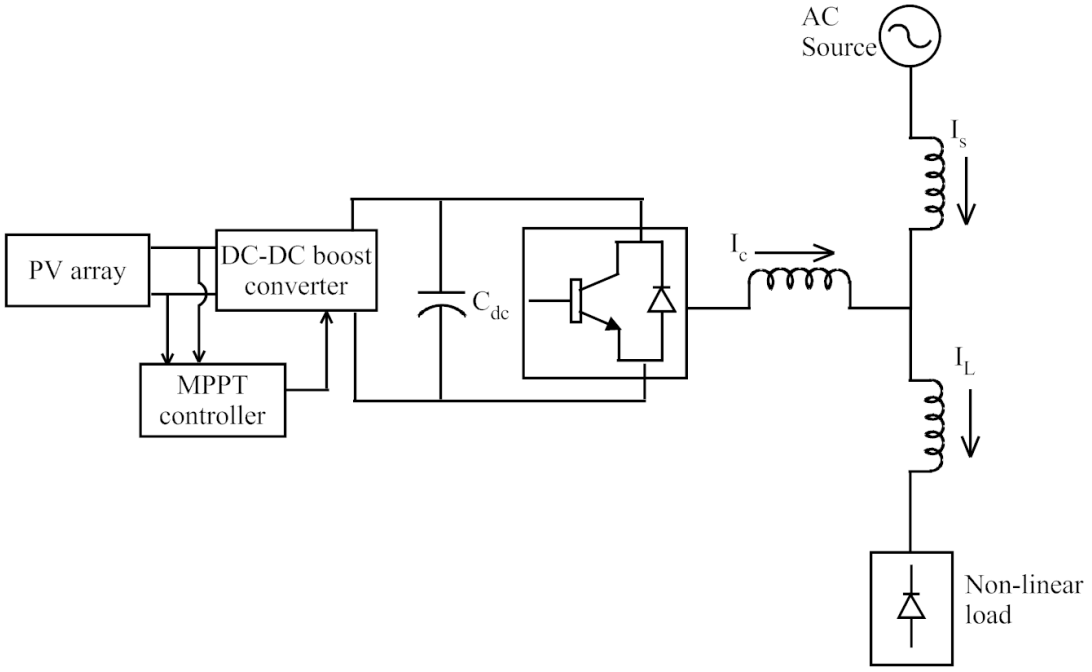

Figure 5.4: Schematic of shunt active power line conditioner system

Characteristics of Harmonic Compensation

The instantaneous voltage V_s and current I_s from grid can expressed as follows

$$V_s(t) = V_{sm} \sin(\omega t) \tag{5.3}$$

$$I_s(t) = I_L(t) - I_C(t) \tag{5.4}$$

The nonlinear load current I_L includes the fundamental and harmonic current components, which is represented as

$$\begin{aligned} I_L(t) &= \sum_{h=1}^{\infty} I_h \sin(n\omega t + \phi_h) \\ &= I_1 \sin(\omega t + \phi_1) + \sum_{h=2}^{\infty} I_h \sin(n\omega t + \phi_h) \end{aligned} \tag{5.5}$$

Load current contains active, reactive and harmonic current components, which can be rewritten as

$$I_L(t) = \underbrace{I_1 \sin(\omega t)}_{active} + \underbrace{I_1 cos(\omega t)}_{reactive} + \sum_{h=2}^{\infty} \underbrace{I_h \sin(n\omega t + \phi_h)}_{harmonics} \tag{5.6}$$

The supply voltage and load current is computed for the instantaneous load current will be calculated as

$$\begin{aligned} P_L(t) &= I_L(t) * V_s(t) \\ &= \left[V_{sm} I_1 \sin^2 \omega t * \cos\phi_1\right] + \left[V_{sm} I_1 \sin\omega t * cos\omega t * sin\phi_1\right] \\ &\quad + \left[V_{sm} \sin\omega t * \left(\sum_{h=2}^{\infty} I_h \sin(n\omega t + \phi_h)\right)\right] \end{aligned} \tag{5.7}$$

Therefore, $P_L(t) = P_f(t) + P_r(t) + P_h(t)$ as follows

$$P_f(t) = V_{sm} I_1 sin^2(\omega t) * cos\phi_1 \tag{5.8}$$

Normally it is expected that supply source would supply active component of current. Therefore APF would be required to supply reactive and harmonic power. If compensation

is perfect, then a sinusoidal current flows from supply and voltage at PCC remain undistorted.

After compensation, the source current can be written as

$$I_s(t) = \frac{P_f(t)}{V_s(t)} = I_1 \cos\phi_1 \sin(\omega t) \tag{5.9}$$

where, $I_1 \cos\phi_1 \sin(\omega t)$ is peak value of source current.

There are some switching losses in VSI, and hence the utility must supply small overhead for the capacitor leakage and inverter switching losses. Therefore, the total peak current supplied by the source is

$$I_{sp} = I_{sm} + I_{sl} \tag{5.10}$$

where, $I_{sp} = I_1 \cos\phi_1 + I_{sl}$ represents peak value of the extracted reference current,

I_{sl}=switching current loss. If the APLC provides the total harmonic and reactive powers, then $I_s(t)$ will be in-phase with supply voltage and almost equal to sinusoidal waveform. In this case, the APLC must provide the compensation current. It should be expressed as

$$I_c(t) = I_L(t) - I_s(t) \tag{5.11}$$

Therefore, the estimation of fundamental component of load current is necessary for accurate and instantaneous compensation of reactive and harmonic currents.

5.4 Synchronous Reference Frame Theory

The conventional and modified synchronous reference frame (SRF) based shunt APLC system is modelled and evaluated through MATLAB/simpower tools, model consists of a three phase VSI that is connected in parallel through the interface inductor with rectifier load. The schematic diagram is shown in Fig. 5.5. The APLC uses the conventional SRF or modified SRF with PWM-VSI current control techniques. The conventional or modified SRF is used to extract the required reference currents from the distorted load currents. The reference current is compared with actual current to generate switching pulses using PWM-VSI to drive the APLC. Then the active power line conditioner provides the

necessary compensating current for current harmonics compensation and reactive power in the connected system. Synchronous reference frame theory based on time domain is used to extract the reference current from the distorted line current. To control the APLC in real time, the SRF control scheme operates in dynamic state as well as in steady state. The calculation of SRF theory is very simple, which involves algebraic calculation [126]. There are two (conventional SRF and modified SRF) types of control schemes derived.

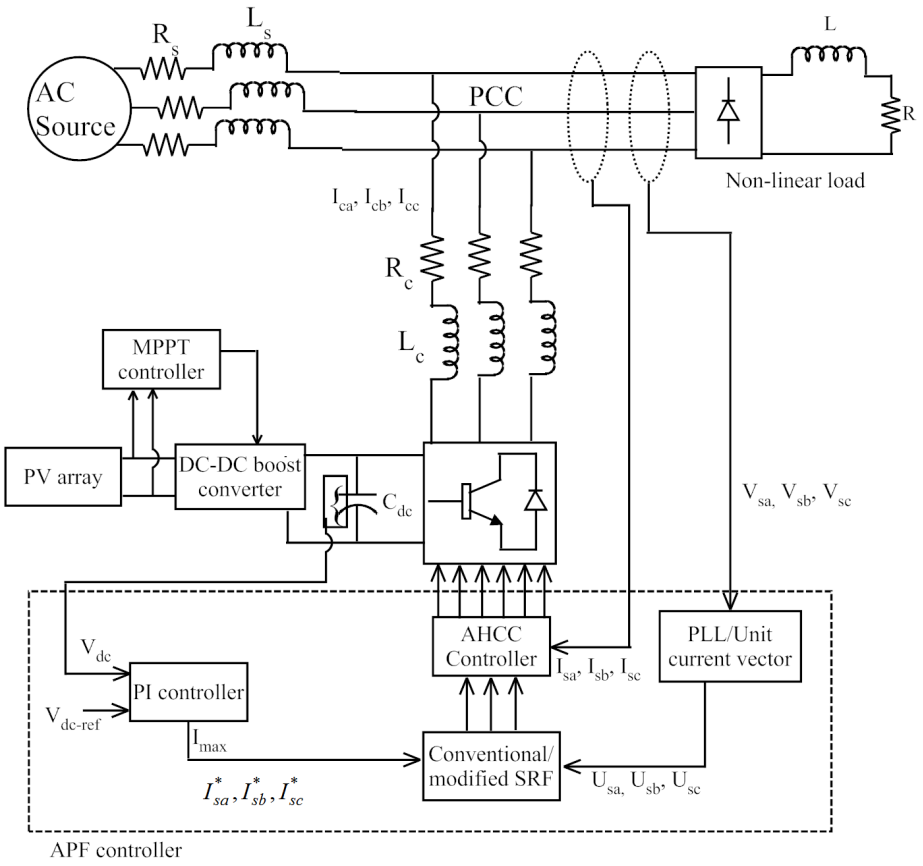

Figure 5.5: Complete schematic of shunt active power filter for PV

5.4.1 Conventional SRF method

The SRF consists of Phase Locked Loop(PLL) circuit and PI controller for vector orientation and DC-link capacitor voltage regulation respectively. The block diagram of conventional SRF method is shown in Fig. 5.6. Here, the three phase load currents i_{la}, i_{lb}, i_{lc} are in stationary coordinates and are converted into two phase direct axis (d) and quadratic

axis (q). The coordinate currents i_d, i_q are represented as

$$\begin{bmatrix} i_d \\ i_q \end{bmatrix} = \frac{2}{3}\begin{bmatrix} \sin\theta & \sin\left(\theta - \frac{2\pi}{3}\right) & \sin\left(\theta + \frac{2\pi}{3}\right) \\ \cos\theta & \cos\left(\theta - \frac{2\pi}{3}\right) & cos\left(\theta + \frac{2\pi}{3}\right) \end{bmatrix}\begin{bmatrix} i_{la} \\ i_{lb} \\ i_{lc} \end{bmatrix} \tag{5.12}$$

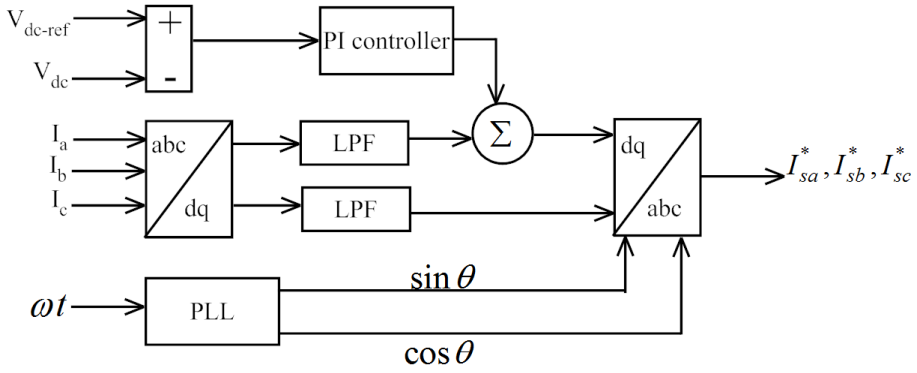

Figure 5.6: Block diagram of conventional SRF

The reference frame is synchronously rotating along with fundamental current, therefore, the time variant current with fundamental frequencies are constant after transformation. So, fundamental and time variant currents are separated simultaneously. The d-axis and q-axis current components are used for harmonic elimination and reactive power compensation respectively. The output of d-q transformation depends on the load current and PLL performance [127].

For synchronization, a PLL circuit is used to obtain fundamental frequency. The $i_d - i_q$ currents are passed through LPF to allow fundamental frequency components and filter out the higher order harmonic components. The steady state error of the DC component is eliminated by the PI controller and maintains the DC-capacitance voltage of the inverter. The gains of PI controller determine the dynamic response and settling time of the DC-bus capacitor voltage [128]. The desired reference current is calculated from $i_d - i_q$ rotating frame using inverse transformation given by

$$\begin{bmatrix} i^*_{sa} \\ i^*_{sb} \\ i^*_{sc} \end{bmatrix} = \begin{bmatrix} \sin\theta & \cos\theta \\ \sin\left(\theta - \frac{2\pi}{3}\right) & \cos\left(\theta - \frac{2\pi}{3}\right) \\ \sin\left(\theta + \frac{2\pi}{3}\right) & \cos\left(\theta + \frac{2\pi}{3}\right) \end{bmatrix}\begin{bmatrix} i_d \\ i_q \end{bmatrix} \tag{5.13}$$

The extracted reference current is then compared with the actual current to generate switching pulses for the inverter by using PWM-VSI controller. Based on the supply voltage, a PLL circuit is required in the conventional SRF control scheme. But, a high performance PLL circuit designing is difficult when the supply voltage is unbalanced.

5.4.2 Modified SRF method

This method consists of a simplified unit vector generation for vector orientation, DC-link capacitor voltage regulation and stationary rotating synchronous frames to extract reference current. Fig. 5.7. shows the modified SRF structure.

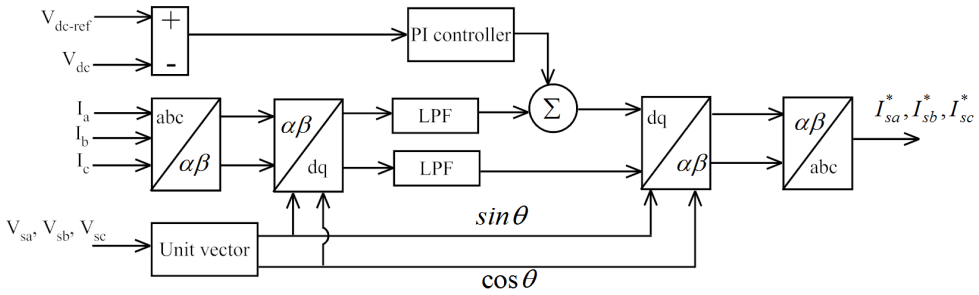

Figure 5.7: Block diagram of the Modified SRF

Unit vector generation

The instantaneous supply voltage is sensed to generate the unit sine vector templates. These voltages are given below

$$V_{sa} = V_{sm}\sin(\omega t)$$

$$V_{sb} = V_{sm}\sin(\omega t - 120^0) \tag{5.14}$$

$$V_{sc} = V_{sm}\sin(\omega t + 120^0)$$

where V_{sm} is the peak of the source voltage, V_{sa}, V_{sb}, and V_{sc} are source voltages. The block diagram of the unit vector generation scheme is shown in Fig. 5.8. The supply voltages are sensed and computed to generate the synchronization vector. The instantaneous three phase source voltages are transformed into two phase voltages by using the $\alpha - \beta$ transformation

(Clarkes transformation) as given in equation (5.15).

$$\begin{bmatrix} v_\alpha \\ v_\beta \end{bmatrix} = \sqrt{\frac{2}{3}} \begin{bmatrix} 1 & \frac{-1}{2} & \frac{-1}{2} \\ 0 & \frac{\sqrt{3}}{2} & \frac{-\sqrt{3}}{2} \end{bmatrix} \begin{bmatrix} v_{sa} \\ v_{sb} \\ v_{sc} \end{bmatrix} \tag{5.15}$$

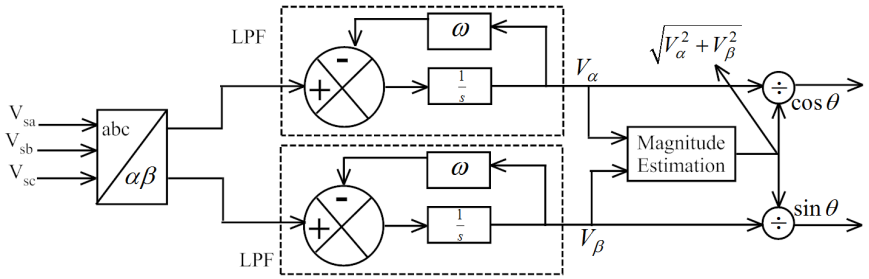

Figure 5.8: Block diagram of unit vector generation

Similarly, the instantaneous space vector current is transformed into $\alpha - \beta$ coordinate currents, which is given as

$$\begin{bmatrix} i_\alpha \\ i_\beta \end{bmatrix} = \sqrt{\frac{2}{3}} \begin{bmatrix} 1 & \frac{-1}{2} & \frac{-1}{2} \\ 0 & \frac{\sqrt{3}}{2} & \frac{-\sqrt{3}}{2} \end{bmatrix} \begin{bmatrix} i_{sa} \\ i_{sb} \\ i_{sc} \end{bmatrix} \tag{5.16}$$

Converting equation (5.19) to $\alpha - \beta$ plane by using equation (5.20), finally we will get the following equations

$$\begin{aligned} v_{s\alpha} &= \tfrac{3}{2} v_m \sin(\omega t) \\ v_{s\beta} &= -\tfrac{3}{2} v_m cos(\omega t) \end{aligned} \tag{5.17}$$

The $\alpha - \beta$ voltages are filtered using first order LPF whose frequency is a fundamental frequency (ω). After filtering, the percentage of h^{th} order harmonics of the sensed supply voltage are reduced by a factor of $\sqrt{2/(h^2+1)}$. It cancels the higher order harmonics and high frequency noise. The estimated magnitude of the space vector generated is as follows:

$$\overrightarrow{V} = \overrightarrow{V_{\alpha\beta}} = v_{s\alpha} + j v_{s\beta} = \sqrt{\left({v_{s\alpha}}^2 + {v_{s\beta}}^2\right)} \tag{5.18}$$

From the above equation, it is clear that the unit vectors can be generated by converting

the supply voltage to $\alpha - \beta$ plane and dividing the components by the magnitude of space vector. Therefore, the unit vector generation is defined as

$$\cos\theta = \frac{v_\alpha}{\sqrt{v_{s\alpha}^2 + v_{s\beta}^2}} = \frac{(3/2)v_m \sin(\omega t)}{(3/2)v_m} = \sin(\omega t)$$
$$\sin\theta = \frac{v_\beta}{\sqrt{v_{s\alpha}^2 + v_{s\beta}^2}} = \frac{-(3/2)v_m cos(\omega t)}{(3/2)v_m} = \cos(\omega t) \tag{5.19}$$

This unit vector generation method results in elimination of supply harmonics, high frequency noise in the distribution of supply voltages.

5.4.3 Case1: Conventional SRF

The adaptive hysteresis current controller (AHCC) technique is used with diode rectifier load with steady state condition. The DC-link capacitor voltage is shown in Fig. 5.9(a), and source current before compensation is shown in Fig. 5.9(b). It indicates that the source current contains fundamental and harmonic current components. The APLC supplies the compensating current shown in Fig. 5.9(c), to compensate harmonic current components. The harmonic current compensation is achieved by injecting equal and opposite harmonic components. Fig. 5.9(d) shows the source current after compensation. It indicates the source current after compensation becomes sinusoidal. Simulation results are validated with real-time digital simulation results are shown in Fig. 5.10. Both simulation and Opal-RT results are showing that the values are same.

5.4.4 Case 2: Modified SRF

The modified SRF with AHCC based shunt APLC under steady state condition is simulated and the simulation results are shown in Fig. 5.11. The instantaneous supply voltages are shown in Fig. 5.11(a), and indicate that the three phase voltages are balanced. The source currents before compensation are shown in Fig. 5.11 (b). These currents contain fundamental and harmonic components due to the rectifier load. The APLC provides necessary compensating currents which is shown in Fig. 5.11(c). The APLC operates as a current source by injecting the harmonic current components generated by the load but the phase shift is 180^0. Thus, the components of harmonic currents in the load currents

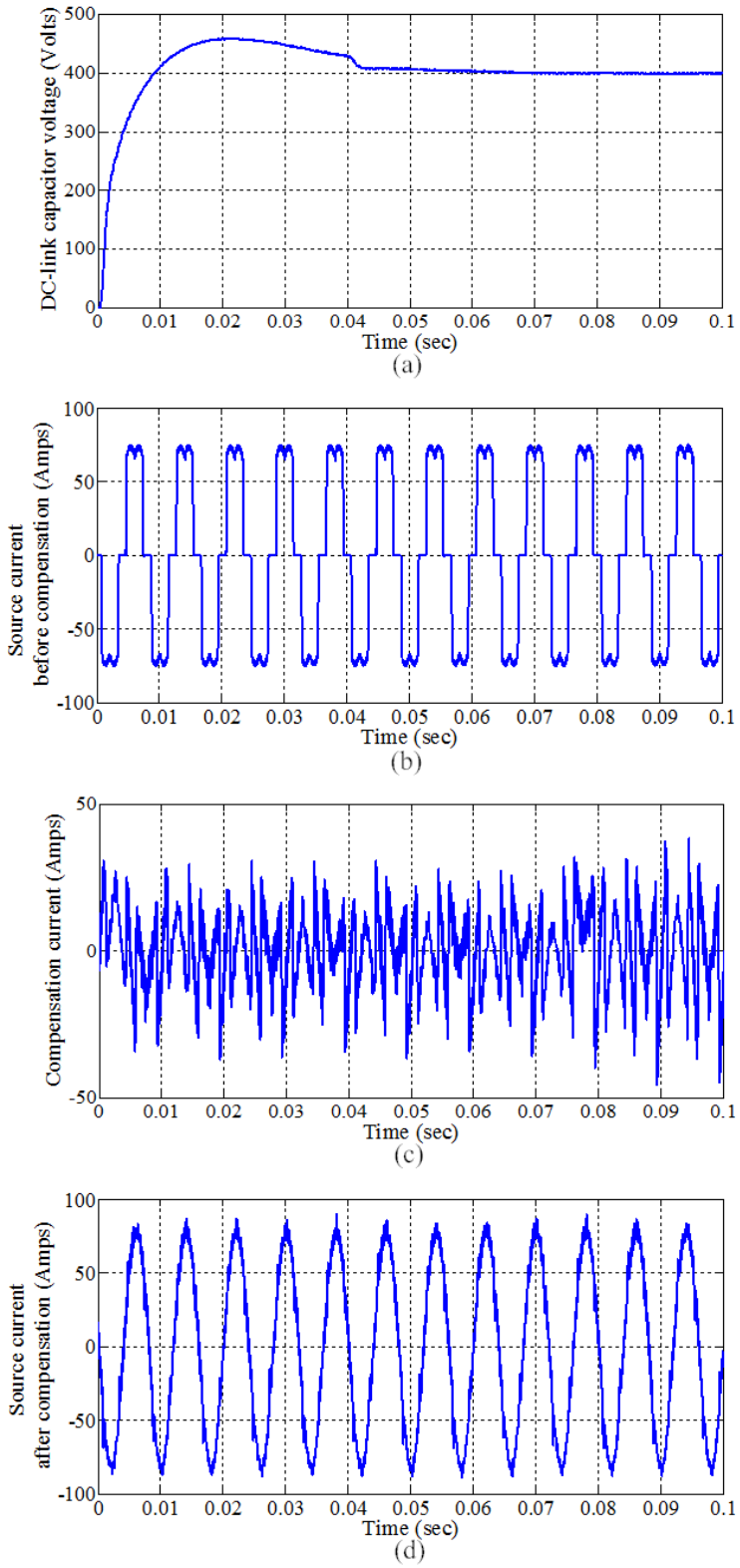

Figure 5.9: Simulation results of Adaptive hysteresis current controller

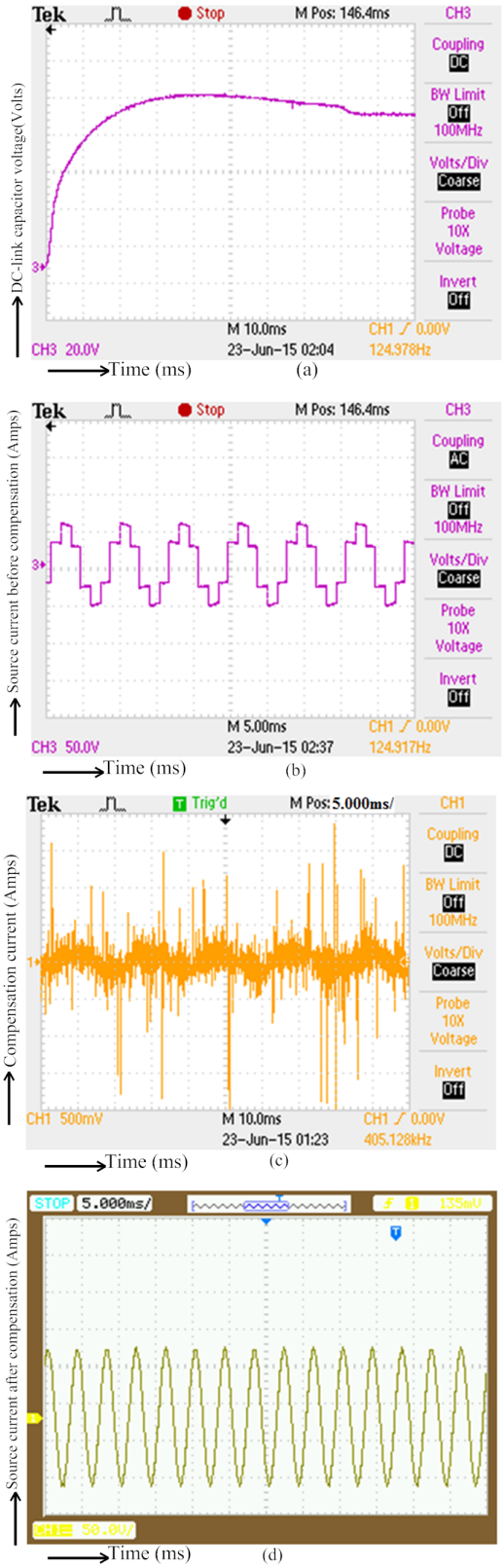

Figure 5.10: Adaptive hysteresis current controller Opal-RT results

can be cancelled by the APLC effect. Source currents after compensation are shown in Fig. 5.11(d), and indicate that the source currents after compensation are sinusoidal and in-phase with the supply voltages. The MATLAB/SIMULINK results are validated wit Opal-RT results are shown in Fig. 5.12. Finally, one can observe that the simulation and Opal-RT results are showing almost equal values. That means, performacne of modified SRF method is a better choice.

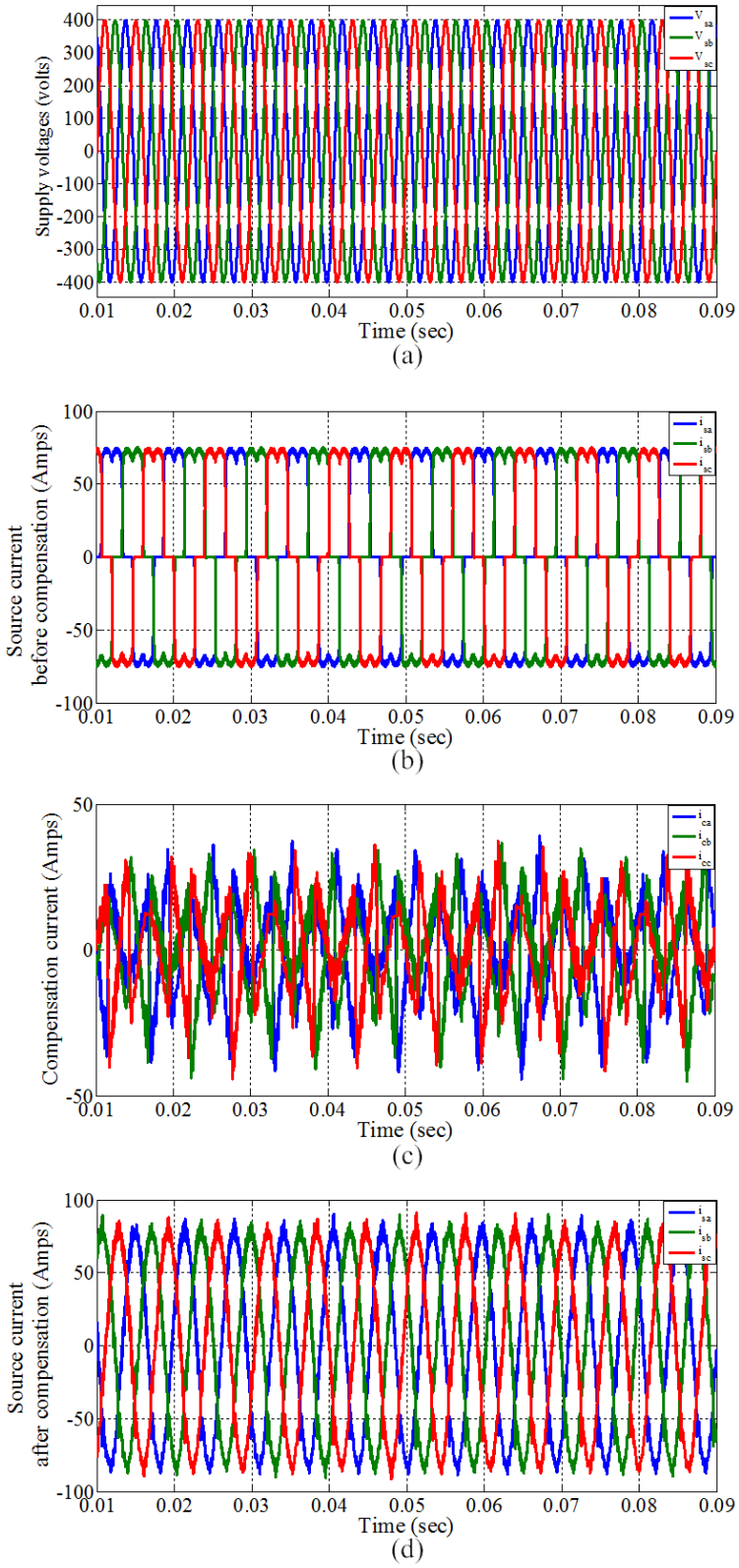

Figure 5.11: APF-AHCC simulation results

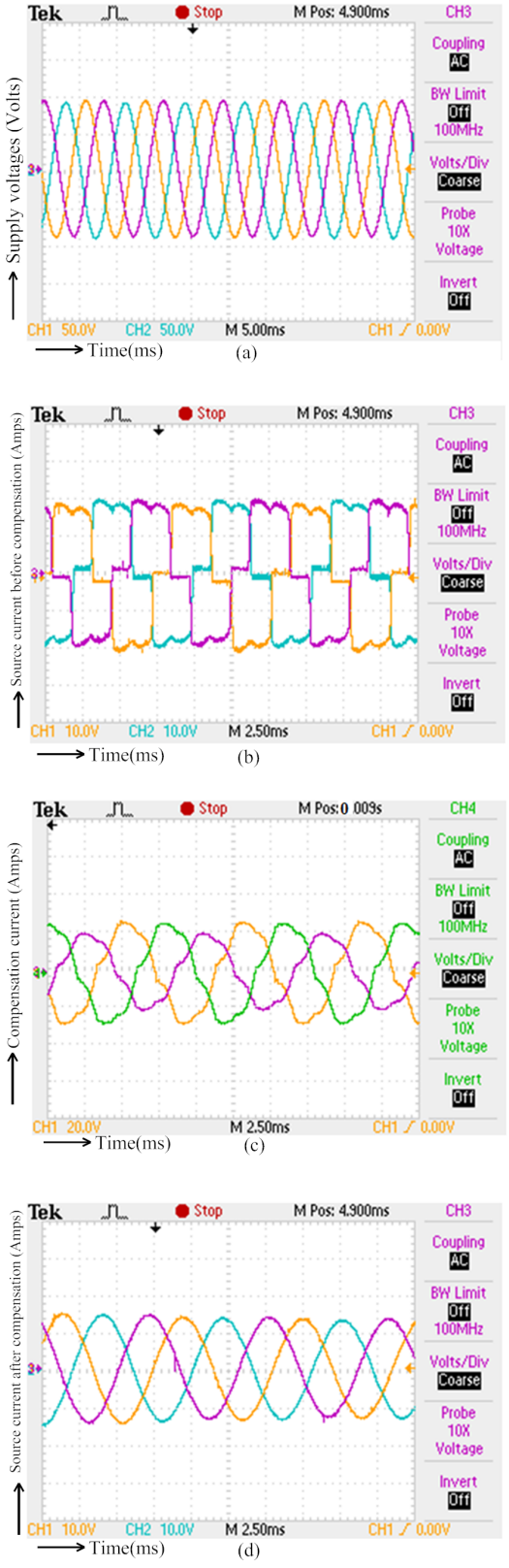

Figure 5.12: APF-AHCC opal-RT results

The comparative analyses of different THD techniques are shown in Fig. 5.13. Without APLC the THD of line currents is 26.66%. When SRF with AHCC based APLC technique is used to compensate the harmonics, then the THD is reduced to 3.92% and THD of line current is measured as 3.74% when modified SRF is used. Thus THD reduction is achieved through the modified SRF to meet the specifications as per the IEEE-519 standard. The detailed comparative analysis of active and reactive powers, THD is summarized in Table 5.1.

Table 5.1: Comparison between SRF and modified SRF with AHCC (diode load)

AHCC		
Controller	Without APLC	With APLC
SRF	P=8.99kW	P=9.22kW
		Q=104 V A R
		THD =3.92%
Modified SRF	Q=239 VAR	P=9.32 kW
		Q=102 V A R
	THD =26.6%	THD = 3.74%

The simulated results indicate that the conventional and modified SRF with AHCC based APLC providing of the reactive power and improve the power quality. From the aforementioned compensation discussion, it is observed that the modified SRF with AHCC performs better than the conventional one in terms of THD, active and reactive powers.

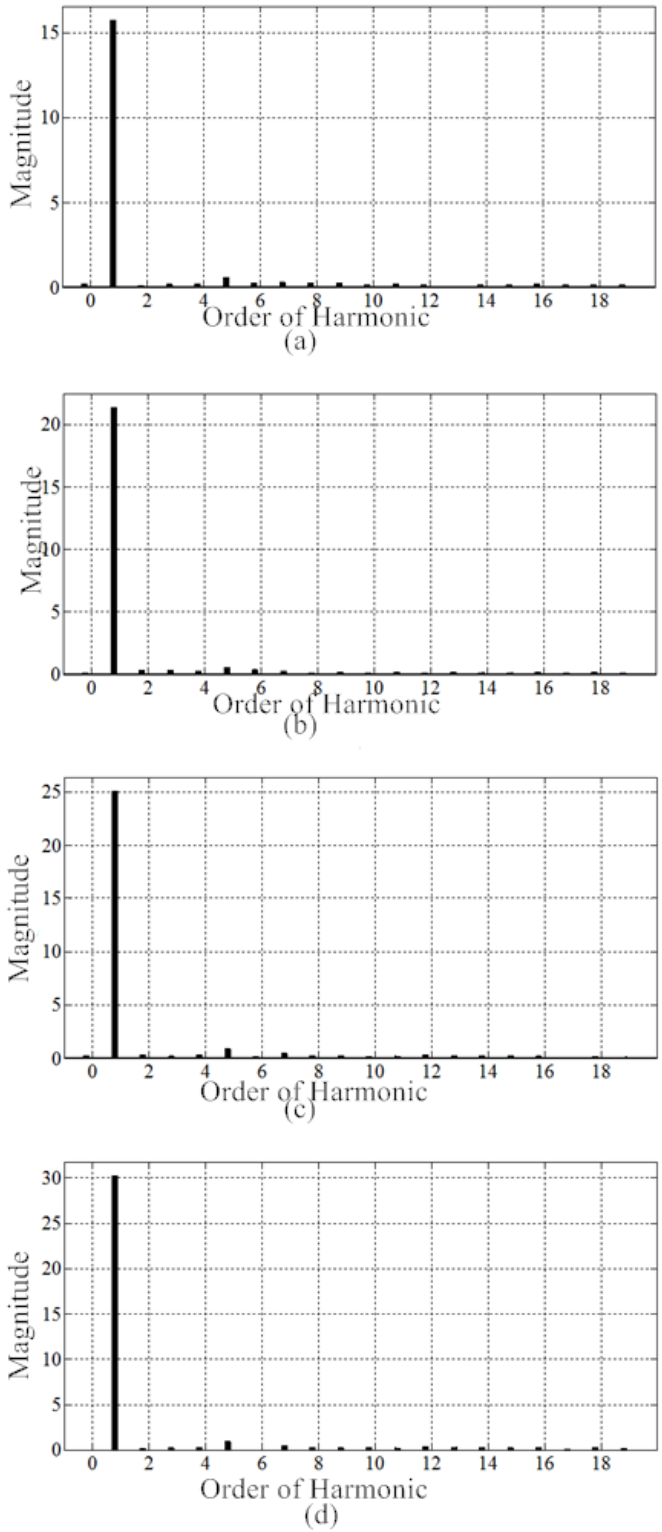

Figure 5.13: Comparison of different techniques of THD (a) SRF without APLC, (b) SRF with APLC, (c) Modified SRF without APLC, and (d) Modified SRF with APLC.

5.5 Chapter Summary

In this chapter we demonstrated that PV system can also be used for APF if rquired while it usually acts as a back-up power supply. A modified incremental conductance MPPT controller with variable step size is proposed in this chapter for a grid connected PV system. The duty cycle step size is varied according to the voltage and current variations. This chapter describes the modelling and control of PV system with active power filter under different loads. With help of the modified Inc Cond MPPT with varible step size, the harmonics are mitigated. Simulation in MATLAB/SIMULINK and real-time simulation in Opal-RT are used to validate the efficiency of the proposed approach. One common inverter is used to improve the power quality at PCC and to inject power generated to the grid. The simulation and real-time results demonstrate that the new Inc Cond controller with variable step exhibits improved tracking performance with SAPF with a non-linear load. For active filtering purpose, we have used SRF and modified SRF rechniques for extracting the fundamental component of the load current, while adaptive hysteresis current control is used for current control within the inverter. These methods are validated through extensive simulation and Opal-RT experimental results.

Chapter 6

Conclusion and Suggestion for future work

This chapter presents the overall conclusion and also suggests some future scope of research work as an extension of the work pursued in this thesis.

6.1 Overall Conclusions

This thesis has presented new algorithms for parameter extraction of a PV panel and maximum power control problems of a stand-alone and a grid connected PV systems. An extensive review on mathematical modeling of PV panels, different parameter extraction techniques and maximum power control techniques, DC-DC converter, DC-AC inverter and Shunt active power filter have been pursued and presented in chapter 1. The MPPT algorithms are presented with broad categorization of existing parameter extraction techniques into three groups such as direct and indirect techniques. Further, merits and demerits of the available parameter extraction techniques reported in the literature are discussed.Further, necessity of designing new MPPTs to achieve higher MPPT efficiency is explored.

A new algorithm called Integral Sliding Mode Controller and modified P&O MPPT algorithm are proposed for MPPT in Chapter 2. The proposed Integral Sliding Mode Controller is faster and more accurate than that of the conventional PI MPPT controller. But, this ISMC suffers to reach staedy state. Thus, a modified P&O MPPT algorithm is designed and compared with ISMC and different conventional MPPT controllers. It is observed that, the proposed P&O MPPT controller is tracking MPPT fastly and reaching the

steady state condition quickly. It may not be suitable for fast changing weather conditions and partial shading conditions. Simulation results are validated with Opal-RT results and verified with FPGA based experimental setup results.

A new algorithm called modified Incremental Conductance MPPT algorithm for varying weather conditions and partial shading conditions (PSCs) is proposed in Chapter 3. This modified Inc Cond MPPT algorithm is designed and compared with conventional Inc Cond MPPT controller. It is observed that, the proposed Inc Cond MPPT controller is tracking MPPT fastly and reaching the steady state condition quickly at PSC. The results obtained from MATLAB simulation are compared with that of Opal-RT and FPGA.

A new Model Predictive MPPT Controller for a grid connected PV system with global maximum power point tracking is proposed in Chapter 4. The proposed MPC is compared with Hysteresis current controller (HCC) and Adaptive hysteresis current controller (AHCC), and from the results obtained it is observed that proposed MPC performance is quite better than the conventional controllers in case of uneven switching and power loss due to high frequency switching. The MATLAB simulation results are verifed with Opal-RT and with FPGA based experimental setup results.

Finally, a new modified Incremental Conductance MPPT controller with variable step size is proposed in Chapter 5 with a Shunt Active Power Filter, reducing the current harmonics to 3.7% of THD which is satisfying the IEEE-1547 grid code.

6.1.1 Contributions of the Thesis

- An integral sliding mode MPPT controller and a modified P&O MPPT controller is developed for standard test conditions of a PV array.
- A modified incremental conductance MPPT controller is developed for handling partial shading conditions of a PV array.
- A model predictive MPPT control scheme is developed for a grid connected PV system.
- A modified variable step incremental conductance MPPT with active power filter for a grid connected PV is developed.

6.2 Suggestions for future work

In this thesis, modelling of PV system with DC-DC boost converter and VSI were developed. These models can be modified taking into account some realistic situations such as grid perturbations etc. Further, the thesis proposed new MPPT algorithms and their implementations on FPGA at STC and PSC for standalone as well as grid connected PV systems. Some suggested new directions of the thesis are follows.

- Grid synchronization can be pursued by using multi level inverter (MLI) in place of VSI and to investigate the power losses and flexibility of implementing filtering and synchronisation issues.
- Subsequently, implementation of MLI can be attempted by using ASIC design, which may reduce the hardware requirement.

Bibliography

[1] M. G. Villalva, J. R. Gazoli, et al. Comprehensive approach to modeling and simulation of photovoltaic arrays. *IEEE Transactions on Power Electronics*, 24(5):1198–1208, 2009.

[2] O. Isabella. *Light management in thin-film silicon solar cells*. Delft University of Technology, 2013.

[3] W. H. Wai, R. J. Wang and C. Y. Lin. High-performance stand-alone photovoltaic generation system. *IEEE Transactions on Industrial Electronics*, 55(1):240–250, 2008.

[4] S. Ravaee, H. Farahat and F.z Sarhaddi. Artificial neural network based model of photovoltaic thermal (pv/t) collector. *The Journal of Mathematics and Computer Science*, 4(3):411–417, 2012.

[5] Pv light house. http://www.pvlighthouse.com.au/.

[6] B. S. G. Dzimano. *Modelling of photovoltaic systems*. The Ohio state University, 2008.

[7] Renewable. http://www.altenergy.org/renewables/renewables.html.

[8] P.P Dash. *Design methodology and stability analysis for a photovoltaic plant interfaced with a distribution network*. The university of Western Ontario, 2008.

[9] T. Mates. *Structure and properties of thin silicon films for solar cells Studied by combined atomic force microscopy*. Charles University, Czech Republic, 2006.

[10] M. Mohamed, A. Elshaer and O. Mohammed. Control enhancement of power conditioning units for high quality pv systems. *Electric Power Systems Research*, 90:30–41, 2012.

[11] J. A. Gow and C. D. Manning. Development of a model for photovoltaic arrays suitable for use in simulation studies of solar energy conversion systems. *IET*, 1996.

[12] E. Lorenzo. *Solar Electricity: Engineering of Photovoltaic Systems*. Progensa, 1994.

[13] Solar wiki http://en.wikipedia.org/wiki/timeline of solar cells.

[14] M. Bouzidi, K. Chegaar and A. Bouhemadou. Solar cells parameters evaluation considering the series and shunt resistance. *Solar Energy Materials and Solar Cells*, 91(18):1647–1651, 2007.

[15] A. N. Celik and N.ır Acikgoz. Modelling and experimental verification of the operating current of mono-crystalline photovoltaic modules using four-and five-parameter models. *Applied energy*, 84(1):1–15, 2007.

[16] V. L. Brano, A. Orioli, G. Ciulla, and A. Gangi. An improved five-parameter model for photovoltaic modules. *Solar Energy Materials and Solar Cells*, 94(8):1358–1370, 2010.

[17] V. R. Kolluru, K. K. Mahapatra, and B. Subudhi. Development and implementation of control algorithms for a photovoltaic system. In *Students Conference on Engineering and Systems (SCES)*, pages 1–5. IEEE, 2013.

[18] B. Subudhi and R. Pradhan. A comparative study on maximum power point tracking techniques for photovoltaic power systems. *IEEE Transactions on Sustainable Energy*, 4(1):89–98, 2013.

[19] P. L. Esram, T. Chapman and et al. Comparison of photovoltaic array maximum power point tracking techniques. *IEEE Transactions on Energy Conversion*, 22(2):439, 2007.

[20] A. Safari and S. Mekhilef. Simulation and hardware implementation of incremental conductance mppt with direct control method using cuk converter. *IEEE Transactions on Industrial Electronics*, 58(4):1154–1161, 2011.

[21] A. D. Savino M. Attivissimo, F. Nisio and M. Spadavecchia. Uncertainty analysis in photovoltaic cell parameter estimation. *IEEE Transactions on Instrumentation and Measurement*, 61(5):1334–1342, 2012.

[22] K. Ishaque and Z. Salam. A review of maximum power point tracking techniques of pv system for uniform insolation and partial shading condition. *Renewable and Sustainable Energy Reviews*, 19:475–488, 2013.

[23] J. J. Wu D. S. Su, J. H. Chen. Learning feedback controller design of switching converters via matlab/simulink. *IEEE Transactions on Education*, 45(4):307–315, 2002.

[24] Md. E. Gargoom A. Lyden, S. Haque and M. Negnevitsky. Review of maximum power point tracking approaches suitable for pv systems under partial shading conditions. In *IEEE Conference on Power Engineering (AUPEC), Australasian Universities*, pages 1–6, 2013.

[25] S. Armstrong and W. G. Hurley. A new methodology to optimise solar energy extraction under cloudy conditions. *Renewable Energy*, 35(4):780–787, 2010.

[26] S. Spiazzi G. Scarpa, V. Buso. Low-complexity mppt technique exploiting the pv module mpp locus characterization. *IEEE Transactions on Industrial Electronics*, 56(5):1531–1538, 2009.

[27] H. Patel and V. Agarwal. Matlab-based modeling to study the effects of partial shading on pv array characteristics. *IEEE Transactions on Energy Conversion*, 23(1):302–310, 2008.

[28] E. Barrado A. Salas, V. Olias and A. Lazaro. Review of the maximum power point tracking algorithms for stand-alone photovoltaic systems. *Solar energy materials and solar cells*, 90(11):1555–1578, 2006.

[29] R. Pradhan. *Development of New Parameter extraction Schemes and Maximum Power Point Controllers for Photovoltaic Power Systems*. 2014.

[30] B. Subudhi and R. Pradhan. Characteristics evaluation and parameter extraction of a solar array based on experimental analysis. In *9th International Conference on Power Electronics and Drive Systems (PEDS)*, pages 340–344. IEEE, 2011.

[31] S. B. Kjaer. *Design and control of an inverter for photovoltaic applications*. Institute of Energy Technology, Aalborg University, 2005.

[32] Z. Blaabjerg, F. Chen and S. B. Kjaer. Power electronics as efficient interface in dispersed power generation systems. *IEEE Transactions on Power Electronics*, 19(5):1184–1194, 2004.

[33] Utility aspects of grid www.iea-pvps.org.

[34] O. H. A. Onar, O.C. Shirazi and A. Khaligh. Grid interaction operation of a telecommunications power system with a novel topology for multiple-input buck-boost converter. *IEEE Transactions on Power Delivery*, 25(4):2633–2645, 2010.

[35] S. D. Odeh and H. I. Abu-Mulaweh. Design and development of experimental setup of hybrid pv/thermal collector. *Global Journal of Engineering Education*, 14(2):170–176, 2012.

[36] R. D. Patidar and S. .P Singh. Active and reactive power control and quality management in dg-grid interfaced systems. *ARPN Journal of Engineering and Applied Sciences*, 4(3):81–90, 2009.

[37] M. Meinhardt and G. Cramer. Past, present and future of grid connected photovoltaic-and hybrid-power-systems. In *IEEE Power Engineering Society Summer Meeting,*, volume 2, pages 1283–1288. IEEE, 2000.

[38] M. Tauseef and E. Nowicki. A simple and cost effective maximum power point tracker for pv arrays employing a novel constant voltage technique. In *25th IEEE Canadian Conference on Electrical & Computer Engineering (CCECE)*, pages 1–4. IEEE, 2012.

[39] M. R. Patel. *Wind and solar power systems: design, analysis, and operation*. CRC press, 2005.

[40] D. S. H. Phang, J. C. H. Chan and J. R. Phillips. Accurate analytical method for the extraction of solar cell model parameters. *Electronics Letters*, 20(10):406–408, 1984.

[41] P. Denholm and R. Margolis. Evaluating the limits of solar photovoltaics (pv) in traditional electric power systems. *Energy policy*, 35(5):2852–2861, 2007.

[42] D. L. Jiang, L. L. Maskell and J. C. Patra. A novel ant colony optimization-based maximum power point tracking for photovoltaic systems under partially shaded conditions. *Energy and Buildings*, 58:227–236, 2013.

[43] G. Chegaar, M. Azzouzi and P. Mialhe. Simple parameter extraction method for illuminated solar cells. *Solid-State Electronics*, 50(7):1234–1237, 2006.

[44] H. Hua, C. Chiang and C. Chuang. New boost converter based on sheppard–taylor topology. *IET Power Electronics*, 7(1):167–176, 2014.

[45] P. Mousavi, A.Das and G. Moschopoulos. A comparative study of a new zcs dc–dc full-bridge boost converter with a zvs active-clamp converter. *IEEE Transactions on Power Electronics*, 27(3):1347–1358, 2012.

[46] J. Maki A. Messo T. Huusari J. Jokipii J. Viinamaki J. Lobera D. Valkealahti S. Nousiainen, L. Puukko and T. Suntio. Photovoltaic generator as an input source for power electronic converters. *IEEE Transactions on Power Electronics*, 28(6):3028–3038, 2013.

[47] I. Altintas, N. Aksoy and etal. A novel zvt-zct-pwm boost converter. *IEEE Transactions on Power Electronics*, 29(1):256–265, 2014.

[48] R. Middlebrook and S. Cuk. *Advances in switched-mode power conversion*, volume 1. TESLAco, 1983.

[49] D. Petrone G. Spagnuolo G. Femia, N. Granozio and M. Vitelli. Optimized one-cycle control in photovoltaic grid connected applications. *IEEE Transactions on Aerospace and Electronic Systems*, 42(3):954–972, 2006.

[50] M. T. Lopez, O. Penella and M. Gasulla. A new mppt method for low-power solar energy harvesting. *IEEE Transactions on Industrial Electronics*, 57(9):3129–3138, 2010.

[51] Y. Zhang Y. Liu, F. Kang and S. Duan. Comparison of p&o and hill climbing mppt methods for grid-connected pv converter. In *3rd IEEE Conference on Industrial Electronics and Applications, ICIEA*, pages 804–807. IEEE, 2008.

[52] K. S. Tey and S. Mekhilef. Modified incremental conductance mppt algorithm to mitigate inaccurate responses under fast-changing solar irradiation level. *Solar Energy*, 101:333–342, 2014.

[53] W. G. Palmer P. Xiao, W. Dunford and A. Capel. Application of centered differentiation and steepest descent to maximum power point tracking. *IEEE Transactions on Industrial Electronics*, 54(5):2539–2549, 2007.

[54] Y. S. Kottas, T. L. Boutalis and A. D. Karlis. New maximum power point tracker for pv arrays using fuzzy controller in close cooperation with fuzzy cognitive networks. *IEEE transactions on Energy conversion*, 21(3):793–803, 2006.

[55] T. Hiyama and K. Kitabayashi. Neural network based estimation of maximum power generation from pv module using environmental information. *IEEE Transactions on Energy Conversion*, 12(3):241–247, 1997.

[56] Y. Tan, S. C. Lai and C. Tse. *Sliding mode control of switching power converters: techniques and implementation*. CRC press, 2011.

[57] D. Shmilovitz. On the control of photovoltaic maximum power point tracker via output parameters. In *IET Proceedings of Electric Power Applications*, volume 152, pages 239–248. IET, 2005.

[58] J. M. Peng F. Z. Rosas, J. C Ramirez and A. Valderrabano. A dc-dc multilevel boost converter. *IET Power Electronics*, 3(1):129–137, 2010.

[59] A. Chini and F. Soci. Boost-converter-based solar harvester for low power applications. *Electronics letters*, 46(4):296–298, 2010.

[60] F. Ledwich G. Ghosh A. Zabihi, S. Zare and H. Akiyama. A new pulsed power supply topology based on positive buck-boost converters concept. *IEEE Transactions on Dielectrics and Electrical Insulation*, 17(6):1901–1911, 2010.

[61] V. G. Yang J. Coutellier D. Choi, S. Agelidis and . P Marabeas. Analysis, design and experimental results of a floating-output interleaved-input boost-derived dc–dc high-gain transformer-less converter. *IET power electronics*, 4(1):168–180, 2011.

[62] T. Mishima and M. Nakaoka. A practical zcs-pwm boost dc-dc converter with clamping diode-assisted active edge-resonant cell and its extended topologies. *IEEE Transactions on Industrial Electronics*, 60(6):2225–2236, 2013.

[63] F. Mayo-Maldonado J. C. Gonzalez-Lopez J. M. Torres-Espinosa H. L. Rosas, J. C. Mancilla-David and J. E. Valdez-Resendiz. A transformer-less high-gain boost converter with input current ripple cancelation at a selectable duty cycle. *IEEE Transactions on Industrial Electronics*, 60(10):4492–4499, 2013.

[64] Y. Shenkman A. Axelrod, B. Berkovich and G. Golan. Diode-capacitor voltage multipliers combined with boost-converters: topologies and characteristics. *IET Power Electronics*, 5(6):873–884, 2012.

[65] G. C. Teixeira L. M. Caracas, J. V. M. Farias and L. A. S. Ribeiro. Implementation of a high-efficiency, high-lifetime, and low-cost converter for an autonomous photovoltaic water pumping system. *IEEE Transactions on Industry Applications*, 50(1):631–641, 2014.

[66] M. Slibar P. Milanovic, M. Truntic and D Dolinar. Reconfigurable digital controller for a buck converter based on fpga. *Microelectronics Reliability*, 47(1):150–154, 2007.

[67] S. H. Danyali, S. Hosseini and G. B. Gharehpetian. New extendable single-stage multi-input dc–dc/ac boost converter. *IEEE Transactions on Power Electronics*, 29(2):775–788, 2014.

[68] L. Kjaer S. B. Bordonau J. Xue, Y. Chang and T. Shimizu. Topologies of single-phase inverters for small distributed power generators: an overview. *IEEE Transactions on Power Electronics*, 19(5):1305–1314, 2004.

[69] L. G. Bialasiewicz J. T. Galvan E. Guisado R. C. P. Prats M. M. Leon J. I. Carrasco, J. M. Franquelo and N. M. Alfonso. Power-electronic systems for the grid integration of renewable energy sources: A survey. *IEEE Transactions on Industrial Electronics*, 53(4):1002–1016, 2006.

[70] Y. M. Tan S. C. Chen, S. Lai and C. K. Tse. Fast response low harmonic distortion control scheme for voltage source inverters. *IET Power Electronics*, 2(5):574–584, 2009.

[71] L. Yao, Z. Xiao and Y. Yan. Seamless transfer of single-phase grid-interactive inverters between grid-connected and stand-alone modes. *IEEE Transactions on Power Electronics*, 25(6):1597–1603, 2010.

[72] Z. Lu T. He, F. Zhao and L. Yuan. Predictive dc voltage control for three-phase grid-connected pv inverters based on energy balance modeling. In *2nd IEEE International Symposium on Power Electronics for Distributed Generation Systems (PEDG)*, pages 516–519. IEEE, 2010.

[73] D. Velasco D. Garcera G. Figueres E. Rodriguez, C. T. Fuente and J. A. G. Moreno. Reconfigurable control scheme for a pv microinverter working in both grid-connected and island modes. *IEEE Transactions on Industrial Electronics*, 60(4):1582–1595, 2013.

[74] E. Koutroulis and F. Blaabjerg. Design optimization of transformerless grid-connected pv inverters including reliability. *IEEE Transactions on Power Electronics*, 28(1):325–335, 2013.

[75] A. Kulkarni and V. John. Mitigation of lower order harmonics in a grid-connected single-phase pv inverter. *IEEE Transactions on Power Electronics*, 28(11):5024–5037, 2013.

[76] D. Guinjoan F. Poveda A. Masana F. Chavarria, J. Biel and E. Alarcon. Fpga-based design of a step-up photovoltaic array emulator for the test of pv grid-connected inverters. In *IEEE 23rd International Symposium on Industrial Electronics (ISIE)*, pages 485–490. IEEE, 2014.

[77] R. Selvamuthukumaran and R. Gupta. Rapid prototyping of power electronics converters for photovoltaic system application using xilinx system generator. *IET Power Electronics*, 7(9):2269–2278, 2014.

[78] H. Patel and V. Agarwal. Investigations into the performance of photovoltaics-based active filter configurations and their control schemes under uniform and non-uniform radiation conditions. *Renewable Power Generation*, 4(1):12–22, 2010.

[79] A. S. A. Talib N. Hairul M. D. Lazi J. M. Isa M. Noormiza S. Ibrahim, Z. Hasim and R. Mustafa. Performance investigation of photovoltaic grid connection for shunt active power filter with different pwm generation. *Journal of Theoretical & Applied Information Technology*, 57(2), 2013.

[80] M. Hamza, D. Qiu and P. K. Jain. Application and stability analysis of a novel digital active emi filter used in a grid-tied pv microinverter module. *IEEE Transactions on Power Electronics*, 28(6):2867–2874, 2013.

[81] A. Hatti M. Belaidi, R. Haddouche and M. Larafi. Shunt active power filter connected to a photovoltaic array for compensating harmonics and reactive power simultaneously. In *Fourth International Conference on Power Engineering, Energy and Electrical Drives (POWERENG)*, pages 1482–1486. IEEE, 2013.

[82] I.H. Altas and A. M. Sharaf. A photovoltaic array simulation model for matlab-simulink gui environment. In *International Conference on Clean Electrical Power, ICCEP'07*, pages 341–345. IEEE, 2007.

[83] K. Michihira M. Tsuyoshi A. Amako K. Yamashita, H. Tamahashi and M.n. Park. A novel simulation technique of the pv generation system using real weather conditions. In *Proceedings of the Power Conversion Conference, PCC-Osaka*, volume 2, pages 839–844. IEEE, 2002.

[84] A. V. Vokas, G. A. Machias and J. L. Souflis. Computer modeling and parameters estimation for solar cells. In *Proceedings of the 6th Mediterranean Electrotechnical Conference*, pages 206–209. IEEE, 1991.

[85] T. Khaehintung, N. Wiangtong and P Sirisuk. Fpga implementation of mppt using variable step-size p&o algorithm for pv applications. In *International Symposium on Communications and Information Technologies*, pages 212–215. IEEE, 2006.

[86] W. G. Palmer P. R. Xiao, W. Dunford and A. Capel. Regulation of photovoltaic voltage. *IEEE Transactions on Industrial Electronics*, 54(3):1365–1374, 2007.

[87] K. Kennerud. Analysis of performance degradation in cds solar cells. *IEEE Transactions on Aerospace and electronic systems*, 6(AES-5):912–917, 1969.

[88] K. Seo, G. Lee and B. Cho. A new dc anti-islanding technique of electrolytic capacitor-less photovoltaic interface in dc distribution systems. *IEEE Transactions on Power Electronics*, 28(4):1632–1641, 2013.

[89] R. Panigrahi, P. C. Panda, and B. Subudhi. A robust extended complex kalman filter and sliding-mode control based shunt active power filter. *Electric Power Components and Systems*, 42(5):520–532, 2014.

[90] V. R. Kolluru, K. K. Mahapatra, and B Subudhi. Design and implementation of modified sliding mode controller for a photovoltaic system. In *International Conference on Advances in Electrical Engineering (ICAEE),*, pages 1–6. IEEE, 2014.

[91] M. Steurer M. Dinavahi V. Noda T. Filizadeh S. Chevrefils A. R. Matar M. Iravani R. Dufour C. Ren, W. Sloderbeck. Interfacing issues in real-time digital simulators. *IEEE Transactions on Power Delivery*, 2(26):1221–1230, 2011.

[92] M. Park and I. Yu. A novel real-time simulation technique of photovoltaic generation systems using rtds. *IEEE Transactions on Energy Conversion,*, 19(1):164–169, 2004.

[93] L Li H. Zhou, Y. Liu and L. Wang. Real time digital simulation (rtds) of a novel battery-integrated pv system for high penetration application. In *2nd IEEE International Symposium on Power Electronics for Distributed Generation Systems (PEDG)*, pages 786–790. IEEE, 2010.

[94] C. Xiaoyun, G. Jinmei and L. Qihui. Real-time and grid-connected control of pv power system. In *International Conference on Advanced Power System Automation and Protection (APAP)*, volume 2, pages 923–928. IEEE, 2011.

[95] V. R. Kolluru, K. K. Mahapatra, and B. Subudhi. Real time implementation and comparison of pi and modified inc cond control algorithms for solar applications. 2014.

[96] P. L. H. Gonzalez. *String level I-V curves from different module types under partial shade*. Cheli, 2012.

[97] C. Urayai and G. A. J. Amaratunga. Single-sensor maximum power point tracking algorithms. *Renewable Power Generation*, 7(1):82–88, 2013.

[98] Ni www.india.ni.com/crio.

[99] Ni www.india.ni.com/9201/concepts.

[100] Ni www.india.ni.com/9263/concepts.

[101] Lem "lem datasheet: Lv 25-p," lem, japan, 1996.

[102] Lem "lem datasheet: La 55-p," lem, japan, 1996.

[103] F. Zare and G. Ledwich. A hysteresis current control for single-phase multilevel voltage source inverters: Pld implementation. *IEEE Transactions on Power Electronics*, 17(5):731–738, 2002.

[104] B. K. Bose. An adaptive hysteresis-band current control technique of a voltage-fed pwm inverter for machine drive system. *IEEE Transactions on Industrial Electronics*, 37(5):402–408, 1990.

[105] GH Bode and DG Holmes. Implementation of three level hysteresis current control for a single phase voltage source inverter. In *IEEE 31st Annual Power Electronics Specialists Conference, PESC*, volume 1, pages 33–38. IEEE, 2000.

[106] J. Bauer. Single phase voltage source inverter photovoltaic application. *Acta Polytechnica*, 50(4), 2010.

[107] F. Zare and G. Ledwich. A hysteresis current control for single-phase multilevel voltage source inverters: Pld implementation. *IEEE Transactions on Power Electronics*, 17(5):731–738, 2002.

[108] D. M. Brod and D. W. Novotny. Current control of vsi-pwm inverters. *IEEE Transactions on Industry Applications*, (3):562–570, 1985.

[109] S.and Akagi H. Nabae, A. Ogasawara. A novel control scheme for current-controlled pwm inverters. *IEEE Transactions on Industry Applications*, 4(IA-22):697–701, 1986.

[110] C. Qi Q. Yan Z. Ni Y. Zhang B. L. Chen S. Zeng, J. Yu and F. F Wu. A novel hysteresis current control for active power filter with constant frequency. *Electric power systems research*, 68(1):75–82, 2004.

[111] S. K. Karuppanan, P. Ram and K. K. Mahapatra. Three level hysteresis current controller based active power filter for harmonic compensation. In *International Conference on Emerging Trends in Electrical and Computer Technology (ICETECT)*, pages 407–412. IEEE, 2011.

[112] M. Kale and E. Ozdemir. An adaptive hysteresis band current controller for shunt active power filter. *Electric Power Systems Research*, 73(2):113–119, 2005.

[113] B. Mazari and F. Mekri. Fuzzy hysteresis control and parameter optimization of a shunt active power filter. *Journal of Information Science and Engineering*, 21(6):1139–1156, 2005.

[114] N. Gupta, S. P. Singh, and S. P. Dubey. Dsp based adaptive hysteresis-band current controlled active filter for power quality conditioning under non-sinusoidal supply voltages. *International Journal of Engineering, Science and Technology*, 3(4), 2011.

[115] J. Wang. *Model predictive control of power electronics converter*. Norwegian university of science and technology, Norway, June 2012.

[116] R. Panigrahi, B. Subudhi, and P. C. Panda. Model predictive-based shunt active power filter with a new reference current estimation strategy. *IET Power Electronics*, 8(2):221–233, 2014.

[117] C. N. Jones. *Reconfigurable flight control*. Camebridge university, March 2005.

[118] Rickey Dubay, Guy Kember, and Bambang Pramujati. Well-conditioned model predictive control. *ISA transactions*, 43(1):23–32, 2004.

[119] M. L. Darby and M. Nikolaou. Mpc: Current practice and challenges. *Control Engineering Practice*, 20(4):328–342, 2012.

[120] G. Wills, A. G. Knagge and B. Ninness. Fast linear model predictive control via custom integrated circuit architecture. *IEEE Transactions on Control Systems Technology*, 20(1):59–71, 2012.

[121] L. Gyugyi and E. C. Strycula. Active ac power filters. In *Proc. IEEE/IAS Annual Meeting*, volume 19, pages 529–535, 1976.

[122] L. Cheng and R. Cheung. New rotating transformation for efficient dsp control of active power-line conditioners. *IEEE Transactions on Power Systems*, 15(1):382–387, 2000.

[123] N. Gupta, S. P. Singh, and S. P. Dubey. Dsp based adaptive hysteresis-band current controlled active filter for power quality conditioning under non-sinusoidal supply voltages. *International Journal of Engineering, Science and Technology*, 3(4), 2011.

[124] J. P. Krim F. Chaoui, A. Gaubert and G. Champenois. Pi controlled three-phase shunt active power filter for power quality improvement. *Electric Power Components and Systems*, 35(12):1331–1344, 2007.

[125] H. Benalla and H. Djeghloud. Shunt active filter controlled by fuzzy logic. *Journal of King Saud University*, 2005.

[126] K. Singh, B. Al-Haddad and A. Chandra. A review of active filters for power quality improvement. *IEEE Transactions on Industrial Electronics*, 46(5):960–971, 1999.

[127] V. M. Pigazo, A. Moreno and E. J. Estebanez. A recursive park transformation to improve the performance of synchronous reference frame controllers in shunt active power filters. *IEEE Transactions on Power Electronics*, 24(9):2065–2075, 2009.

[128] P. Karuppanan and K. K. Mahapatra. A novel srf based cascaded multilevel active filter for power line conditioners. In *Annual IEEE India Conference (INDICON)*, pages 1–4. IEEE, 2010.

[129] H. Komurcugil and O. Kukrer. A new control strategy for single-phase shunt active power filters using a lyapunov function. *IEEE Transactions on Industrial Electronics,*, 53(1):305–312, 2006.

[130] H. Zheng. *Solar photovoltaic energy generation and conversion- from devices to grid integration*. The university of Alabama, Alabama, 2013.

[131] O. S. Ramon R. P.J. Sergio V. Marcelo, C. E. P. Gabriel and F. Leopoldo. Model predictive control of an interter with output lc filter for ups applications. 2010.

Thesis Dissemination

Journals

1. **V. R. Koluru** , K. K. Mahapatra, and B. Subudhi "Real-Time Digital Simulation and Analysis of Sliding Mode and P&O MPPT Algorithms for a PV System," *International Journal of Emerging Electric Power Systems*, 2015, vol. 16, no. 4, pp: 313-322.

2. **V. R. Koluru** , K. K. Mahapatra, and B. Subudhi "Design and implementation of an optimized sliding mode controller and compared with a conventional MPPT controller for a solar system," *WSEAS Transactions on Systems and Control*, 2014, vol. 9, no. 1, pp: 558-565.

Conferences

1. **V. R. Koluru** , G. Sahu, K. K. Mahapatra, and B. Subudhi "Design and simulation of a modified sliding mode controller evaluated with a conventional P&O MPPT controller for solar applications," *IEEE International Conference on Signal Processing, Informatics, Communication and Energy Systems, SPICES 2015*, Calicut, 19-21 Feb.

2. **V. R. Koluru** , K. K. Mahapatra, B. Subudhi and R. Tejavathu "Real time implementation and comparison of PI and modified Inc Cond control algorithms for solar applications," *6th India International Conference on Power Electronics, IICPE-2014*, Kurukshetra, 8-10 Dec.

3. **V. R. Koluru** , K. K. Mahapatra, and B. Subudhi "Design and implementation of modified sliding mode controller for a Photovoltaic system," *International Conference on Advances in Electrical Engineering, ICAEE 2014*, Vellore, 9-11 Jan.

4. **V. R. Koluru** , K. K. Mahapatra, and B. Subudhi "A new approach to fast tracking and low cost single exponential model photovoltaic system," *Asia Pacific Conference on Postgraduate Research in Microelectronics and Electronics,* Prime Asia 2013, Visakhapatnam, 19-21 Dec.

5. **V. R. Koluru** , K. K. Mahapatra, and B. Subudhi "Development and implementation of control algorithms for a photovoltaic system," *Students Conference on Engineering and Systems,* SCES 2013, Allahabad, 12-14 Apr.